Technical Report Documentation Page

1. Report No.	2. Government Accession No.	3. Recipient's Catalog No.
FHWA/TX-01/1851-1		

4. Title and Subtitle	5. Report Date
CRACKING IN RC BENT CAPS	October 2000
	6. Performing Organization Code

7. Author(s)	8. Performing Organization Report No.
Joseph M. Bracci, Peter B. Keating, and Mary Beth D. Hueste	Report 1851-1

9. Performing Organization Name and Address	10. Work Unit No. (TRAIS)
Texas Transportation Institute The Texas A&M University System College Station, Texas 77843-3135	11. Contract or Grant No. Project No. 0-1851

12. Sponsoring Agency Name and Address	13. Type of Report and Period Covered
Texas Department of Transportation Research and Technology Implementation Office P. O. Box 5080 Austin Texas 78763-5080	Research: September 1998 - August 2000
	14. Sponsoring Agency Code

15. Supplementary Notes

Research performed in cooperation with the Texas Department of Transportation and the U.S. Department of Transportation, Federal Highway Administration

Research Project Title: Study of Flexural Cracking in Cantilever Standard Design Interior Bent Caps

16. Abstract

This final project report documents the findings of a Texas Department of Transportation sponsored research program to determine the causes of unexpected cracking in reinforced concrete bent caps at outside column locations (cantilevered regions) during service load conditions. Sixteen full-scale bent cap specimens were constructed and tested under quasi-static monotonic loading up to service level loading and through failure. Researchers considered and evaluated the following bent cap parameters in regard to their influence on cracking: longitudinal reinforcement stress, size, and spacing; embedment of longitudinal reinforcement near the discontinuous end of the cap; transverse reinforcement detailing and shear strength; critical section for flexure; and skin reinforcement. Researchers measured and recorded cracks from initial cracking through failure, and reinforcement strain data was recorded continuously throughout the loading history for each specimen. The experimental program confirmed that the observed flexural cracking during service load conditions is directly proportional to the level of stress in the flexural reinforcement. In addition, enhancing the shear strength of the bent cap leads to a reduction in inclined flexure-shear cracks during service and ultimate load conditions.

17. Key Words	18. Distribution Statement
Reinforced Concrete, Bent Cap, Cracking, Service Loading, Reinforcement Stress, Shear Strength, Strut and Tie, Specimens	No restrictions. This document is available to the public through NTIS: National Technical Information Service 5285 Port Royal Road Springfield, Virginia 22161

19. Security Classif.(of this report)	20. Security Classif.(of this page)	21. No. of Pages	22. Price
Unclassified	Unclassified	270	

Form DOT F 1700.7 (8-72) **Reproduction of completed page authorized**

CRACKING IN RC BENT CAPS

by

Joseph M. Bracci
Associate Research Engineer
Texas Transportation Institute

Peter B. Keating
Associate Research Engineer
Texas Transportation Institute

and

Mary Beth D. Hueste
Assistant Research Engineer
Texas Transportation Institute

Report 1851-1
Project Number 0-1851
Research Project Title: Study of Flexural Cracking in Cantilever Standard Design Interior Bent Caps

Sponsored by the
Texas Department of Transportation
In Cooperation with the
U.S. Department of Transportation
Federal Highway Administration

October 2000

TEXAS TRANSPORTATION INSTITUTE
The Texas A&M University System
College Station, Texas 77843-3135

DISCLAIMER

This research was performed in cooperation with the Texas Department of Transportation. The content of this report reflects the views of the authors, who are responsible for the facts and accuracy of the data presented herein. The contents do not necessarily reflect the official view or policies of the TxDOT. This report does not constitute a standard, specification, or regulation, nor is it intended for construction, bidding, or permit purposes. Trade names were used solely for information and not for product endorsement. The engineer in charge was Joseph M. Bracci, P.E. (TX 79855).

ACKNOWLEDGMENTS

The authors gratefully acknowledge the financial support from the Texas Department of Transportation (TxDOT), in cooperation with the U.S. Department of Transportation Federal Highway Administration, to conduct this research (project number 0-1851). In addition, the authors are grateful to the project director (PD), David Hohmann, for his involvement and assistance throughout the project.

Structural Metals, Inc. of Seguin, Texas, through Paul Fredrickson, is also acknowledged for donating the reinforcing steel for the specimens of the experimental program.

The authors would also like to thank Andrew Fawcett, Jeff Perry, and Gerry Harrison of the Testing, Machining, and Repair Facility at Texas A&M University for their efforts, dedication, and commitment to experimental research.

Finally, the authors wish to thank the graduate research assistants on the project, Bradley Young and Suraphong Powanusorn, for their hard work and contributions.

TABLE OF CONTENTS

LIST OF FIGURES

LIST OF TABLES

1. INTRODUCTION

1.1 PROBLEM STATEMENT

In Texas, unexpected top and side face cracking in reinforced concrete (RC) bent caps at outside column locations (cantilevered regions) exists within the Texas Department of Transportation (TxDOT) bridge inventory. This cracking has primarily initiated during service load levels, and in some cases initiated under only dead load conditions. American Association of State Highway and Transportation Officials (AASHTO) Standard Specifications for allowable stress design (ASD) require that the service load stress in the main longitudinal reinforcement (Grade 60) be limited to 24 ksi in an effort to adequately control flexural cracking (AASHTO, 1996). Alternatively, AASHTO specifications for load and resistance factor design (LRFD) limit the service load stress to 60 percent of the reinforcement yield stress (AASHTO, 1998). In an effort to better control bent cap cracking, TxDOT also limits the dead load stress in the main longitudinal reinforcement within negative moment regions to 22 ksi.

However, it is unknown if these reinforcement stress limits are effective in controlling cracks. It is also uncertain whether other variables may influence this cracking and which of these variables might be economically controlled in an effort to mitigate cracking at these critical locations. There is also some uncertainty regarding the effectiveness of code serviceability requirements to control cracking in RC flexural members with small shear span-to-depth ratios (less than about 2.0) such as bridge bent caps. Along with being visible eyesores, these cracks allow the propagation of corrosive materials through the concrete cover to the steel reinforcement, which can potentially compromise the strength and long-term durability of these highway bridge structures.

1.2 OBJECTIVE

The objective of this research project is to determine the causes of excessive cracking in TxDOT standard design RC bent caps near the column-to-bent cap negative moment joint locations during service load conditions. Researchers investigated various design and detailing parameters that are believed to directly affect cracking in RC

members. Researchers also evaluated the effectiveness and applicability of past and current code requirements for crack control.

The goal of this project is to develop new design recommendations for RC bent caps and similar structural members that more accurately reflect the relationship between these design parameters and cracking. Ultimately, these design recommendations for crack mitigation should lead to improved long-term performance of bridge structures with reduced maintenance costs.

1.3 SCOPE

In conjunction with the project objectives, researchers designed, constructed, and tested 16 full-scale bent cap specimens in an experimental testing program. The project investigated a variety of bent cap design requirements and detailing arrangements, including service stress in the main longitudinal reinforcement, reinforcement arrangement, location of design critical section for flexure, bar development length, shear strength and code serviceability requirements for crack control in terms of their influence on cracking. Strain levels in the main longitudinal reinforcement were monitored, and crack widths were measured and recorded in an effort to determine a relationship between these factors and associated surface crack widths. Quasi-static force-controlled actuators applied loading to the specimens, simulating bridge girder loading up to service conditions through failure. To complement the experimental program, researchers conducted nonlinear finite element modeling of the bent cap specimens to correlate with the experimental findings and then modified the models to highlight certain parameters that may influence such cracking.

The following information provides an overview of the organization in this final report. Section 1 presents the problem statement, research objectives, and scope of work. Section 2 presents the previous and current state of practice for flexural and shear design of RC members based on serviceability and factored strength levels, per American Concrete Institute (ACI) 318 and AASHTO codes. Previous and current TxDOT procedures for the design of standard RC bent caps are discussed. Section 2

also provides a literature review of research on cracking in similar RC members. In addition, findings from a limited field investigation of TxDOT bent caps currently in service is highlighted. Section 3 describes the organization of the experimental program and design details for three groups of bent cap specimens. This section also describes the experimental test set-up, including specimen instrumentation, data acquisition, and analytical tools used for comparative purposes. Section 4 presents the experimental results from the three groups of specimen tests. This section includes results that were based on observations, as well as those that were based upon acquired data from strain gauge readings and other instrumentation. Section 5 provides a brief presentation on the application of strut-and-tie modeling for the design of RC bent caps. Advantages and shortcomings of strut-and-tie design approach, as well as a simple model to reflect the specific application of a typical bent cap, are presented. Section 6 presents the findings from the non-linear finite element modeling of the bent cap specimens in the experimental program, as well as some parametric studies that highlight certain design and detailing variables that influence cracking. Section 7 summarizes the findings of the entire research program and presents conclusions and design recommendations based upon these findings. Suggestions are also made for further research, which may help to further validate the results of the experimental program and reduce cracking in such members. Several appendices are included that illustrate important behavioral characteristics for each test specimen via strain gauge data. Photographs within the appendices show the cracking behavior in each specimen at various loading stage.

2. BACKGROUND

2.1 PREVIOUS STATE OF PRACTICE

The ACI Building Code Requirements for Structural Concrete (ACI 318, 1995) specifies that flexural reinforcement should be distributed throughout the tension region such that flexural cracking is reasonably controlled. Prior to revisions made in 1999, this specification took the form of a 'z' factor, which was a function of the level of tensile stress in the longitudinal reinforcement as well as the amount and arrangement of flexural tension reinforcement (which emphasized the flexural reinforcement details). Limiting this 'z' factor to below certain values, 175 k/in. and 145 k/in. for interior and exterior exposures, respectively, corresponds to expected crack widths of 0.016 and 0.013 in., respectively. Along with aesthetic reasons for limiting surface crack widths, these crack widths were thought to be reasonably effective in limiting the amount of corrosive chemical agents penetrating the surface cracks and contacting the reinforcement. The 'z' factor expression in the ACI 318 (1995) code is as follows:

$$z = f_s \sqrt[3]{d_c A} \tag{2.1}$$

where: f_s = Service stress in the flexural tension reinforcement (in ksi), can be taken as 60 percent of the specified yield strength of the reinforcement ($f_s = 0.60 * f_y$).

d_c = Distance from extreme concrete fiber in tension to the centroid of the closest layer of reinforcement (in in.).

A = Effective tension area of concrete surrounding the flexural reinforcement divided by the number of flexural bars (in in.^{2}/bar).

This expression is a modified version of the Gergely-Lutz (1968) equation, which was the result of a statistical analysis of crack width data from a collection of extensive investigations into cracking of RC members (further discussed in Section 2.4.3). The form taken by this 'z' factor is such that an arrangement of several bars at moderate spacing would be much more effective in controlling surface crack widths than an equivalent amount of reinforcement made up of larger bars at a larger spacing. It

should be noted that no limitations were placed upon the values for concrete cover (d_c) to be used in calculations of this 'z' factor. It is also common practice to reduce the service stress in the longitudinal reinforcement (f_s) by the ratio of the area of steel required to the area of steel provided. In effect, according to this equation, this ratio will reduce the associated 'z' value and reduce crack widths.

Prior to 1989, ACI 318 also specified a minimum amount of side face (skin) reinforcement to be evenly spaced through the depth of relatively deep members in order to control web-flexural cracking. Much of this skin reinforcement was ineffective in controlling cracks because only a portion was placed within the web-tension zone, where it could be effective in crack control.

2.2 CURRENT STATE OF PRACTICE

2.2.1 ACI 318 Requirements

Provisions were made in the 1999 edition of ACI 318 that replaced the 'z' factor approach to crack control in favor of one that emphasizes flexural tension reinforcement spacing. This new expression as it appears in ACI 318 (1999) is as follows:

$$s = \frac{540}{f_s} - (2.5 * c_c) \leq 12 * \left(\frac{36}{f_s}\right) \tag{2.2}$$

where: s = Maximum spacing of flexural tension reinforcement (in in.).

f_s = Service load stress in the tension reinforcement (in ksi), can be taken as $0.60*f_y$.

c_c = Clear cover from the nearest concrete surface in tension to the surface of the flexural tension reinforcement (in in.).

This code revision, discussed further in Section 2.4.3, was motivated by the fact that the previous 'z' factor expression was unworkable for concrete covers greater than 2.5 in. Some researchers explained that a weak correlation exists between surface crack width and total corrosion in the reinforcing steel (Darwin et al., 1985). Because of this,

the new expression limits crack width to tolerable levels based on aesthetics only. In addition, no specifications are made for exposure conditions as had existed in the previous serviceability expression. Due to the large amount of scatter associated with cracking in RC members and the fact that the 'z' factor expression becomes practically unworkable for larger and commonly specified cover dimensions, ACI 318 replaced the 'z' expression in favor of the above expression that emphasizes bar spacing. This expression served as a design basis for some of the test specimens within Group #3 of the experimental phase of this project in an effort to make a comparison between bents designed based upon the previous 'z' factor expression and this new expression.

ACI 318 (1999) also contains serviceability requirements for reinforcing the side faces of flexural members where the member effective depth exceeds 36 in. The motivation for this revision, discussed further within the literature review, was the fact that researchers commonly observed larger than expected web-diagonal cracks in relatively deep flexural members near mid-depth, and they could not be controlled adequately by the arrangement of flexural tension reinforcement. Specifications for detailing side face reinforcement within ACI 318 (1999) are stated as follows:

ACI 318-99 (10.6.7)

If the effective depth (d) of a beam or joist exceeds 36 in., longitudinal skin reinforcement shall be uniformly distributed along both side faces of the member for a distance d/2 nearest the flexural tension reinforcement. The area of skin reinforcement (A_{sk}) per foot of height on each side face shall be / 0.012(d-30). The maximum spacing of the skin reinforcement shall not exceed the lesser of d/6 and 12 in. It shall be permitted to include such reinforcement in strength computations if a strain compatibility analysis is made to determine stress in the individual bars or wires. The total area of longitudinal skin reinforcement in both faces need not exceed one-half of the required flexural tensile reinforcement.*

This modification was introduced into the ACI 318 code in 1989 and into the AASHTO code shortly after. Therefore, a significant portion of the bent caps within the TxDOT bridge inventory currently in service do not reflect this detail. As stated previously, earlier specifications called for an even distribution of side face reinforcement along the vertical face of flexural members to control web cracking.

2.2.2 AASHTO Requirements

AASHTO LRFD (1998) and Standard Specifications (1996) contain a serviceability expression that is very similar to the ACI 318 (1995) 'z' factor expression. This expression places a limit on service load stress levels in the flexural tension reinforcement based upon reinforcement details and is shown below as it appears in AASHTO (1998):

$$f_{sa} = \frac{z}{\sqrt[3]{d_c A}} \leq 0.6 f_y \tag{2.3}$$

where: f_{sa} = Allowable service stress in flexural tension reinforcement (in ksi).

z = Crack width parameter: 170 and 130 k/in. for moderate and severe exposure to corrosive environments, respectively.

d_c = Distance from the extreme tensile fiber to the center of the nearest reinforcing bar, not to be taken greater than 2.0 in.

A = Area of the tension concrete having the same centroid as the reinforcement divided by the number of flexural tension bars (in in.^{2}/bar).

AASHTO limits the value for concrete cover (d_c) to 2.0 in. for calculation purposes. In doing so, the designer is not penalized on a serviceability level for specifying covers greater than 2.0 in. AASHTO sites a weak correlation between surface crack width and corrosion in its justification for this limit. It states that expected surface cracks should be larger for increased cover dimensions, but that this increased crack width should not be detrimental to corrosion protection. This assertion differs from the expression that appears in ACI 318 (1995), which did not limit the concrete

cover dimension (d_c) for calculation purposes. The exposure criteria for the 'z' values differ in the ACI 318 and AASHTO codes. While ACI 318 has 'z' values corresponding to interior and exterior exposure conditions, AASHTO includes 'z' values based upon moderate and severe exposure conditions. The corresponding exposure classification differences also offer slightly different values for the 'z' term for these two codes.

Commentary within AASHTO (1998) Section 5.7.3.4 states that the most effective means to control cracking is to provide well distributed longitudinal reinforcement throughout the tension region of the member. An orthogonal grid of skin reinforcement is required when design is based upon strut-and-tie modeling, which will be discussed in the next section, as well as in Section 5.

2.3 DEEP BEAM CONSIDERATIONS

2.3.1 ACI 318

2.3.1.1 Flexure Design

Slender beam theory is based primarily upon the assumption that plane sections perpendicular to the member longitudinal axis remain plane and perpendicular to the longitudinal axis throughout bending. From this assumption, a linear strain profile is taken to exist through the member depth and width, thus allowing for simple analysis of stresses throughout the load history of the member. Typical analysis of flexural members for strength purposes assumes that slender beam behavior exists, or that it is a reasonably close representation of the actual behavior. However, this assumption of a linear strain profile is not accurate for certain types of deep flexural members (Chow et al., 1953). ACI 318 (1995) classifies members as being deep for flexural strength calculations based upon their span-to-depth ratios in the following manner:

> **ACI 318-99 (10.7)**
>
> *Flexural members with overall depth-to-clear span ratios greater than 2/5 for continuous spans, or 4/5 for simple spans, shall be designed as deep flexural members taking into account nonlinear distribution of strain and lateral buckling.*

Specific recommendations for the design of members classified as deep for flexure are not explicitly given. However, the code does site several references that suggest the use of strut-and-tie modeling or alternative methods such as conventional beam design with an approximate reduced internal moment arm that accounts for this nonlinear strain distribution (Park and Paulay, 1975).

2.3.1.2 Shear Design

ACI 318 (1999) includes special provisions for the design of deep members for shear strength. These provisions offer alternative expressions for the concrete shear strength contribution (V_c) and require a minimum area of vertical shear reinforcement (A_v) and horizontal shear reinforcement (A_{vh}) to be included in the design of members meeting the following clear span-to-depth ratios:

ACI 318-99 (11.8)

The provisions of 11.8 shall apply to members with l_n/d less than 5 that are loaded on one face and supported on the opposite face so that compression struts can develop between the loads and the supports.

Here, l_n is the clear span distance between two adjacent supports, and d is the effective depth of the member. At the cantilever end, the clear span dimension was taken to be the distance between two adjacent applied loads. Mentioned in the commentary of Section 11.8 is an allowance for shear design procedures based upon satisfaction of equilibrium and strength requirements. Such an alternative design procedure could be the use of strut-and-tie modeling, which is discussed further in Section 5.

The common scope of application of the ACI 318 code is in the design of building structures, where flexural members are acted upon primarily by distributed loading. This loading allows members to be categorized as deep based upon their clear span-to-depth ratios. Large concentrated loads acting near supports, which would cause nonlinear longitudinal strain distributions and thus exhibit deep beam characteristics, are not considered in detail. Regardless of the member geometry, deep beam behavior is

more a function of the load transfer path and may exist at localized positions along members of any size.

2.3.2 AASHTO

AASHTO LRFD (1998) does not explicitly categorize members as being deep in the same manner as ACI 318. It makes suggestions for alternative design procedures in the following manner for members that exhibit nonlinear longitudinal strain distribution where conventional beam theory is not an accurate representation of actual behavior:

> **AASHTO (1998) (5.6.3.1)**
>
> *The strut-and-tie model should be considered for the design of deep footings and pile caps or other situations in which the distance between the centers of the applied load and the supporting reactions is less than about twice the member thickness.*
>
> **AASHTO (1998) (C5.6.3.1)**
>
> *Where the conventional methods of strength of materials is not applicable because of non-linear strain distributions, the strut-and-tie modeling may provide a convenient way of approximating load paths and force effects in structures.*

While the scope of application of the ACI 318 code is primarily in building design, the scope of the AASHTO code is primarily in bridge and highway design, where large, concentrated loads more commonly act upon flexural members. For this reason, AASHTO makes reference to the distance from the concentrated load to the support in determining if a non-linear strain distribution is to be considered in design. Unlike ACI 318, AASHTO makes explicit reference to the use of the strut-and-tie model for design when a nonlinear strain distribution is expected. AASHTO (1998) Section 5.6.3 also provides some design specifications for use in strut-and-tie modeling.

AASHTO LFD (1996) specifications include ***no basis*** for classifying a deep flexural member.

2.3.3 Bent Cap Applications

The nature of the load path determines if conventional beam theory can be applied to a situation. If a typical TxDOT bent cap with a shear span to depth ratio of about 1.5 was designed per ACI 318 (1999) guidelines, it would probably not be considered deep for flexure or shear design. However, the same bent cap designed per AASHTO LRFD (1998) standards would require consideration of non-linear strain distributions based upon typical shear span-to-depth ratios, and thus it would require an alternative means of design, such as the strut-and-tie model. Because dimensions such as clear span, shear span, and depth vary somewhat in bent caps throughout Texas, it is difficult to classify these members as being deep members by ACI 318 or AASHTO specifications.

As stated previously, it may be more appropriate to use AASHTO LRFD (1998) recommendations when determining whether to classify a particular bent cap span as deep. Typical loading upon a bent cap structure consists of a series of concentrated loads from support of the longitudinal deck girders. In this case, it would be common to find concentrated loads acting near the support, and thus AASHTO LRFD recommends alternative methods for design, including the strut-and-tie model. As stated previously, it is important to understand the load transfer path through a member in determining if a linear strain distribution can be reasonably assumed. Methods in which codes classify members as being deep are simplifications based upon an assumed loading pattern and may not be an accurate representation of all situations. Macgregor (1997) suggests a more general definition of a deep beam as being: "...a beam in which a significant amount of the load is carried to the supports by a compression thrust joining the load and the reaction. This occurs if a concentrated load acts closer than about $2d$ to the support, or for uniformly loaded beams with a span-to-depth ratio, l_n/d, less than about 4 to 5."

2.4 LITERATURE REVIEW AND PAST RESEARCH

2.4.1 General

The literature in this filed documents significant research efforts to determine the parameters that affect cracking in RC members. However, there is still a great deal of uncertainty associated with which parameters directly affect cracking. This uncertainty can be attributed to many factors, including the high degree of variability associated with cracking in concrete, as well as the variability within experimental parameters such as member geometry and loading. Prior to the experimental phase of this project, researchers reviewed past work related to cracking in RC bent caps, as well as RC structures in general. The purpose of this section is to present a brief overview of the literature review.

2.4.2 Design of Bent Cap Structures

In Texas, research was conducted specifically dealing with the design criteria for the overhang regions of RC bent caps (Ferguson, 1964). In this particular investigation, 36 bent cap specimens, each with a depth of 36 in., were constructed and tested in an attempt to establish, in part, proper numerical values for the shear strength of typical bent caps designed throughout Texas. Variables examined in this project included shear span dimensions, end anchorage of longitudinal steel, web reinforcement arrangement, reinforcement bar size, column support geometry, and material properties such as steel grade. Ferguson (1964) made certain conclusions regarding the role of these variables in strength and serviceability of these bent caps. Based upon results from this investigation, Ferguson presented design suggestions to enhance the durability and long-term performance of these structures. Ordinary beam flexure theory was determined to be an accurate means for design. An alternative expression for calculating concrete shear strength, in lieu of the typical expression ($V_c = 2\sqrt{f'_c}bd$), was presented as well.

Regarding column support geometry, both circular and square columns were constructed and tested. In both cases, researchers observed that cracks intruded upon the support area along the side face, suggesting that the crack surface, and thus the strain profile, was not constant through the cross-section from side to side. Such cracking

indicates that the strain toward the sides of the specimen was higher than the strain on the same cross-sectional plane toward the center of the specimen.

With regard to flexural strength, Ferguson (1964) observed that nearly all specimens failed at a load well beyond the load that caused initial yielding of the longitudinal steel, suggesting a desirable ductile failure mechanism. By plotting maximum achieved loads, Ferguson was also able to conclude that vertical stirrups offered little contribution to shear strength for shear spans within the range of his study ($0.5 \leq [a/d] \leq 1.2$). Conventional design calculations based upon superposition of strength contributions from the stirrups and the concrete showed these vertical stirrups significantly contributing to the nominal member shear strength.

Ferguson (1964) also concluded that bond failure at the discontinuous end of the bent could be eliminated by providing a minimum of 12 in. end anchorage length on #8 bars or 15 in. on #11 bars. End anchorage refers to the extension of longitudinal bars past the center of the load point, away from the support, so that enough mechanical bond exists to fully develop the steel strength capacity.

A primary inefficiency with the design of overhanging ends of bent caps seemed to be the inability to effectively control larger than expected side face crack widths with the code specifications used at that time (prior to 1989) for horizontal skin reinforcement.

2.4.3 Crack Control in RC Flexural Members

Frantz and Breen (1978) examined the cause of excessive mid-depth side face cracking in large RC beams designed according to ACI and AASHTO standards. Attention was given to variables that affect side face cracking, which include beam depth, cover dimensions, amount and distribution of side face (skin) reinforcement, and web width. A total of 50 specimens (inverted T-beams) were constructed and tested. Initial flexural cracking occurred at a longitudinal steel stress of about 20 ksi, a stress level that might exist under dead load conditions. Section 4 also discusses this

observation, where tests on bent cap specimens show flexural microcracking to initiate at approximately 5 ksi. Following this initial cracking, reinforcement strains increased to approximately 20 ksi, with very little increase in applied load.

The ACI and AASHTO philosophies seem to dictate setting a minimum allowable cover so that the steel reinforcement is an adequate distance from the surface to avoid the corrosive environment. Alternatively, the Comitě Euro-International du Běton (CEB) Code (1991) takes a different approach by establishing a maximum allowable cover in an attempt to keep the steel reinforcement relatively close to the surface, thus tightly controlling cracking and protecting against advancement of corrosive materials. These philosophies illustrate two very different approaches to the same problem. Moreover, there continues to be some debate regarding whether or not a direct relationship can be made between crack width and corrosion (Darwin et al., 1985).

Frantz and Breen (1978) conclude that the most effective means to control side face cracking in relatively deep members is through the combined use of horizontal skin reinforcement distributed throughout the tension region along with a longitudinal steel arrangement that consists of many smaller, well-distributed bars. Another factor having a direct effect on crack width is the level of steel stress nearest the concrete surface. Therefore, increasing the steel area provided would prove to be an effective means for flexural crack control by lowering the stress levels in the longitudinal bars under the same loading. This is a philosophy similar to that of the previous ACI serviceability 'z' factor (ACI 318, 1995). The authors emphasize the importance of the horizontal skin reinforcement and mention that the increased cost of adding this reinforcement can be offset by using slightly less longitudinal steel, if the flexural strength contribution of the skin reinforcement is considered in design through strain compatibility.

Gergely and Lutz (1968) analyzed data from six extensive crack width experimental investigations. The six groups of data used in this study were taken from investigations by Rüsch and Rehm (1964), Broms (1965), Hognestad (1962), Kaar and Hognestad (1965), Kaar and Mattock (1963), and Clark (1956). By performing

correlation and regression analysis upon this data, the authors proposed equations for predicting crack width in RC flexural members. In general, this approach was an attempt to better define expressions for crack width by employing numerical tools upon data from previous investigations into cracking in RC members. These expressions reflected the results of the six investigations as a whole, thus reducing the tendency for one crack width expression to be dependent upon characteristics unique to one particular investigation. Gergely and Lutz (1968) proposed expressions for crack width along the tension face of flexural members, as well as along the member side faces. The variables that were found to be important factors in cracking were: steel stress levels, cover dimensions, effective area of concrete in tension, and number of reinforcing bars. The expressions for crack width based on these factors (see Appendix F for variable descriptions) are:

For side face crack width (w_s):

$$w_s = .076 \frac{\sqrt[3]{A t_s}}{1 + \frac{2}{3}\frac{t_s}{h_1}} f_s \tag{2.4}$$

For bottom (tension) face crack width (w_b):

$$w_b = .076 \sqrt[3]{A t_s}\, R\, f_s \tag{2.5}$$

The crack width expression for the bottom (tension) face of a member formed the basis of the ACI 318 serviceability requirement for crack control until it was replaced in 1999. The form that appeared in the ACI code was a more practical design version of the Gergerly-Lutz equation, dictating an effective distribution of longitudinal reinforcement such that cracks were limited to some allowable width based upon exposure conditions (see Eq. 2.1). For practical purposes, '*R*' in Eq. 2.5 was set to a value of 1.2 (ratio of the distances to the neutral axis from the extreme compression face and to the centroid of the main tension reinforcement). Then by setting the crack width

'w' in the Gergely-Lutz expression to a value of 0.016 in. (a crack width deemed acceptable for corrosion resistance in interior exposure conditions), the expression defined as 'z' by ACI must be equivalent to 175 k/in. From a designer's standpoint, satisfying the 'z' term involves properly arranging and sizing longitudinal reinforcement within the tension region. AASHTO also refers to the Gergely-Lutz expression as a serviceability requirement. ACI 318 and AASTHO codes suggest slightly different values for 'z' depending on interior or exterior exposure in ACI and moderate or extreme exposure conditions in AASHTO.

Adebar and van Leeuwen (1999) investigated the serviceability performance of 21 large RC hybrid beams (steel flanges with a concrete web) reflecting a variety of code requirements for side face (skin) reinforcement. Substantial differences existed within various codes regarding the amount of side face reinforcement necessary to control primarily flexural cracking in beam webs. The authors were also concerned with the ability of these code requirements to control simultaneous inclined shear cracking along the side face of these members, which for certain shear spans were as much as twice as wide as flexural cracks at the same load.

From research by Ferguson (1964) and Frantz and Breen (1978) on crack control in large RC members, ACI and AASHTO codes adopted requirements for side face reinforcement that depended solely upon the member depth. Alternatively, the Canadian Concrete Code (CSA) and the Canadian Highway Bridge Code (CHBDC) require side face reinforcement in the form of a reinforcement ratio, related to the cross-sectional area of the member. Initial full-scale tests showed that ACI and AASHTO standards are reasonably effective in controlling flexural cracking, while the CSA and the CHBDC proved to be overly conservative (Adebar, 1999). It should be noted that these conservative requirements may be necessary to control simultaneous inclined flexure-shear cracks at mid-depth.

The results of the Adebar and van Leeuwen study (1964) indicated that the most effective way to reduce web cracking is by increasing the amount of well-distributed

side face longitudinal reinforcement. In comparing several of the North American code requirements for crack control, it seems that the ACI 318 and AASHTO requirements are adequate for limiting crack widths to within the range of 0.008 - 0.016 in. However, this may not be suitable for certain severe exposure conditions. These requirements were developed in an attempt to control vertical flexural cracking and may be somewhat unconservative for controlling simultaneous inclined flexure-shear cracks. Conversely, the Canadian Highway Bridge Code requirement may be conservative for many mild exposure conditions but may provide the necessary reinforcement for controlling flexure-shear cracking in more severe exposure conditions.

Frosch (1999) took another look at cracking and crack control in RC beams in an effort to develop a more generalized expression for predicting crack widths. Motivation for this study was threefold. First, the 'z' expression for crack control was considered to represent cracking accurately in members with concrete cover less than 2.5 in. For covers greater than 2.5 in., which is common in larger members in severe exposure environments, this equation diverges. Second, researchers have suggested that crack width may play a rather minor role in the total amount of corrosion along the reinforcement (Darwin et al., 1985). Other factors, such as the quality and permeability of concrete surrounding the reinforcement, may play a much more dominant role in overall corrosion than any localized contribution due to crack width. Also, large covers are often specified as a means to avoid corrosion. At the same time, the ACI 318 (1995) 'z' expression penalized engineers for specifying larger covers. Finally, with the high degree of variability associated with cracking in RC members, it was thought to be unrealistic to attempt to target certain crack width limits through a serviceability expression. In this investigation, Frosch used a physical cracking model in order to formulate a rational expression for cracking and crack control. Below is a summary of the formulation behind Frosch's crack width expression.

Beginning with the relationship that the crack width (w_c) at the level of main tension reinforcement can be expressed as the product of the steel strain (ε_s) at that level multiplied by the crack spacing (s_c):

$$w_c = \varepsilon_s * s_c \tag{2.6}$$

a linear strain gradient can project the maximum strain occurring at the level of the flexural reinforcement to the corresponding crack width at the concrete surface. Research by Broms (1965) concluded that crack spacing is primarily a function of the maximum concrete cover and that the maximum expected crack spacing can be accurately assumed to be twice the minimum spacing. These relationships along with the strain gradient β allow the above expression to be expressed in terms of a maximum crack width in the form:

$$w_c = 2 * \frac{f_s}{E_s} \beta \sqrt{d_c^2 + \left(\frac{s}{2}\right)^2} \tag{2.7}$$

This expression can then be rewritten in a more practical form that dictates bar spacing (s) by linear interpolation of data falling between curves generated from setting permissible crack width (w_c) to 0.016 and 0.02 in.:

$$s = 12\alpha \left[2 - \frac{d_c}{3\alpha_s} \right] \leq 12\alpha_s$$
$$where\ \alpha_s = \frac{36}{f_s} \tag{2.8}$$

In 1999, ACI adopted a form of this expression modified somewhat for simplification. The following equation shows this modified form as it appears in ACI 318 (1999):

$$s = \frac{540}{f_s} - 2.5c_C \leq 12 * \left(\frac{36}{f_s}\right) \tag{2.9}$$

where: s = Maximum spacing of flexural tension reinforcement (in in.).

c_c = Clear cover from concrete tension surface to the reinforcement (in in.).

f_s = Working stress taken to be $0.60 f_y$ (in ksi).

The above expression limits crack widths to tolerable limits for aesthetic reasons only. Therefore, no classifications are made for exposure conditions. Should special environmental considerations be needed for exposure levels, it is left for the judgment of the engineer to reduce the maximum bar spacing and service bar stresses in order to reduce expected crack widths. As well as being a more practical approach to crack control, this expression was shown to be a comparable fit to the crack width data from the six independent studies that served as the basis for the Gergely-Lutz expression.

As a result of this code change, some questions developed as to its applicability for beams of certain dimensions. Nawy (1999) questioned the removal of the 'z' equation in favor of Eq. 2.9, stating that it may be sufficient to make provisions similar to those in AASHTO (1998), where the cover distance need not be taken greater than 2 in. for computation purposes. This adaptation would seem to be a fix to the problem, thus avoiding complete removal of the previous expression. For some flexural members with typical cover distances, Eq. 2.9 yields maximum bar spacing values that may be of limited use as upper bounds. For example, for a beam with a clear cover of 2.5 in. and a working stress (f_s) of 36 ksi, Eq. 2.9 yields a maximum bar spacing of 8.75 in. Most practical beams will have bar spacing well below this value, and thus serviceability will likely not control the design. However, it was not the intention of Eq. 2.9 to control cracking by increasing bar spacing. Rather it serves as a less restrictive expression, thus avoiding some of the controversy surrounding the past serviceability expression (Eq. 2.1) and its ability to control crack widths on the order of accuracy with which it implies. Application to specific, unique situations is left to the judgment of the engineer. Nawy (1999) suggested that the above expression may be more useful in RC slab applications where the larger upper bound on bar spacing may be of more practical use.

2.5 FIELD INVESTIGATION

As a part of this research project, researchers conducted field investigations on multiple highway bridges within Texas with unexpected cracking at the column-to-bent cap joint locations. These affected bent caps, currently in service throughout the state, show a distinct cracking pattern (see Figs. 2.1 and 2.2). Smaller flexural cracks exist primarily within the width of the column support, initiating at the top of the bent cap and extending vertically downward. Along with these smaller flexural cracks, larger shear or flexure-shear diagonal cracks commonly exist within the shear span region of the bent cap, inclined at approximately 45 degrees and extending from the base of the load point toward the column face. It should be mentioned that crack width measurements were not taken on site, and conclusions were made by visual observations alone.

Along with these site visits, TxDOT furnished drawings for one particular overpass consisting of three separate bent cap structures with such unexpected cracking. These drawings provided typical bent cap design details that served as benchmark designs for the initial specimens within the experimental study. Fig. 2.3 shows typical TxDOT details for a series of bent caps constructed in 1988. Examination of these drawings showed that the new specifications (ACI 318 and AASHTO) for side face reinforcement (skin) had not yet been introduced, as the nominal amount of skin reinforcement was distributed evenly throughout the member depth.

Calculations for serviceability criteria based upon the cross-section from Fig. 2.3 show that the bent cap was conservatively designed for crack control according to AASHTO (1998) but unconservatively designed for crack control based upon ACI 318 (1995). According to Eq. 2.3, the actual working stress should be limited to below 36 ksi in order to adequately control cracking. From Eq. 2.1, the working stress would have to be limited to 28 ksi in order to adequately control cracking. The difference in these two expressions lies in the values that are used for clear cover (d_c) as well as the acceptable values each code specifies for the 'z' term. Table 2.1 highlights these differences.

Table 2.1. Bent Cap Serviceability Criteria Case Study.

Parameter	ACI 318-95	AASHTO (1996)
Z	145 k/in.	170 k/in.
d_c	3.5 in.	2 in.
A	39.1 in^2/bar	22.3 in^2/bar
f_s	28 ksi	36 ksi

Site visits to various highway bridge overpasses confirmed that standard design RC bent caps have experienced excessive flexural and shear cracking at the column-to-bent cap joint locations, with the widest cracks occurring near the cantilevered ends in the form of inclined shear-flexure cracks. Cracks at these locations were clearly visible to the naked eye from the vantage point of a passenger traveling on the underpass road. Most cracking was observed to be within the negative moment regions of the bent caps, with only very minor cracking observed along the bottoms of these bents in the positive moment region.

Figure 2.1. Cracking in TxDOT Bent Cap at the Cantilevered End, View #1.

Figure 2.2. Cracking in TxDOT Bent Cap at the Cantilevered End, View #2.

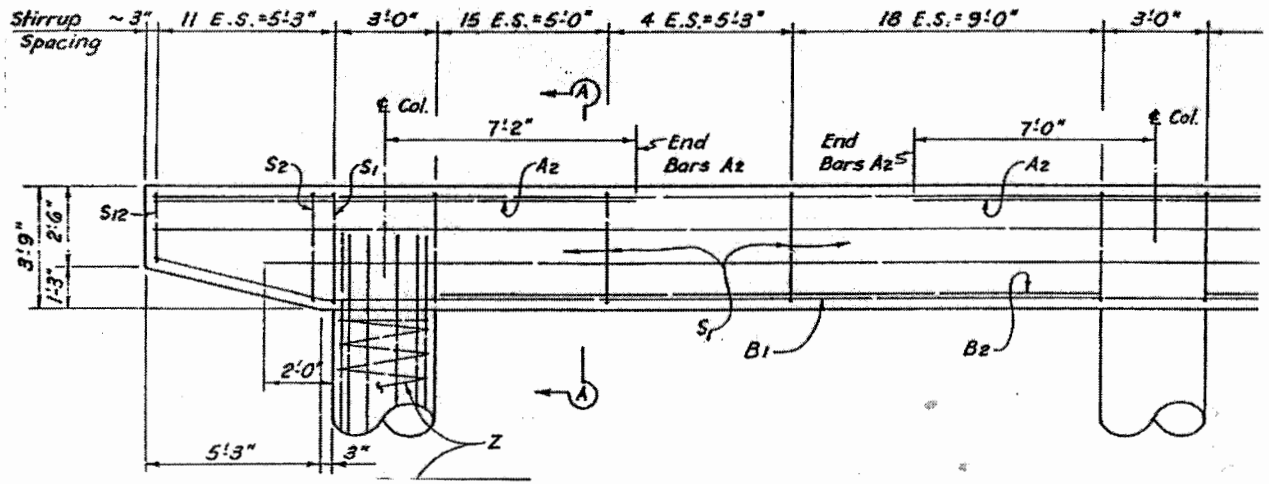

Bar	No.	Size	Length
A1	3	#10	141'-1"
A2	24	#10	14'-0"
B1	3	#10	136'-9"
B2	20	#10	19'-3"
D	4	1¼"ϕ	1'-6"
S1	151	#5	13'-4"
S2-12	22	#5	12'-1"
T1	2	#5	ϕ127'-5"
T2	2	#5	ϕ119'-6"

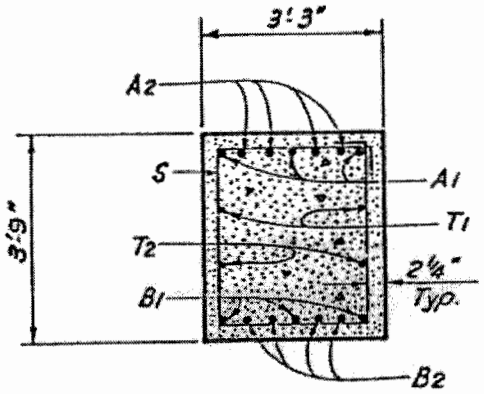

Figure 2.3. Typical TxDOT (1988) Design Specifications for the Cantilevered Portion of a Multi-Column Continuous Bent Cap.

2.6 SUMMARY

The subject of crack control in RC members has been an active area of research over the past 40 years. There still continues to be many questions regarding the reliability of current code level serviceability expressions to control cracking within tolerable limits. Current building and bridge codes such as ACI 318 and AASHTO contain serviceability requirements that reflect the research conducted in the area of crack control. As more data are collected, a better understanding of the factors that affect cracking will follow. Thus, the rationale for expressions to predict crack widths will improve.

Much of what has been presented here was utilized to direct this research investigation and used to develop the initial specimen designs in the experimental program. Most TxDOT bridge design procedures are based upon AASHTO LFD (1996) Standard Specifications. In many cases, these AASHTO specifications are directly correlated with ACI 318 specifications. Some variation does exist between these two codes due to the fact that the AASHTO scope of application is primarily for bridge structures, while the ACI 318 scope of application is primarily for building structures. Both AASHTO and ACI 318 code requirements are covered in an effort to not only establish the basis for TxDOT specifications but also to examine the relationship between the ACI 318 and AASHTO code specifications regarding cracking.

As a result of this literature review, review of past and current state of practice, and observations made from the field investigations, the project team determined a plan of action for the experimental phase of the research project. The team considered several design details for the bent cap specimens based upon potential dominant factors in cracking. The following section discusses the design basis behind each bent cap specimen, along with other aspects of the experimental program, including the experimental setup, instrumentation, and data acquisition.

3. EXPERIMENTAL PROGRAM

3.1 PROGRAM OVERVIEW

In an attempt to evaluate the causes of excessive cracking in RC bent caps, a total of 16 full-scale bent caps were designed, constructed, and tested at the Texas Engineering Experiment Station (TEES) Testing, Machining and Repair Facility high-bay laboratory. The experimental program consists of three groups of specimens thatsub-divide these 16 specimens. Group #1 consists of four specimens, while Groups #2 and #3 consist of six specimens each. The design philososphy for each of these specimens are discussed below.

Researchers assigned each specimen an alphanumeric identification (e.g., 1A), where the number identifies the reinforcement detail of the bent cap and the letter denotes the associated concrete batch. For example, bent cap specimen 1A can be identified by reinforcement detail #1 and concrete compressive strength associated with concrete batch A.

Specimens represented the cantilevered portion of a multi-column bent cap. One end of the specimen represented the continuous end of the bent, where a portion of the main longitudinal bars was hooked to reflect the continuous bars that actually extended along the length of the multi-column bent cap. The hooked detail ensured that slip due to bond failure was not a factor contributing to cracking or failure at this continuous end during testing. At the cantilevered end, the main longitudinal reinforcement extended 17 in. beyond the center of the applied load. This detail was not only reflective of typical TxDOT specifications, but it also agreed with conclusions made by Ferguson (1964) stating that embedment length exceeding 15 in. eliminated the concern for bond failure at the cantilevered end of the cap. To alleviate congestion of reinforcement at the column-to-bent cap joint location, half of the compression steel was cut off prior to intrusion upon the joint. This detail also reflected current TxDOT practice.

Designs provided a nominal amount of transverse shear reinforcement, consisting of #5 closed stirrups spaced at 6.25 in. center-to-center. This reinforcement detail also reflected current TxDOT practice. Reinforcement details for the column were chosen to closely reflect TxDOT design but were not a point of focus in this investigation. All other design details varied according to their association with one of the three specimen groups. Fig. 3.1 shows typical design details for the bent cap specimens and highlights the aspects of design and layout that remain constant throughout the experimental program.

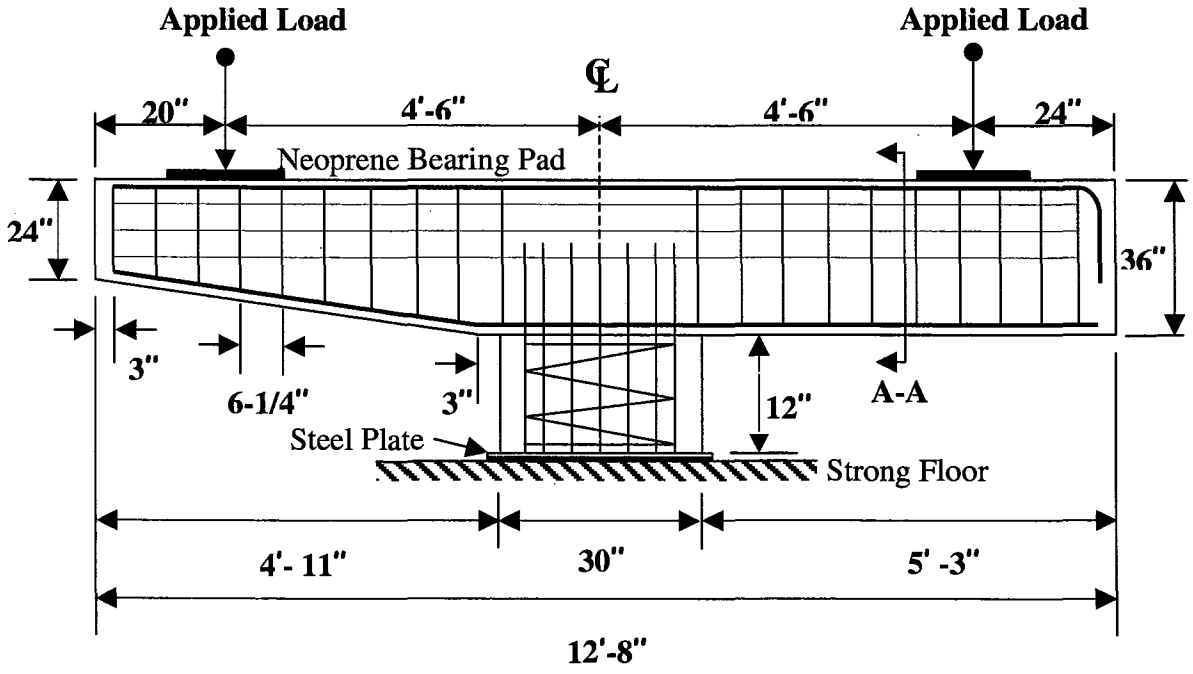

Figure 3.1. Typical Bent Cap Specimen Reinforcement Details.

In summary, the experimental program consisted of 16 full-scale bent cap specimens that were divided into three groups based on their design details. Within each group, researchers isolated and studied certain design characteristics. Each specimen can be identified by its alphanumeric identification, indicating its associated design detail and particular concrete compressive strength. The following section describes the specific details for each specimen group.

3.2 GROUP #1 – EXISTING TxDOT DETAILS

To determine the cause of excessive cracking in standard design RC bent caps, it was first necessary to reproduce the observed field cracking behavior in the laboratory, under simulated loading conditions. The first phase of the experimental program consisted of the design, construction, and testing of four full-scale bent cap specimens. Researchers designed two specimens according to previous (prior to 1989) AASHTO specifications and two according to current AASHTO specifications. The difference was the distribution of horizontal side face reinforcement for controlling flexural cracking in the beam web.

Specimens designed according to previous TxDOT specifications had two layers of #5 horizontal side face reinforcement spaced evenly throughout the member depth. Since this detail reflects code specifications prior to 1989, these specimens are reflective of the majority of bent caps in service throughout the state. For testing, these two particular bent caps are identified as Specimens 1A and 1B.

As discussed in Section 2.4.3, previous code specifications for side face reinforcement were not adequate for crack control in beam webs with relatively small shear span-to-depth ratios. This characteristic is common among members with relatively deep webs and applied loads near the support (Frantz and Breen, 1978). Many codes have adopted new specifications for side face (skin) reinforcement distributed throughout the tension region of the web, as a function of beam depth. To reflect this code change, researchers design specimens 2A and 2B using three layers of #4 horizontal bars concentrated within the web tension region (within a distance d/2 from the main longitudinal reinforcement).

All specimens from Group #1 consisted of eight #8 main longitudinal tension reinforcement at 3.75 in. center-to-center spacing placed in one layer. The compression steel also consisted of eight #8 bars, half of which were cut off prior to intrusion upon the supporting column. These details are representative of one particular TxDOT design and serve as a basis for comparison throughout the experimental program. Fig. 3.2

shows detailed drawings, and Table 3.1 highlights the design details for Group #1 bent cap specimens.

Table 3.1. Group #1 Specimen Design Description.

Specimen ID	Longitudinal Reinforcement	Skin Reinforcement	'z'[1] (k/in.)	Design Critical Section	f'c[2] (psi)
1A	8-#8 bars	4-#5 bars	164	Column face	6,217
1B	8-#8 bars	4-#5 bars	164	Column face	5,820
2A	8-#8 bars	6-#4 bars	164	Column face	6,217
2B	8-#8 bars	6-#4 bars	164	Column face	5,820

[1] Calculated at the column face, using $f_s = 0.6f_y$.
[2] Determined from an average of three standard 28-day compression tests.

3.3 GROUP #2 – MODIFIED DETAILS

Group #2 was composed of six total specimens, consisting of three separate bent designs with two separate concrete batches used for each design. As specimens with alphanumeric identification numbers 1 and 2 belong to Group #1, specimens with identification numbers 3, 4, and 5 belong to Group #2. This next phase of testing consisted of specimens with modified reinforcement details in an effort to focus on specific design parameters and to study their influence on cracking.

Design of specimens within Group #2 emphasized certain serviceability and ultimate strength requirements were met. Two variables within this group included:

- location of critical section for flexure design of the bents; i.e., column face vs. column centerline, and
- arrangement of flexural tension reinforcement to vary the ACI 318 (1995) '*z*' factor calculated at the column face.

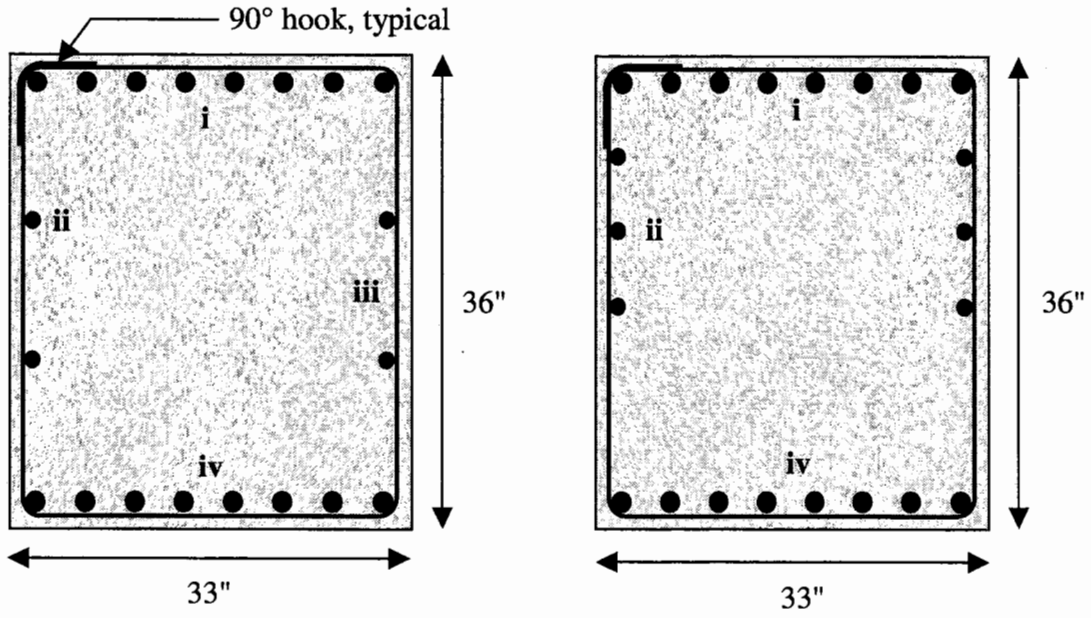

(a) Specimen 1A and 1B Details

(b) Specimen 2A and 2B Details

i. Main Tension Reinforcement:
8-#8 bars @ 3.75 in. spacing (A_s = 6.32 in.^{2})

ii. Side-face (skin) Reinforcement:
(a) 2-#5 bars each side @ 9.75 in. spacing
(b) 3-#4 bars each side @ 5.5 in. spacing

iii. Transverse Reinforcement:
5 Stirrups @ 6.25 in. spacing

iv. Compression Reinforcement:
8-#8 bars
4 cut off prior to column support

● Continuous Bars Through Joint
● Discontinuous Bars at Joint face

Figure 3.2. Group #1 Reinforcement Details, Section A-A (See Fig. 3.1).

In relatively deep members with supports that are not as wide as the bent itself, designing for flexural demands that exist at the face of support may significantly underestimate maximum demands. It can be visualized that for smaller beams framing into much larger columns, the critical section for flexural design purposes would be at the column face, as the strain would be relatively constant throughout the rigid column region. However, for a large beam framing into a somewhat smaller column, the longitudinal strain in the beam tension reinforcement may continue to increase within the column support region, as the bearing axial support of the column is not substantial. The geometry of the bent cap specimens indicates that if a linear strain gradient is assumed to exist from the point of applied load to the centerline of support, then designing for demands at the column face correspond to a 20 percent underestimation of maximum demands in the bent cap reinforcement. Of course, it is doubtful that a linear strain gradient exists along this span, especially within the column support region. However, the idea is that some type of strain gradient does exist within the column support region, and the difference in designing for stresses that exist at the column face as opposed to the column centerline may be substantial, in some cases.

Using the design critical section at the column centerline instead of at the column face ultimately results in a higher moment demand, which implies that more flexural tension reinforcement is needed. Column supports within this investigation are circular in cross-section, and any reference to the column face location refers to the location of the face of a square support of equivalent area.

Members within Group #2 also met serviceability requirements in the form of the ACI 318 (1995) 'z' factor. All calculations made for the 'z' factor were made in relation to the column face location. Therefore, the values used for working stress were adjusted from the suggested value of $0.60f_y$ by the ratio of the area of steel required (based on eight #8 bars, or 6.32 in^2) to the area of steel provided ($f_s = 0.60f_y(A_{st}/A_{sp})$). Isolating this design parameter was motivated by questions surrounding the ability of this expression and the similar AASHTO expression (see Eq. 2.3) to control cracking in these types of members. These design parameters also serve as an attempt to determine if in fact the

ACI 318 (1995) 'z' expression and the similar AASHTO serviceability expression (AASHTO 1998) are effective in predicting crack widths in members with geometry and loading typical of bridge bent caps.

Researchers designed and constructed specimens in Group #2 according to a combination of these two variables, so that members with certain 'z' values may be compared to members with differing design critical sections, and vise versa. Table 3.2 summarizes the serviceability and ultimate strength design basis for each specimen within Group #2, while Fig. 3.3 illustrates Group #2 cross-sections.

Table 3.2. Group #2 Specimen Design Description.

Specimen ID	Longitudinal Reinforcement	Skin Reinforcement	'z'[1] (k/in.)	Design Critical Section	f'c[2] (psi)
3C	11-#7 bars	6-#4 bars	140	Column face	6,035
3D	11-#7 bars	6-#4 bars	140	Column face	5,508
4C	7-#10 bars	6-#4 bars	125	Column centerline	6,035
4E	7-#10 bars	6-#4 bars	125	Column centerline	7,722
5D	11-#8 bars	6-#4 bars	107	Column centerline	5,508
5E	11-#8 bars	6-#4 bars	107	Column centerline	7,722

[1] Calculated at the column face using $f_s = 0.6f_y$ and adjusted by (A_{sr}/A_{sp}) accordingly.
[2] Determined from an average of three standard 28-day compression tests.

By isolating these strength and serviceability design parameters, conclusions could be made about the effectiveness of each parameter individually. Specifically, the effectiveness of the ACI 318 'z' factor in predicting service level crack widths in bent cap members can be determined. Also, any advantages that may exist in designing for demands at the column centerline as opposed to the column face in bent cap structures may become apparent. The strain gradient profile along the main longitudinal reinforcement from the load point to the column centerline will also aid in locating a reasonable design critical section.

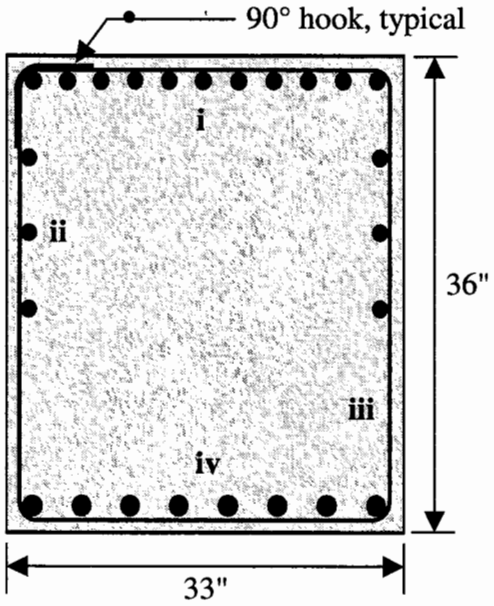

(a) Specimen 3C and 3D Details

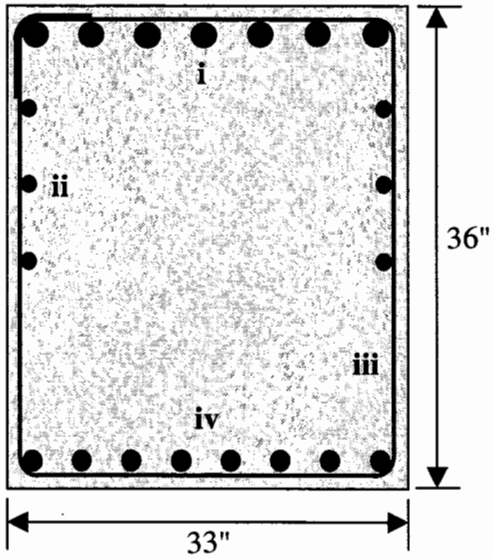

(b) Specimen 4C and 4D Details

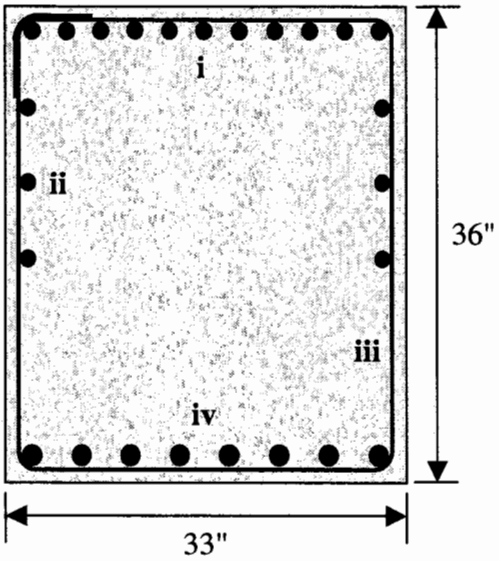

(c) Specimen 5D and 5E Details

i. Main Longitudinal Reinforcement:
   (a) 11-#7 bars @ 2.6 in. spacing (A_s = 6.60 in.^{2})
   (b) 7-#10 bars @ 4.3 in. spacing (A_s = 8.89 in.^{2})
   (c) 11-#8 bars @ 2.6 in. spacing (A_s = 8.69 in.^{2})

ii. Side-face (skin) Reinforcement:
   3-#4 bars each side @ 5.5 in. vertical spacing

iii. Transverse Reinforcement:
   #5 Stirrups @ 6.25 in. longitudinal spacing

iv. Compression Reinforcement: 8-#8 bars
   4 cut off prior to column support

● Continuous Bars through Joint
● Discontinuous Bars at Joint Face

Figure 3.3. Group #2 Reinforcement Details, Section A-A (See Fig. 3.1).

3.4 GROUP #3 – MODIFIED DETAILS

Within Group #3, six specimens were designed, constructed and tested. Similar to Group #2, these six specimens consisted of three separate designs and two concrete batches. Specimens within Group #3 have identification numbers 6, 7, and 8, and contain the following design modifications:

- increased shear strength using overlapping stirrups for transverse reinforcement throughout the length of the bent caps, and
- varied amount and arrangement of flexural tension reinforcement to satisfy code serviceability requirements.

Each specimen within Group #3 contained overlapping stirrups at the typical 6.25 in. spacing for enhanced shear resistance (see Fig. 3.4). This detail was based upon an analysis of the bent cap using a strut-and-tie model, in an attempt to improve the behavior of the bent cap by adjusting the load transfer mechanism in the member. Strut-and-tie models, discussed further in Section 5, simplify the mechanics of a cracked RC member at ultimate loading conditions through the use of an analogous truss model consisting of tension ties, compression struts, and nodal zones. Strut-and-tie analysis of a typical bent cap specimen showed a large percentage of the applied load was being transferred directly to the support through a main diagonal compression strut, with little help from compression fan struts developed by the stirrups. Concentrating the load path into one area in this way results in a brittle failure mechanism. High principal tensile stresses acting perpendicular to this main strut result in cracking parallel to the strut. To increase the ductility of the system, overlapping stirrups enhance shear resistance and distribute the load through more desirable compression fans, alleviating stresses in the main compression strut. Thus, the new construction might more effectively control observed inclined flexure-shear cracks in the field and in the specimens of Groups #1 and #2.

The main longitudinal reinforcement of Group #3 specimens was detailed to satisfy certain code level serviceability requirements. With the introduction of the new

ACI 318 (1999) Building Code, the previous expression for '*z*,' which indirectly limited crack widths based upon the reinforcement detail, was replaced by an expression that primarily emphasizes spacing of longitudinal reinforcement (see Eq. 2.2). In an attempt to examine the performance of this new serviceability expression, specimens 6F and 6G within Group #3 were detailed according to Eq. 2.2, and the maximum allowable bar spacing was used in design. Although specimens 6F and 6G within Group #3 were detailed according to the updated ACI 318 (1999) serviceability expression, researchers calculated its value for the previous '*z*' factor approach in order to remain consistent throughout the experimental program and for the sake of comparison. Fig. 3.4 shows reinforcement details for Group #3 specimens, and Table 3.3 highlights the code level serviceability criteria and design parameters.

Table 3.3. Group #3 Specimen Design Description.

Specimen ID	Longitudinal Reinforcement	Skin Reinforcement	'z'[1] (k/in.)	Design Critical Section	f'c[2] (psi)
6F	5-#10 bars	6-#4 bars	196	Column face	5,460
6G	5-#10 bars	6-#4 bars	196	Column face	5,320
7F	11-#8 bars	6-#4 bars	107	Column centerline	5,460
7H	11-#8 bars	6-#4 bars	107	Column centerline	5,727
8G	8-#8 bars	6-#4 bars	164	Column face	5,320
8H	8-#8 bars	6-#4 bars	164	Column face	5,727

[1] Calculated at the column face using $f_s = 0.6f_y$ and adjusted by (A_{sr}/A_{sp}) accordingly.
[2] Determined from an average of three standard 28-day compression tests.

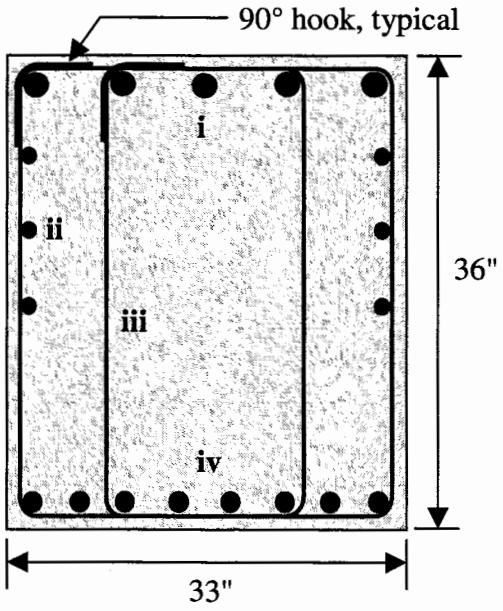

(a) Specimen 6F and 6G Details

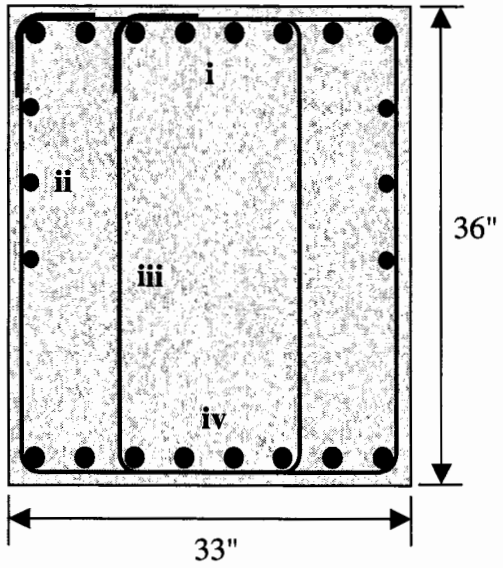

(b) Specimen 8G and 8H Details

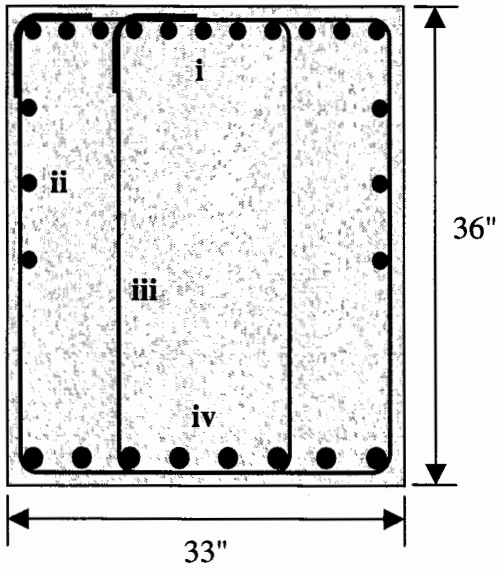

(c) Specimen 7F and 7H Details

i. Main Longitudinal Reinforcement:
   (a) 5-#10 bars @ 6.5 in. spacing (A_s = 6.35 in.^{2})
   (b) 8 -#8 bars @ 3.7 in. spacing (A_s = 6.32 in.^{2})
   (c) 11-#8 bars @ 2.6 in. spacing (A_s = 8.69 in.^{2})

ii. Side-face (skin) Reinforcement:
   3-#4 bars each side @ 5.5 in. spacing

iii. Transverse Reinforcement:
   #5 bars @ 6.25 in. longitudinal spacing

iv. Compression Reinforcement: 8-#8 bars
   (4 cut off prior to column support)

- Continuous Bars through Joint
- Discontinuous Bars at Joint Face

Figure 3.4. Group #3 Reinforcement Details, Section A-A (See Fig. 3.1).

3.5 EXPERIMENTAL TEST SET-UP

3.5.1 General

Specimen testing in the experimental program was performed at the Texas Engineering Experiment Station - Testing, Machining, and Repair Facility high-bay laboratory at Texas A&M University. Specimens were loaded in a quasi-static fashion using two 600-kip force controlled actuators, placed symmetrically at a distance 4.5 ft. from the centerline of the column support as shown in Fig. 3.5. This loading configuration reflects the location of longitudinal bridge deck girders at 9 ft. centers, seated upon the transverse bent cap. A common actuator load was transferred from each actuator to each end of the specimen through the use of W14x398 steel wide flange sections acting as load distributors. Neoprene bearing pads, arranged as shown in Fig. 3.5(c), were used for bearing support and represent the type of load transfer that exists in practice at typical deck girder bearing locations. The specimens were loaded monotonically in 40 kip load increments to failure. After each 40 kip increment, the load was temporarily held constant and researchers visually identified, measured, and recorded cracks. Crack widths were measured using crack width identification cards and were recorded on the specimen along with the corresponding actuator load. As load increased and cracks widened to 0.013 and 0.016 in., the corresponding loads were again recorded on the specimen. Respectively, these crack widths correspond to benchmark maximum crack widths for moderate and extreme exposure (AASHTO, 1998). This process was continued out to an applied load of 360 kips. Beyond this load, very few new cracks formed, and existing cracks widened beyond meaningful values. Thus, crack widths were no longer recorded and loading was increased up to 500 kips, or until failure. A photograph of the experimental test set-up within the high-bay lab is shown in Fig. 3.6.

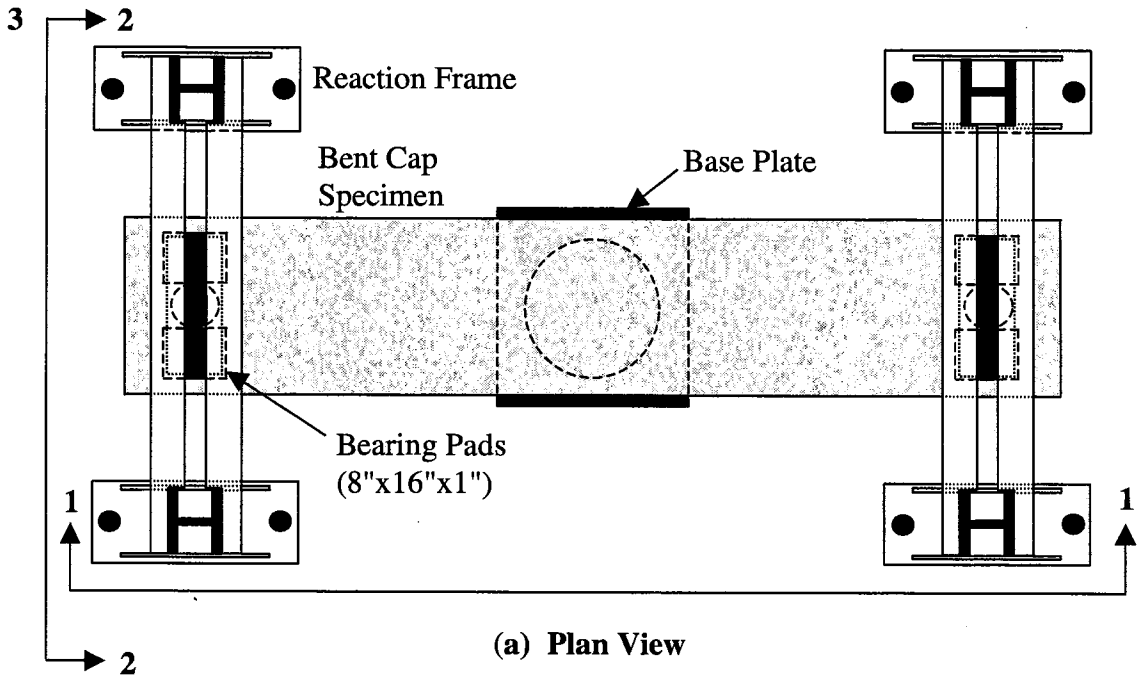

(a) Plan View

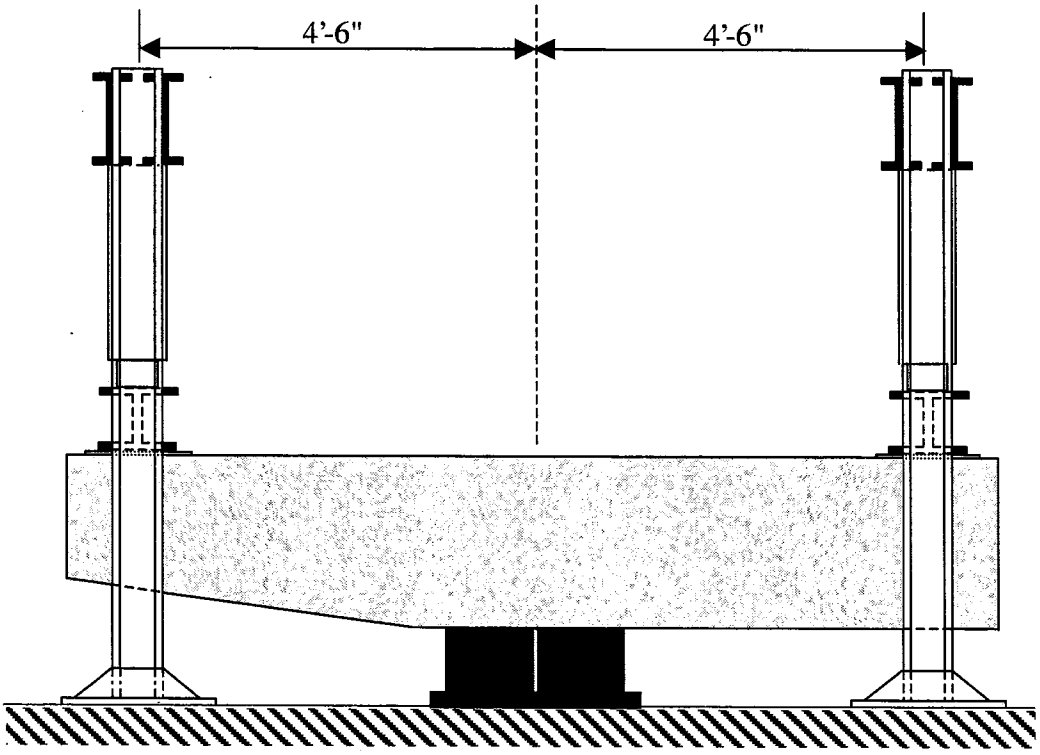

(b) Section 1-1

Figure 3.5. Experimental Test Set-Up.

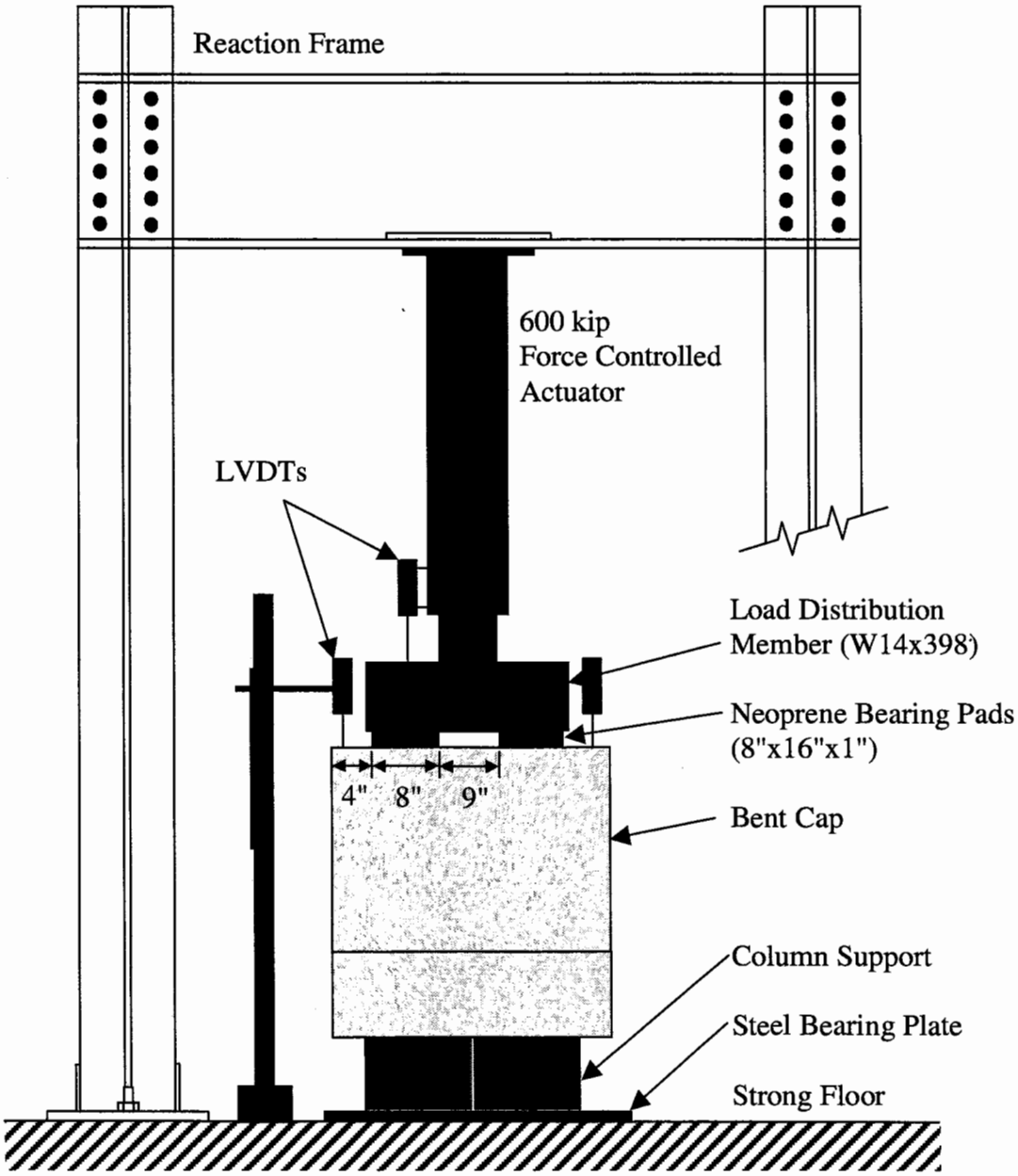

(c) Section 2-2

Figure 3.5. (continued).

3.5.2 Instrumentation

Strain gauge placement at various locations along the reinforcement of each specimen was similar for Group #1 and #2 and was somewhat modified for Group #3 based upon results collected from the previous 10 specimens. Fig. 3.7 shows the strain gauge locations for Group #1 and #2 specimens, while Fig. 3.8 shows the strain gauge locations for Group #3 specimens. The number associated with each strain gauge was used as the gauge identification name. Researchers placed linear variable differential transformers (LVDTs) at the loading points on the bent cap, as well as on the actuators, as shown in Fig. 3.5(c). These LVDTs measured deflections of the specimen ends during testing.

Figure 3.6. High Bay Laboratory Experimental Test Set-Up.

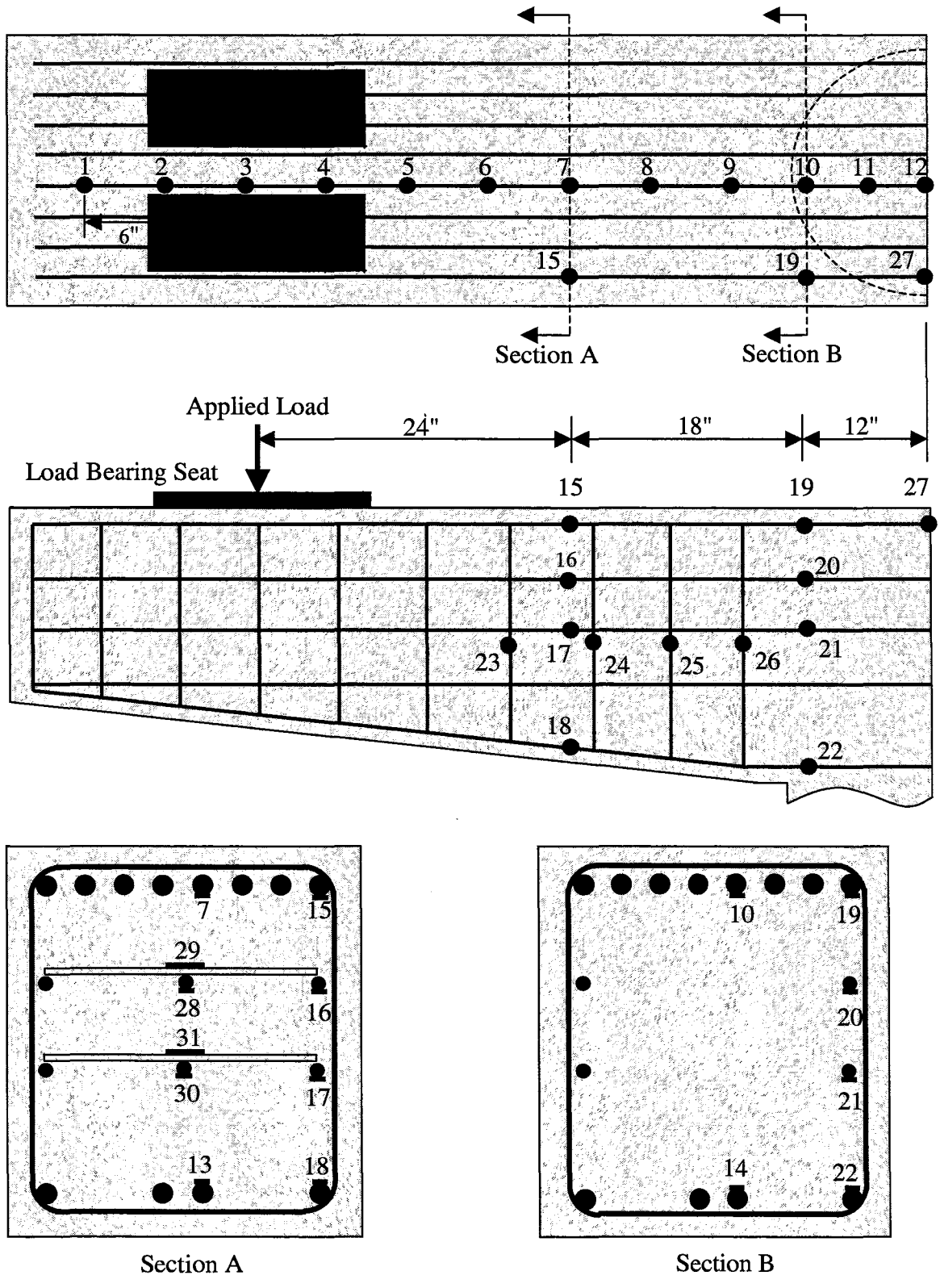

Figure 3.7. Strain Gauge Placement for Group #1 and-#2 Specimens.

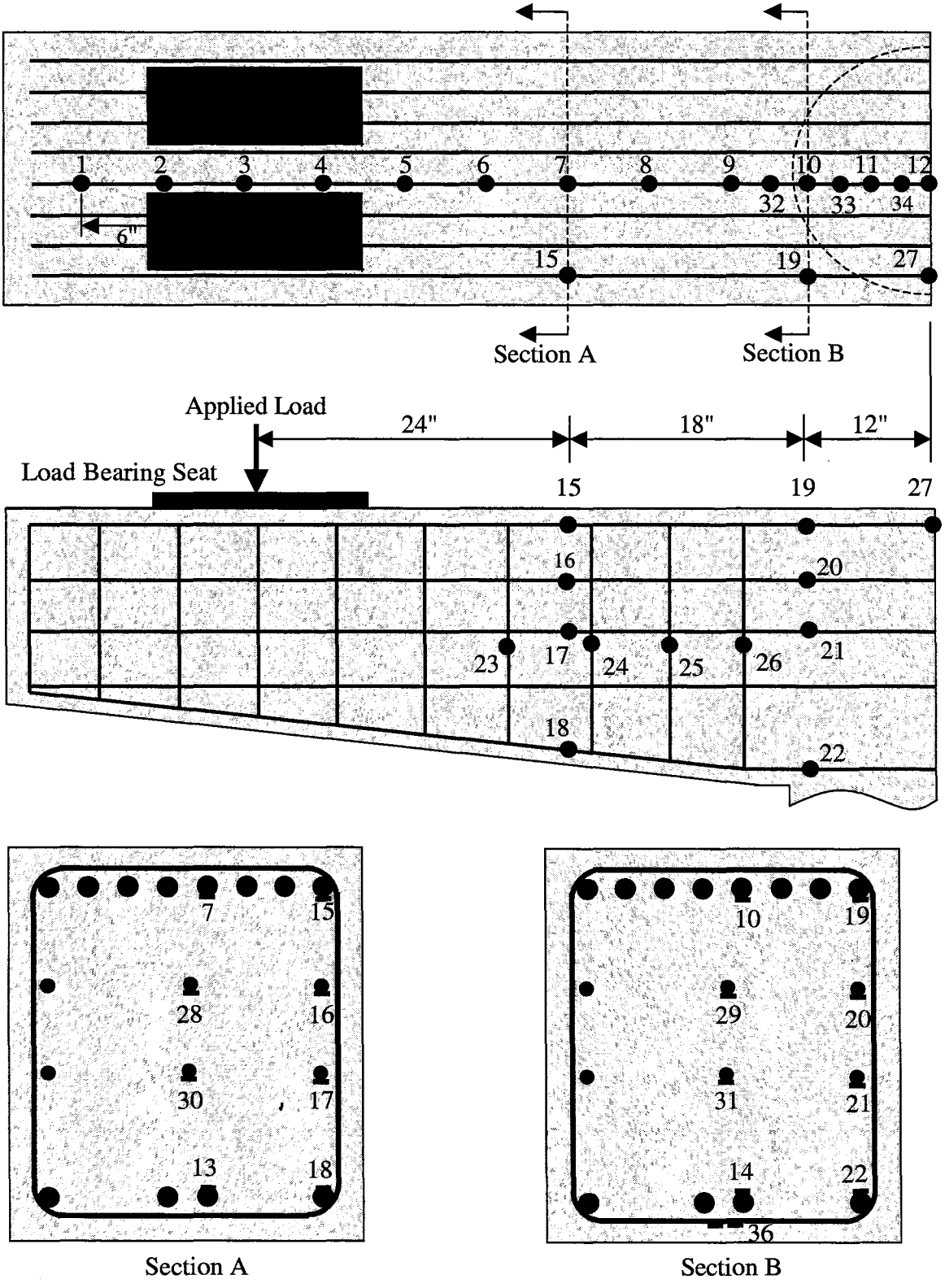

Figure 3.8. Strain Gauge Placement for Group #3 Specimens.

3.5.3 Data Acquisition

Measured response from the instrumentation was acquired using of a commercially available PC-based data acquisition system. The system recorded measurements at a rate of two readings per second during loading. At each 40 kip load increment, the applied loading and data acquisition was temporarily paused while crack widths were measured and recorded. Along with the instrument readings, crack width measurements during testing were also acquired through observation and crack identification card measurements. Specimen photographs with recorded crack widths and associated applied loads were taken at each 40 kip load increment up to 400 kips, as stated previously. Since the actuators utilized air pressure for loading, the pressure (and therefore, the load) typically dropped slightly during the time that cracks were being measured and recorded.

3.6 ANALYTICAL MODEL

Prior to testing each specimen, models predicted the applied actuator load and corresponding steel stress at initial surface cracking at initial yielding of the main longitudinal steel and at ultimate flexural failure of each specimen. The model was based entirely on beam flexural behavior, including the following principals and assumptions:

- maximum concrete compressive strain = 0.003 in./in.,
- concrete tensile strength = $7.5*[f'_c]^{1/2}$, with f'_c in psi,
- f_y = 75 ksi (per uniaxial tensile coupon tests),
- plane sections perpendicular to the longitudinal axis of the member remain plane and perpendicular to the member axis throughout bending, and
- a prismatic cross-section exists.

This model uses equations of equilibrium and compatibility, along with a constitutive relationship to predict stresses in the main longitudinal reinforcement corresponding to a given applied load. For the conditions of equilibrium, the model checks the internal resistive moments against externally applied moments, as well as

checking that internal compressive forces balance internal tensile forces. The compatibility relationship is based upon the assumption of complete bond between the steel reinforcement and the surrounding concrete. This assumption ensures, for calculation purposes, that strain in the main longitudinal reinforcement is exactly equivalent to strain in the concrete at that same level. Included within this compatibility condition is the assumption that plane sections perpendicular to the member neutral axis prior to bending remain plane and perpendicular after bending. Thus, a linear strain profile is assumed to exist through the depth of the member. It is also assumed that all tension bars in a transverse plane are stressed to the same level. The constitutive relationship states that stress can be determined directly from the product of the strain and the modulus of elasticity up to the yield stress of the reinforcement. Following yielding, perfectly plastic behavior is assumed.

Fig. 3.9 shows these three relationships and their applications to a typical RC bent cap section. This analytical model was not only useful in verifying calibration factors on all data acquisition instruments, it also served as a means for comparing the actual behavior of the bent cap with behavior that was predicted based upon the above listed assumptions regarding pure beam flexure.

3.7 SUMMARY

In an attempt to evaluate the causes of excessive cracking in RC bent caps, researchers designed, constructed, and tested a total of 16 full-scale specimens. These 16 specimens were broken down into three groups, based upon certain design parameters which are highlighted below:

Group #1:

- Arrangement of side face reinforcement.

Group #2:

- Location of design critical section for flexure.
- Value for serviceability 'z' factor at column face location.

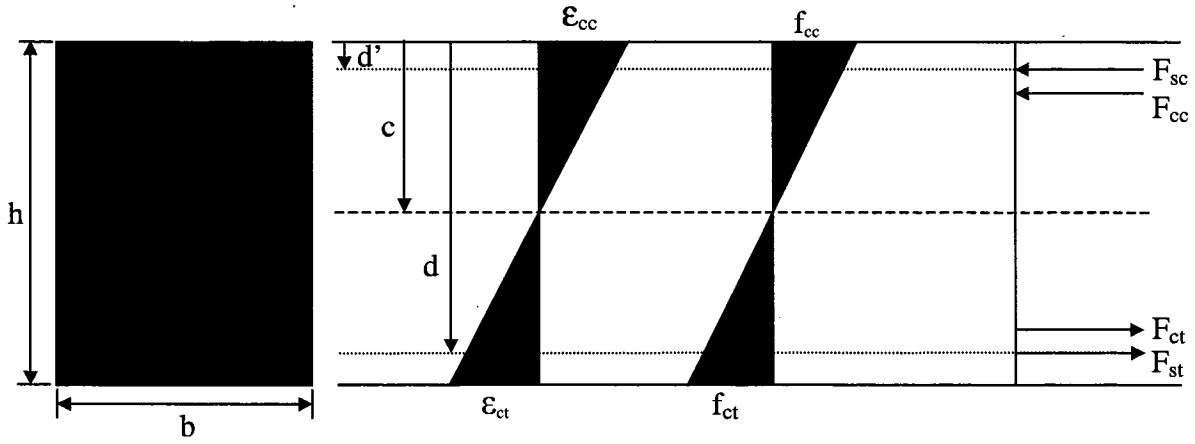

Compatibility Relationships

$$\frac{\varepsilon_{cc}}{c} = \frac{\varepsilon_{sc}}{c-d'} = \frac{\varepsilon_{ct}}{h-c} = \frac{\varepsilon_{st}}{d-c}$$

Constitutive Relationships

$$\frac{\frac{f_{cc}}{E_c}}{c} = \frac{\frac{f_{sc}}{E_s}}{c-d'} = \frac{\frac{f_{ct}}{E_c}}{h-c} = \frac{\frac{f_{st}}{E_s}}{d-c}$$

Equilibrium Relationship

$$\sum M_{internal} = \sum M_{external}$$

$$\sum F = 0$$

(a) Uncracked Bent Cap Behavior

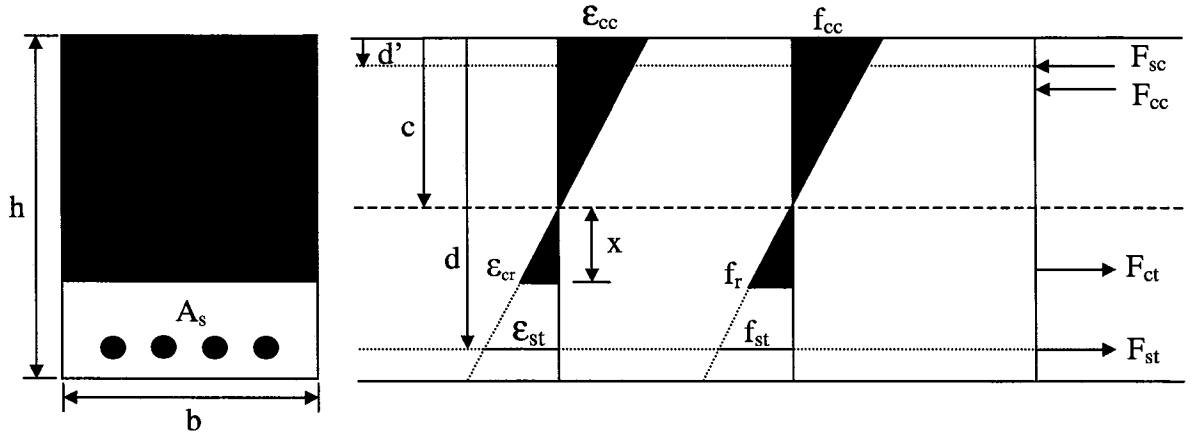

Compatibility Relationships

$$\frac{\varepsilon_{cc}}{c} = \frac{\varepsilon_{sc}}{c-d'} = \frac{\varepsilon_{cr}}{x} = \frac{\varepsilon_{st}}{d-c}$$

Constitutive Relationships

$$\frac{\frac{f_{cc}}{E_c}}{c} = \frac{\frac{f_{sc}}{E_s}}{c-d'} = \frac{\frac{f_r}{E_c}}{x} = \frac{\frac{f_{st}}{E_s}}{d-c}$$

Equilibrium Relationship

$$\sum M_{internal} = \sum M_{external}$$

$$\sum F = 0$$

(b) Cracked Bent Cap Behavior

Figure 3.9. Illustrative Description of Relationships Used in Analytical Model.

Group #3:

- Previous vs. current ACI 318 serviceability expressions.
- Effect of enhanced shear strength through the use of overlapping transverse (stirrup) reinforcement.

Specimen were loaded in a quasi-static, monotonic fashion using 40 kip increments. Researchers continually collected data throughout loading in the form of strain gauge and displacement readings. Crack widths were also measured and recorded at each 40 kip load increment, and observations were made as to general cracking behavior of each specimen. Strain gauge data were compared to an analytical model for comparison purposes, which was based upon certain assumptions associated with beam flexural theory.

4. EXPERIMENTAL RESULTS

4.1 GROUP #1 RESPONSE (SPECIMENS 1A, 1B, 2A, AND 2B)

The primary objectives for testing of Group #1 specimens were to:

(1) Reproduce the cracking in laboratory specimens that occurs in RC bent caps currently in service throughout Texas. This includes a combination of flexural and shear cracking during primarily service load stress levels,

(2) Evaluate the performance of the varying side face reinforcement details between previous and current code specifications discussed in Section 2, and

(3) Serve as a benchmark when attempting to improve the performance of bent caps within the later specimen groups.

Appendix A has all graphical data for specimens within Group #1, and Figs. E-1 through E-8 in Appendix E show photographs of Group #1 specimens during testing.

In general, flexural cracking in the bent cap specimens of Group #1 initiated near the column support at an applied load of approximately 100 kips (roughly corresponding to reinforcement stresses of 4 to 7 ksi). These cracks spread, gradually widened, and rapidly propagated down the side faces of the specimens. At approximately 160 kips (roughly corresponding to stresses of 36 ksi), the vertical flexural cracks in the bent span began to incline toward the column support. At higher load levels, inclined flexure-shear cracks initiated, propagated, and widened, while the original flexural cracks stabilized. At higher applied loads, the number of new cracks diminished, and the inclined flexure-shear cracks widened appreciably more than the vertical flexural cracks. This cracking pattern was very similar to observed cracking in the field investigation of in-service TxDOT bent caps (see Figs. 4.1 and 4.2), thus accomplishing one of the objectives in this phase of testing.

As stated in Section 2, the most recent ACI 318 and AASHTO codes specify a nominal amount of side face reinforcement to be concentrated within the web

Figure 4.1. Typical Field Observed Cracking Pattern.

Figure 4.2. Typical Laboratory Observed Cracking Pattern of Group #1 Specimens at P = 160 Kips.

tension region of flexural members with effective depths exceeding 36 in. Specimens 2A and 2B reflect this code provision, while specimens 1A and 1B reflect the previous requirement of an even distribution of the nominal side face reinforcement throughout the web depth. Examination of crack widths and patterns from Group #1 tests (see Fig. 4.3 and Tables 4.1-4.12) shows a slight advantage in favor of the side face reinforcement concentrated within the web tension region. At service load levels (approximately 160 kips, roughly corresponding to a flexural tensile stress of 36 ksi), Table 4.8 shows that the maximum observed side face crack widths (w_{max}) for specimens 1A and 1B were slightly larger than for those occurring on specimens 2A and 2B. Examination of crack widths corresponding to a load of 200 kips from Table 4.9 shows that the maximum observed crack widths were very similar for specimens 1A, 1B, 2A and 2B (about 0.016 in.). This trend continued out to higher loads, beyond service conditions.

At service loads, the skin reinforcement concentrated in the web tension region was more effective in controlling the widths of vertical flexural cracks by intersecting the cracks at near 90 degrees. At higher load levels, when shear deformations were more significant and inclined flexure-shear cracks widened more rapidly than vertical flexure cracks, the skin reinforcement became less effective in crack control. Since observed flexural cracking occurred primarily at service load levels, it is reasonable to conclude that concentration of skin reinforcement within the web tension region is advantageous in flexural crack mitigation at service load levels. However, at higher loads the effect of the skin reinforcement diminished as inclined cracks widened and the horizontal steel became less effective in counteracting the high principal tensile stresses acting perpendicular to the inclined cracks. Tables 4.1 through 4.12 show that the location of maximum crack widths during service loads typically occurred between the equivalent column face and the column center (in Fig. 4.3, 'CF' and 'CL,' respectively). These tables also show that the maximum crack widths at post-serviceability loads typically correspond to inclined flexure-shear cracks occurring within the shear span

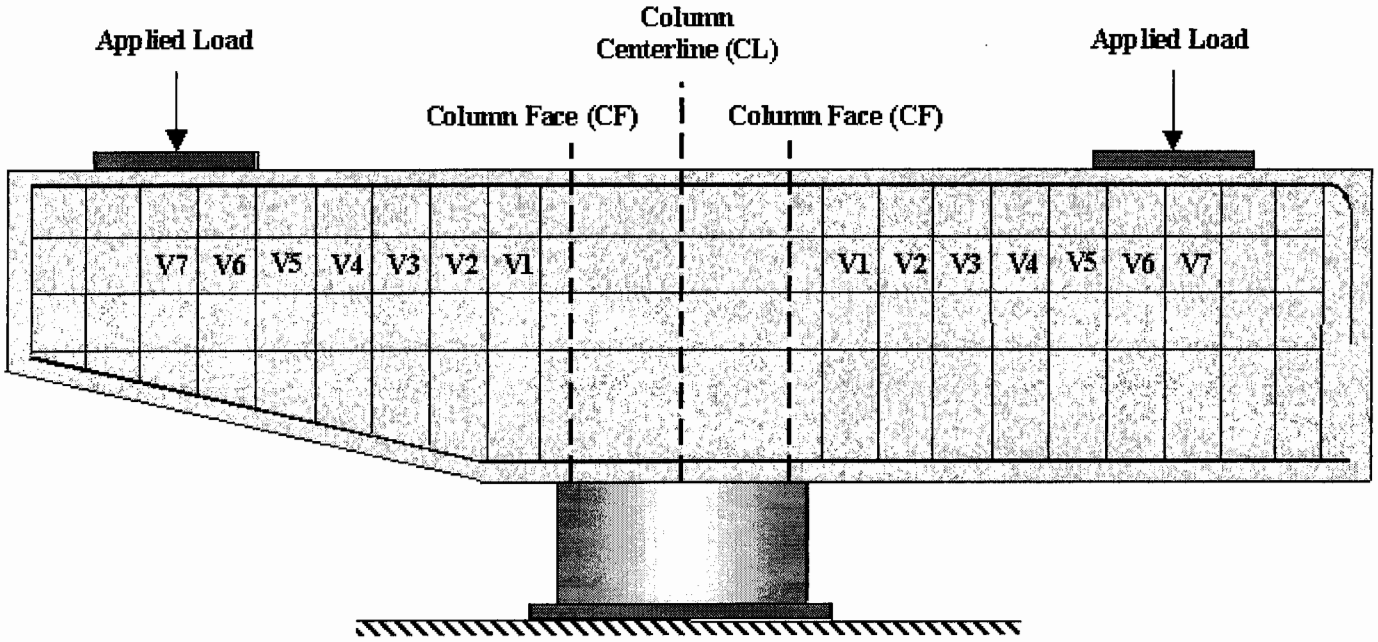

Figure 4.3 Bent Cap Crack Location Key

TABLE 4.1. Maximum Top Face Crack Widths at P = 120 kips

Specimen	Wmax (in.)	Location
1A	0.007	CF
1B	0.009	CF
2A	0.009	CL
2B	0.01	V3/CF
3C	0.009	CF/CL
3D	0.01	CF
4C	0.007	CF
4E	0.003	CL
5D	0.007	CF
5E	0.002	CF
6F	0.003	CF/CL
6G	0.007	CL
7F	0.003	CF
7H	0.005	CL
8G	0.009	CF
8H	0.005	CF

TABLE 4.2. Maximum Top Face Crack Widths at P = 160 kips

Specimen	Wmax (in.)	Location
1A	0.013	V2
1B	0.013	V2
2A	0.013	CF/V4
2B	0.013	V4
3C	0.016	V2/V3
3D	0.016	V4
4C	0.007	CF/V4
4E	0.009	CF/V4
5D	0.009	V2/V3
5E	0.007	CL/V2
6F	0.013	V2
6G	0.013	V3
7F	0.007	V3
7H	0.009	V2
8G	0.016	V4
8H	0.01	CF/V3

TABLE 4.3. Maximum Top Face Crack Widths at P = 200 kips

Specimen	W_{max} (in.)	Location
1A	0.016	V5
1B	0.016	V5
2A	0.016	CF
2B	0.02	V4
3C	0.02	V4
3D	0.025	V4
4C	0.016	V3
4E	0.013	CF
5D	0.016	V4
5E	0.013	V2
6F	0.016	CF/V3
6G	0.02	V2
7F	0.013	CF
7H	0.01	CL/V2
8G	0.016	CF/V4
8H	0.013	V3

TABLE 4.4. Maximum Top Face Crack Widths at P = 240 kips

Specimen	W_{max} (in.)	Location
1A	0.02	V2
1B	0.02	V2
2A	0.02	V4
2B	0.03	V4
3C	0.03	V2/V3
3D	0.03	V3/V4
4C	0.02	V3/V5
4E	0.016	CF
5D	0.02	CF/V4
5E	0.02	V3
6F	0.025	V3
6G	0.02	V2
7F	0.016	CF/V4
7H	0.013	CF/V4
8G	0.025	V3
8H	0.016	V3

TABLE 4.5. Maximum Top Face Crack Widths at P = 280 kips

Specimen	W_{max} (in.)	Location
1A	0.03	V4
1B	0.025	V4
2A	0.025	V4
2B	0.04	V4
3C	0.04	V2/V3
3D	0.05	V4
4C	0.025	V5
4E	0.02	CF/V5
5D	0.02	CF/V4
5E	0.03	V4
6F	0.02	V3
6G	0.02	V3
7F	0.02	V4
7H	0.016	CF/CL/V4
8G	0.03	V3
8H	0.02	V3/V5

TABLE 4.6. Maximum Top Face Crack Widths at P = 320 kips

Specimen	W_{max} (in.)	Location
1A	0.03	V4
1B	0.035	V4
2A	0.03	CF/CL/V4
2B	0.05	V4
3C	0.05	V4
3D	0.05	V4
4C	0.03	V5
4E	0.025	CF/V5
5D	0.025	V4/V2
5E	0.025	V4
6F	0.04	V3
6G	0.025	CL/CF
7F	0.025	V4
7H	0.025	V4
8G	0.04	V3
8H	0.025	CF/V5

TABLE 4.7. Maximum Side Face Crack Widths at P = 120 kips

Specimen	W_{max} (in.)	Location
1A	0.005	CF
1B	0.01	CF
2A	0.009	CL
2B	0.005	V3/CF
3C	0.007	CF/CL
3D	0.003	CF
4C	0.005	CF
4E	0.003	CL
5D	0.003	CF
5E	0.003	CF
6F	0.003	CF/CL
6G	0.005	CL
7F	0.005	CF
7H	0.005	CL
8G	0.005	CF
8H	0.005	CF

TABLE 4.8. Maximum Side Face Crack Widths at P = 160 kips

Specimen	W_{max} (in.)	Location
1A	0.013	V2
1B	0.013	V2
2A	0.009	CF/V4
2B	0.01	V4
3C	0.013	V2/V3
3D	0.013	V4
4C	0.005	CF/V4
4E	0.005	CF/V4
5D	0.007	V2/V3
5E	0.007	CL/V2
6F	0.013	V2
6G	0.01	V3
7F	0.007	V3
7H	0.007	V2
8G	0.013	V4
8H	0.007	CF/V3

TABLE 4.9. Maximum Side Face Crack Widths at P = 200 kips

Specimen	Wmax (in.)	Location
1A	0.016	V5
1B	0.016	V5
2A	0.016	CF
2B	0.016	V4
3C	0.02	V4
3D	0.016	V4
4C	0.016	V3
4E	0.016	CF
5D	0.013	V4
5E	0.013	V2
6F	0.016	CF/V3
6G	0.013	V2
7F	0.013	CF
7H	0.007	CL/V2
8G	0.016	CF/V4
8H	0.013	V3

TABLE 4.10. Maximum Side Face Crack Widths at P = 240 kips

Specimen	Wmax (in.)	Location
1A	0.025	V2
1B	0.035	V2
2A	0.02	V4
2B	0.025	V4
3C	0.03	V2/V3
3D	0.02	V3/V4
4C	0.03	V3/V5
4E	0.016	CF
5D	0.02	CF/V4
5E	0.016	V3
6F	0.02	V3
6G	0.016	V2
7F	0.02	CF/V4
7H	0.013	CF/V4
8G	0.02	V3
8H	0.016	V3

TABLE 4.11. Maximum Side Face Crack Widths at P = 280 kips

Specimen	Wmax (in.)	Location
1A	0.03	V4
1B	0.04	V4
2A	0.03	V4
2B	0.03	V4
3C	0.03	V2/V3
3D	0.03	V4
4C	0.03	V5
4E	0.025	CF/V5
5D	0.02	CF/V4
5E	0.02	V4
6F	0.02	V3
6G	0.016	V3
7F	0.02	V4
7H	0.016	CF/CL/V4
8G	0.02	V3
8H	0.02	V3/V5

TABLE 4.12. Maximum Side Face Crack Widths at P =320 kips

Specimen	Wmax (in.)	Location
1A	0.04	V4
1B	0.04	V4
2A	0.04	CF/CL/V4
2B	0.04	V4
3C	0.04	V4
3D	0.03	V4
4C	0.05	V5
4E	0.03	CF/V5
5D	0.03	V4/V2
5E	0.03	V4
6F	0.025	V3
6G	0.03	CL/CF
7F	0.025	V4
7H	0.02	V4
8G	0.04	V3
8H	0.025	CF/V5

(in Fig. 4.3, 'V1' through 'V7'). Table 4.13 highlights the advantages of the concentration of side face reinforcement (specimens 2A and 2B) within the web tension region at varying load levels (P = 160 kips corresponds to service load levels).

Table 4.13. Maximum Observed Side Face Crack Widths for Group #1 Specimens.

	W_{max}(in.)		
Specimen	P = 160 k	P = 200 k	P = 320 k
1A	0.013	0.016	0.04
1B	0.013	0.016	0.04
2A	**0.009**	**0.016**	**0.04**
2B	**0.01**	**0.016**	**0.04**

The mode of failure for each specimen within Group #1 was shear (diagonal tension) failure. Although the ultimate shear failure was sudden, the failure mechanism did exhibit minimal levels of ductile response, as some yielding of the longitudinal steel took place before the onset of shear distress (see Fig. E-8). However, considering that the bent cap specimens were not subjected to any cyclic loading, which can significantly reduce the shear strength of the concrete, bent caps detailed in this fashion may be susceptible to a brittle-type shear failure. Therefore, researchers recommend additional shear reinforcement to achieve more appropriate ductile response in ultimate bending conditions.

Three of the four specimens within Group #1 (1B, 2A, and 2B) failed along a shear plane extending from the load point inclined toward the column support on the *cantilevered* side of the bent cap (see Appendix E). Specimen 1A failed in a similar manner, except that the failure took place on the side of the bent cap that was detailed as *continuous* (see Fig. E-2). This failure on the *continuous* end, combined with the observed symmetry of cracking on either side of the bent cap, reduces the possibility that slip of the longitudinal reinforcement due to bond failure is a significant factor in the observed cracking in cantilevered bent cap regions. This also supports the observations

from the field investigation, where some cracks occurred at interior, as well as exterior, joint locations.

Results from Group #1 testing can be summarized in the following manner:

- Laboratory specimens successfully reproduced field-observed cracking patterns. Therefore, researchers considered the test specimens to accurately reflect the conditions and behavior of existing bent caps currently in service.

- New code requirements for concentration of side face reinforcement (ACI 318, 1995 and AASHTO, 1998) within the web tension region aided in flexural crack mitigation of the bent caps under service load conditions. However, improvements diminished as loading increased beyond the service load range, as inclined flexure-shear cracks widened.

- Slip of the flexural steel at the cantilevered end of the bent due to bond failure can be discounted as a significant variable contributing to cracking during service conditions. One specimen failed in shear on the continuous side of the bent cap that was detailed with proper hook anchorage. Symmetric crack patterns also appeared on the cantilevered and continuous sides of each specimen.

4.2 GROUP #2 RESPONSE (SPECIMENS 3C, 3D, 4C, 4E, 5D, AND 5E)

The primary variables for specimens within Group #2 were the location of the bent cap critical section for flexural design and the distribution of the flexural tension reinforcement related to the ACI 318 (1995) 'z' expression (Eq. 2.1) and the AASHTO (1998) expression (Eq. 2.3). The two critical section locations were the equivalent column face and the column center.

All Group #1 specimens, along with specimens 3C and 3D from Group #2, were designed based upon moment demand at the column face (A_s = 6.32 in.^{2} for Group #1 specimens, and 6.60 in.^{2} for specimens 3C and 3D). Specimens 4C, 4E, 5D and 5E from

Group #2 represented bent caps that were designed based upon moment demands at the column center, and therefore contained more flexural tension reinforcement (A_s = 8.89 in.^{2} and 8.69 in.^{2}, respectively). For a given applied load, the increased reinforcement effectively reduces the flexural stress levels when compared to bents designed for moments existing at the column face. Since it is known that steel stress has a primarily influence on cracking (Nawy, 1968), designs based upon demands at the column center can significantly reduce cracking.

Figs. E-9 through E-19 show Group #2 specimens during testing. Fig. E-7 shows specimen 2B (A_s = 6.32 in.^{2}) with significant flexural cracking and initiation of flexure-shear cracks at an applied load of 160 kips. Fig. E-15 shows specimen 4E (A_s = 8.89 in.^{2}) at the same applied load, with markedly less cracking. Examination of Tables 4.1 through 4.12 shows that additional flexural steel resulted in smaller maximum crack widths during low applied loads through to post-serviceability load levels. Table 4.2 shows that the maximum top face crack widths at an applied load of 160 kips were in the range of 0.007-0.009 in. for Specimens 4C, 4D, 5D and 5E. For Specimens 1A, 1B, 2A and 2B, as well as specimens 3C and 3D, the range of maximum top face crack widths at the same applied load was 0.013-0.016 in. This trend reoccurred throughout the load history of the specimens. Because those specimens with larger amounts of longitudinal reinforcement exhibited reduced cracking for any given applied load, results verified that flexural tensile stress in the main longitudinal reinforcement plays a major role in limiting cracks in bent caps. Table 4.14 highlights these findings. Specimens shown in bold were designed based upon flexural demands at the column center with more flexural steel.

Table 4.14. Maximum Observed Top Face Crack Widths for Group #1 and #2 Specimens.

Specimen	W_{max}(in.)	
	P = 160 k	P = 320 k
1A	0.013	0.03
1B	0.013	0.035
2A	0.013	0.03
2B	0.013	0.05
3C	0.016	0.05
3D	0.016	0.05
4C	**0.007**	**0.03**
4E	**0.009**	**0.025**
5D	**0.009**	**0.025**
5E	**0.007**	**0.025**

Because bent caps designed to meet TxDOT standards have columns somewhat smaller than the width of the bent cap itself, the column support does not provide complete bearing support for the bent. Therefore, it is possible that the bent cap longitudinal strain is not completely constant through the width of the column support. Designing for stresses that exist at the column center can be justified if strain data shows a substantial strain increase in the tensile reinforcement from the column face to the column center. Comparing the strain readings at the column center location (gauge #12) and the column face (gauge #10), Figs. 4.4 and 4.5 show that higher strain values exist at the column center for most bent cap specimens. This trend was most visible at post-serviceability load levels. Prior to cracking, the strain values at the column face and column center were similar. After cracking, strain at the column center became larger than the corresponding strain at the column face. Fig. 4.5 shows that the strain at the column center was on average approximately 10 percent higher than at the column face. This variation corresponds to about a 6.0 ksi difference in stress from the column face to the column center. Thus, in order to design for the highest flexural stresses in the bent cap, it may be necessary to define the critical section to be within the column width, as opposed to the column face.

It is also possible to investigate the accuracy of the previous ACI 318 (1995) 'z' expression in predicting maximum crack widths in the bent cap specimens. By identifying the flexural tensile stress at the column face corresponding to a maximum observed crack width of 0.013 and 0.016 in, it was possible to measure the accuracy of this expression. For example, the amount and distribution of flexural tension reinforcement along with a 'z' value of 145 k/in. allows for calculation of an expected stress corresponding to the occurrence of a 0.013 in. crack width (see Eq. 2.1). This expected stress value was then compared with the actual stress that was measured at the load level corresponding to the first observed crack of 0.013 in. Figs. 4.6 and 4.7 illustrate the comparison of the expected versus measured flexural steel stress at the column face, which corresponds to the occurrence of these benchmark crack widths. Specimens along the x-axis are arranged in order from lowest to highest expected flexural stress at the first occurrence of a 0.013 and 0.016 in. top face crack, as predicted by Eq. 2.1.

Figs. 4.6 and 4.7 show that the stress levels in the flexural steel were the predominant factor to influence cracking. Factors such as the 'd_c' and 'A' terms in Eq. 2.1, which imply that the arrangement of flexural steel within the tension region can affect cracking, did not seem to play an important role in cracking in these bent cap specimens. The first occurrences of 0.013 and 0.016 in. cracks coincided more consistently with attainment of a certain stress level than with any specific arrangement of flexural steel. Thus, researchers concluded that the previous serviceability 'z' expression as it appeared in ACI 318 (1995), as well as a modified version in AASHTO (1998) (see Eqs. 2.1 and 2.3, respectively) may not be conservative enough for crack width predictions in bent cap structures. Specimens 5D, 5E, 7F, 7H, 3C and 3D represent a more favorable arrangement of flexural steel according to Eq. 2.1 and would be expected to exhibit slightly higher stresses at the first occurrence of the benchmark crack widths. However, these specimens actually showed lower stress levels corresponding to these crack widths (see Figs. 4.6 and 4.7). Although the arrangement of flexural reinforcement is recognized to only marginally influence crack control

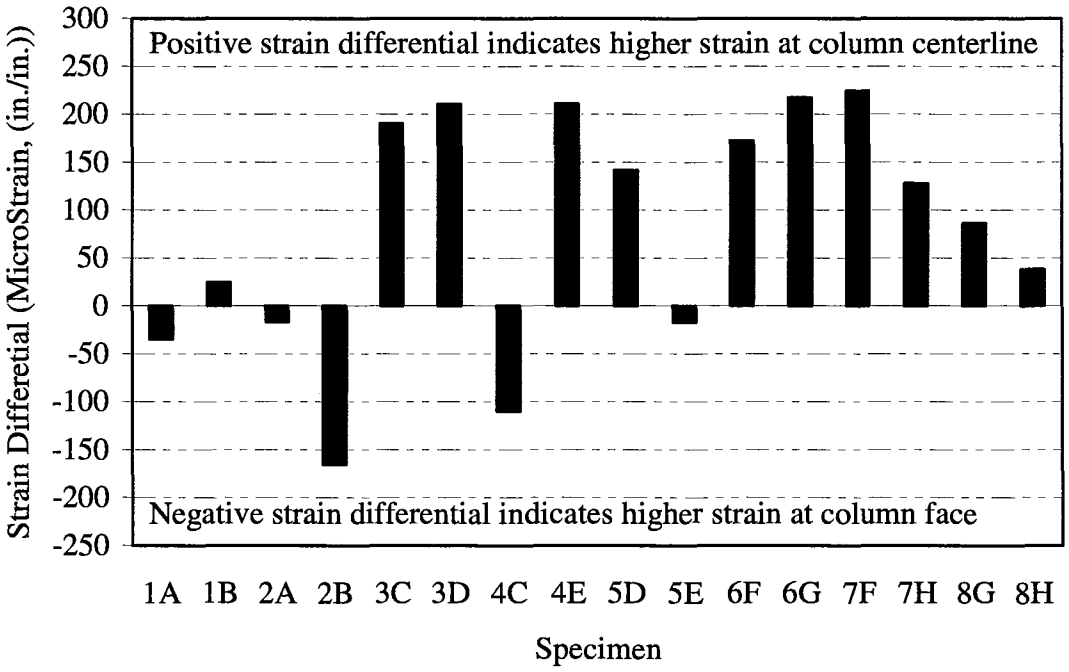

Figure 4.4. Strain Difference at the Column Face and Center at P = 160 kips.

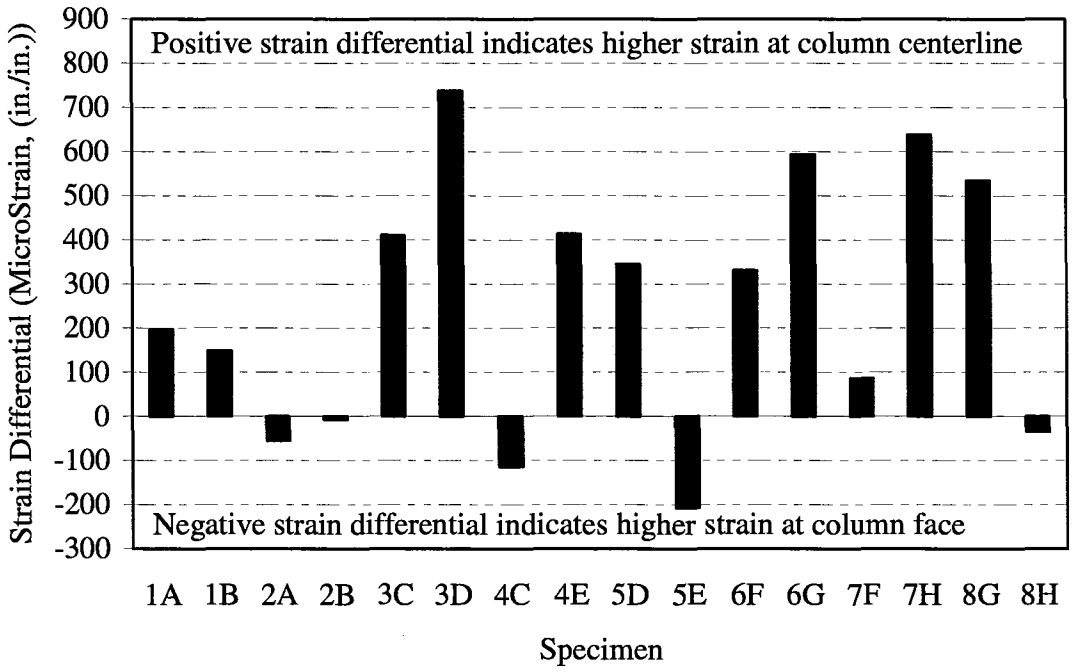

Figure 4.5. Strain Difference at the Column Face and Center at P = 300 kips.

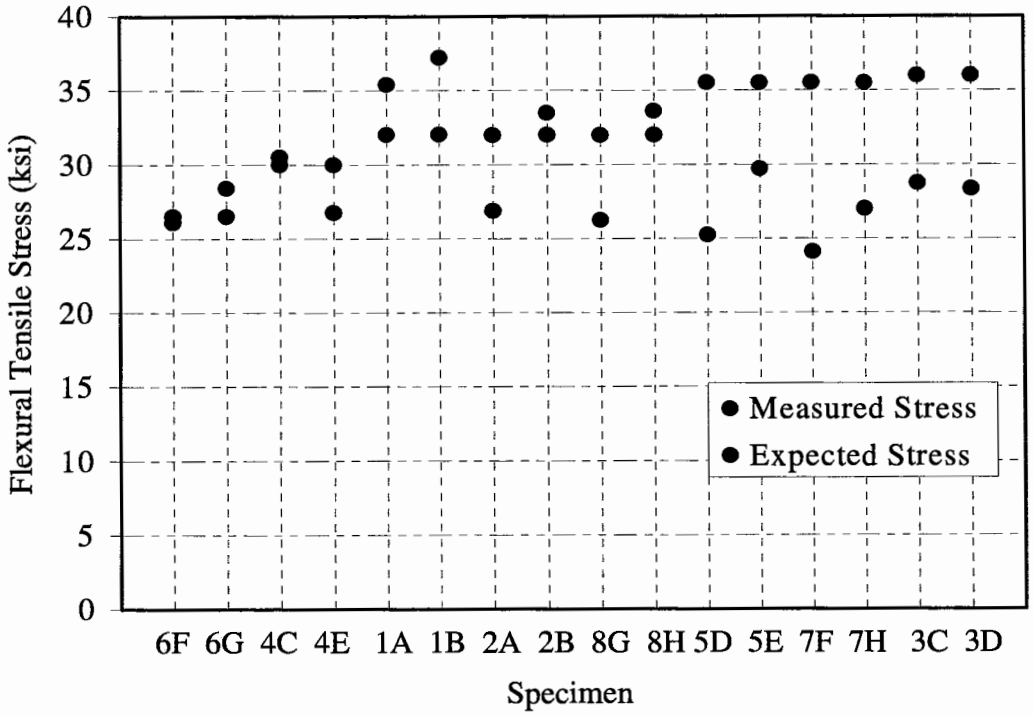

Figure 4.6. Measured vs. Expected Flexural Stress at the First Occurrence of a Top Face Crack Width of 0.013 in.

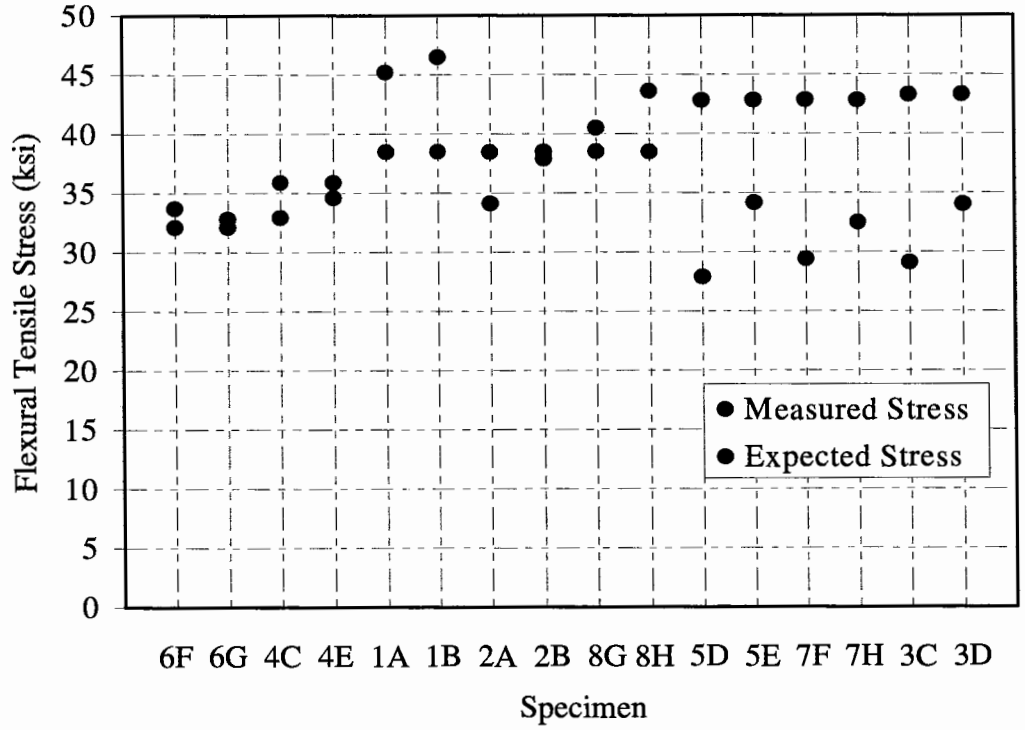

Figure 4.7. Measured vs. Expected Flexural Stress at the First Occurrence of a Top Face Crack Width of 0.016 in.

(d_c and A appear in a cubed-root in Eqs. 2.1 and 2.3), Figs. 4.6 and 4.7 show that these terms were unconservative in predicting cracks in the bent cap specimens. Results indicate that crack mitigation in bent cap structures can be achieved by reducing stress levels in the flexural reinforcement. Fig. 4.6 indicates that limiting stress levels in the flexural steel to approximately 24 ksi was effective in limiting crack widths in these specimens to below 0.013 in. This agrees well with AASHTO ASD (1996) requirements for crack control, where f_s is limited to 24 ksi. Fig. 4.7 indicates that crack widths in the bent cap specimens can be limited to below 0.016 in. if the stress in the flexural steel was below approximately 30 ksi.

Looking at the results from the testing of Group #2 specimens, the following conclusions were drawn:

- After cracking, higher tensile reinforcement strains existed at the column center (gauge # 12) when compared to strain at the column face (gauge # 10). This implies that a more appropriate and conservative location for the critical section for flexural design may be at the column center (the location of highest stress following the onset of initial cracking).

- The ACI 318 (1995) serviceability 'z' expression (Eq. 2.1) for crack control may be somewhat unconservative for bent cap structures. Test results show that the single most important factor in crack control was the stress level (f_s) in the flexural steel. The ACI 318 (1995) 'z' expression seems to overestimate the ability of the arrangement of flexural steel to control cracking. Results show that crack width was virtually independent of the arrangement of flexural steel but was directly related to the flexural stress level in the bent cap specimens.

4.3 GROUP #3 RESPONSE (SPECIMENS 6F, 6G, 7F, 7H, 8G, AND 8H)

Within Group #3 specimens, several variables were examined. Three different arrangements of flexural tension reinforcement were included as an extension of the investigation into the accuracy of the 'z' expression from Groups #1 and #2. One specimen was detailed according to the current ACI 318 (1999) serviceability expression (see Eq. 2.2), which emphasizes a maximum bar spacing for controlling flexural cracking, as discussed in Sections 2.2.1 and 3.4. Group #3 specimens contained overlapping transverse reinforcement for increased shear resistance to control inclined flexure-shear cracking. The basis for inclusion of overlapping stirrups can be justified in a strut-and-tie model, which is discussed further in Section 5. The additional shear strength alleviates the main compression strut through better development of the compression fan regions for load transfer. Figs. E-20 through E-28 show Group #3 specimens and their cracking patterns during testing.

Because the data and discussion from Group #3 specimens relating to the accuracy of the code serviceability expressions were included within Section 4.2, this section does not discuss it further. However, the performance of specimens 6F and 6G reflect a distribution of the flexural tension reinforcement as required by the latest ACI 318 (1999) serviceability expression (Eq. 2.2). Previous serviceability approaches in the form of the 'z' expression would indicate poor detailing of specimens 6F and 6G for crack control, with a small number of larger bars arranged within the flexural region. Conversely, a comparison between the cracking behavior of specimens 6F, 6G, 8G, and 8H (A_s = 6.35 in.^{2} [five #10] and 6.32 in.^{2} [eight #8], respectively) from Group #3 showed no significant differences in general cracking behavior. Tables 4.1 through 4.6 also verify that no significant difference in the maximum top face crack width occurs for specimens 6F, 6G, 8G, and 8H. Results from Group #3 specimens further reinforce what researchers previously concluded; the arrangement of flexural steel within the tension zone did not play a major role in controlling cracks in the bent cap specimens. Because only a limited amount of experimental data were obtained from this investigation, conclusions cannot be drawn as to the applicability or accuracy of the

current ACI 318 (1999) serviceability expression (Eq. 2.2) in controlling cracks for the general case. Table 4.15 highlights these findings.

Table 4.15. Maximum Observed Top Face Crack Widths for Specimens with A_s = 6.35 in.^{2}.

Specimen	'z'	W_{max}(in.)	
		P = 160 k	P = 320 k
1A	164	0.013	0.03
1B	164	0.013	0.035
2A	164	0.013	0.03
2B	164	0.013	0.05
3C	140	0.016	0.05
3D	140	0.016	0.05
6F	**196**	**0.013**	**0.04**
6G	**196**	**0.013**	**0.025**
8G	164	0.016	0.04
8H	164	0.01	0.025

Specimens within Group #3, which were reinforced with overlapping transverse stirrups for enhanced shear resistance, showed a clear reduction in inclined flexure-shear cracking at higher loads when compared to similar specimens without overlapping transverse stirrups. In comparing specimens 5D, 5E, 7F, and 7H (A_s = 8.69 in.^{2}), specimens 7F and 7H (with overlapping stirrups) lacked the steep inclined shear cracking that was evident on specimens 5D and 5E at the same load. Fig. E-24 shows specimen 7F at an applied load of 500 kips, which had not reached failure. The steep inclined flexure-shear cracks acting along the main compression strut had not developed. This indicates more involvement of the compression fans in load transfer as a result of the increased strength provided by the overlapping stirrups. Fig. E-18 shows specimen 5D (with single stirrups) at 470 kips, where diagonal tension failure had occurred along the main compression strut at a lower applied load. Additionally, Tables 4.7 through 4.12 show slightly smaller maximum side face cracks at higher loads for specimens 7F and 7H when compared to specimens 5D and 5E. Fig. E-25 shows specimen 7H at an applied load of 480 kips. The large number of inclined cracks on the right side of the

specimen indicates good participation from the compression fan region at high loads due to the overlapping stirrups.

Specimens 2A, 2B, 8G, and 8H (A_s = 6.32 in.^{2}) can be compared in the same manner. Fig. E-8 shows specimen 2B after diagonal tension failure along the main compression strut at an applied load of 390 kips. Fig. E-27 shows specimen 8G prior to failure at an applied load of 440 kips. Specimen 8G, reinforced with overlapping stirrups, had increased strength as well as good participation from the compression fan region as a result of the increased load-carrying capacity from the overlapping stirrups. At lower service load levels, the overlapping reinforcement had little effect in controlling the vertical flexural cracks. This reinforcement became effective at higher load levels, when inclined flexure-shear cracks widened more rapidly than the vertical flexural cracks, engaging the vertical stirrups and activating the compression fan mechanism. Tables 4.10 through 4.12 also indicate slightly smaller maximum crack widths along the side face of specimens 6F, 6G, 8G, and 8H when compared to specimens 1A, 1B, 2A, 2B, 3C, and 3D (all with similar amounts of flexural reinforcement). Table 4.16 highlights these findings as well. Here, the specimens shown in bold contain enhanced shear resistance with overlapping stirrups. These specimens exhibited smaller maximum crack widths at higher load levels when compared to specimens with single stirrups for transverse reinforcement.

Because the bent cap specimens within Group #3 exhibited favorable behavior as a result of enhanced shear strength, quantification of a desirable amount of shear reinforcement for design purposes is desired. In order to ensure ductile behavior at ultimate load levels, the calculated nominal shear resistance of the bent cap ($\phi V_c + \phi V_s$) should exceed the maximum probable shear demand during flexural failure (M_{pr}/a, where 'a' is the corresponding shear span to the column face, and M_{pr} is the probable flexural capacity of the bent cap using standard beam theory and flexural rebar stresses of $1.25f_y$, which is similar to ACI 318 (1999) seismic code provisions). For design purposes of bent cap members with similar shear span ratios, nominal strength values should be used for calculation of V_c ($2\sqrt{f'_c}bd$) and V_s ($A_v f_y d / s$ where f_y = 60 ksi).

Table 4.17 shows these calculated values for the specimens within the experimental program. The nominal shear strengths (ϕV_n) for Group #1 and #2 specimens are considerably lower than the applied load to cause a maximum probable flexural failure (M_{pr}/a). This indicates that these specimens may be susceptible to a brittle shear failure prior to flexural failure. The overlapping stirrups in Group #3 specimens provides enhanced shear strength, ensuring a desirable ductile response with significant yielding of flexural steel prior to the onset of shear distress. Enhanced shear resistance does not necessitate the specific use of overlapping stirrups. However, this detail may be beneficial in that it provides additional confinement to the relatively large, unreinforced concrete core of the bent cap.

Table 4.16. Maximum Observed Side Face Crack Widths for Specimens with A_s = 6.35 in.^{2}.

Specimen	W_{max}(in.)		
	P = 160 k	P = 240 k	P = 280 k
1A	0.013	0.025	0.03
1B	0.013	0.035	0.04
2A	0.009	0.02	0.03
2B	0.01	0.025	0.03
3C	0.013	0.03	0.03
3D	0.013	0.02	0.03
6F	**0.013**	**0.02**	**0.02**
6G	**0.01**	**0.016**	**0.016**
8G	**0.013**	**0.02**	**0.02**
8H	**0.007**	**0.016**	**0.02**

Table 4.17. Specimen Nominal Strength and Demand.

Specimen	V_c (kips)	V_s (kips)	ϕV_n (kips)	M_{pr} (kip-ft)	M_{pr}/a (kips)
1A	174	194	313	1246	366
1B	169	194	308	1243	366
2A	174	194	313	1246	366
2B	169	194	308	1243	366
3C	172	195	312	1300	382
3D	165	195	306	1295	381
4C	176	193	314	1718	505
4E	197	193	332	1737	511
5D	169	194	309	1680	494
5E	197	194	333	1707	502
6F	163	387	467	1240	365
6G	161	387	466	1239	364
7F	169	388	473	1679	494
7H	172	388	476	1684	495
8G	162	388	468	1239	364
8H	167	388	472	1242	365

From the testing of Group #3 specimens, the following conclusions can be drawn:

- Specimens 6F and 6G, with flexural steel detailed according to the current ACI 318 (1999) serviceability expression limiting bar spacing (Eq. 2.2), showed similar cracking patterns and widths when compared to specimens that had been detailed based upon the previous ACI 318 (1995) 'z' expression emphasizing flexural steel distribution. This reinforces the conclusions drawn from Group #2 specimens that flexural stress was a more influential factor than the arrangement of the flexural tension reinforcement in controlling cracks in these bent cap specimens.

- Specimens reinforced for enhanced shear strength with overlapping transverse stirrups showed favorable cracking behavior when compared to similar specimens without overlapping stirrups. These specimens not only

showed increased shear strength as a result of these overlapping stirrups, but the formation of wider inclined shear cracks along the main compression strut was also delayed.

4.4 GENERAL RESPONSE

Appendices A through C present strain data collected from each specimen arranged in a consistent manner. Figs. A-1 through A-43 show results from Group #1. Group #2 results are shown in Figs. B-1 through B-62, and Group #3 results are shown in Figs. C-1 through C-66. These appendices consist of the following graphical comparisons for each specimen within each of the three groups:

- Actuator force (P) versus reinforcement strain (ε) at the following strain gauge locations:
  - Column face, bent center (gauge #10) and column center, bent center (gauge #12) strain.
  - Column face, bent center (gauge #10) and column face, bent side face (gauge #19) strain.
  - Mid-span, bent center (gauge #7) and mid-span, bent side face (gauge #15) strain.
  - Column center, bent center (gauge #12) and column center, bent side face (gauge #27) strain.
  - Mid-span, through-depth side face strain profile (gauges 15, 16, 17 and 18).
  - Column face, through-depth side face strain profile (gauges 19, 20, 21 and 22).
  - Transverse stirrups strain profile at mid-depth (gauges 23, 24, 25 and 26).
  - Mid-span, through-depth bent center strain (gauges 7, 13, 28 and 30).
  - Mid-span, bent side face (gauge #16) and mid-span bent center (gauge #28) strain, for Groups #1 and #2 only.
  - Column face, through-depth bent center strain (gauges 10, 14, 29 and 31), for Group #3 only.

- Actuator force (P) versus bent cap end displacement.
- Actuator force (P) versus tensile reinforcement strain (ε) for gauges 1 through 12, at 50 kip load increments.

The experimental program successfully reproduced the observed cracking pattern in TxDOT bent caps currently in service. Flexural cracks initiated early in the load history (approximately 100 kips) at the top of the bent cap within the column support. This load corresponds to a tensile stress in the flexural steel in the range of 4 to 7 ksi at the column face location. After initial flexural cracking and redistribution of internal tensile forces, the flexural steel stress increased rapidly to approximately 20 ksi with little increase in applied load. As loading continued, these flexural cracks widened only slightly and extended down the side faces of the bent cap. As load was further increased, flexural cracks initiated at the top of the bent between the load point and the support, and began to propagate down the side face of the bent cap. These cracks then began inclining toward the column support and resembled inclined flexure-shear cracking. At this point, the newly formed flexure-shear cracks tended to widen more quickly with increased load than the initial flexural cracks. Once the total number of cracks had stabilized, few new cracks initiated, and existing cracks widened as load was increased.

Cracks were typically largest along the top face of the bent cap and at the level of the flexural tension reinforcement on the side face. Vertical flexural cracks became smaller in width as they propagated down the side face toward the support. Inclined flexure-shear cracks displayed a more uniform width throughout the member depth due to the combination of high flexural stresses at the concrete tension surface and the high shear stresses at the mid-depth. After initial yielding of the flexural tension reinforcement of Group #1 and #2 specimens, steep inclined shear cracks typically formed near mid-depth of the web, propagating from the load point and to the column support. These shear cracks propagated quickly and ultimate shear failure typically occurred along this plane, as shown in Fig. E-8. As stated previously, Group #3

specimens avoided or at least delayed the onset of these inclined flexure-shear cracks with enhanced shear strength from overlapping transverse stirrups.

Prior to cracking, the strain in the flexural steel was constant along any plane transverse to the bent cap longitudinal axis. However, after initial cracking, the strain profile did not remain constant along the transverse plane. Strain readings at gauge #15 (side face) were consistently higher than readings taken at gauge #7 (center), which lie on the same transverse plane (see Fig. C-14). A similar but somewhat less pronounced trend existed along a transverse plane taken at the column face by comparing strain readings from gauges #10 and #19 (see Fig. C-2). This trend weakened near the column center, where strain along a transverse plane was constant throughout the load history of the specimens. Appendices A through C graphically illustrate these trends. Because the strain in the side face longitudinal reinforcement was consistently higher than the strain in the longitudinal reinforcement at the bent center along a similar transverse plane, researchers concluded that plane sections prior to bending did not remain plane during bending. The allowable working stress for crack control (f_{sa}) specified by Eq. 2.3 assumes a constant stress along a transverse plane. Because higher strains (and thus, higher stresses) existed at the bent cap side face as compared to the bent cap center, cracks measured near the side face of the bent cap may be expected to be slightly larger than originally predicted from these types of code serviceability expressions.

Examination of the strain data for the bent cap reinforcement showed that the through-depth strain profile at high loads was also nonlinear. Strain gauge readings through the depth of the member indicate that the highest longitudinal strain appeared to be located some distance below the extreme concrete fiber in tension, toward mid-depth of the member. Pure bending stress would yield a maximum flexural strain at the extreme tension fiber, while pure shear on a rectangular section would produce highest shear strain at the mid-depth of the section. For slender members dominated by flexural stresses, the combination of high flexural stresses with relatively low shear stresses allows the assumption that shear deformation is minimal. The strain distribution can

then be considered linear, reflecting the flexural strain distribution. For the case of relatively deep members subjected to high shear, shear deformations are not negligible. High shear strains can cause the strain distribution to more closely reflect that of pure shear, with highest strain occurring near the mid-depth. The through-depth strain distribution in the bent cap specimens did not follow a consistent pattern. Some specimens indicated high longitudinal strain near mid-depth of the member, reflecting high shear strains. Other specimens more closely resembled pure flexural behavior with higher longitudinal strains at the level of the flexural steel. This can be seen by examining the graphical results in Appendices A through C, and the strain profiles for gauges 15 through 18, 19 through 22, as well as 7, 28, 30, and 13. Fig. 4.8 also shows sample through-depth strain profiles for four of the specimens within this study. Behavior of these four specimens can be considered as representative of the specimens as a whole.

Comparison of the measured versus analytical strain data at the column face (see Appendix D) shows relatively good correlation between the two. However, significant differences exist between the predicted and measured strains associated with initial cracking. This is evident from the separation of the two trend lines in Figs. D-1 through D-16 at approximately 60 kips. Contributing to this discrepancy may be the initiation of flexural microcracking, which is known to initiate at extremely low flexural stress levels (Nawy, 1968). This is an important observation in the study of cracking in bent cap structures under service loads. Typical assumptions for design simplification regarding strain linearity may not be valid for bent caps, thus overestimating the load corresponding to initial cracking.

These trends can be seen graphically within Appendices A through C, and general results are highlighted below:

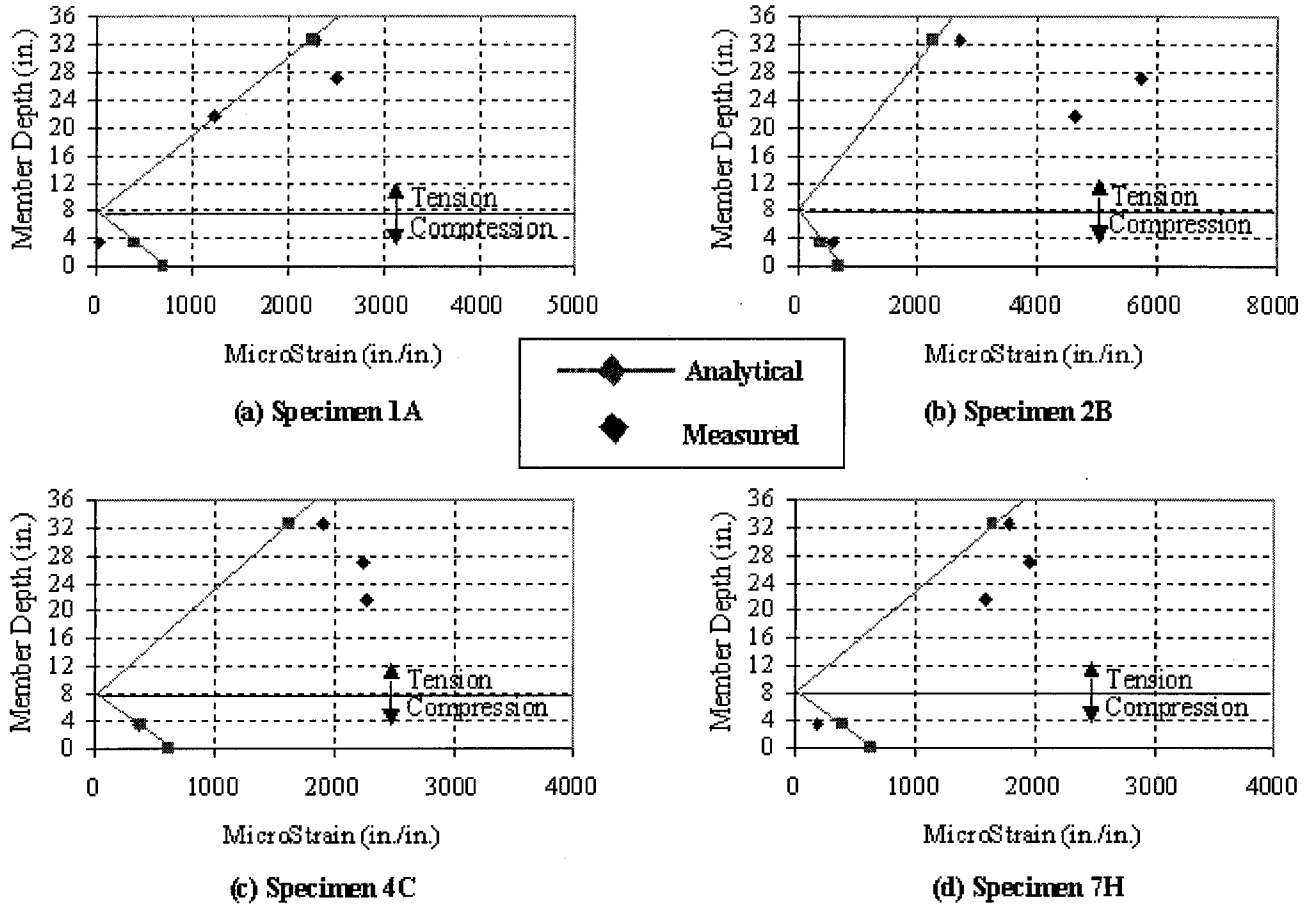

Figure 4.8. Sample Measured vs. Analytical Through-Depth Strain Profiles at P = 300 kips.

- Throughout loading, strain along a plane transverse to the member longitudinal axis was not uniform. Higher strains were typically measured at the side face when compared to strains at the bent cap center, along a common transverse plane. Because the level of flexural stress was the predominate factor influencing cracking, and this flexural stress was typically larger at the side face, larger crack widths along the side face might be expected.

- The through-depth strain profile of the bent caps was also nonlinear. The highest longitudinal strain typically existed at some distance below the extreme concrete fiber in tension, more toward the mid-depth. This indicates some amount of shear deformation, and typical flexural design assumptions based upon linear strain become invalid away from the level of the main longitudinal reinforcement.

- In some cases, the analytical model overestimated the load corresponding to initial cracking. The model was based upon assumptions associated with pure bending and did not consider the possible effects of shear deformation or flexural microcracking at low load levels. However, flexural strength at failure was adequately predicted.

5. STRUT-AND-TIE MODELING

5.1 INTRODUCTION

Two types of regions are generally identified in the design of reinforced concrete (RC) flexural members: main regions and local regions. Main regions are defined by a linear strain distribution through the member depth, resulting in a clearly defined internal tension-compression force couple to counteract applied loads through bending. Conversely, local regions exhibit nonlinear through-depth strain distributions, resulting in an internal tension-compression force couple that cannot be clearly defined. Therefore, an alternative means for design and analysis within these local regions is necessary. The strut-and-tie model is one alternative approach for design within these local regions.

Strut-and-tie modeling involves representing the components of a RC member through an analogous truss model. Specifically, concrete compression forces are represented as strut members, reinforcing steel tensile forces are represented as tie members, and member connecting points are represented as nodes within the analogous truss model. Assuming that the ties develop yield stress, the system can be analyzed as a determinate system of forces, and rational load transfer paths are easily visualized. The RC member can then be dimensioned and detailed to satisfy strength requirements dictated by this analogous plastic truss. The strut-and-tie method, based upon conditions of equilibrium, offers a systematic alternative design approach for RC members when traditional beam theory is not an accurate representation of actual behavior.

5.2 BACKGROUND AND THEORY

As stated in the previous section, designers make certain assumptions about the behavior of RC beam members for the purpose of design and analysis simplicity. One central assumption is that a linear strain distribution exists through the depth of the member (plane sections remain plane). However, it is known that strain distribution through deep members can actually be far from linear in certain situations (Park and Paulay, 1975). For example, regions of high shear, where a significant amount of load is

transferred to the support by a compression strut, can exhibit nonlinear strain distribution due to significant shear deformations. Also, localized disturbances such as concentrated loads and sharp changes in member geometry can cause stress concentrations where the strain distribution can become nonlinear. These regions, referred to previously as local regions, are also known as discontinuous regions or D-regions. Here, a significant portion of the load is transferred through in-plane forces rather than a tension-compression force couple (MacGregor, 1997).

A strut-and-tie model that most accurately represents the actual load carrying mechanism of the member is one that allows the most direct, efficient load transfer path from the point of applied load to the support. This is done through the use of a truss model to represent the load transfer system composed of tension ties, compression struts, and nodal zones. Fig. 5.1 shows a simple truss model.

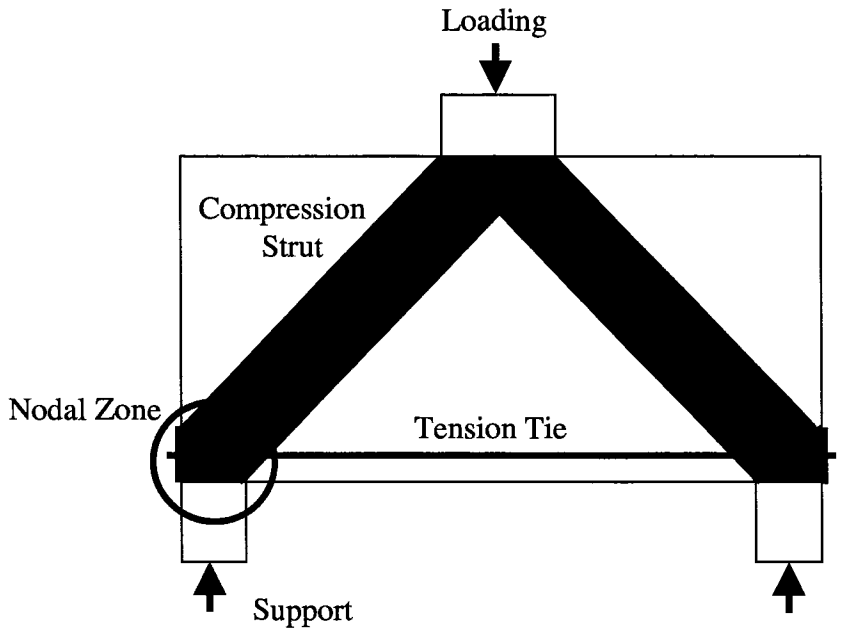

Figure 5.1. General Truss Model Showing Basic Components (after MacGregor, 1997).

Member forces in the tension ties and compression struts are determined through simple statics. Then, the tension reinforcement can be designed and the compression

strength can be analyzed for adequate strength of the strut. Assuming that the longitudinal reinforcement has fully yielded for ultimate strength design, an adequate amount of steel can be specified to carry the full tensile load determined from the truss model. Once the compression forces have been determined from the truss model, the compressive capacity of the concrete can be checked for adequacy. There are several recommended approaches for determining the effective compressive strength of the concrete strut (f_{ce}). MacGregor (1997) suggests the following:

$$f_{ce} = v_1 v_2 f'_c \tag{5.1}$$

along with suggested values for the v_1 and v_2 coefficients. The v_2 coefficient is a function of f'_c, and v_1 is a function of the type of confinement of the strut at a nodal region. The value for v_2 varies from 0.30 to 1.0. Nodal zones of the truss model must also be checked for adequate capacity based upon these same principles. Other sources suggest values for the compressive strength of the concrete struts that are based upon modified compression field theory, where concrete strength is a function of the angle of inclination of a strut referenced from a tension tie axis (AASHTO, 1998). For many members requiring design by the strut-and-tie method, it is important that adequate anchorage be provided for the tension ties. Fig. 5.1 shows a tied-arch mechanism where the tensile force in the tie is constant along its length. Because high tensile stresses exist near the support (in contrast to normal beam theory where the stresses diminish toward the support), mechanical anchorage in the form of anchorage plates or hooks must be provided to avoid slip of the reinforcement resulting from inadequate bond strength.

The validity of any strut-and-tie model depends primarily upon whether it accurately reflects the actual behavior of a member. Therefore, this approach can be applied to virtually any structural system provided that the analogous truss is correctly constructed. Common applications of the strut-and-tie approach include the design of dapped end beams, corbels, joint regions, beams with discontinuities such as holes, deep beams, and transfer girders. These types of members are typically dominated by D-regions, where conventional beam theory does not apply. The following section

discusses applications of the strut-and-tie model for the design of bent cap structures, which can be considered to exhibit deep beam characteristics. It also discusses advantages and disadvantages of the strut-and-tie method.

5.3 BENT CAP APPLICATION

According to ACI 318 (1999), flexural members are classified as being deep based upon their clear span-to-depth ratio. Alternatively, AASHTO (1998) classifies flexural members as being deep based upon the distance from an applied concentrated load to the support. The AASHTO approach has a more direct application to bent caps, which are typically loaded by a series of concentrated loads from bearing of the longitudinal bridge deck girders. From typical shear span-to-depth ratios associated with bent caps in the TxDOT bridge inventory, it can be expected that nonlinear strain distributions exist near the column support in the negative moment regions of these structures. Thus, slender beam theory may not be an accurate representation of actual behavior and may lead to inadequate design. Strut-and-tie modeling may, therefore, be a valid design alternative for bent cap structures.

Applying the principles from Section 5.2 to a typical bent cap specimen used in the experimental program described previously, a simple truss model (shown in Fig. 5.2) can be constructed. Including transverse reinforcement in the truss model to more accurately reflect the detailing in a typical bent cap can change the tied arch mechanism shown in Fig. 5.2 to the truss models shown in Figs. 5.3 and 5.4, which consist of main compression struts as well as compression fan regions. Fig. 5.3 shows a strut-and-tie mechanism where the majority of the applied load is being transmitted through the main compression strut into the support, while Fig. 5.4 shows a strut-and-tie mechanism where the applied load is distributed more evenly through the main compression strut and the compression fan regions.

Once the member has cracked, the transverse reinforcement intersecting these cracks is engaged and is capable of carrying tensile load while resisting further opening of these cracks. This will alleviate some of the load transfer burden from the main

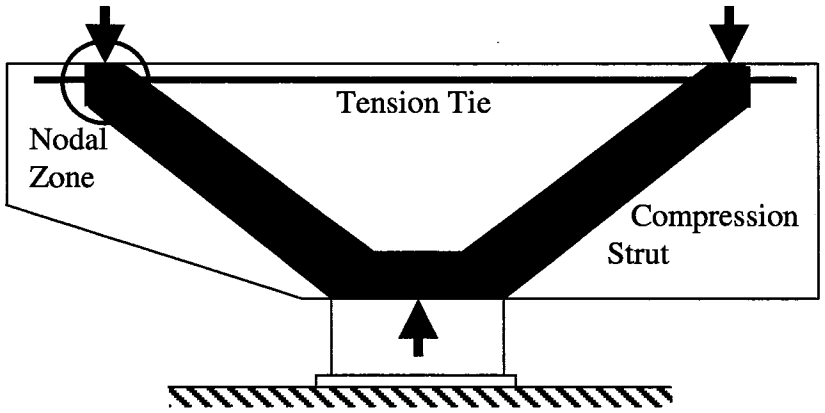

Figure 5.2. Bent Cap Structure and Tied-Arch Truss Model.

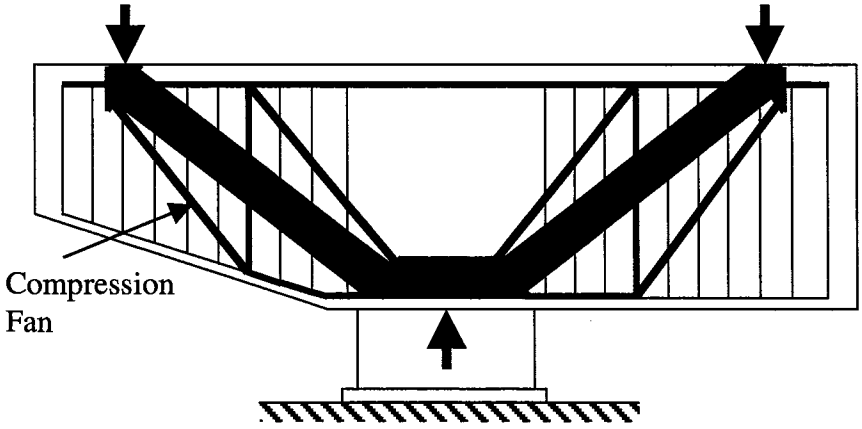

Figure 5.3. Bent Cap Truss Model with Few Active Stirrups.

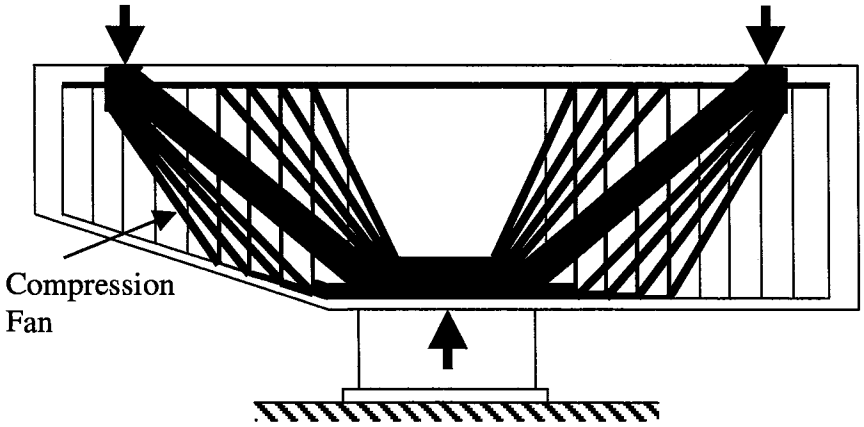

Figure 5.4. Bent Cap Truss Model with Many Active Stirrups.

compression strut. An assumption in this modeling is that the transverse reinforcement has fully yielded at ultimate conditions so that the vertical tensile forces in the ties are known and the system becomes determinate. Compression fans resulting from the inclusion of transverse reinforcement aid in the ductility of the overall system because they increase the number of paths capable of carrying load (see Fig. 5.4). They do not, however, contribute proportionally to the shear capacity of the system because cracks within these D-regions often intersect this vertical reinforcement at angles much steeper than 45 degrees and often intersect very few stirrups. MacGregor (1997) recommends that a compromise between ductility and cost-effectiveness be made so that approximately 25-35 percent of the shear is transferred through the stirrups, or compression fans.

Referring to the left side of the bent cap shown in Fig. 5.4, the compression and tension members within the truss model can be solved by equilibrium, as shown in Fig. 5.5. This process is iterative due to the fact that the location of the node within the support region can vary somewhat depending upon the width of the support. While varying the location of this node, tensile and compression forces also change. Thus, the truss must be reevaluated in order to sustain equilibrium within the truss model. After the actual geometry of the node has been estimated by convergence, it is possible to determine the validity of the original assumption for its location. For a predetermined applied load, the location of the support node must be located in order to satisfy equilibrium of the truss model.

The first step of the process is to define an initial location for the node within the support region, shown as node Q in Fig. 5.5 (which represents the left side of the truss in Figs. 5.3 and 5.4). For purposes of this analysis, the location of node Q is assumed to be at a distance 3 in. away from the face of the circular column and 5.8 in. above the bent cap compression face. Thus, the internal moment arm shown in Fig. 5.5 (jd) is found to be 26.45 in. It is also necessary to determine which vertical stirrups will be active in the truss model. (For Table 5.1, the member forces are shown for the tied arch mechanism with no active stirrups in Fig. 5.2 for comparison purposes). Stirrups

denoted as A-I, B-J, and H-P were ignored in the truss model since their angle of inclination is greater than 65 degrees, as recommended by MacGregor (1997). Stirrups C-K, F-N, and O-G are also ignored since the compression struts spanning between these stirrups interfere with the main compression strut (A-Q). Stirrups D-L and E-M are active tension members within the truss and are shown in bold in Fig. 5.5. Assuming these stirrups have yielded at ultimate load levels, the truss member forces and a corresponding applied load can be determined. For an applied load of 220 kips, these member forces are shown in Table 5.2.

For the specimen shown in Fig. 5.5 with single transverse #5 stirrups at 6.25 in. longitudinal spacing, the main compression strut (A-Q) carries a vertical shear force of 145 kips, which is about 66 percent of the total shear force of 220 kips. To alleviate this main compression strut, a similar specimen reinforced with overlapping #5 transverse stirrups at the same 6.25 in. spacing under the same externally applied load of 220 kips is considered. The corresponding truss member forces are shown in Table 5.3.

Comparison of observations in Tables 5.1, 5.2, and 5.3 reveals that several advantages exist when increasing the amount of transverse reinforcement through the use of overlapping stirrups. Fig. 5.4 shows that the bent cap reinforced with overlapping #5 stirrups allows more of the total applied load to be carried by the compression fans, thus alleviating some of the demands on the main compression strut. Here, the main compression strut is required to carry about 32 percent of the total shear force of 220 kips. Alleviating the main compression strut may be effective in reducing inclined cracks, which initiate along this strut due to high principle tensile stresses that act perpendicular to this strut. While MacGregor (1997) suggests that the compression fan carry approximately 25-35 percent of the total vertical shear, this simple comparison illustrates the ability of the strut-and-tie model in expressing the load transfer mechanism and how it might be adjusted to improve performance.

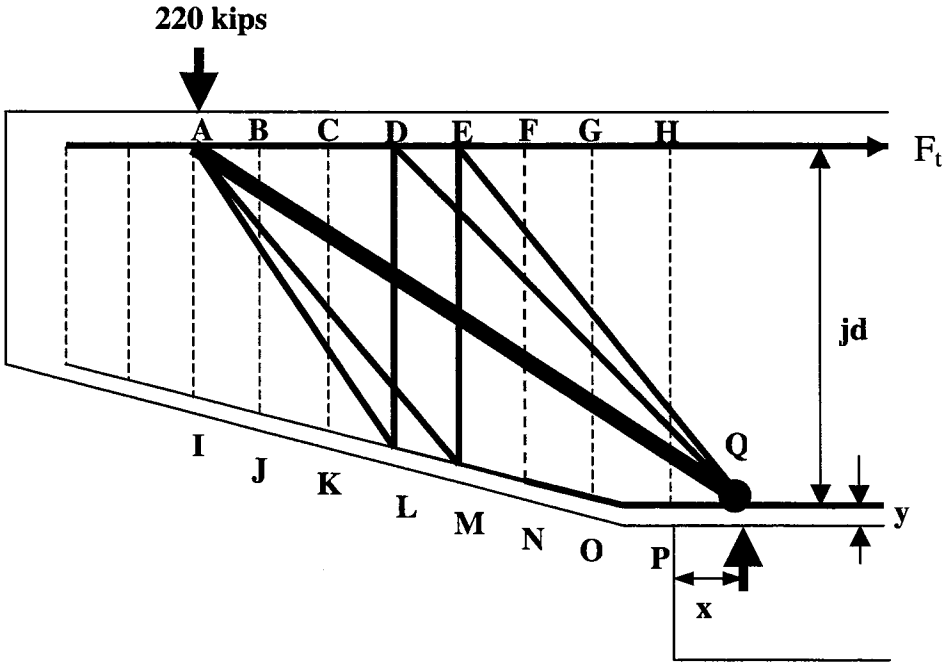

Figure 5.5. Truss Model: Cantilevered End of a Typical Bent Cap Specimen.

Table 5.1. Truss #1 Member Forces (see Fig. 5.2).

Strut	Vertical Force (kips)	Horizontal Force (kips)	Member Force (kips)
A-L	0	0	0
A-M	0	0	0
A-Q	220	388	447
Q-D	0	0	0
Q-E	0	0	0

Transverse Stirrups = #5 @ 6.25 in. spacing

Flexural Tensile Force (F_t) = 388 kips

Table 5.2. Truss #2 Member Forces (see Fig. 5.5).

Strut	Vertical Force (kips)	Horizontal Force (kips)	Member Force (kips)
A-L	37.2	26.6	45.8
A-M	37.2	33.7	50.2
A-Q	145	253	292
Q-D	37.2	39.8	54.4
Q-E	37.2	29.4	47.4

Transverse Stirrups = #5 overlapping @ 6.25 in. spacing
Flexural Tensile Force (F_t) = 383 kips

Table 5.3. Truss #3 Member Forces (see Fig. 5.5).

Strut	Vertical Force (kips)	Horizontal Force (kips)	Member Force (kips)
A-L	74.4	53.2	91.5
A-M	74.4	67.5	100.5
A-Q	71	124	143
Q-D	74.4	79.5	109
Q-E	74.4	58.8	95

Transverse Stirrups = #5 overlapping @ 6.25 in. spacing
Flexural Tensile Force (F_t) = 383 kips

Once these member forces have been found, it is possible to determine the widths associated with each truss element. For example, the main compression strut (A-Q) from Table 5.2 carries a load of 292 kips. From Eq. 5.1, using f'_c of 5500 psi and recommendations for v_1 (.80) and v_2 (.75) (MacGregor, 1997), the effective concrete strength (f_{ce}) for this strut is 3300 psi. For a member width of 33 in., this main strut width would be about 2.75 in. where it joins with the nodal zones. Dimensions for all

compressive members can be determined in this manner, and a general node geometry can be identified.

TxDOT bent cap structures with excessive cracking at the column-to-bent cap joint locations typically exhibit largest cracks along a similar main compression strut shear plane (see Figs. 2.1 and 2.2). Within the experimental program, Group #3 specimens have been reinforced using overlapping transverse reinforcement and have exhibited reduced diagonal shear cracking when compared to bent caps without overlapping reinforcement. The strut-and-tie model is an effective tool for visualizing the load paths through a bent cap structure. At the negative moment regions, where a large compression strut typically exists, it may be beneficial to provide enhanced shear reinforcement using overlapping transverse reinforcement for mitigating inclined shear cracking by reducing compressive forces within the main strut.

5.4 SHORTCOMINGS OF THE STRUT-AND-TIE MODEL

The strut-and-tie method offers several advantages for the design of a wide variety of RC structures that may not be suited for conventional beam theory. An understanding of the load transfer paths from the applied loads through the member to the support is inherent in the strut-and-tie approach and is necessary for a complete understanding of the mechanics of the structural system. Thus, the strut-and-tie method is advantageous in that it requires these load transfer paths to be identified. However, there are some shortcomings associated with this approach as well. There is a great amount of difficulty associated with determining the geometry of the nodal zones for compression fan regions. Initially, for purposes of solving for the truss member forces, researchers assumed that these members act through one common point. Therefore, nodes initially consist of a group of truss elements (tension ties and compression struts) joined at one point. Once widths are determined for the compression struts based upon the effective concrete compressive strength (see Eq. 5.1), the points at which these struts intersect each other near the node defines the geometry of that node, as shown in Fig. 5.6(a). This newly defined node geometry, however, does not represent a completely hydrostatic node with measurable dimensions. Some adjustments must therefore be

made to the compression struts to arrive upon a completely hydrostatic node, as shown in Fig. 5.6(b). Once these adjustments are made, the angle of each individual strut has changed, and therefore the internal forces have changed as well. However, equilibrium must still be preserved. Note that in Fig. 5.6(b) the truss elements no longer intersect at one point; their angles have been changed in order to produce a completely hydrostatic node element.

For some applications of the strut-and-tie model, it may not be of much concern to the engineer to have an exact representation of the nodal geometry, and the truss model may suffice. For applications such as bent caps, however, where the support region is fairly wide, it may be of importance to have a better representation of the nodal geometry in order to determine if the originally assumed location for the support node was accurate. If the location of this node is not assumed accurately, and the face of the node does not correspond to the face of the support, the truss does not represent an accurate model for the RC system. However, a direct approach for determining the exact geometry of a hydrostatic nodal element is unknown to the authors at this time.

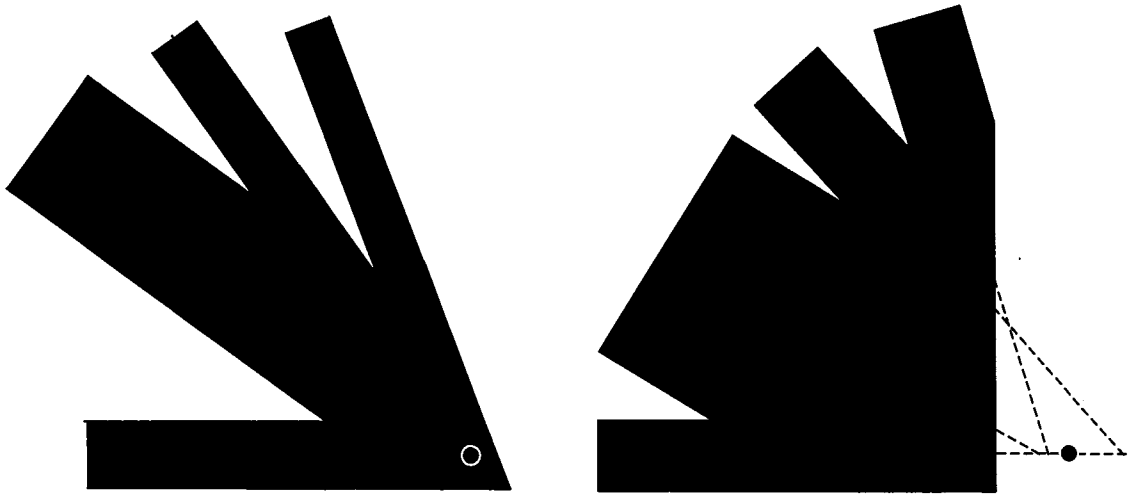

(a) Truss Model Nodal Region

(b) Adjusted Hydrostatic Nodal Region

Figure 5.6. Comparison of Nodal Regions in a General Strut-and-Tie Model.

Also, the strut-and-tie approach is somewhat tedious because in addition to questions regarding node dimensioning, the forces in every strut and tie must be calculated and proportioned rather than treating the beam as a whole and simplifying design (Hsu, 1993).

Other concerns in applying the strut-and-tie method also exist. It is necessary to assume that some amount of transverse stirrup reinforcement is effective in the truss model, while some reinforcement remains inactive, depending on the angle of inclination of the developing strut. It is also necessary to assume that the active transverse stirrups have fully yielded so that the vertical tensile forces are known and the truss remains determinate. Test data from the experimental program show that only a few of the transverse stirrups are active in load transfer (as was assumed in Fig. 5.5). However, there is still some uncertainty associated with these assumptions and their ability to accurately represent the actual behavior of the RC member for all situations. Although the strut-and-tie model may be a valid approach to the design of certain members where assumptions associated with conventional beam theory do not apply, there are still a fair number of assumptions and simplifications required for this method. Also, serviceability aspects of design must still be considered separate from the strut-and-tie model, which is concerned solely with performance at the ultimate limit state.

6. PRELIMINARY NON-LINEAR FEM ANALYSIS

6.1 INTRODUCTION

In this section, a non-linear finite element model is developed to correlate with the measured response from the experimental program. The section examines three factors in a parametric study to represent the experimental data:

(1) tensile strength of concrete,

(2) shear retention factor across cracks, and

(3) concrete confinement effect.

The validity of the model is examined by comparing the analytical prediction to the experimental data. The goal of this section is to develop a reliable non-linear finite element model for RC bent caps that can be used in later sensitivity analyses to evaluate effects of stirrups and reinforcement details, bent geometry, and various shear span-to-depth ratios on the cracking behavior.

6.2 SCOPE OF STUDY AND METHODOLOGY

In general, there are two major sources of non-linearity in finite element analysis, namely geometric non-linearity and material non-linearity. The effect of geometric non-linearity appears to be insignificant in the present study as the deflection of RC bent caps is relatively small, even at failure. Therefore, the project considered only the material non-linearity in two constituents, concrete brick elements and reinforcing steel bar elements. The non-linear stress-strain relationship of concrete, incorporating the effect of confinement from stirrups proposed by Mander et al. (1988), is used. The constitutive relationship for the steel reinforcement is assumed to take the bi-linear form, with approximately 3 percent strain hardening. ANSYS 5.5 (SAS IP, Inc., 1998) is used to conduct the non-linear finite element analysis via the supercomputing facility at Texas A&M University.

6.2.1 Concrete Constitutive Model

This section briefly discusses the concrete constitutive models, as applied for finite element analysis in the open literature. In general, there are two physical characteristics contributing to the non-linear response of concrete. Non-concurrent crushing or yielding of the aggregates at the microscopic level can cause the non-linearity in compression, while the cracking of concrete can cause non-linearity in tension. Advantages and disadvantages of these models are discussed below, and the influence of concrete confinement on the stress-strain relationship is also emphasized. Finally, the details of the models used in this research project are presented.

6.2.1.1 Non-Linearity in Compression (Crushing of Micro-Mechanical Components)

Concrete is a composite material formed by cement paste, sand, a large number of aggregates with different sizes and characteristic strengths, and special additives for strength, performance, and workability. Yielding or crushing of aggregates does not occur simultaneously at the microscopic level. This non-concurrent yielding of material leads to the non-linear macroscopic stress-strain behavior. Numerous forms of constitutive models for concrete are available in the literature. Chen and Saleeb (1982) summarized the comprehensive treatment of the failure criterion for concrete material based on continuum plasticity theory. William and Warnke's five-parameter failure model (1974) is also discussed. The relative merit of the five-parameter model lies in the facts that the elliptic yield surface proposed by William and Warnke (1974) does not violate the rules of plasticity theory and that both uniaxial strength and biaxial strength of concrete can be degenerated from their general three-dimensional failure surface. Chen et al. (1982) also discussed the general approach for formulating a non-linear elastoplastic stress-strain relationship for concrete.

ANSYS 5.5 (SAS IP, Inc, 1998) employs the five-parameter model proposed by William and Warnke (1974). The five parameters that define the three-dimensional elliptic failure surface are: (1) ultimate uniaxial tensile strength (f_t), (2) ultimate uniaxial compressive strength (f'_c), (3) ultimate biaxial compressive strength (f_{cb}), (4) ultimate compressive strength for a state of biaxial compression superposed on hydrostatic stress

(f_1), and (5) ultimate compressive strength for a state of uniaxial compression superposed on hydrostatic stress (f_2).

In this research project, the only parameter tested in the laboratory was the ultimate uniaxial compressive strength of concrete (f'_c). Approximations for the remaining four parameters were made as follows:

$$f_t = 7.5\sqrt{f'_c} \qquad per \quad ACI\ 318\ (1999)\ (psi) \tag{6.1}$$

Preliminary analysis runs showed that the tensile strength recommended by ACI 318 (1999) was too high when compared with the experimental results. This may be attributed to the coupling effect with shear deformations because the bent caps have a small shear span-to-depth ratio. Therefore, the tensile strength used in the subsequent modeling was 70 percent of the ACI 318 value.

According to William and Warnke (1974), the last three parameters can be approximated by the following:

$$f_{cb} = 1.2 f'_c \ (psi) \tag{6.2}$$

$$f_1 = 1.45 f'_c \ (psi) \tag{6.3}$$

$$f_2 = 1.2 f'_c \ (psi) \tag{6.4}$$

6.2.1.2 Non-Linearity in Tension (Cracking)

For concrete structures, cracking occurs when the stress at a point exceeds the tensile strength. The influence of cracks on the response of RC structures is extremely complicated because of their randomness and their subtle effect on reducing the transfer of stress across the cracks. Ideally, the topology of a finite element mesh for the structure should change when cracks occur. Ngo and Scordelis (1967) first applied the concept of discrete crack models in two-dimensional finite element analysis of RC beams. Basically, redefinition of nodes is required when the tensile stress demand exceeds the cracking strength of concrete in tension. Ngo (1975) reported the inconvenience of applying this method to general problems because the computation

cost is too high. In contrast to the discrete crack model, Rashid (1968) proposed the smeared or average crack model. In this model, the redefinition of nodes and elements is replaced by reducing the stiffness matrix of the cracked element. The original model by Rashid (1968) completely ignored the transfer of stress across the crack, which introduced premature numerical instability (Cedolin et al., 1982). Subsequently, Hand et al. (1975) suggested the use of shear retention factors to capture the partial shear transfer across cracks. Improvements over Rashid's model were reported (Cedolin et al., 1982).

This investigation employed the smeared crack model proposed by Hand et al. (1975), as incorporated in ANSYS 5.5 (SAS IP, Inc, 1998), for concrete. The shear retention factor for open cracks was obtained by simulation where this factor was varied between 0.05 and 0.30 to best compare with the experimental results. A complete shear transfer was adopted along closed cracks.

6.2.1.3 Effect of Confinement on the Concrete Stress-Strain Relationship

Confinement has a significant influence on the compressive strength and ductility of RC members. Conceptually, stirrups or hoops provide confining pressure to concrete. Because the failure surface of concrete is enlarged by an increase in confining pressure, significant strength gain can be achieved for confined concrete. Mander et al. (1988) proposed a constitutive model for confined concrete with various stirrup configurations. The model is also applied in the present investigation and is explained subsequently.

An explicit uniaxial compressive stress-strain relationship for confined concrete, as proposed by Mander et al. (1988), was employed. Because ANSYS does not allow direct definition of the stress and strain relationship, a multi-linear piecewise stress-strain curve for concrete was adopted at 20 equal intervals. The stress at each strain interval was calculated according to Mander et al. (1988):

$$f_c = \frac{f'_{cc}\, xr}{r - 1 + x^r} \tag{6.5}$$

where, f'_{cc} = Peak compressive strength of confined concrete = $K f'_{c0}$ (psi)

$$\varepsilon_{cc} = \varepsilon_{co}\left(1 + 5\left(\frac{f'_{cc}}{f'_{co}} - 1\right)\right)$$

f'_{co} = Uniaxial unconfined compressive strength of concrete (defined as f_c' previously) (psi)

K = Confinement factor, which is a function of the hoop reinforcement configuration and is obtained from alignment chart (psi)

x = Ratio between the current compressive strain (ε_c) and the strain corresponding to the peak confined strength (ε_{cc}) = $\frac{\varepsilon_c}{\varepsilon_{cc}}$

E_c = Tangent modulus of elasticity of concrete = $57000\sqrt{f'_{co}}$ (psi)

$$r = \frac{E_c}{E_c - E_{sec}}$$

$$E_{sec} = \frac{f'_{cc}}{\varepsilon_{cc}} \text{ (psi)}$$

ε_{co} = Strain corresponding to the unconfined compressive strength

Fig. 6.1 shows the difference between stress-strain curves for unconfined concrete and confined concrete, where the plotted curves are: (1) unconfined concrete with f'_c= 5.82 ksi, (2) confined concrete with #5 bars, single stirrups, and (3) confined concrete with #5 bars, double stirrups.

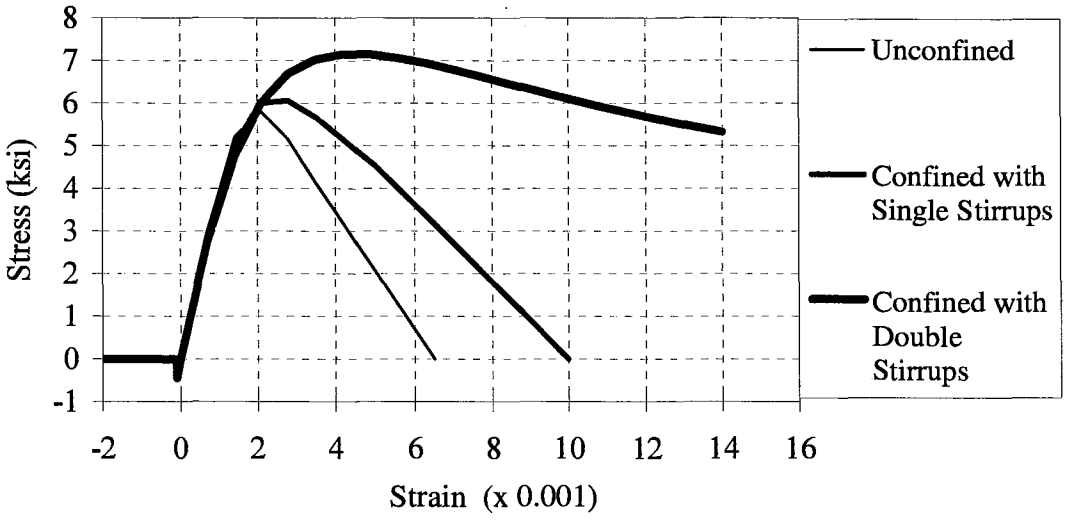

Figure 6.1 Idealized Stress-Strain Relationship of Concrete.

6.2.2 Steel Constitutive Model

A bilinear stress-strain relationship for steel was assumed with a yield stress of 65 ksi, based on mill reports for the reinforcement used in the bent cap specimens. The initial modulus of elasticity for steel was taken to be 29,000 ksi and 3 percent strain hardening was assumed. Fig. 6.2 shows the idealized stress-strain curve of the steel reinforcement.

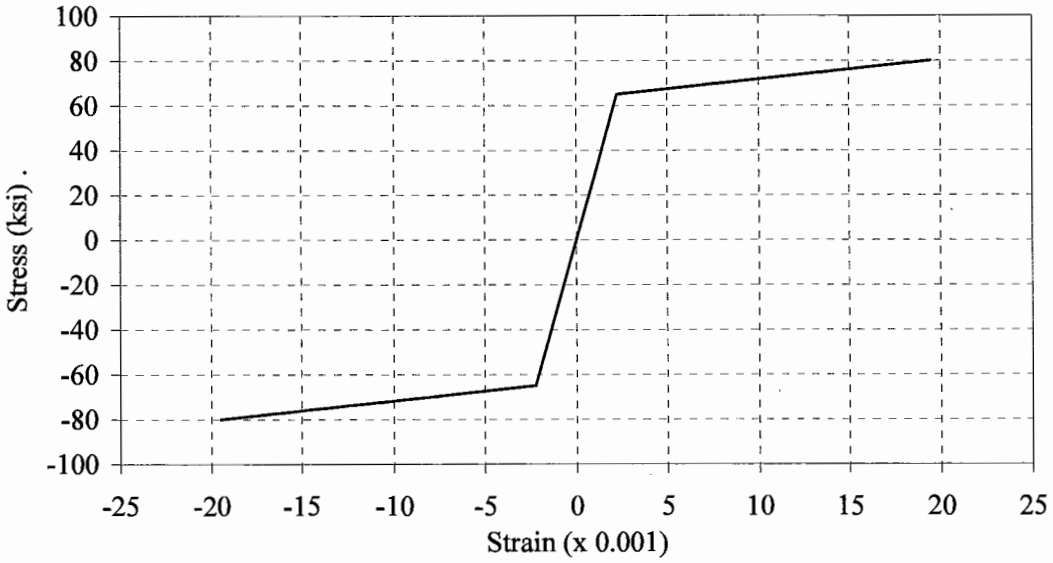

FIG 6.2 Idealized Stress-Strain Relationship of Reinforcing Steel

6.2.3 Incremental Analysis

Several methods are available for solving non-linear problems numerically. Hinton and Owen (1980) summarized the general methods for performing the analysis of structures by finite elements in a plasticity context. Pavlovic et al. (1995) made a comparison of the performance of three iterative techniques applied to non-linear analysis of concrete structures: (1) Tangent Stiffness or Full Newton-Raphson Method, (2) Initial Stiffness Method, and (3) Modified Newton- Raphson Method.

The Full Newton-Raphson Method leads to better convergence rates compared to the other methods (Kotsovos et al., 1995). But it may give rise to the singularity of tangent stiffness of the structure, and a large number of computational steps are required because the stiffness matrix has to be recalculated at all iterations. It may also violate

the symmetry of the stiffness matrix according to Kotsovos et al. (1995). Application of the Initial Stiffness Method should imply unconditional stability of stiffness matrix with slower convergence rates (Hinton and Owen, 1980). However, the initial stiffness in some applications can cause divergence, while the more rapid tangent stiffness method is more successful (Kotsovos et al., 1995). For analysis of concrete structures with cracking, the Modified Newton-Raphson Method becomes more suitable. For this method, the stiffness matrix of the structures is updated when new cracks form.

Several options are available in the current version of ANSYS. This study adopted the Modified Newton-Raphson scheme. The program automatically determines the regularity for updating the stiffness by evaluating the convergence norm of the solutions.

6.2.4 Test Model

As mentioned in the previous section, the tensile strength of concrete, the shear retention coefficient for open cracks, and the effect of concrete confinement were varied in a parametric study to best correlate with experimental findings. Researchers found that a combination of 30 percent reduction in modulus of rupture from that presented in ACI 318 (1999) and a shear retention factor of 0.15 yields adequate comparison with the experimentally measured strain gauge data. The effect of confinement on the load transfer mechanism was examined by comparing the results from two finite element models with two different shear reinforcement details: (1) specimen 2B with eight #8 bars with single stirrups, and (2) specimen 8H with eight #8 bars with double stirrups.

Element Definition

The continuum concrete beam is divided into a finite element mesh of hexahedral three-dimensional brick elements. Steel reinforcement is idealized as three-dimensional bar elements with only axial deformations. By taking advantage of symmetry, only half of the beam is modeled in the finite element mesh. Fig. 6.3 shows the isometric view of the finite element mesh of a specimen with eight #8 bars.

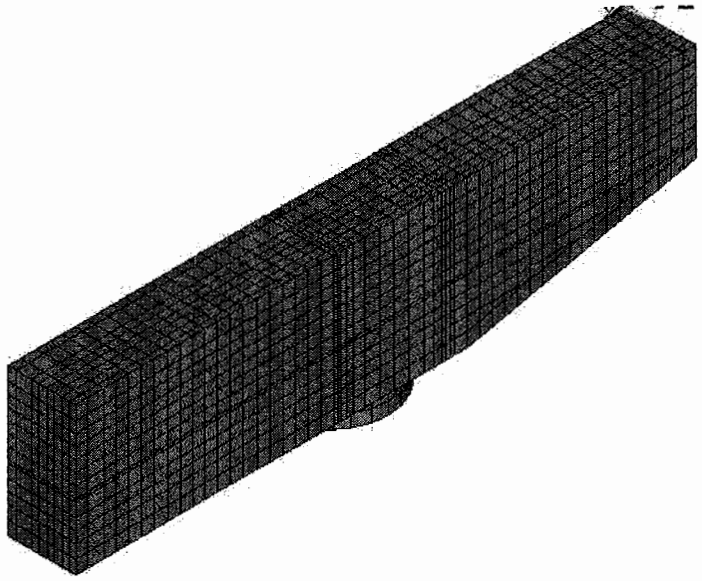

Figure 6.3 Finite Element Mesh for Model with Eight #8 Bars.

6.2.5 Load Increments

The analysis employed three main load steps with different sub-steps to monitor the change in strain of the longitudinal bars: (1) eight sub-steps of 40 kips increments to reach 320 kips at the end of first main load step, (2) four sub-steps of 10 kips increments to 360 kips, and (3) five sub-steps of 2 kips increments to 370 kips. The output, composed of the nodal displacements and stresses in brick and bar elements, were recorded at every sub-step up through the last step. The results from the analytical study, as compared with the experimental results, are shown in the subsequent section.

6.3 RESULTS

This sections makes comparisons between the analytical model previously presented and experimental behavior of Specimens 2B and 8H. Both specimens were reinforced with eight #8 longitudinal bars with the same skin reinforcement details. However, Specimen 8H consisted of double overlapping stirrups and had, accordingly, more confinement and shear strength. The confinement effect was taken into account by modifying the stress-strain relationship of unconfined concrete, as described in Section

6.2. Comparisons are made between the strain gauge data at two locations across the transverse direction of the beam: (1) at an interior reinforcing bar, and (2) at a side face reinforcing bar. Comparisons are made at three different locations along the length of the bent caps: (1) column center, (2) equivalent column face, and (3) at 29.3 in. from the column center. Details of the strain gauge location can be found in Fig. 3.7 for Specimen 2B and in Fig. 3.8 for Specimen 8H.

6.3.1 Transverse Variation of Strain

Analytical and experimental results from strain gauges #7 vs. #15, #10 vs. #19, and #12 vs. #27 are shown in Figs. 6.4-6.9. Strain gauges #7, #10, and #12 are located on a longitudinal bar along the bent center, while gauges #15, #19, and #27 are located on the side face longitudinal bar. Comparisons between the strains at these locations help verify the validity of the engineering beam theory, which assumes the uniformity of stress and strain across the width of the bent caps.

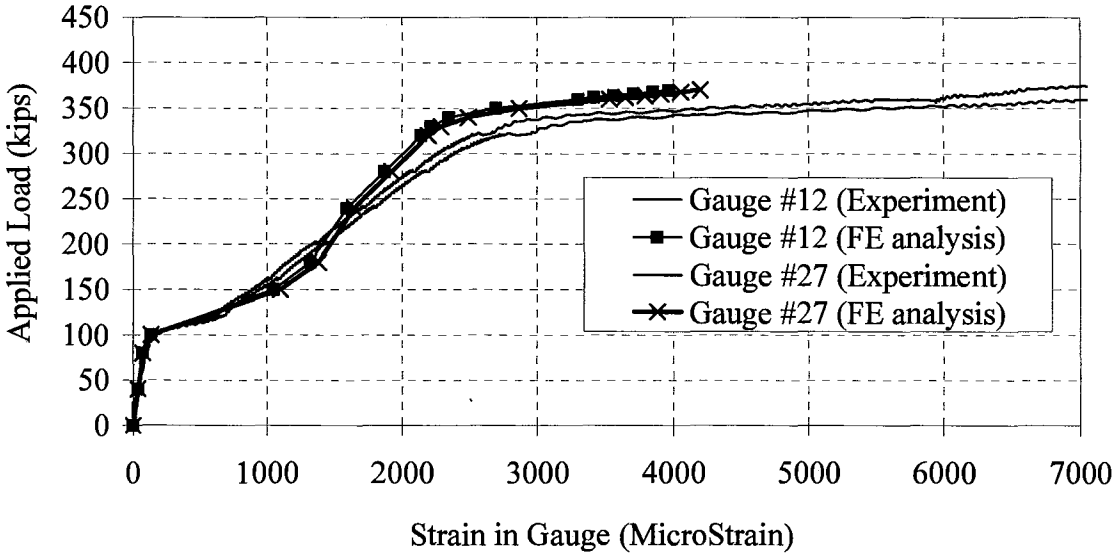

Figure 6.4 Load versus Strain in Gauges #12 and #27 for Specimen 2B (Column Center).

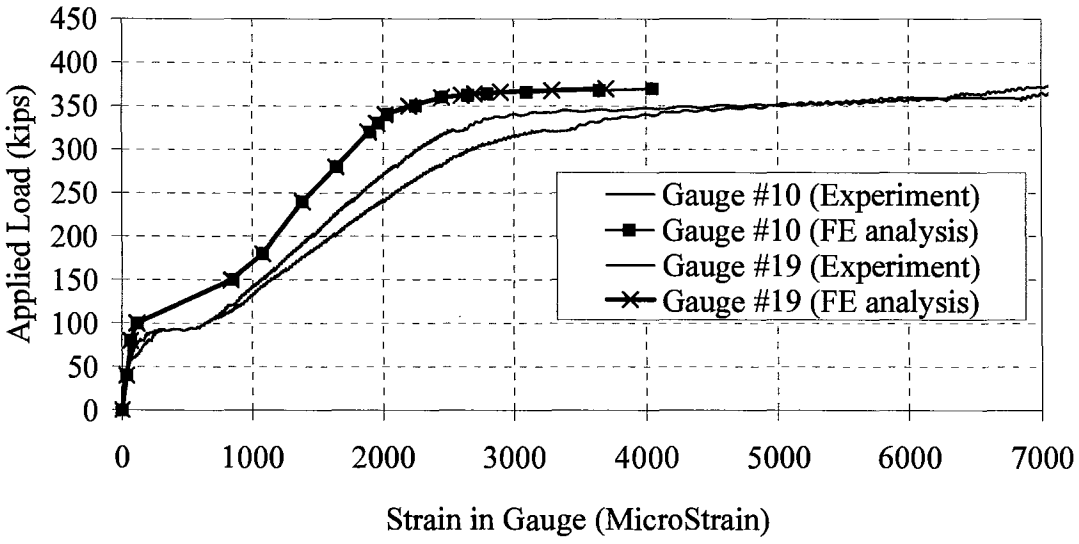

Figure 6.5 Load versus Strain in Gauges #10 and #19 for Specimen 2B (Column Face).

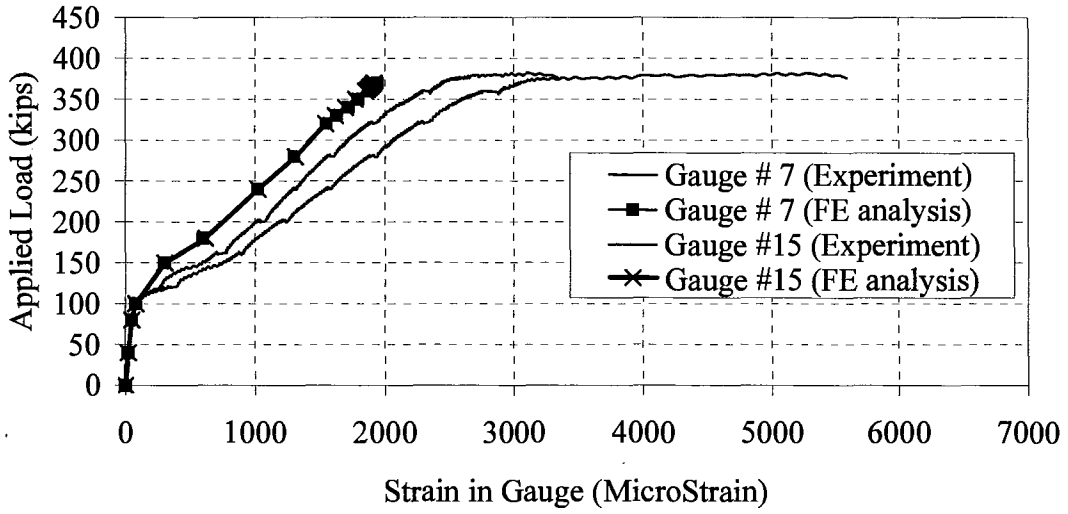

Figure 6.6 Load versus Strain in Gauges #7 and #15 for Specimen 2B (29.3 in. from the Column Center).

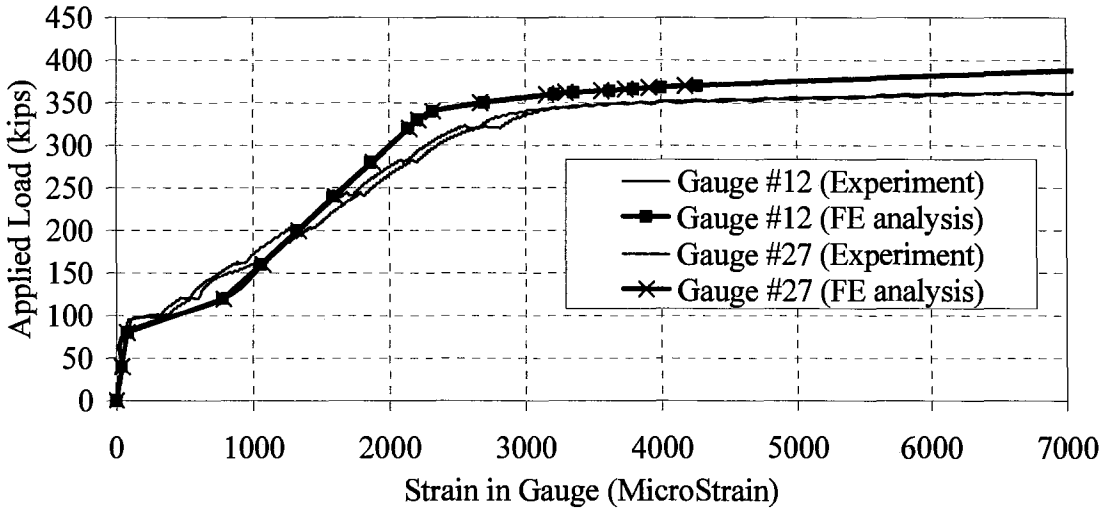

Figure 6.7 Load versus Strain in Gauges #12 and #27 for Specimen 8H (Column Center).

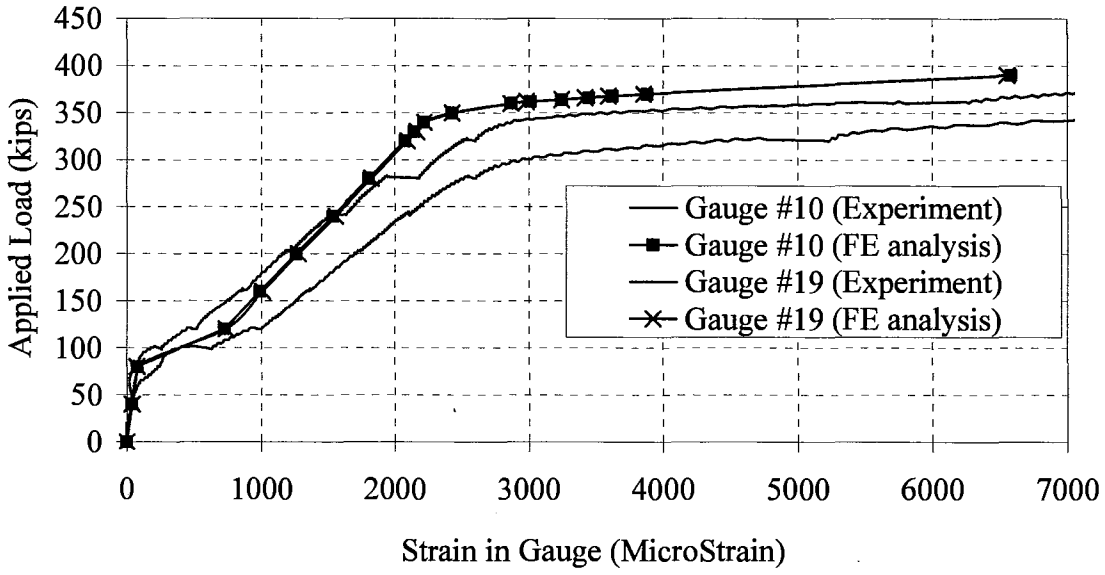

Figure 6.8 Load versus Strain in Gauges #10 and #19 for Specimen 8H (Column Face).

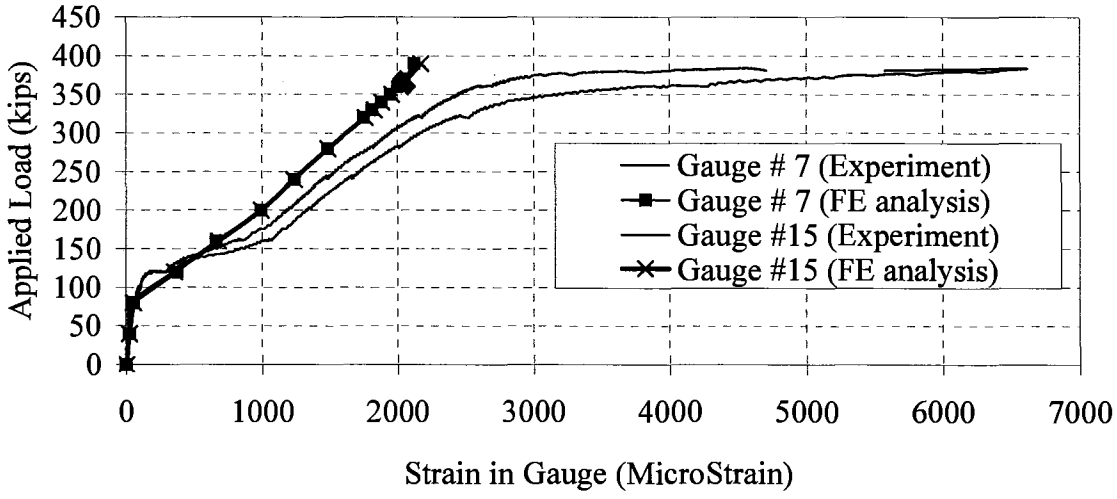

Figure 6.9 Load versus Strain in Gauges #7 and #15 for Specimen 8H (29.3 in. from the Column Center).

Figs. 6.4-6.9 show that the proposed model yields comparative response, up to the yield strength of steel, when compared to the experimental data. The best correlation of the longitudinal bar strains is at the column center. The results deviate as the monitored location moves further from the column center. Side face bars (gauge #19) at the equivalent column face have higher strains than interior bars in both specimens. At a distance 29.3 in. from the column center, strain in the inner bar is higher for specimen 8H, but the contrary is true for specimen 2B. Analytical results show similar trends but the deviation in strain across the width is not as pronounced as in the experiments. Strains in the outer bars are slightly larger than the strains in the inner bar.

Many factors can contribute to the discrepancy between the observed and predicted longitudinal bar strains. For instance, experimentally, if the location of the gauge was coincident with the crack location, erroneous results might be anticipated. An inaccurate shear retention factor can also lead to the same type of problem. In this investigation, researchers assumed a constant value of 0.15 for the shear retention factor for all open cracks. Lower shear retention factors may lead to premature numerical instability. Physically, cracks with different angles of inclination may have different shear transfer mechanisms, and the assumption used may not be sufficiently accurate. Application of lower shear retention factors for the elements near a distance of 29.3 in. from the column center can possibly lead to better correlation without causing numerical instability.

6.3.2 Longitudinal Variation of Strain

Strain variations along the bent cap length are shown in Figs 6.10 and 6.11. Results from this section can be used to examine the possibility of applying the strut and tie model, which assumes the uniform distribution of stress along the beam length at failure. The figures again show that the finite element model under-predicts the reinforcing bar strains throughout the beam length at higher loads.

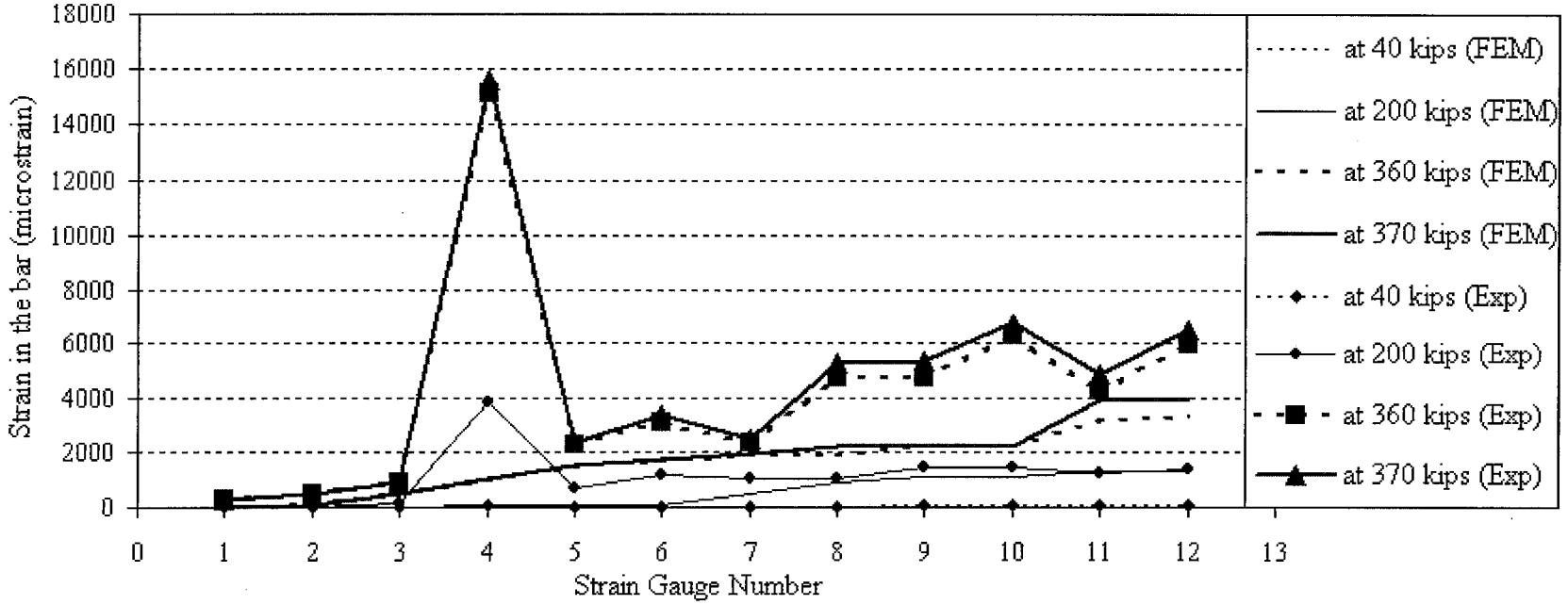

Figure 6.10 Strain along Member Length for Specimen 2B.

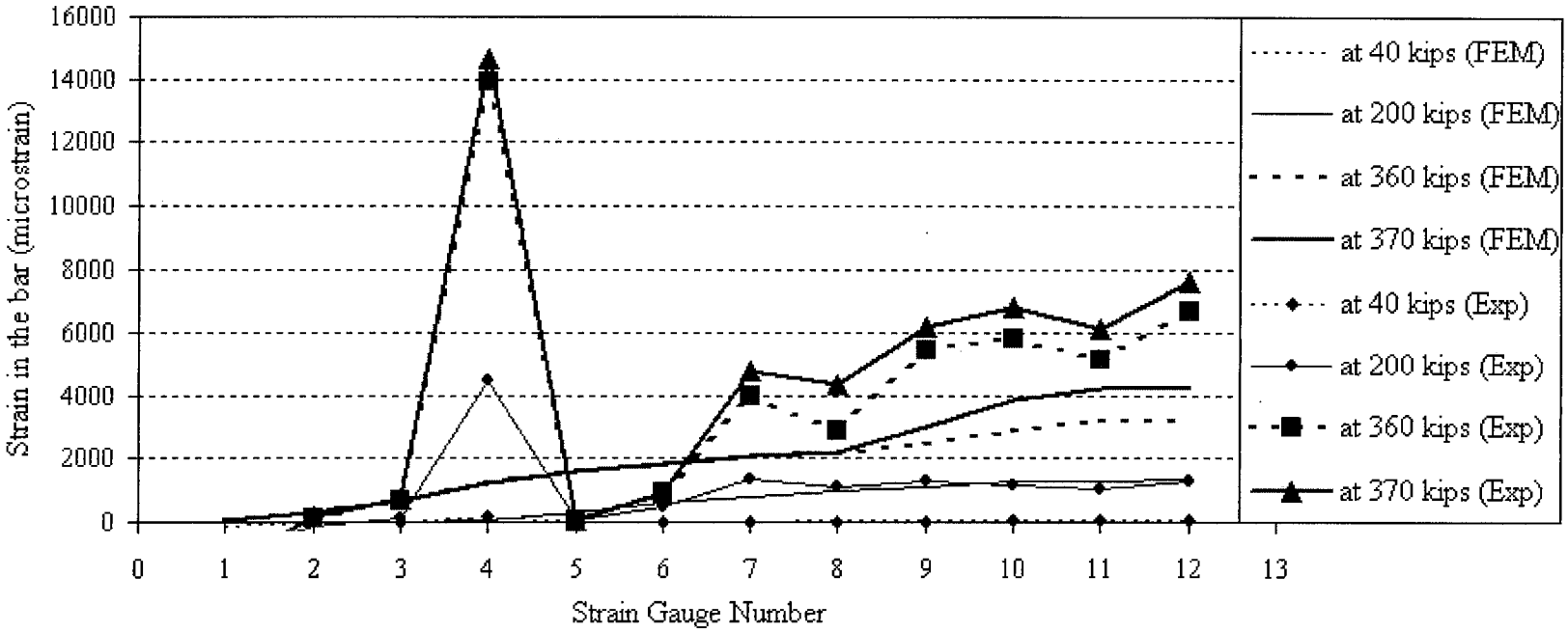

Figure 6.11 Strain along the Member Length for Specimen 8H.

6.3.3 Principal Compressive Stress Contour

Research evaluated the load transfer mechanism from the load points to the column support using the principal compressive stress contour diagram. This section compares the load transfer mechanisms of Specimens 2B and 8H. The stress contours are determined for loads of 40, 200, 360, and 370 kips. The 40 kips load represents the uncracked state of the RC bent caps. At 200 kips, observable cracking occurred throughout the specimens in the experimental program. Loads of 360 and 370 kips are representative of the bent caps near failure. Results in this section indicate that confinement of concrete and additional shear strength from the vertical stirrups affect the load transfer mechanism of the RC bent caps. Figs. 6.12 through 6.16 shows the stress contours at the different load levels.

The interpretation of results of the study of stress contours is presented in two different contexts: (1) the stress redistribution over the entire load history, and (2) the differences in the stress contours when additional shear strength and confinement are used.

6.3.3.1 Stress Redistribution

The principal compressive stress contours reveal that the stress pattern on the bent changes over the entire load history. Or stated another way, the load transfer mechanism or load path continuously changes over the entire load step. After cracking, tension in the concrete is redistributed to the longitudinal reinforcing bars, as observed in the laboratory and the analytical model where a significant jump occurs in longitudinal bar strain. The change in load path is possibly best described in the context of modified compression field theory (Vecchio and Collins, 1986) and strut and tie model analogy. According to the modified compressive field theory, the load path is such that all concrete in compression is in the form of a compressive strut, and reinforcing bars carry all possible tension. At 200 kips (Fig. 6.13), a minor change in the stress contour from elastic response is observed with the initiation of a minor strut near the supporting column. The formation of the main strut is more observable at loads of 360 and 370 kips.

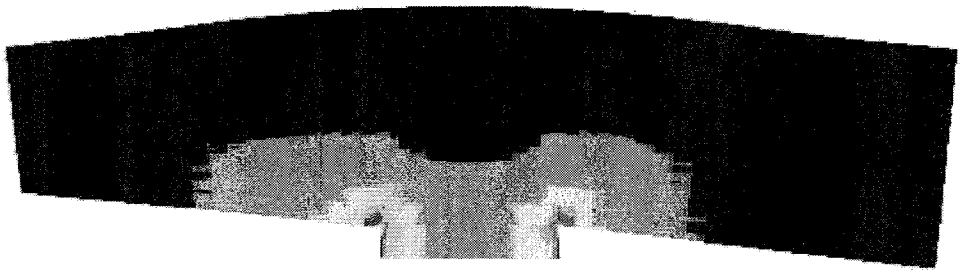

(a). Specimen 2B

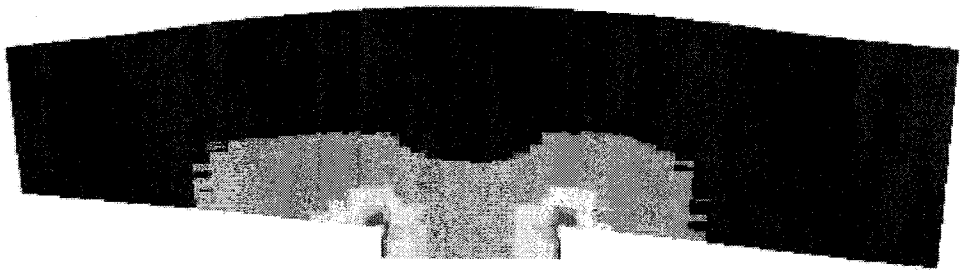

(b) Specimen 8H

Figure 6.12 Principal Compressive Stress Contour at Bent Cap Center at 40 kips.

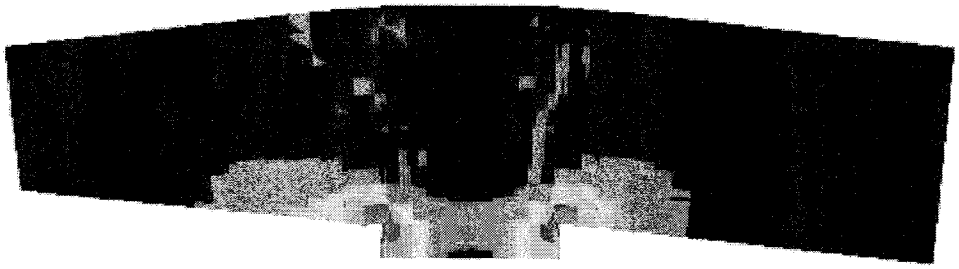

(a) Specimen 2B

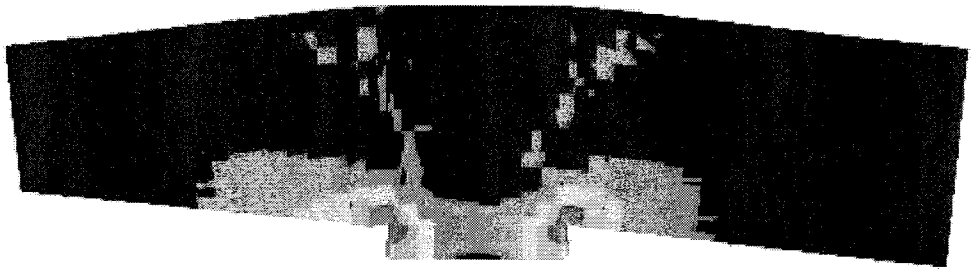

(b) Specimen 8H

Figure 6.13 Principal Compressive Stress Contour at Bent Cap Center at 200 kips.

(a) Specimen 2B

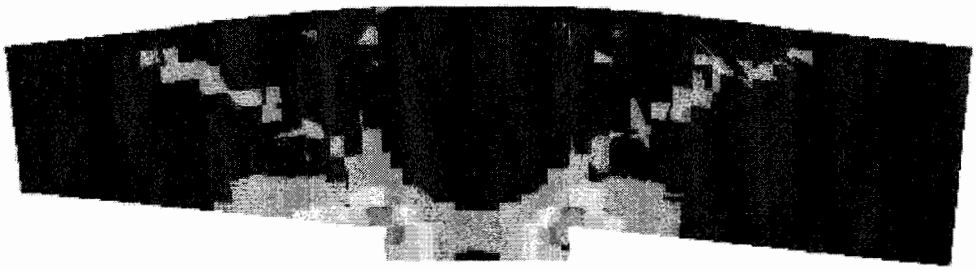

(b) Specimen 8H

Figure 6.14 Principal Compressive Stress Contour at Bent Cap Center at 360 kips.

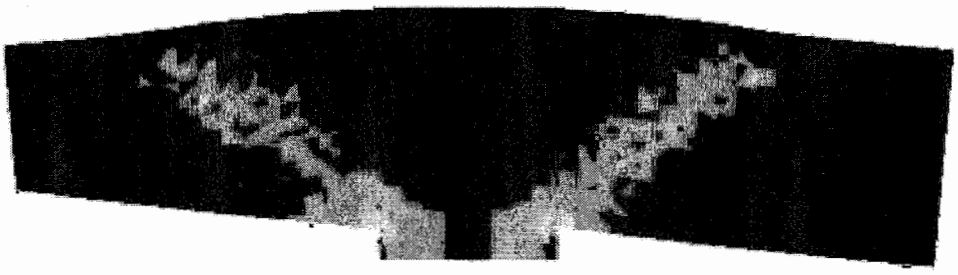

(a) Specimen 2B

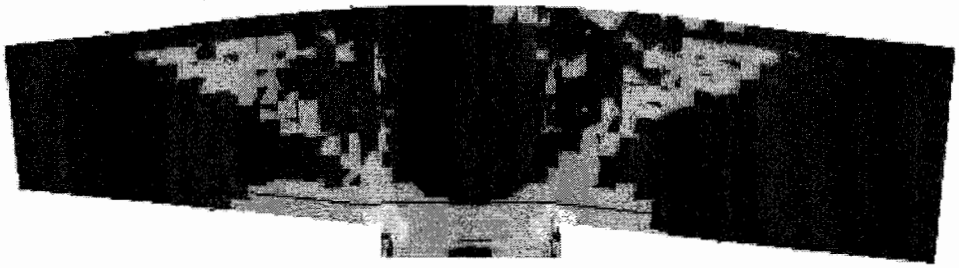

(b) Specimen 8H

Figure 6.15 Principal Compressive Stress Contour at Bent Cap Center at 370 kips.

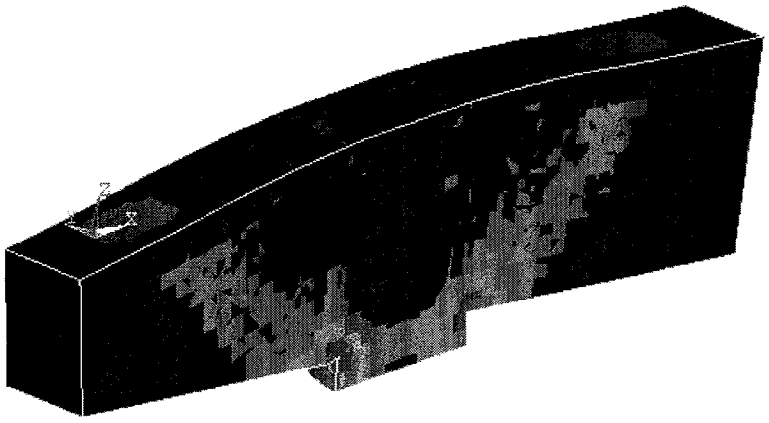

(a) Specimen 2B

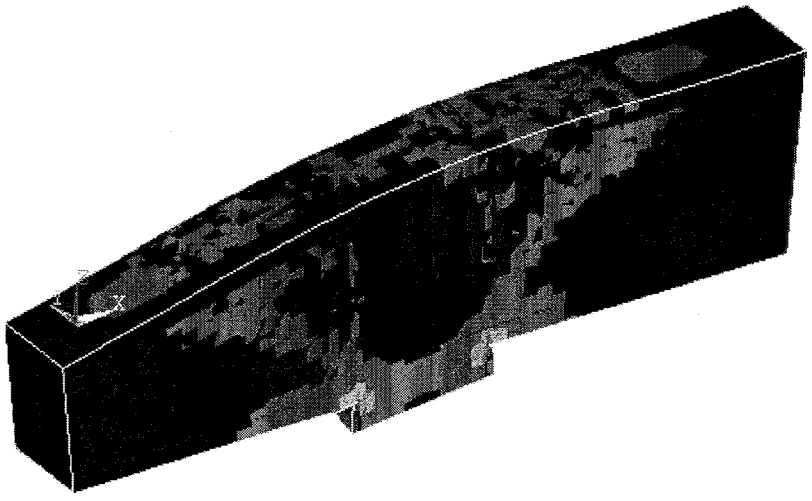

(b) Specimen 8H

Figure 6.16 Principal Compressive Stress Contour at Bent Cap Center at 370 kips – Isometric View.

Fig. 6.14 (at 360 kips) shows a possible formation of a major strut from the load point to the supporting column. The column supporting zone, which is called the nodal zone in strut and tie modeling, is accompanied by the formation of a main diagonal strut and the other two struts from both in front of and behind the column face. The main difference between the stress contours at 360 and 370 kips is the size of the main diagonal strut (see Figs. 6.14-6.15).

6.3.3.2 Effect of Confinement and Enhanced Shear Strength

Fig. 6.16 shows that confinement and enhanced shear strength do have an influence on the load path. Specimen 8H, with more confinement and shear strength, is able to distribute cracking throughout the bent by forming a compression fan region and a smaller diagonal strut. Experimental results showed that Specimen 8H, with overlapping stirrups, also had smaller crack widths than Specimen 2B at the same level of load. This phenomenon may be associated with the dispersion of cracks through several minor compression fans for members with high confinement and shear strength.

6.4 SUMMARY

This section develops non-linear finite element models of RC bent caps. Sections 6.1 and 6.2 presented the general description of the model used to conduct the analytical study. Three parameters of interest were examined: (1) tensile strength of concrete, (2) shear retention factor across cracks, and (3) concrete confinement. The appropriate values for the tensile strength of concrete and the shear retention factor across open cracks were chosen from numerical studies. Results from the analytical models were shown in Section 6.3. Discussions on the distribution of strain across the width and the length of bent caps and the load transfer mechanism were also made in Section 6.3.

Although the finite element analyses were not completely successful (at least in terms of predicting reinforcing bar strains at higher loads), the finite element models provided reasonable prediction of observable stress and strain trends in the experimental

program. The principal stress contours were able to show the positive influence of additional shear strength and confinement on the bent cap behavior by distributing damage or cracking throughout the bent, as compared to being concentrated along one major strut for members with minimal shear reinforcement.

7. SUMMARY

7.1 CLOSING

The purpose of this investigation was to examine the causes of unexpected cracking in multi-column RC bent caps at outside column locations (cantilevered regions) that exist within the TxDOT bridge inventory. The first phase of the research program consisted of a literature review of work performed on cracking in RC members, including design and detailing characteristics specific to bent cap structures. Included in this literature review was a background presentation regarding the past and present state of practice for design issues related to bent caps, including ACI 318 and AASHTO code level serviceability requirements.

Researchers designed, constructed, and tested 16 full scale bent cap specimens in a laboratory setting under quasi-static monotonic loading. Tests isolated several parameters within the specimens to determine their role in cracking: stress levels in the longitudinal reinforcement, arrangement of flexural reinforcement, skin reinforcement, shear resistance, and various code level serviceability requirements for crack control. Deep beam characteristics, as well as alternative approaches for the design of bent caps, were also investigated as a part of this study. Reinforcement strains and critical specimen displacement readings, as well as observed cracking patterns and crack widths, were measured and recorded throughout the experimental program in order to draw conclusions about the role of each of the above mentioned design parameters in cracking of RC bent caps.

Non-linear finite element modeling (FEM) analyses of several bent cap specimens complemented the experimental program. Two parameters used in the modeling, namely the concrete tensile strength and the shear retention factors, were determined in a parametric study in an effort to best correlate with the experimental results. Concrete and reinforcing steel strength parameters were determined from compression cylinder tests and mill records, respectively. The effect of concrete

confinement was accounted for by means of a modified constitutive relationship (stress-strain behavior) which incorporated the effect of closed stirrups or hoops (Mander et al., 1988). Researchers conducted the analyses using a commercial finite element analysis program capable of performing non-linear analysis.

7.2 CONCLUSIONS

Sections below present several primary conclusions based on the findings of this experimental and analytical investigation into cracking in the RC bent caps. All conclusions are related solely to bent caps with shear span-to-depth ratios of approximately 1.5.

- Flexural cracking in RC bent caps typically initiates when longitudinal reinforcement stresses are about 4 to 7 ksi, which are well below service stress limits in current codes. Therefore, some degree of cracking can be expected when using established RC design procedures.

- At low serviceability load levels, concentrating the side face reinforcement within the web tension region, as specified in current AASHTO (1996 and 1998) and ACI 318 (1999) codes, more effectively controlled vertical flexural cracking than evenly distributed horizontal reinforcement placed through the member depth.

- Slip of the longitudinal reinforcement in the cantilever region due to bond failure was not a contributing factor to cracking in the bent cap specimens. Symmetric cracking patterns were typically observed on both sides of the column support. In addition, one specimen developed a shear failure on the side that was detailed to replicate the continuous portion of the bent.

- Tensile stress of the longitudinal reinforcement was the primary factor influencing flexural cracks in the bent cap specimens. Other factors that appear in code serviceability expressions for crack control, implying that the distribution of the flexural reinforcement influences cracking, were shown to have little influence on

the specimen cracking behavior. Test results show that limiting the longitudinal reinforcement stress at service load levels to about 30 ksi and 24 ksi at the equivalent column face corresponds to maximum expected crack widths of 0.016 and 0.013 in., respectively.

- Although standard beam bending theory adequately predicted the flexural capacity of the specimens, it did not accurately predict the actual strain profile in the bent cap specimens. Reinforcement strains at and near the support were typically larger along the side face of the bent caps when compared with reinforcement strains at the bent cap center for the same transverse plane. In addition, the longitudinal strains were generally higher at some distance below the top longitudinal reinforcement level due to significant shear demands.

- Following initial cracking of the specimens, the longitudinal reinforcement strains near the column center were consistently higher than the reinforcement strains near the column face. This trend initiated at serviceability load levels and remained consistent through ultimate failure of the specimen. Therefore, the location of the critical section for flexural design based on ultimate load conditions existed within the column support region and not at the equivalent column face.

- Field investigations of in-service bent caps with similar shear span-to-depth ratios showed that inclined flexure-shear cracks are generally larger than flexural cracks. Bent cap specimens with nominal transverse reinforcement displayed a similar cracking behavior during service loads and failed in a brittle shear manner along about a 45 degree plane between the loading point and the column face. Specimens with enhanced shear strength using overlapping transverse reinforcement had reduced inclined flexure-shear cracking throughout the load history and developed a more desirable (ductile) flexural failure mechanism during ultimate loading. Increasing the shear resistance and concrete core confinement effectively reduced the shear transfer demands on the main compression strut from the applied load to the support by increasing the participation of the compression fan region.

- Non-linear FEM analyses of the RC bent cap specimens satisfactorily represented the experimentally measured response with properly correlated analysis parameters. Observations identified the load transfer mechanisms in the specimens with single and overlapping stirrups during the various loading stages. The size and orientation of the concrete struts changed with increasing applied loads. For specimens with a single stirrup, one major concrete compression strut formed from the applied load to within the supporting column region. Specimens with overlapping stirrups for enhanced shear strength and concrete confinement had an evenly distributed formation of compressive force paths or struts, including a nodal compression fan region.

7.3 DESIGN RECOMMENDATIONS

The following recommendations are provided below based on the experimental and analytical program of bent cap specimens having a shear span-to-depth ratio of about 1.5:

- Since the critical longitudinal reinforcement strains were within the column support region beyond service load conditions and limiting the service load stress in the longitudinal reinforcement proved to be effective for flexural crack mitigation, bent cap flexure design should be based on the critical section being at the column center. Inevitably, this will require additional the longitudinal reinforcement and provide flexural overstrength at the equivalent column face. This, in turn, effectively reduces the longitudinal reinforcement stresses during service load. Longitudinal reinforcement stresses at the column center during service loading should be limited to 36 ksi for moderate exposure cases. This will essentially limit the reinforcement service stress at the equivalent column face to about 30 ksi for similar shear spans and column support widths. For severe exposure cases, longitudinal reinforcement stresses at the column center should be limited to 30 ksi, or about 24 ksi at the equivalent column face.

- To limit undesirable inclined flexure-shear cracks and shear failure mechanisms, the nominal shear resistance of bent caps should exceed: (1) the factored shear demands at the equivalent column face from normal bridge loading, and (2) the shear demand required to develop flexural overstrength of the bent at the equivalent column face. The nominal shear resistance should be computed using the standard expressions for concrete shear strength ($V_c = 2\sqrt{f'_c}bd$) and stirrup shear strength ($V_s = A_v f_y d / s$) for bent caps with similar shear span-to-depth ratios. However, for other ratios, special care should be taken to determine the appropriate bent cap shear strength. Flexural overstrength of the bent cap should be calculated using standard beam theory with a longitudinal reinforcement stress of $1.25 f_y$.

- Along with these flexural and shear aspects of bent cap design, horizontal side face (skin) reinforcement should also be provided within the web tension region to assist in crack control, as per current AASHTO and ACI 318 codes.

7.4 RECOMMENDATIONS FOR FUTURE WORK

Cracking patterns observed throughout the experimental program indicate that the performance of these bent cap specimens was related to the load transfer mechanism. Direct transfer of applied loads to the support element through a main compression strut resulted in inclined flexure-shear cracking during service and ultimate load conditions. Further research is required to study the effects of changing the shear span-to-depth ratio, thus varying this load transfer mechanism and studying its effect on cracking.

Further research is required regarding strut-and-tie modeling and its application to flexural members with geometry similar to bent caps. Strut-and-tie models are an accepted design method for deep reinforced concrete beams. However, the generalization of theory to practical applications has not yet reached the final stage of development. Specifically, the researchers recommend investigation of a straight-forward method for determining nodal geometry and solving for strut forces and

capacities. Member forces within a conceptual strut and tie model can be compared to strain data from full scale testing to evaluate the accuracy of the model in representing the actual behavior of the RC member. Relatively little is known on the distribution of stress in the nodal zone and the orientation and size of the compressive struts in this region. Recently, Yun (2000) proposed a new non-linear strut-and-tie model for RC structures, which leads to improved identification of the load path. The model uses prior knowledge based on the non-linear finite element analysis of concrete structures and several iterations with trial and error. Therefore, using preliminary non-linear analysis may lead to a more realistic model and yield better predictions on the ultimate capacity of the beam.

Further inelastic finite element modeling may also be beneficial for a better understanding of the behavior of the bent caps before and after cracking. A limited number of strain gauges placed throughout the specimens allows for a general understanding of the post-cracking load transfer behavior. However, an accurate finite element model can be beneficial for a more complete understanding of the behavior of the bent cap following cracking. Considerations of out-of-plane effects on cracking can also be made, which cannot easily be accounted for in the laboratory.

In addition, more research should be performed to investigate the relationship between cracking and spacing of the flexural reinforcement. Limited test results from this investigation indicated that the primary factor affecting cracking in bent cap specimens was the tensile stress in the longitudinal reinforcement, and that cracking was virtually independent of bar spacing. However, the bar spacing within this investigation was of limited range, and did not provide broad-based results for general conclusions regarding the role of flexural reinforcement arrangement and cracking. Because recent ACI 318 (1999) code revisions replaced the previous 'z' expression with one that emphasizes bar spacing, more research is needed to determine the ability of such an expression to control cracking in typical bent cap members.

Since it was shown that the non-linear FEM analyses reasonably correlated with the experimental response, non-linear FEM parametric studies should be performed to evaluate the influence of the following variables on cracking in highway bridge bent caps: (1) varying shear span-to-depth ratios, which will significantly affect the load transfer mechanism in the bent caps and lead to different orientation of concrete compressive struts and ties by means of stirrups, and (2) relative size of bent cap and supporting column. Experiments conducted in this project had 30 in. circular columns and 33 in. wide by 36 in. deep bent caps. Varying the size of bent, while keeping the size of column constant, may significantly alter the load transfer mechanism and lead to highly nonlinear behavior in which normal beam theory may not be applicable. This three-dimensional behavior may lead to increasing reinforcement demands and larger cracks.

REFERENCES

AASHTO (1996). *Standard Specifications for Highway Bridges, 16th Edition,* American Association of State Highway and Transportation Officials, Washington D.C.

AASHTO (1998). *LRFD Bridge Design Specifications and Commentary, 2nd Edition,* American Association of State Highway and Transportation Officials, Washington D.C.

ACI Committee 318 (1995). *Building Code Requirements for Structural Concrete and Commentary,* American Concrete Institute, Farmington Hills, Michigan.

ACI Committee 318 (1999). *Building Code Requirements for Structural Concrete and Commentary,* American Concrete Institute, Farmington Hills, Michigan.

Adebar, P. and van Leeuwen, J. (1999). "Side-Face Reinforcement for Flexural and Diagonal Cracking in Large Concrete Beams," *ACI Structural Journal,* American Concrete Institute, Farmington Hills, Michigan, 693-704.

ASCE (1982). "*State-of-the-Art Report. Finite Element Analysis of Reinforced Concrete*," American Society of Civil Engineers, Reston, Virginia.

Breen, J. E. and Frantz, G. C. (1978). "Control of Cracking on the Side Faces of Large Reinforced Concrete Beams," *Texas Highway Department, Report #198-1F,* Center for Highway Research, Austin, Texas.

Broms, B. (1965). "Crack Width and Crack Spacing in Reinforced Concrete Members," *ACI Journal, Proceedings*, 62(10), 1237-1256.

Chen, W.F. and Saleeb, A.F. (1982). "*Constitutive Equations for Engineering Materials Vol.1 Elasticity and Modeling*," John Wiley & Sons, New York, New York.

Clark, A. P. (1956). "Cracking in Reinforced Concrete Members," *ACI Journal, Proceedings*, 52(8), 851-862.

Darwin, D., Beeby, A., Ghowrwal, A., Hognestad, E., Manning, D., and Rice, P. (1985). "Debate: Crack Width, Cover, and Corrosion," *Concrete International,* 7(5), 20-35.

Ferguson, P. M. (1964). "Design Criteria for Overhanging Ends of Bent Caps," *Texas Highway Department, Report #52-1F*, Center for Highway Research, Austin, Texas.

Frosch, R. (1999). "Another Look at Cracking and Crack Control in Reinforced Concrete," *ACI Structural Journal*, American Concrete Institute, Farmington Hills, Michigan, 437-442.

Gergely, P. and Lutz, L. A. (1968). "Maximum Crack Width in Reinforced Concrete Flexural Members," *Causes, Mechanisms, and Control of Cracking in Concrete, SP-20*, American Concrete Institute, Farmington Hills, Michigan, 87-117.

Hand, F.R., Pecknold, D.A., and Schnobrich, W.C. (1973). "Nonlinear Layered Analysis of RC Plates and Shells," *Journal of the Structural Division*, American Society of Civil Engineers, Vol. 99(7), 1491-1505.

Hinton, E. and Owen D.R.J. (1980). "*Finite Element in Plasticity,*" Pineridge Press, Swansea, United Kingdom.

Hognestad, E. (1962). "High Strength Bars as Concrete Reinforcement: Part 2 – Control of Cracking," *Journal, PCA Research and Development Laboratories*, 4(1), 46-62.

Hsu, T. C. (1993). *Unified Theory of Reinforced Concrete*, CRC Press, Boca Raton, Florida.

Karr, P. H. and Hognestad, E. (1965). "High Strength Bars as Concrete Reinforcement: Part 7 – Control of Cracking in T-Beam Flanges," *Journal, PCA Research and Development Laboratories*, 7(1), 42-53.

Karr, P. H. and Mattock, A. H. (1963). "High Strength Bars as Concrete Reinforcement: Part 4 – Control of Cracking," *Journal, PCA Research and Development Laboratories*, 5(1), 15-38.

Kotsovos, M.D. and Pavlovic, M.N. (1995). *Structural Concrete. Finite Element Analysis for Limit-State Design*, Thomas Telford, London, Great Britain.

MacGregor, J. G. (1997). *Reinforced Concrete Mechanics and Design,* Third Edition, Prentice Hall, Upper Saddle River, New Jersey.

Mander, J.B., Priestley, M.J.N., and Park, R. (1988). "Theoretical Stress-Strain Model for Confined Concrete," *Journal of Structural Division*, American Society of Civil Engineers, Vol.114(8), 1804-1826.

Nawy, E. (1968). "Crack Control in Reinforced Concrete Structures," *Journal Proceedings, ACI Journal*, Farmington Hills, Michigan, 825-835.

Nawy, E. (1999). "Proposed Revisions to Building Code Requirements for Structural Concrete (ACI 318-95) and Commentary – ACI 318R-95," *Concrete International,* 21(5), 318/10-318/12.

Ngo, D. (1975). "A Network-Topological Approach to the Finite Element of Progressive Crack Growth in Concrete Members," University of California, Berkeley, Ph.D. Dissertation.

Ngo, D. and Scordelis, A.C. (1967). "Finite Element Analysis of Reinforced Concrete Beams," *ACI Structural Journal*, American Concrete Institute, Farmington Hills, Michigan, Vol. 64(3), 152-163.

Park, R. and Paulay, T. (1975). *Reinforced Concrete Structures,* John Wiley & Sons, New York, New York.

Rashid, Y.R. (1968). "Analysis of Prestressed Concrete Pressure Vessels," *Nuclear Engineering and Design*, Vol. 7(4), 334-344.

Rüsch, H. and Rehm, G. (1964). "Versuche mit Betonformstahlen," *Deutscher Ausschuss für Stahlbeton*, Bulletins 140(1), 160(2), and 165(3).

William, K.J. and Warnke, E.P. (1975). "Constitutive Model for the Triaxial Behavior of Concrete," *Proceedings*, International Association for Bridge and Structural Engineering, Vol.19, 1-30.

Yun, Y.M. (2000). "Nonlinear Strut-Tie Model Approach for Structural Concrete," *ACI Structural Journal*, American Concrete Institute, Farmington Hills, Michigan, Vol. 97(3), 581-590.

APPENDIX A

GROUP #1 EXPERIMENTAL RESULTS

For this Appendix:

- The graphical data were intentionally terminated in order to reflect only that portion of testing necessary for illustrating a particular trend. Therefore, termination of the data series does not indicate failure of the specimen or completion of testing.

- Refer to Fig. 3.7 for illustration of strain gauge identification and locations.

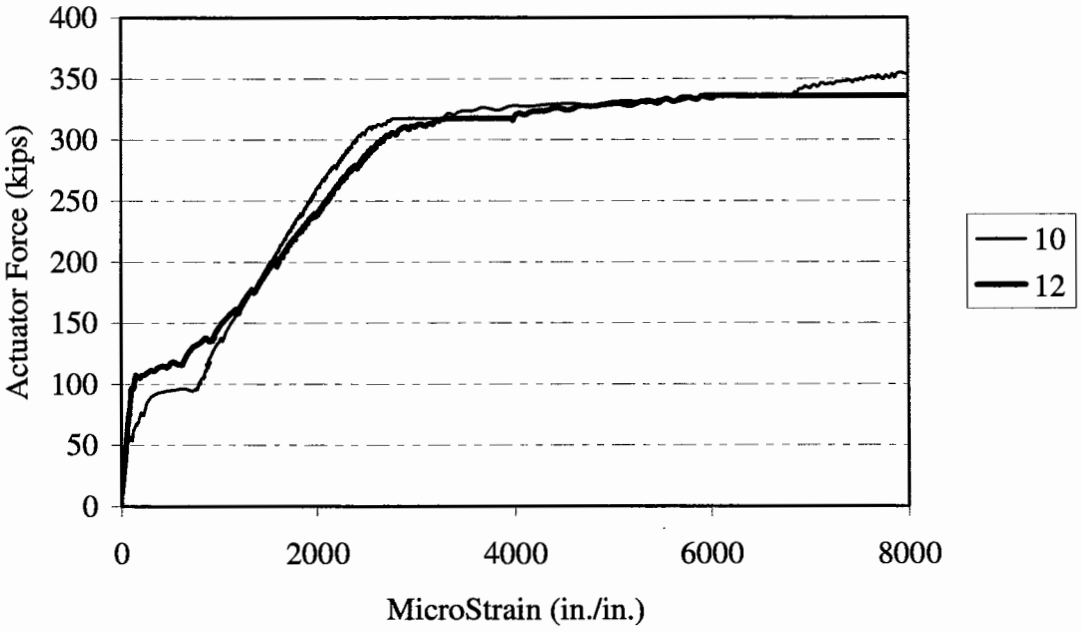

Figure A-1. Specimen 1A Load-Strain History Column Face (10) vs. Column Centerline (12).

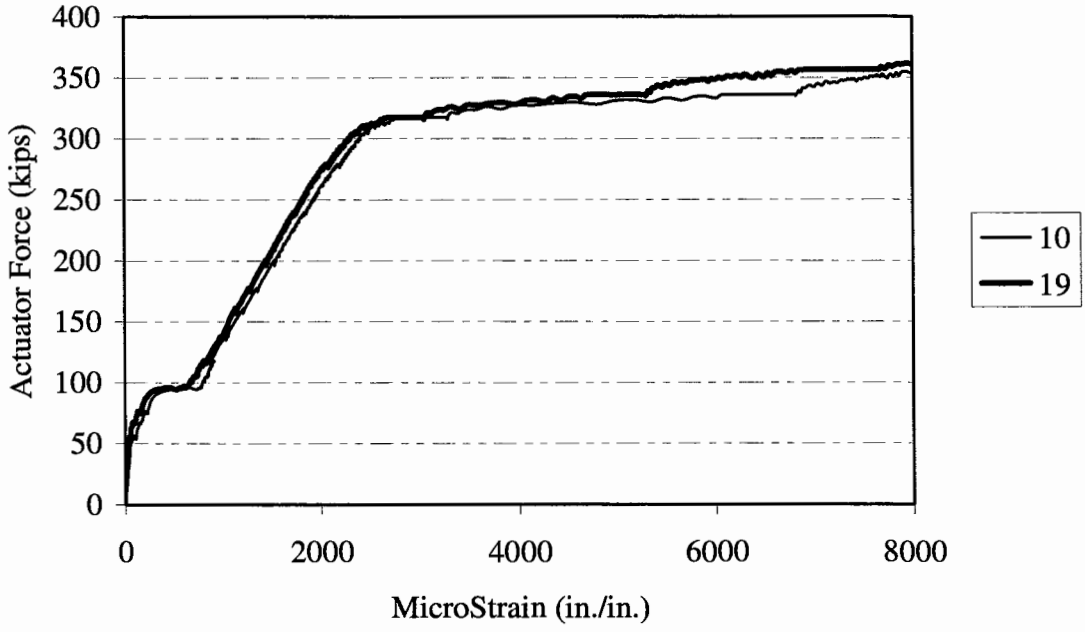

Figure A-2. Specimen 1A Load-Strain History Side (19) vs. Center (10) Transverse Plane.

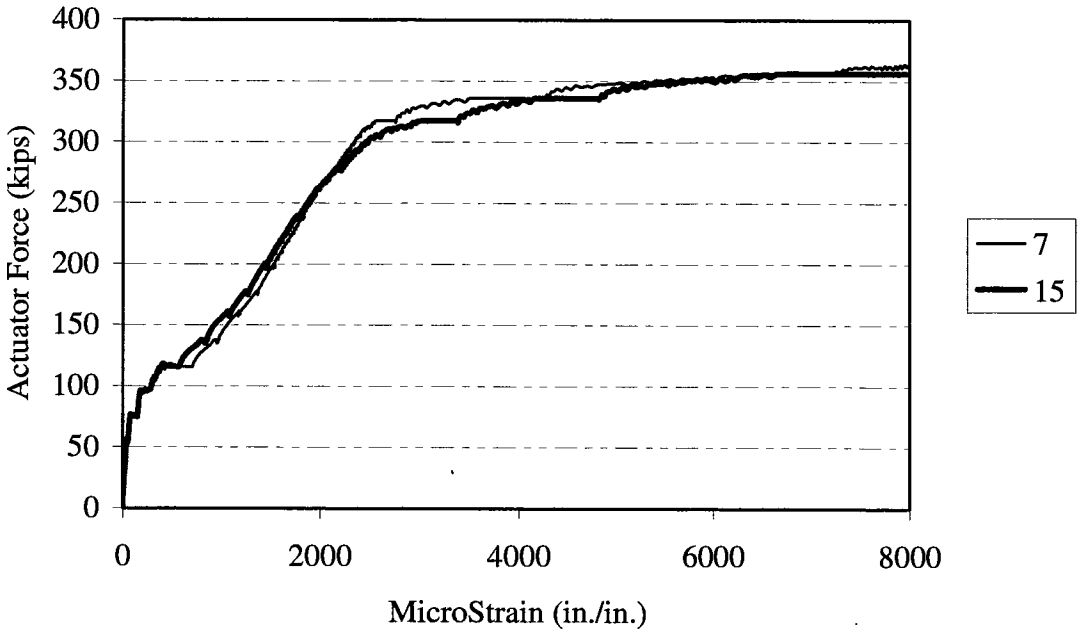

Figure A-3. Specimen 1A Load-Strain History Side (15) vs. Center (7) Transverse Plane.

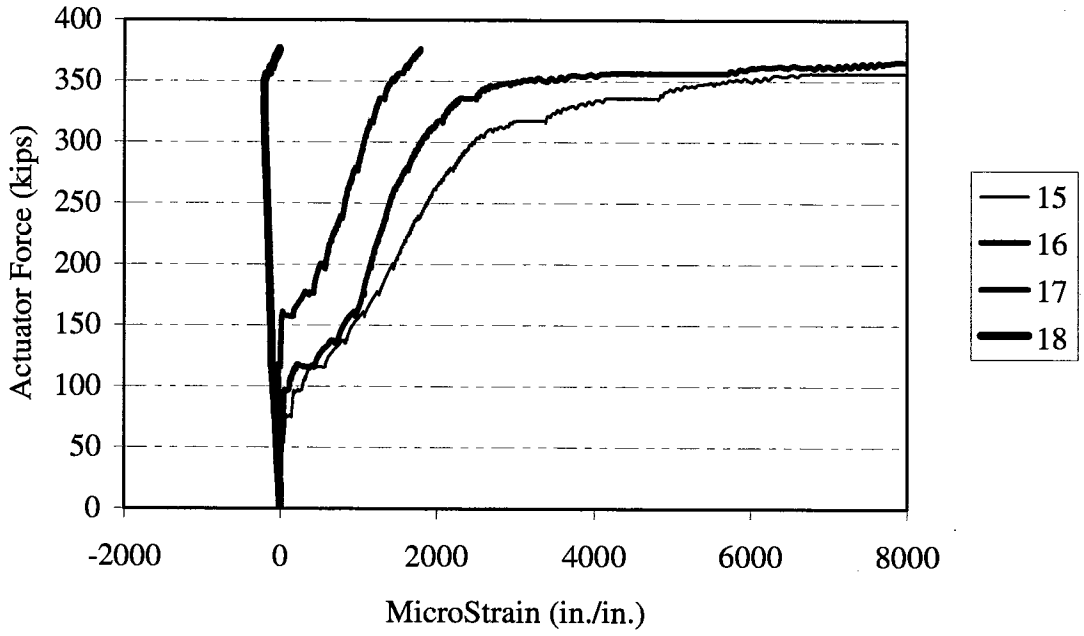

Figure A-4. Specimen 1A Strain Profile Through-Depth Side Face.

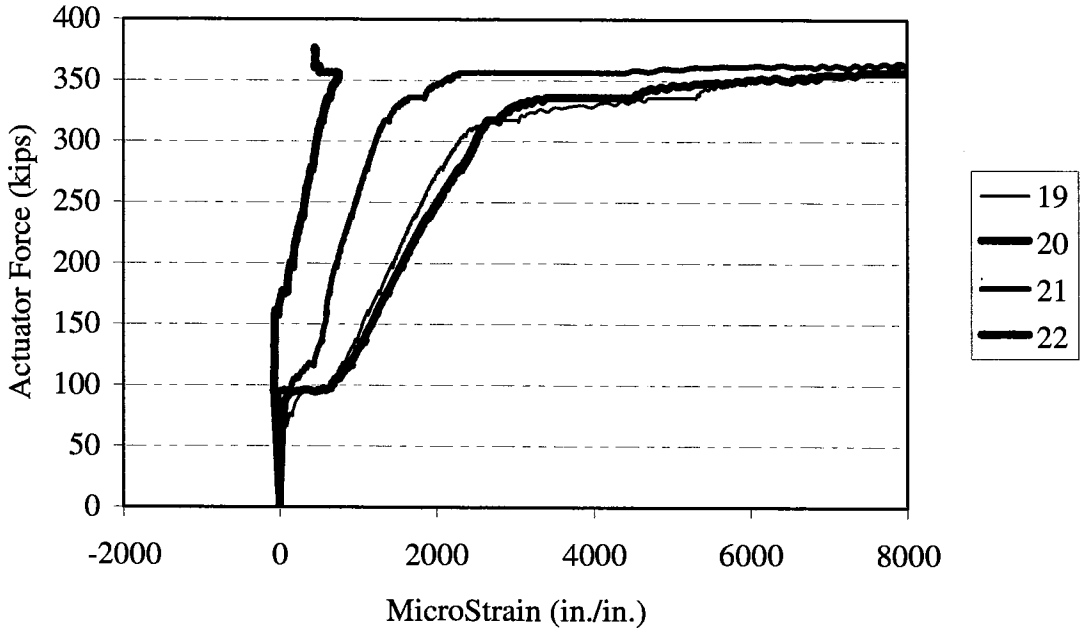

Figure A-5. Specimen 1A Strain Profile Through-Depth Side Face.

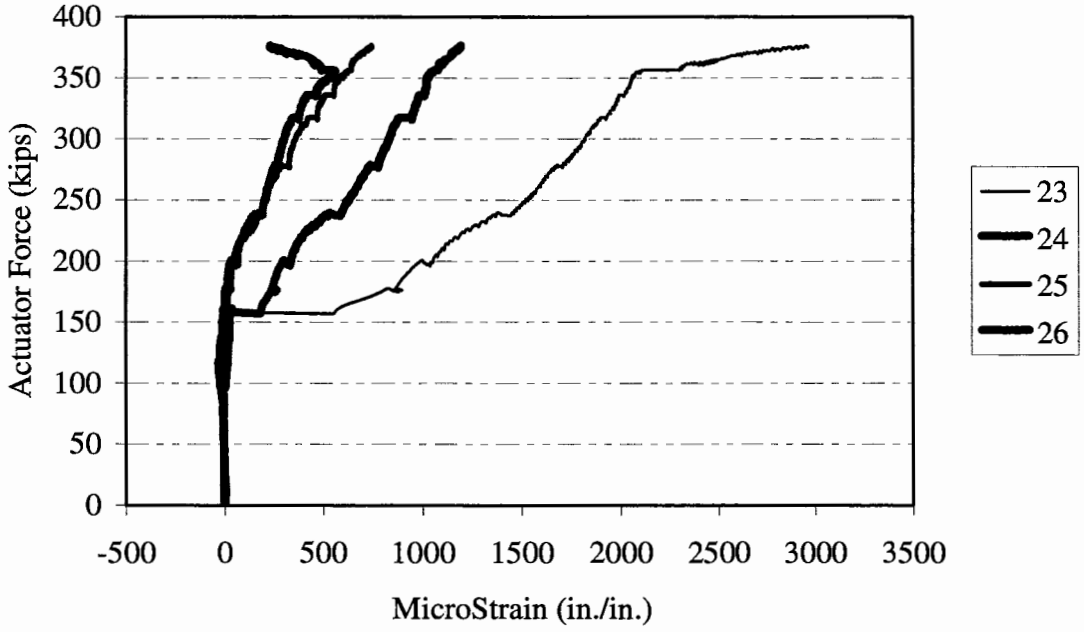

Figure A-6. Specimen 1A Strain Profile Transverse (Stirrup) Reinforcement.

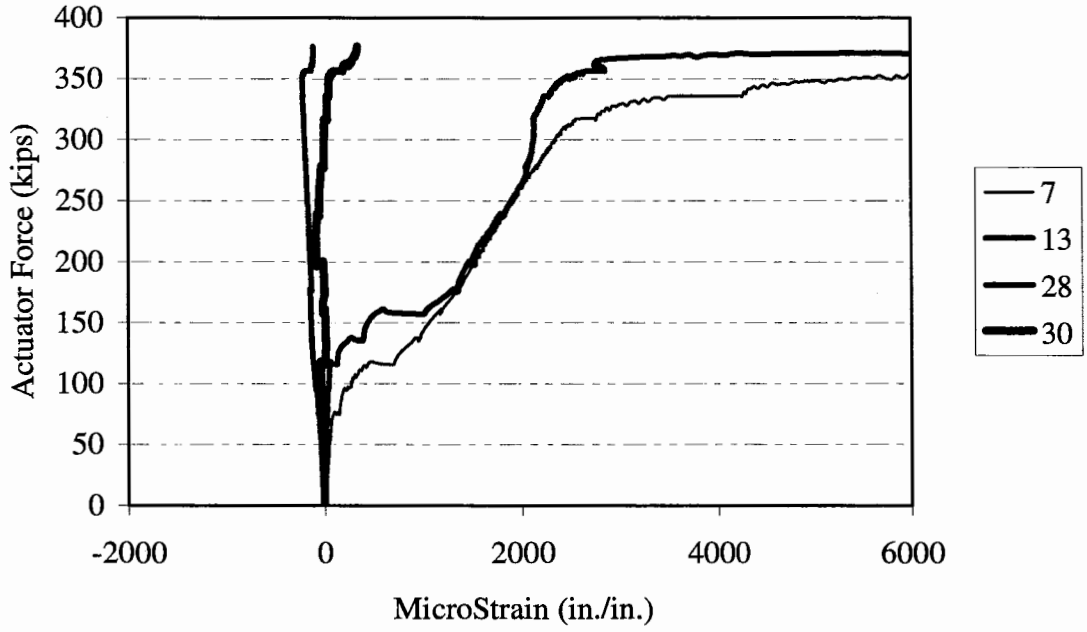

Figure A-7. Specimen 1A Strain Profile Through-Depth Centerline.

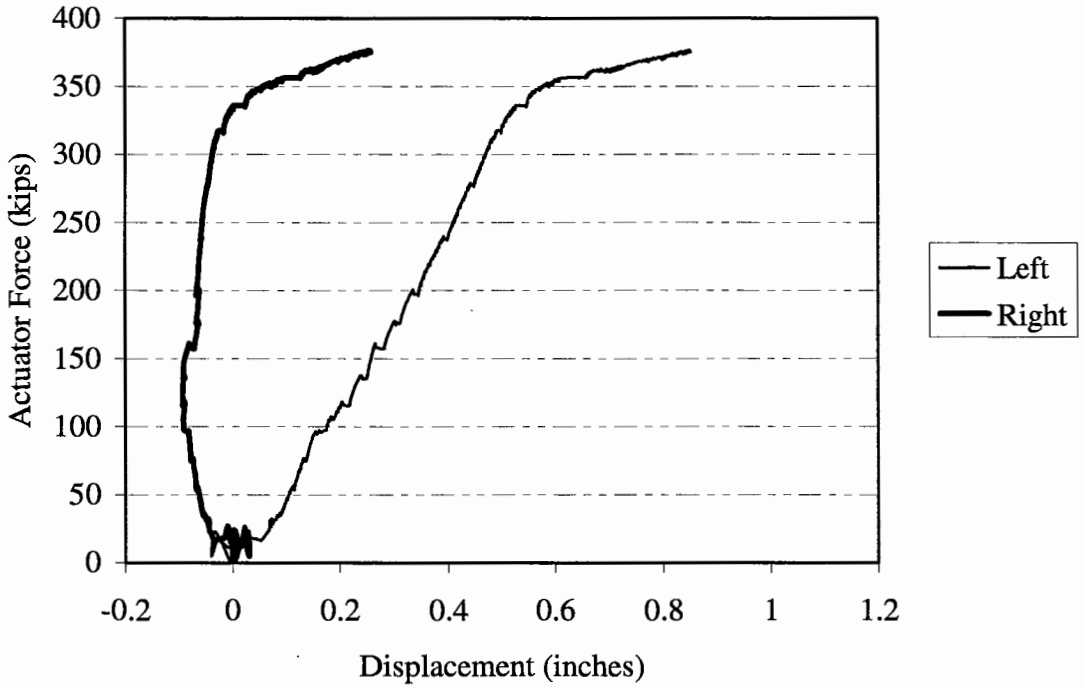

Figure A-8. Specimen 1A Load-Displacement History.

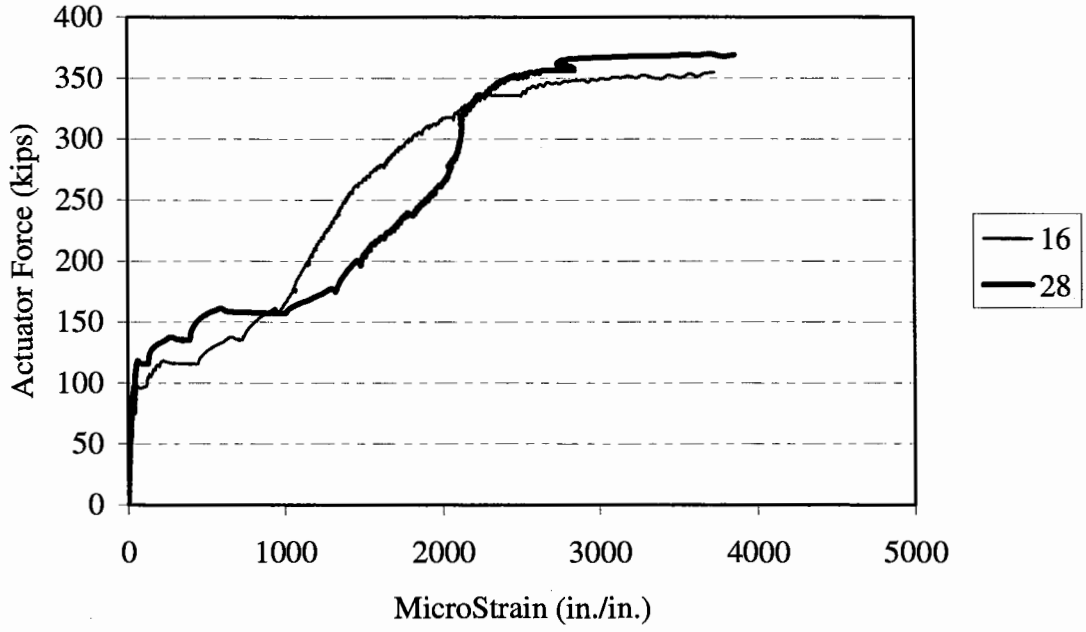

Figure A-9. Specimen 1A Load-Strain History Center (28) vs. Side (16) Transverse Plane.

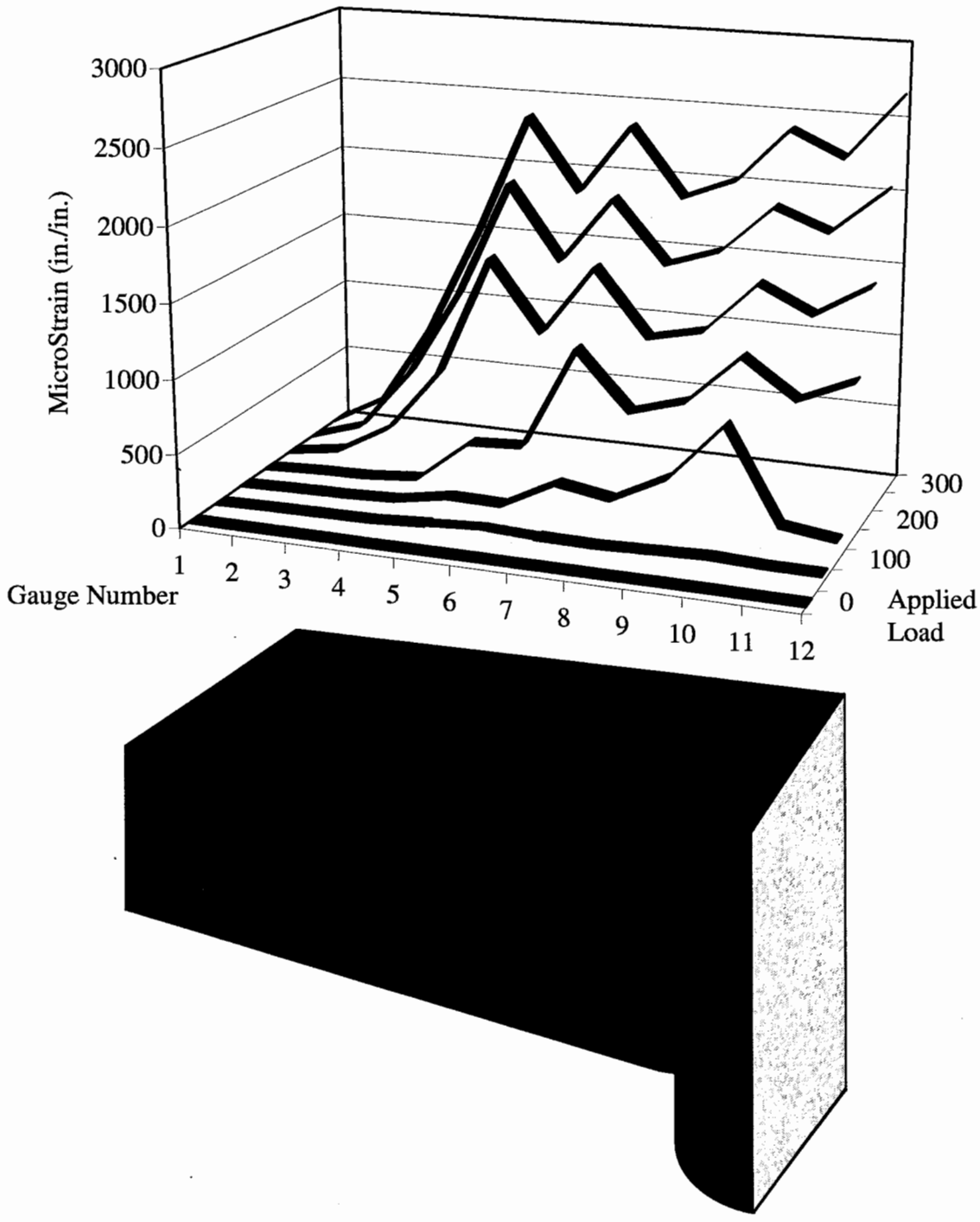

Figure A-10. Specimen 1A Longitudinal Reinforcement Strain Profile for Gauges 1 Through 12.

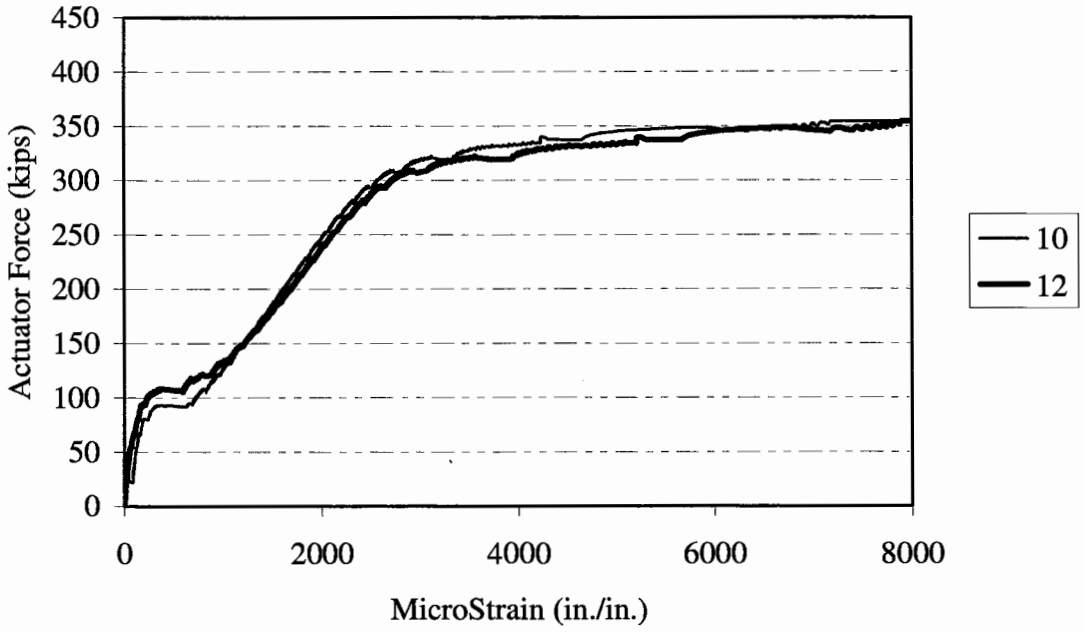

Figure A-11. Specimen 1B Load-Strain History Column Face (10) vs. Column Centerline (12).

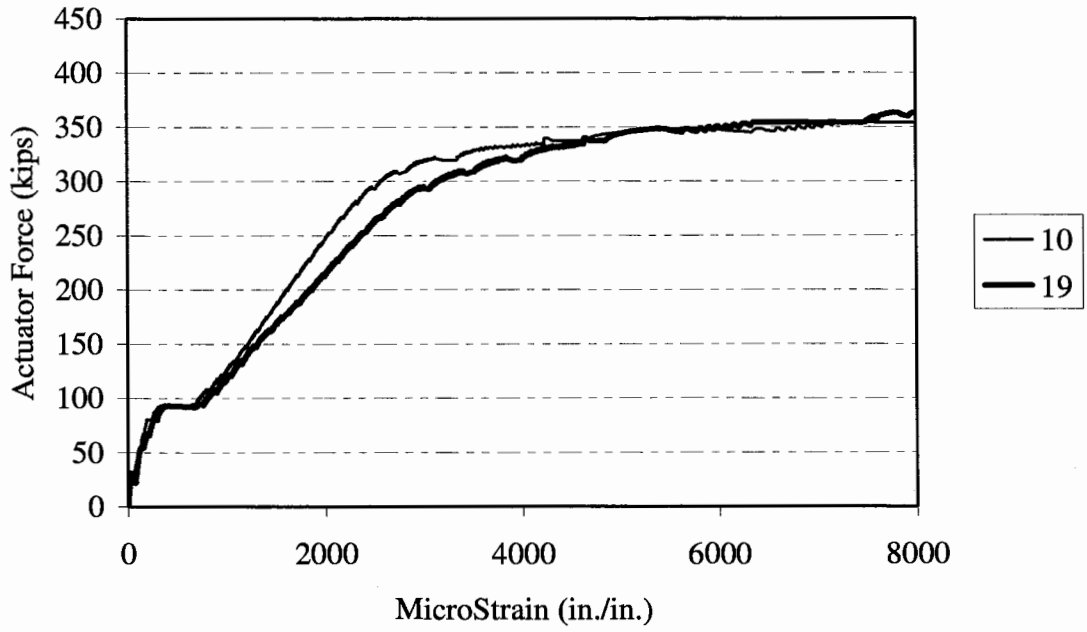

Figure A-12. Specimen 1B Load-Strain History Side (19) vs. Center (10) Transverse Plane.

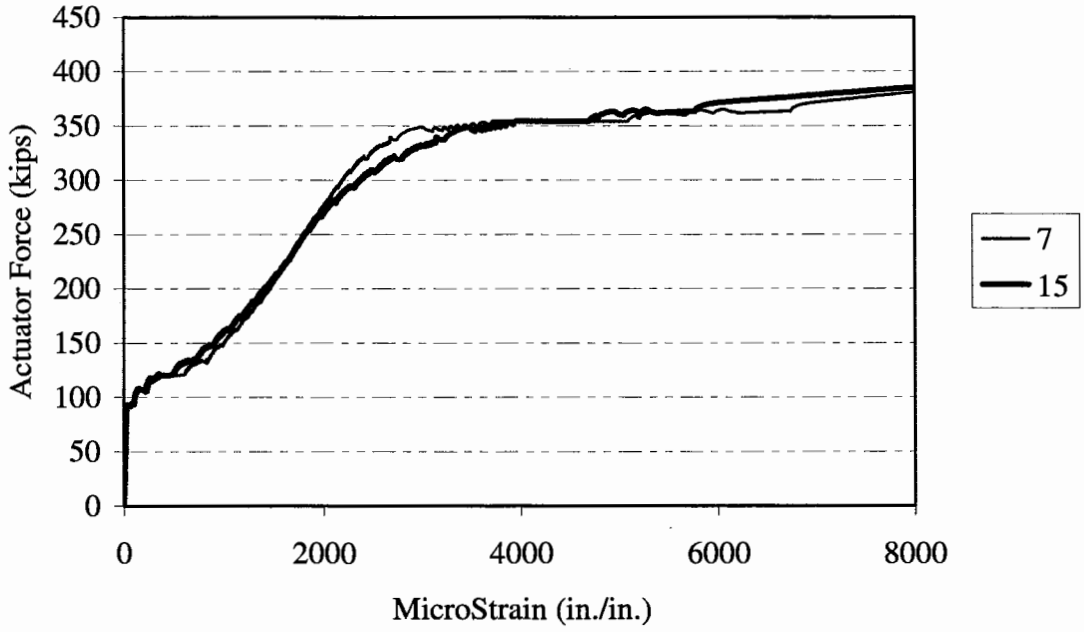

Figure A-13. Specimen 1B Load-Strain History Side (15) vs. Center (7) Transverse Plane.

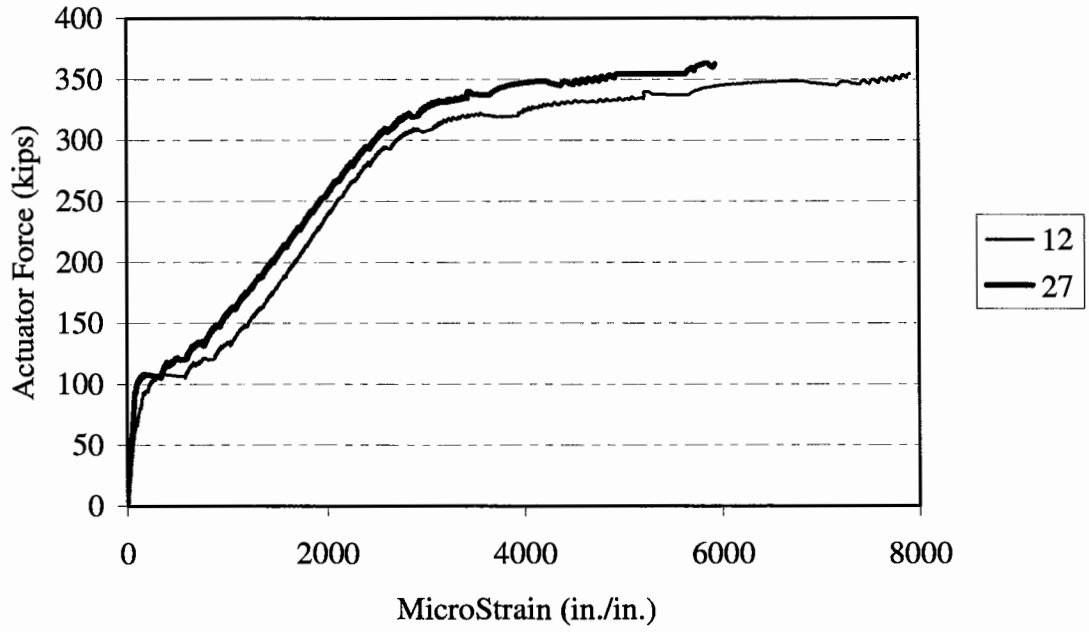

Figure A-14. Specimen 1B Load-Strain History Side (27) vs. Center (12) Transverse Plane.

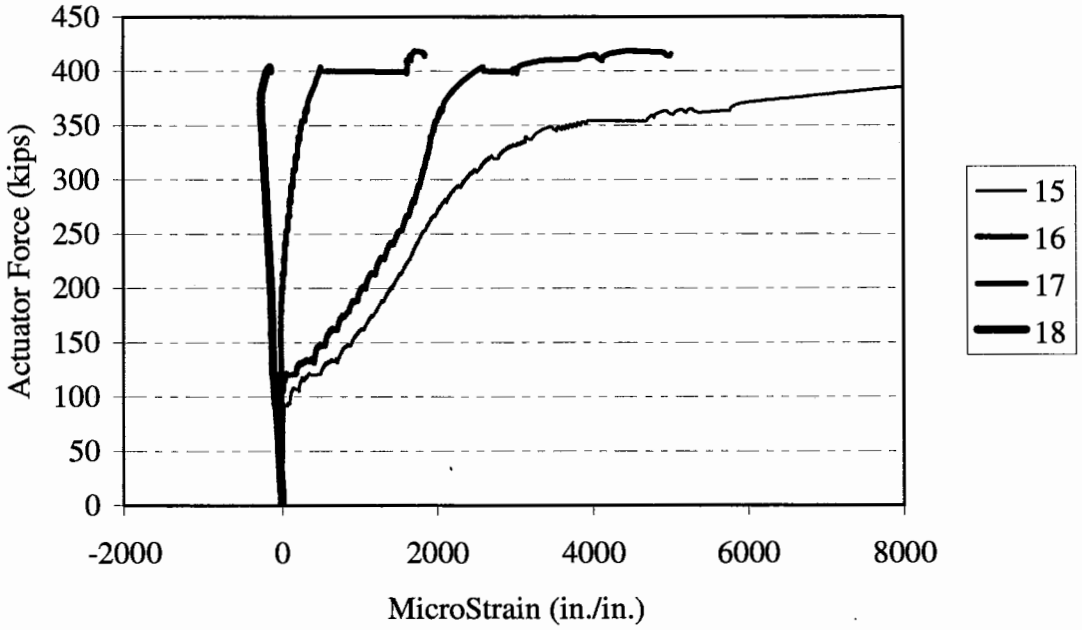

Figure A-15. Specimen 1B Strain Profile Through-Depth Side Face.

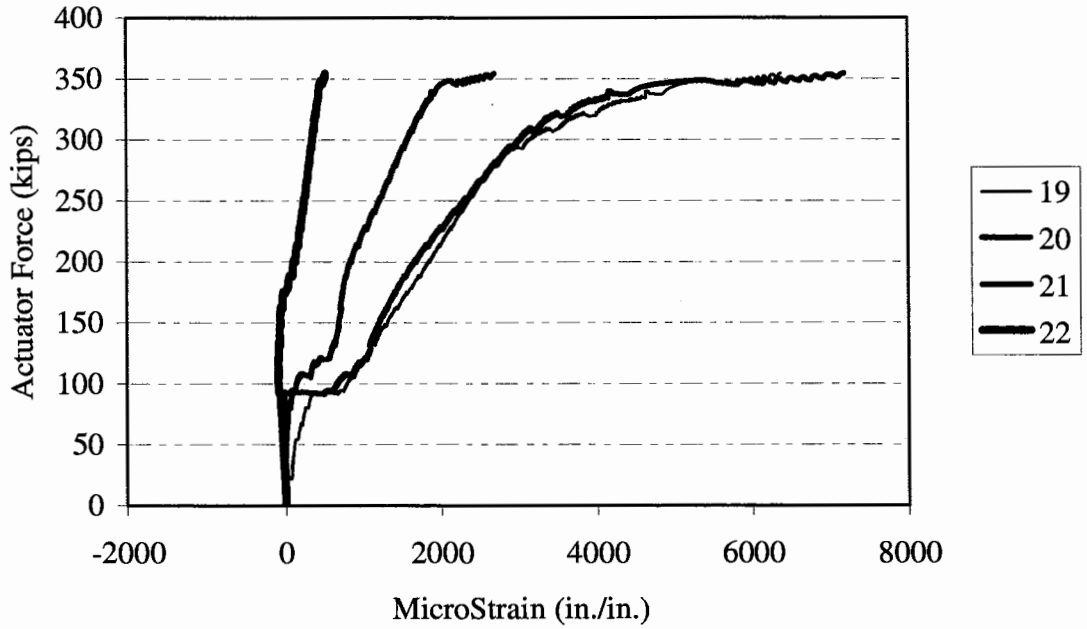

Figure A-16. Specimen 1B Strain Profile Through-Depth Side Face.

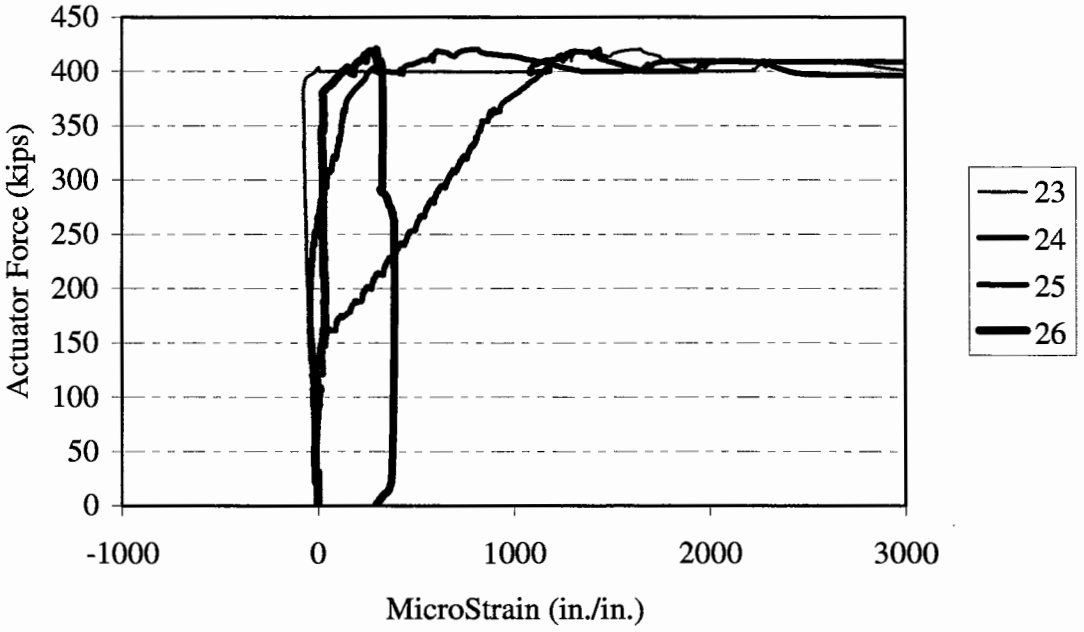

Figure A-17. Specimen 1B Strain Profile Transverse (Stirrup) Reinforcement.

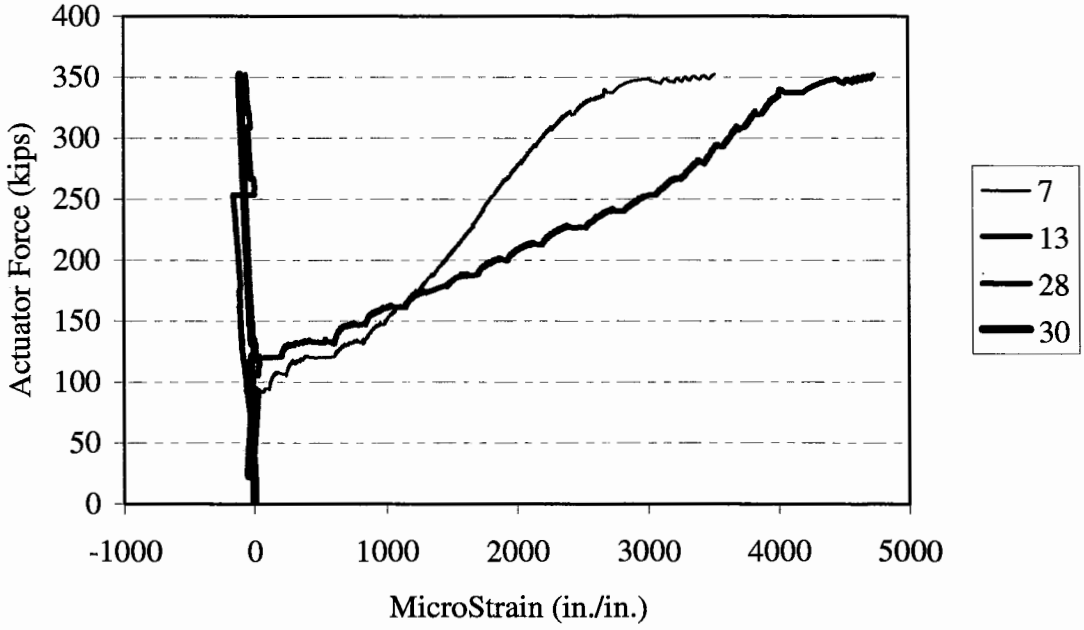

Figure A-18. Specimen 1B Strain Profile Through-Depth Centerline.

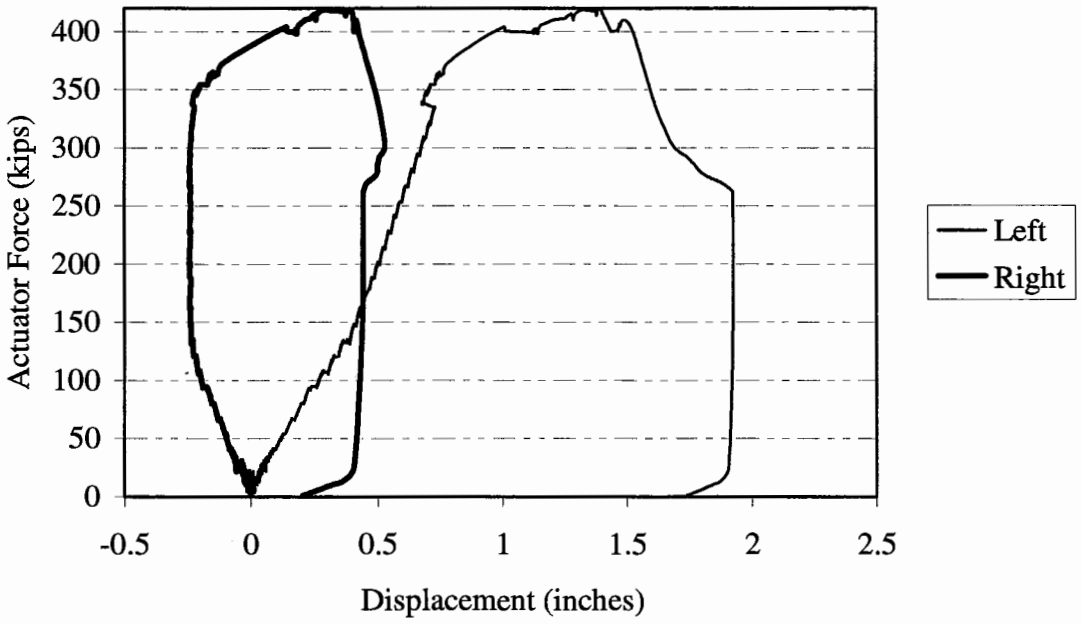

Figure A-19. Specimen 1B Load-Displacement History.

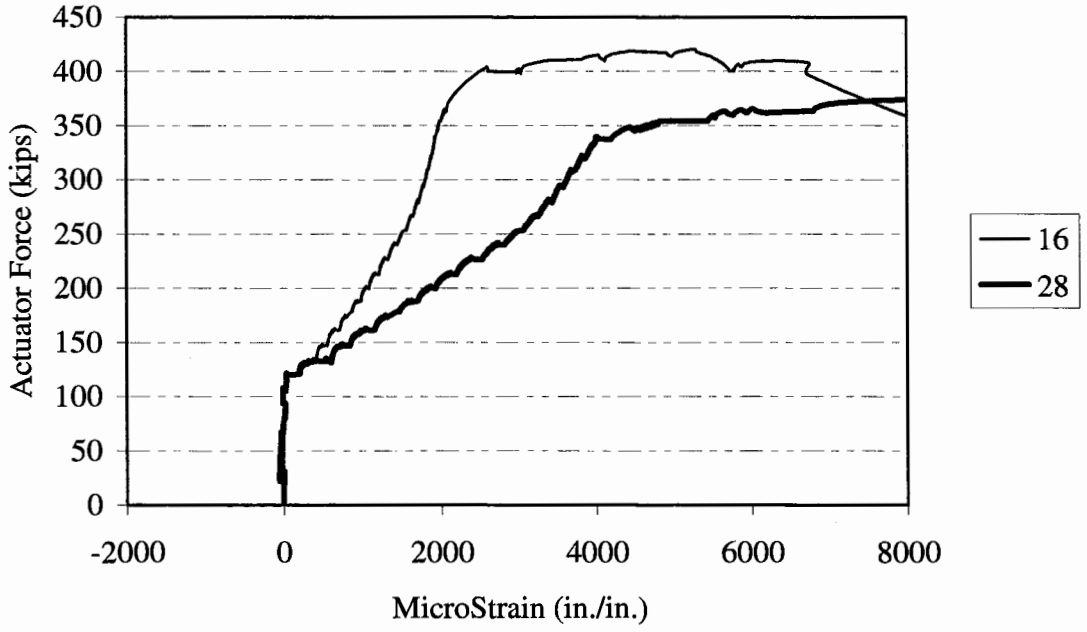

Figure A-20. Specimen 1B Load-Strain History Center (28) vs. Side (16) Transverse Plane.

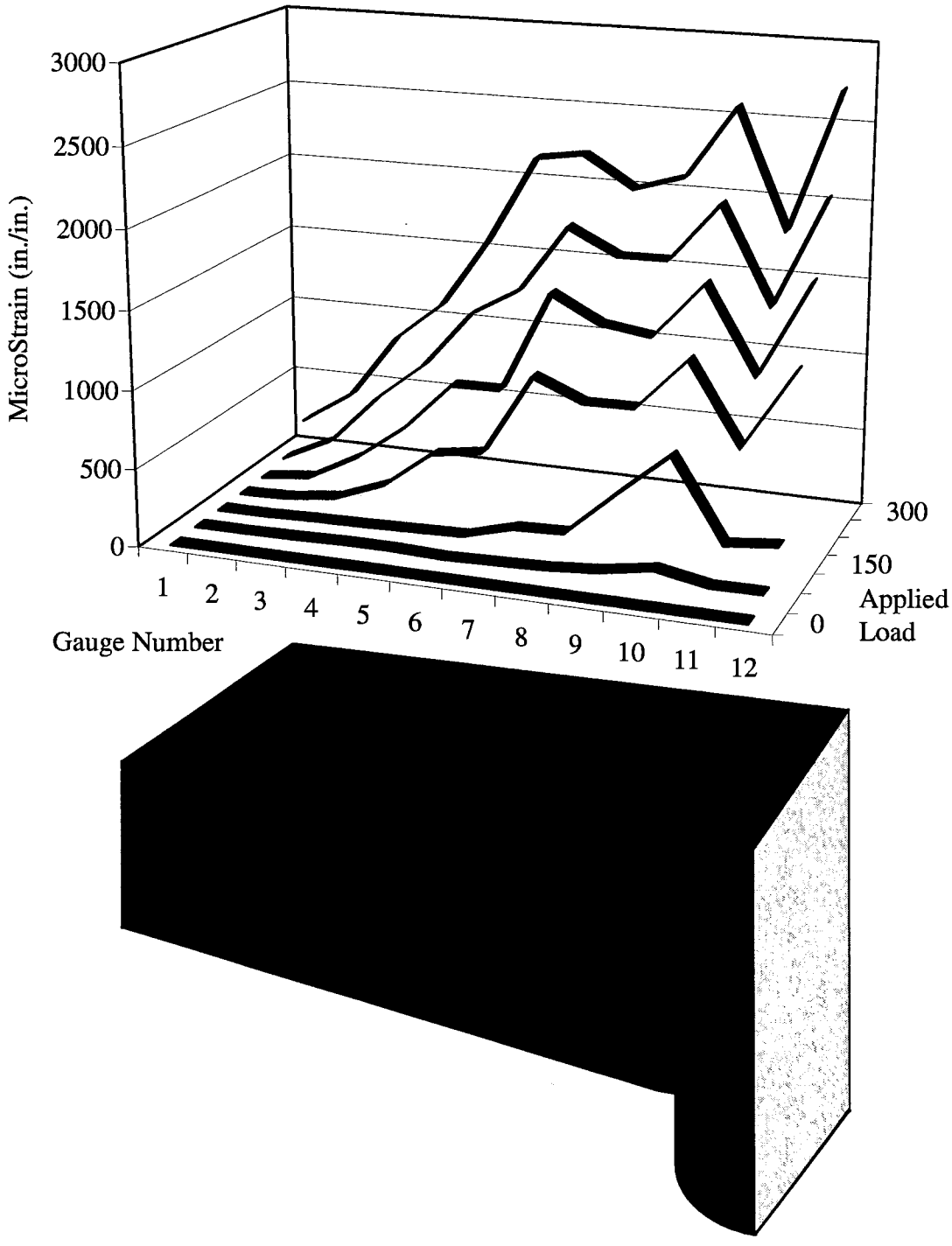

Figure A-21. Specimen 1B Longitudinal Reinforcement Strain Profile for Strain Gauges 1 Through 12.

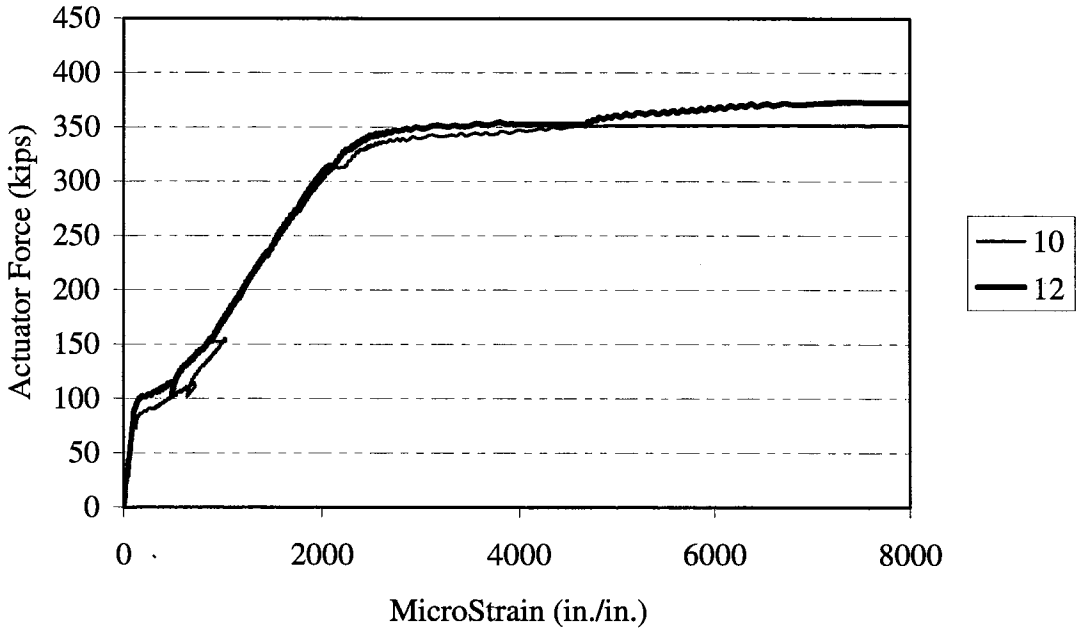

Figure A-22. Specimen 2A Load-Strain History Column Face (10) vs. Column Centerline (12).

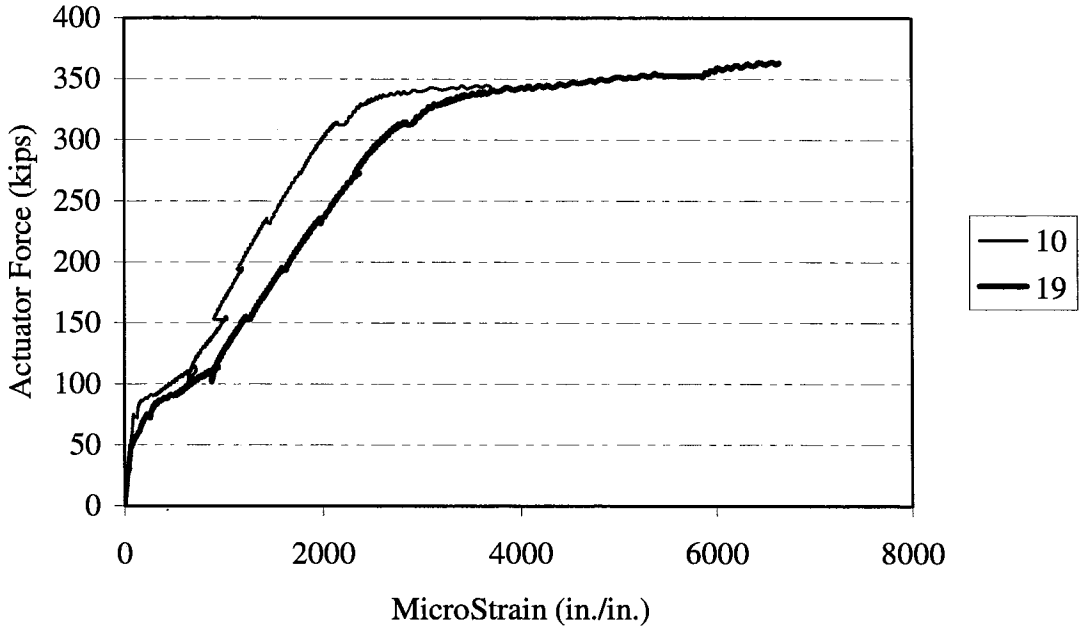

Figure A-23. Specimen 2A Load-Strain History Side (19) vs. Center (10) Transverse Plane.

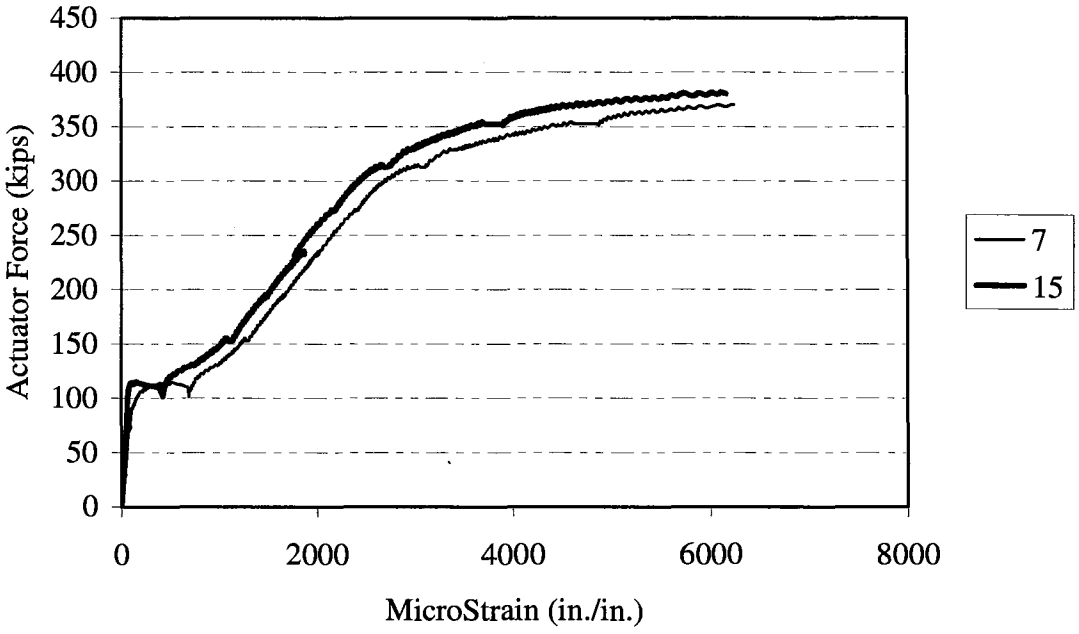

Figure A-24. Specimen 2A Load-Strain History Side (15) vs. Center (7) Transverse Plane.

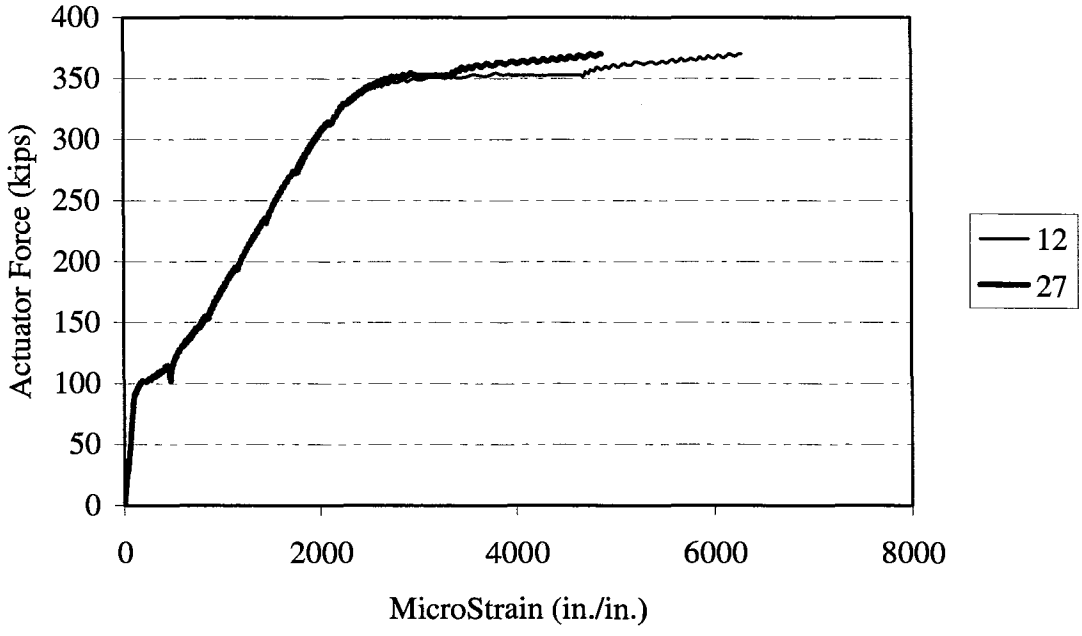

Figure A-25. Specimen 2A Load-Strain History Side (27) vs. Center (12) Transverse Plane.

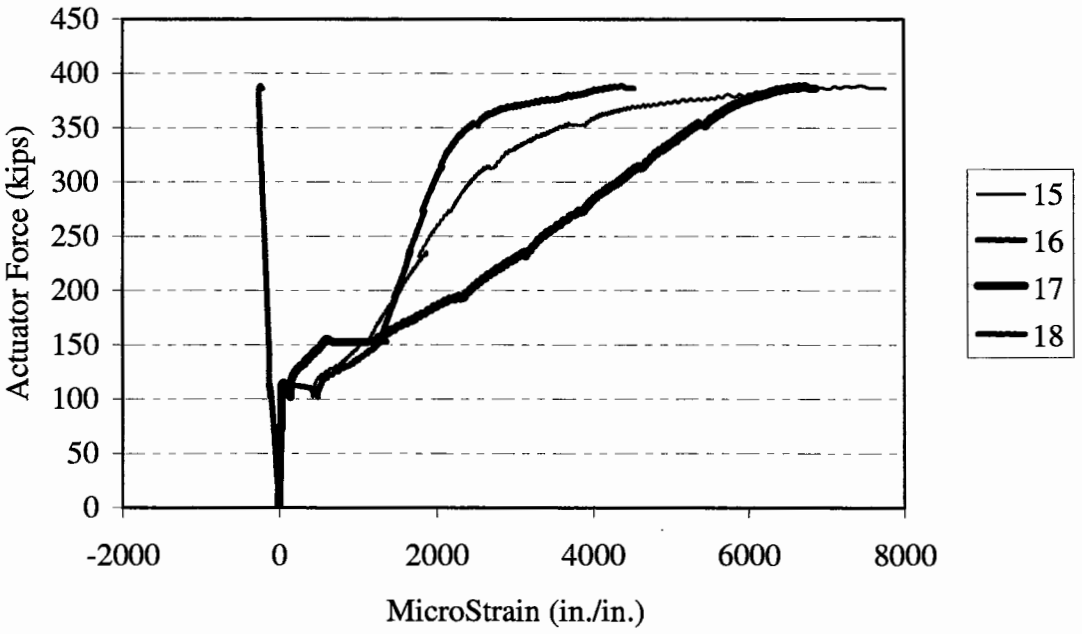

Figure A-26. Specimen 2A Strain Profile Through-Depth Side Face.

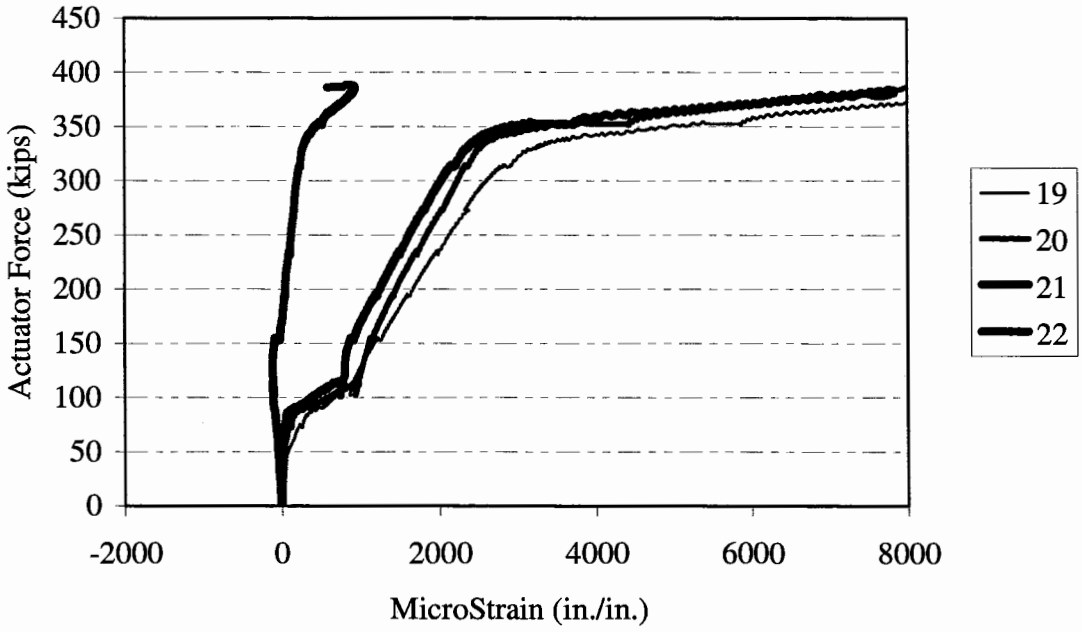

Figure A-27. Specimen 2A Strain Profile Through-Depth Side Face.

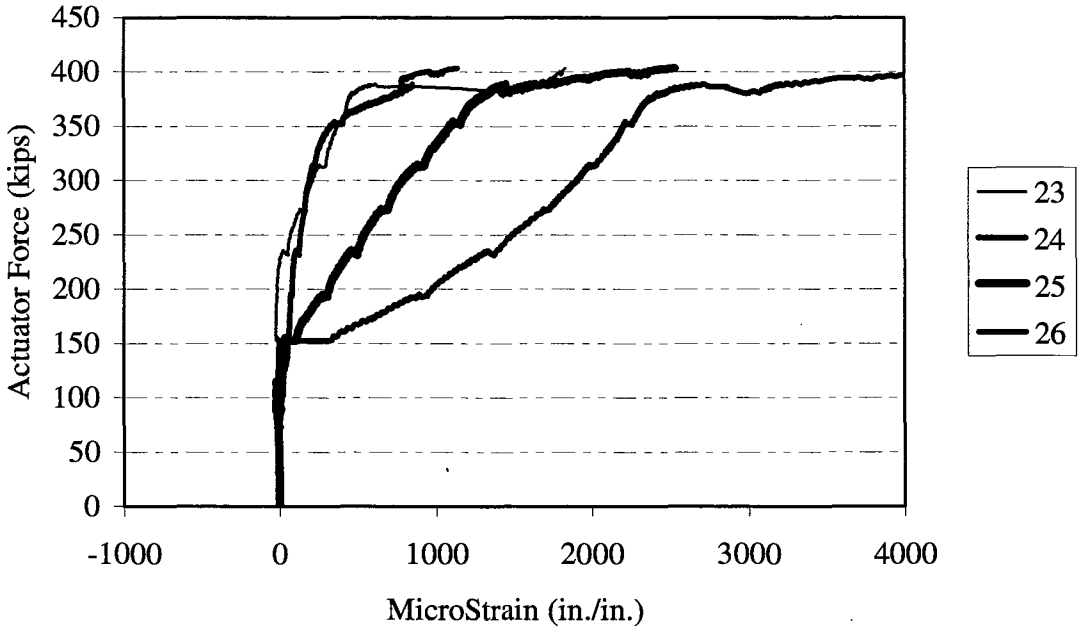

Figure A-28. Specimen 2A Strain Profile Transverse (Stirrup) Reinforcement.

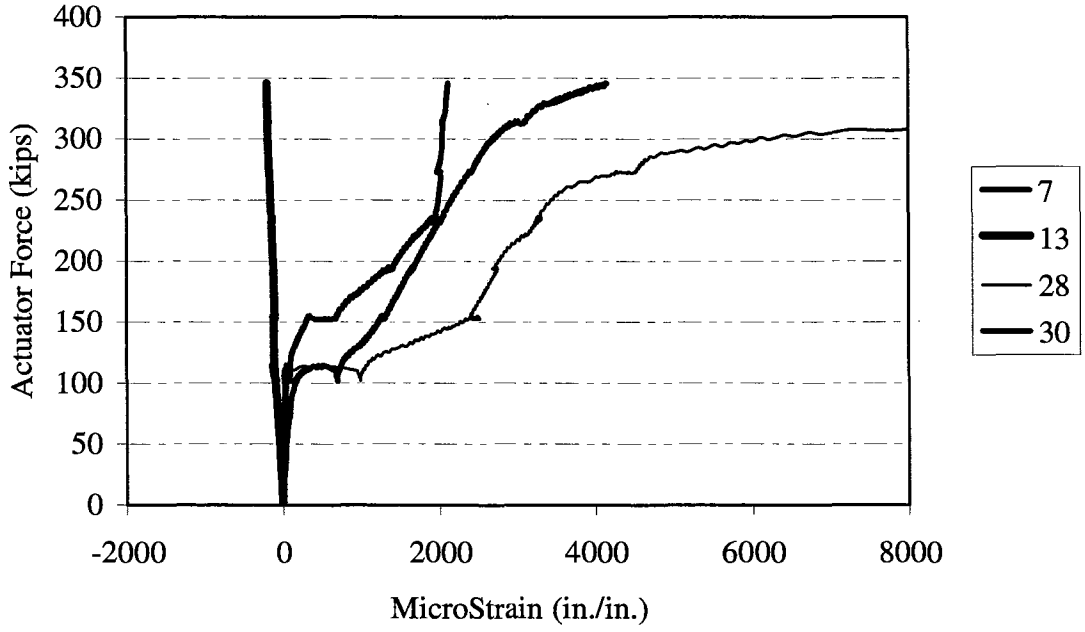

Figure A-29. Specimen 2A Strain Profile Through-Depth Centerline.

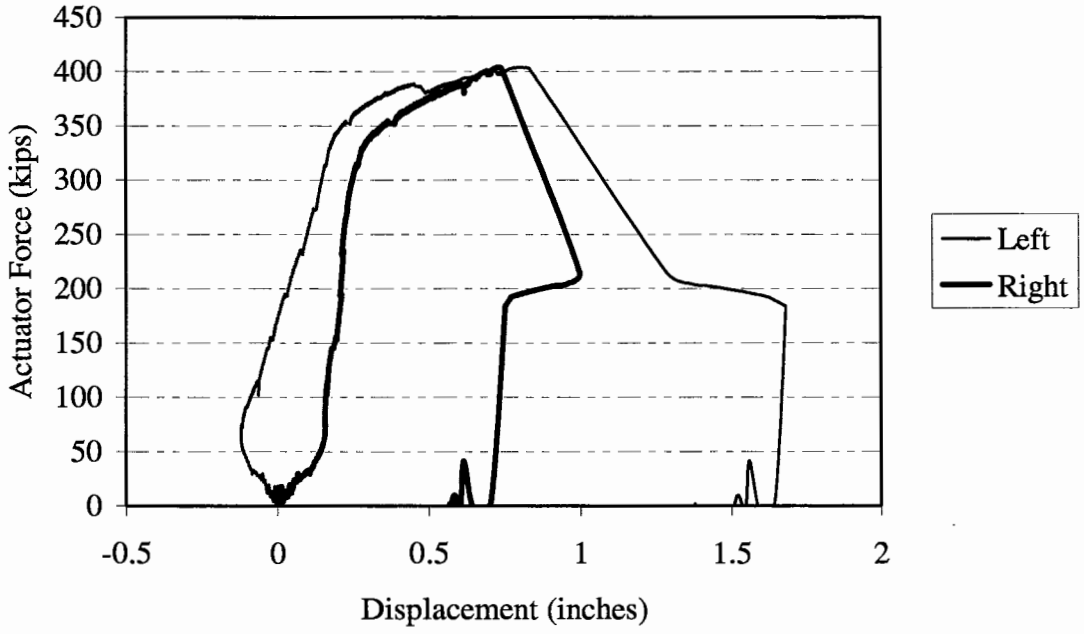

Figure A-30. Specimen 2A Load-Displacement History.

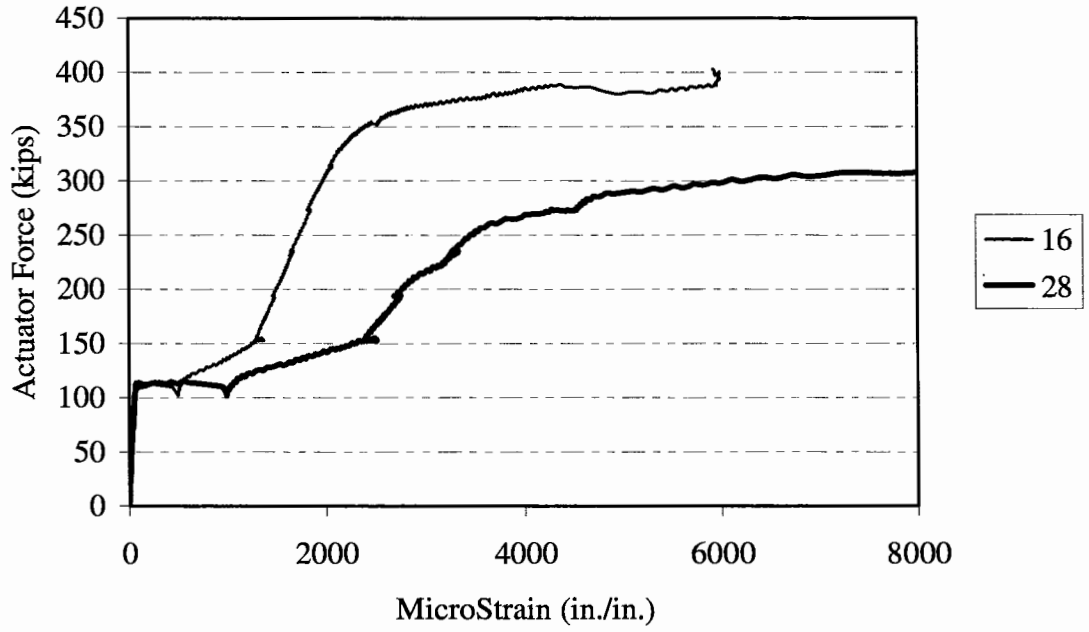

Figure A-31. Specimen 2A Load-Strain History Center (28) vs. Side (16) Transverse Plane.

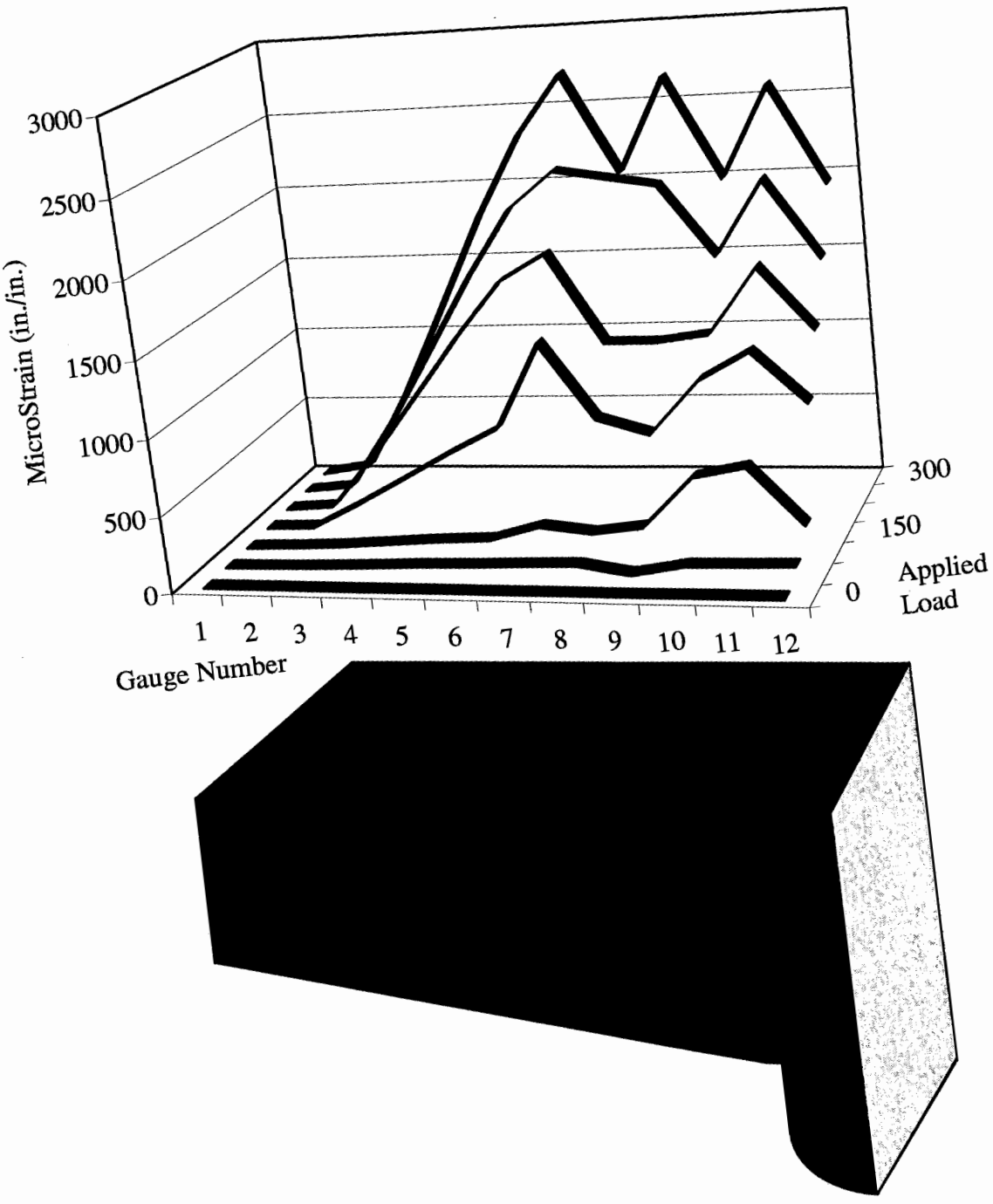

Figure A-32. Specimen 2A Longitudinal Reinforcement Strain Profile for Strain Gauges 1 Through 12.

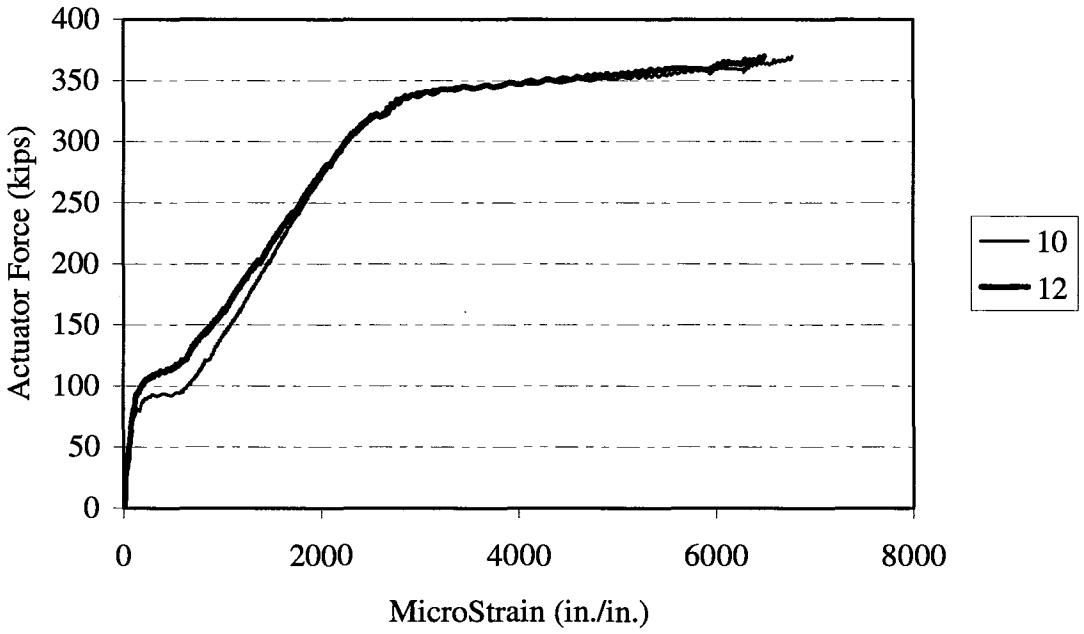

Figure A-33. Specimen 2B Load-Strain History Column Face (10) vs. Column Centerline (12).

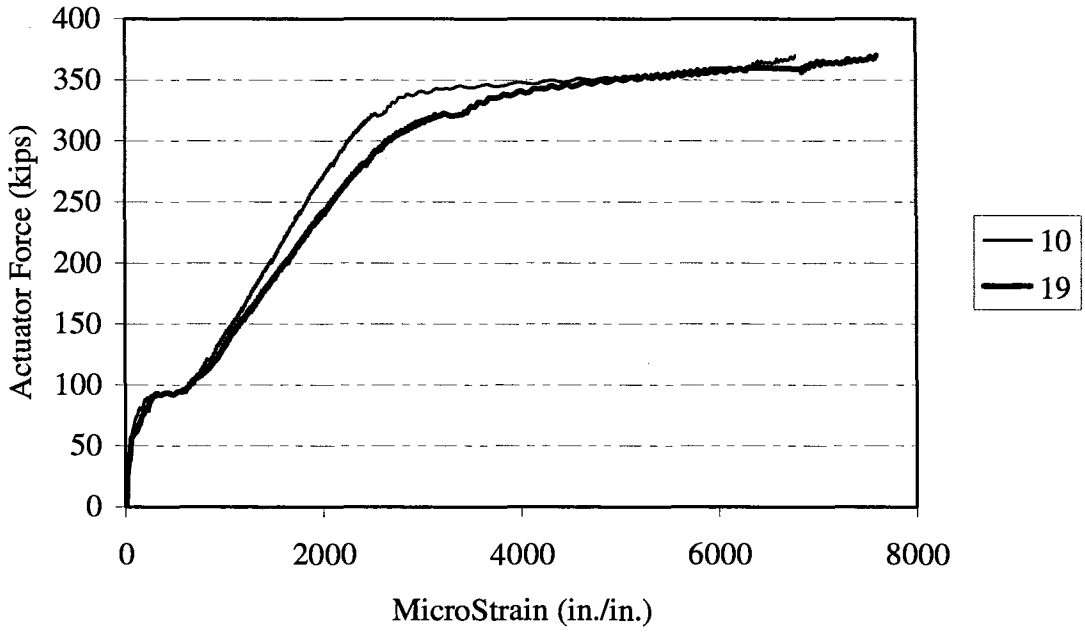

Figure A-34. Specimen 2B Load-Strain History Side (19) vs. Center (10) Transverse Plane.

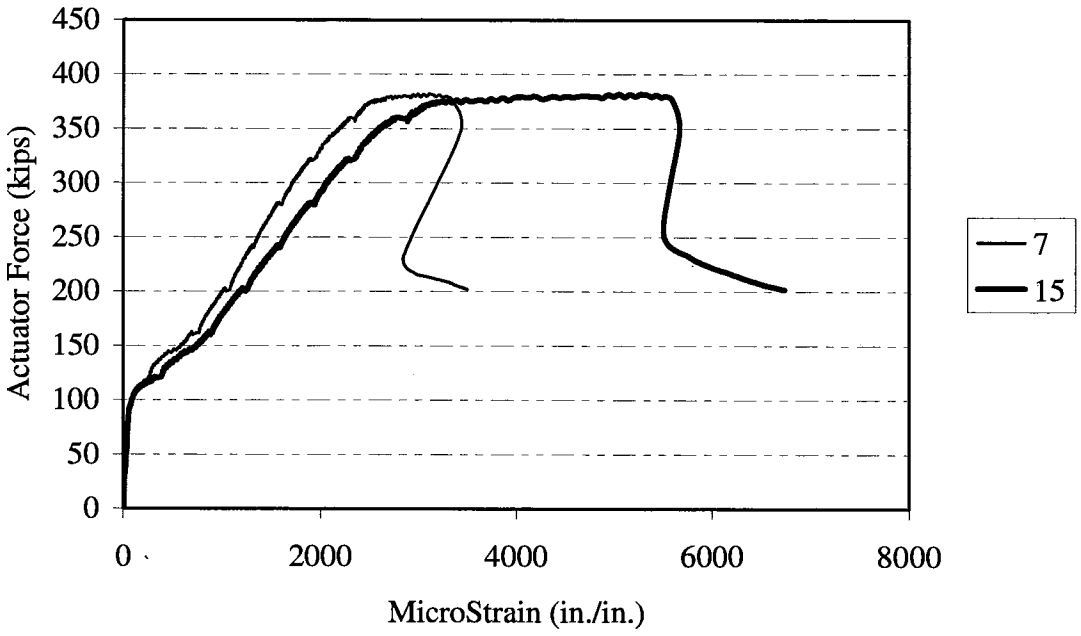

Figure A-35. Specimen 2B Load-Strain History Side (15) vs. Center (7) Transverse Plane.

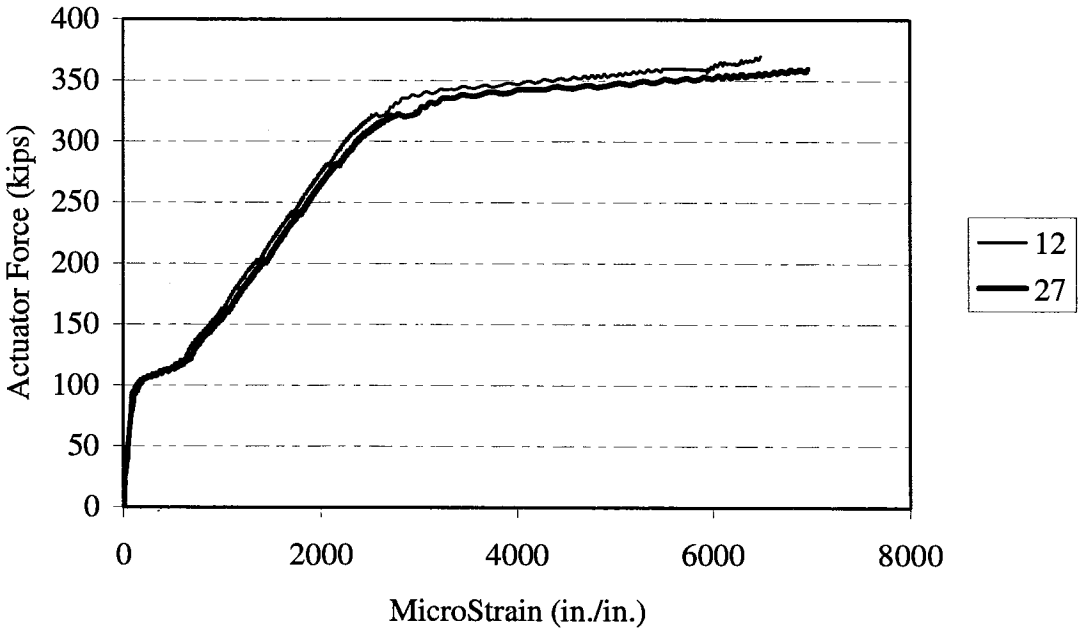

Figure A-36. Specimen 2B Load-Strain History Side (27) vs. Center (12) Transverse Plane.

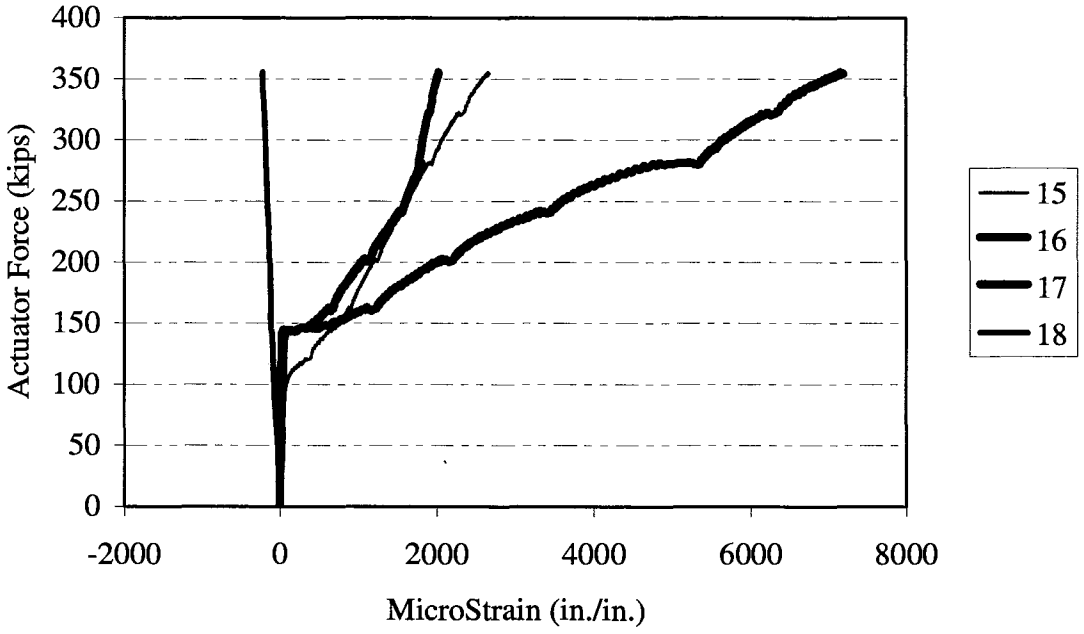

Figure A-37. Specimen 2B Strain Profile Through-Depth Side Face.

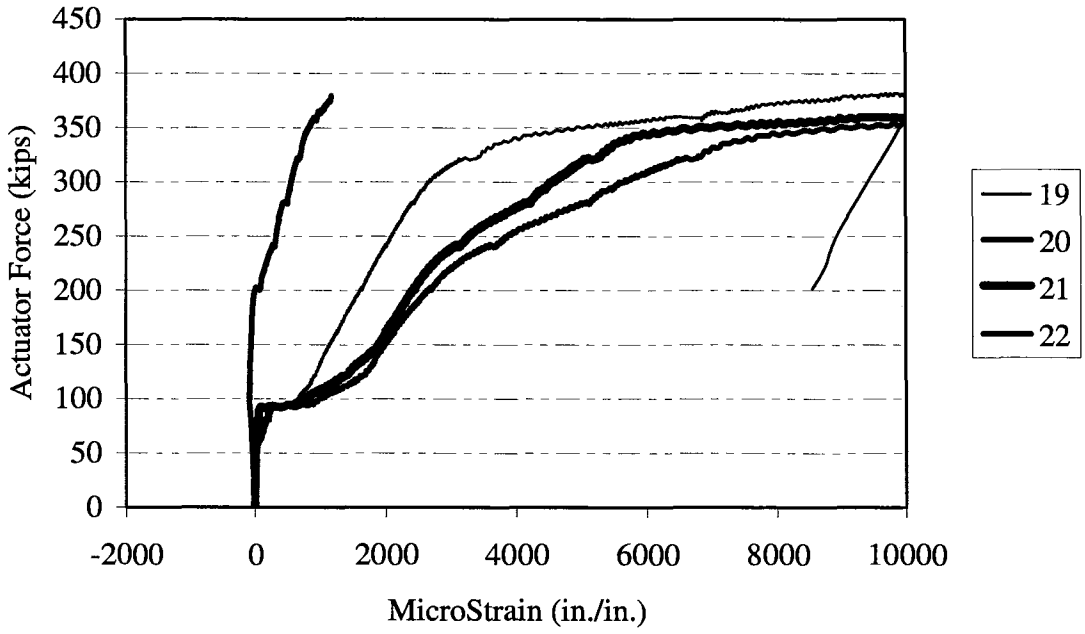

Figure A-38. Specimen 2B Strain Profile Though-Depth Side Face.

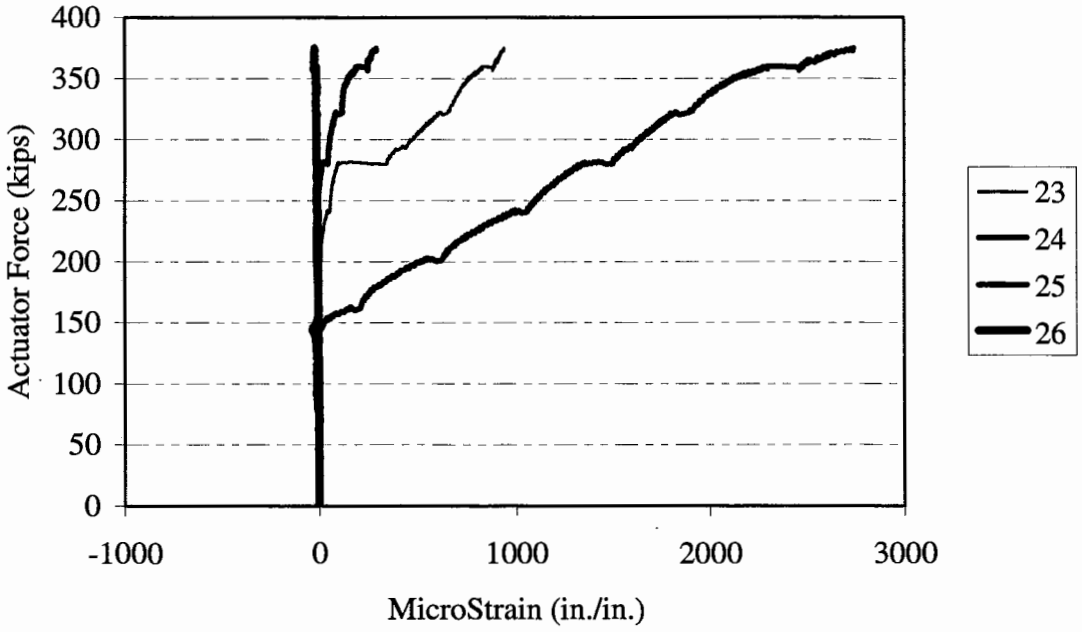

Figure A-39. Specimen 2B Strain Profile Transverse (Stirrup) Reinforcement.

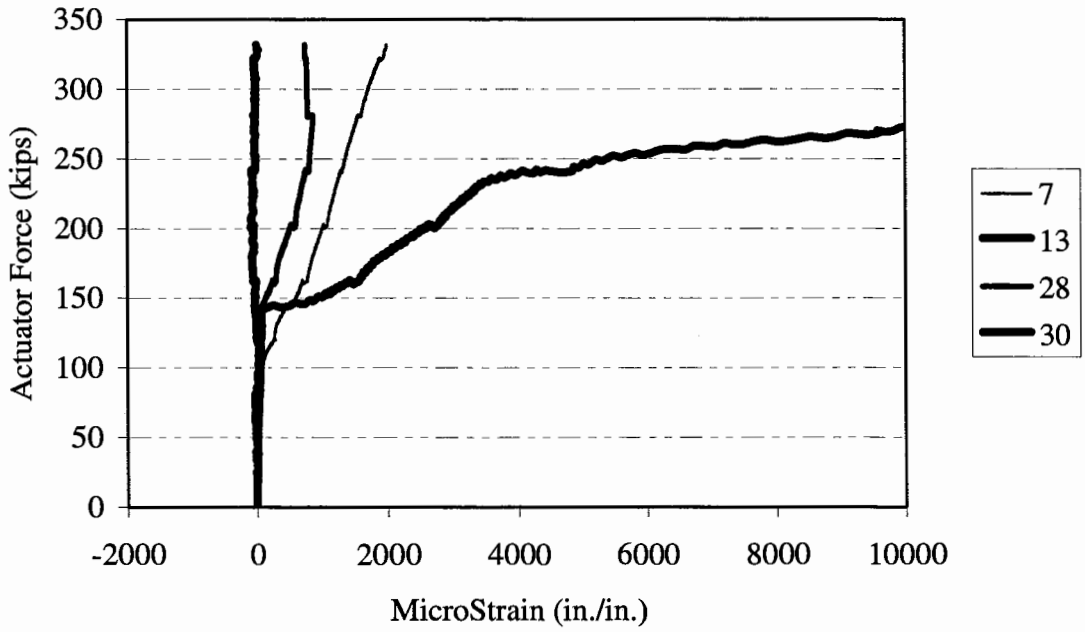

Figure A-40. Specimen 2B Strain Profile Through-Depth Centerline.

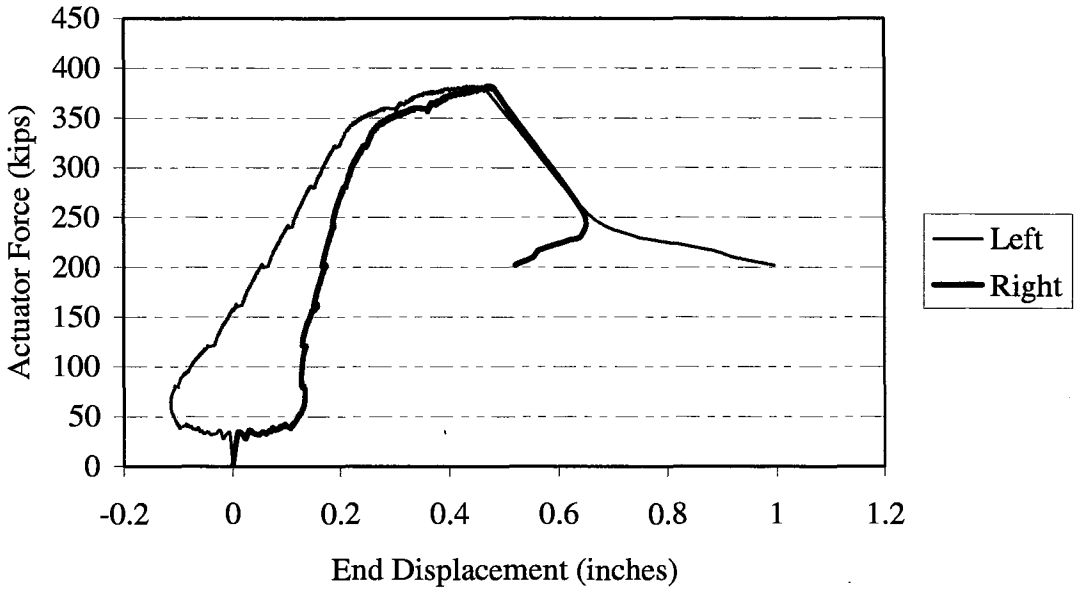

Figure A-41. Specimen 2B Load-Displacement History.

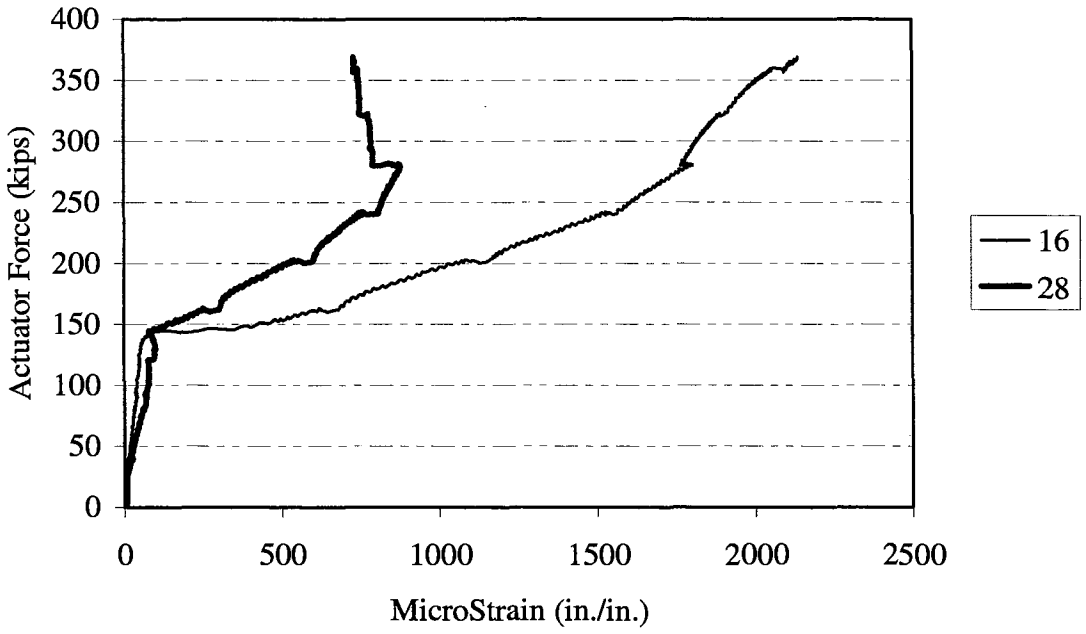

Figure A-42. Specimen 2B Load-Strain History Center (28) vs. Side (16) Transverse Plane.

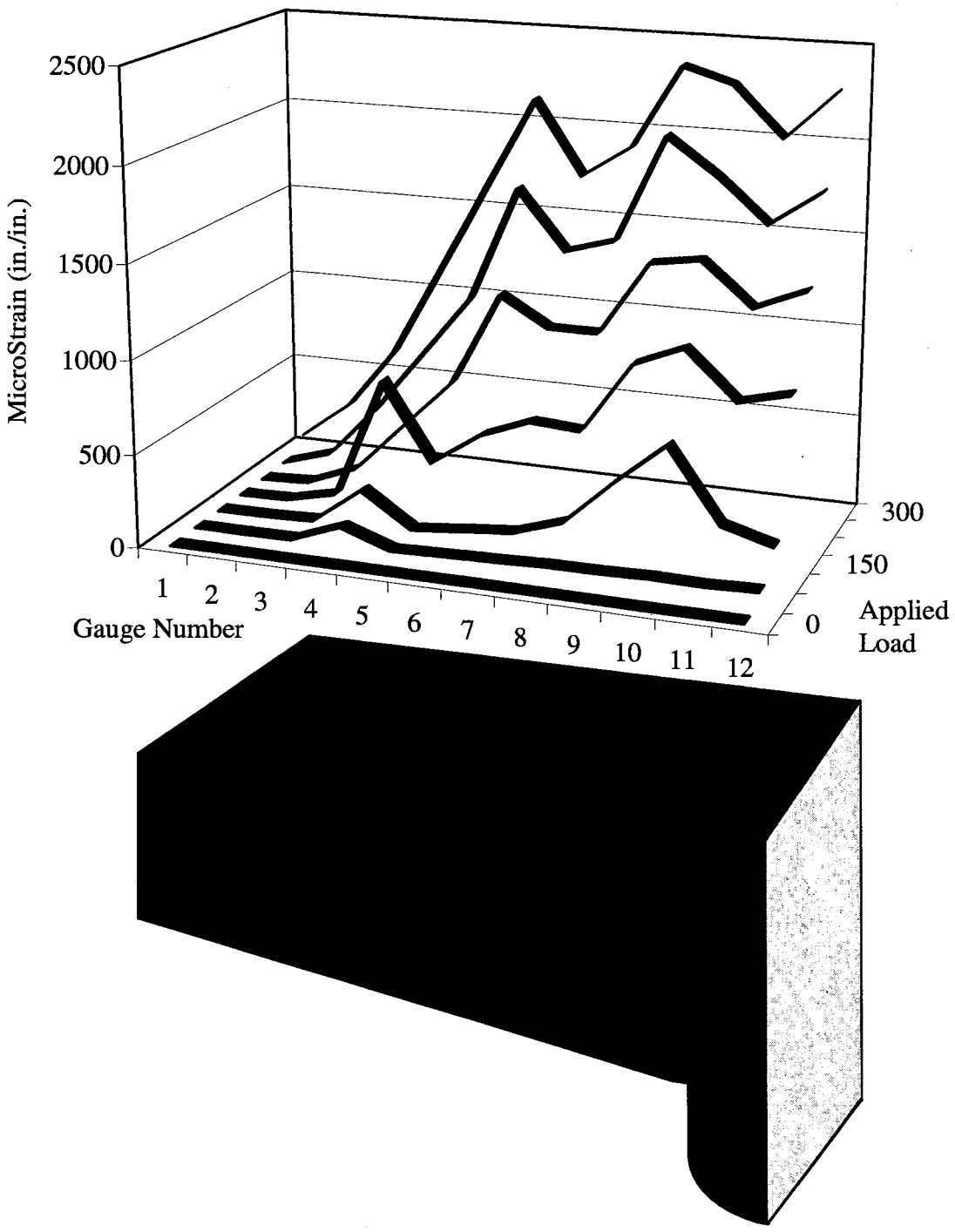

Figure A-43. Specimen 2B Longitudinal Reinforcement Strain Profile for Strain Gauges 1 Through 12.

APPENDIX B

GROUP #2 EXPERIMENTAL RESULTS

For this Appendix:

- The graphical data were intentionally terminated in order to reflect only that portion of testing necessary for illustrating a particular trend. Therefore, termination of the data series does not indicate failure of the specimen or completion of testing.

- Refer to Fig. 3.7 for illustration of strain gauge identification and locations.

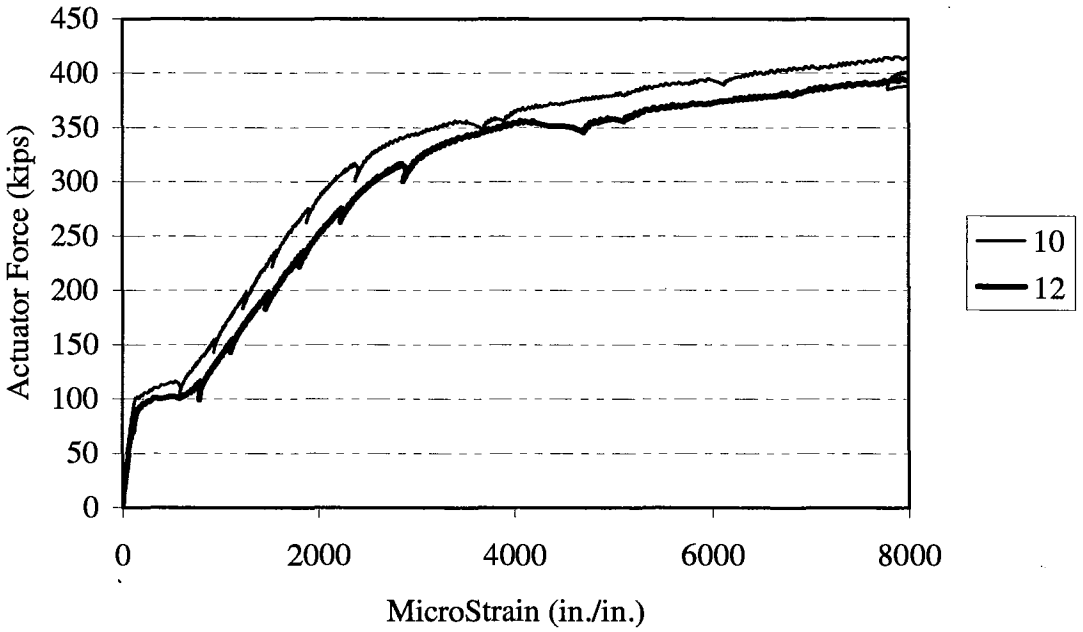

Figure B-1. Specimen 3C Load-Strain History Column Face (10) vs. Column Centerline (12).

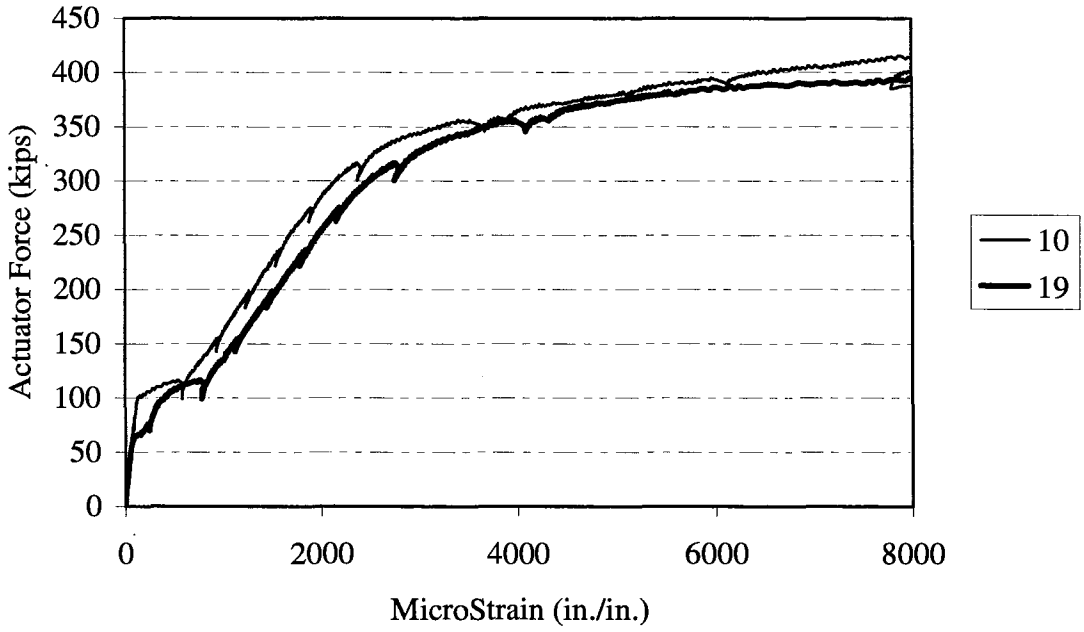

Figure B-2. Specimen 3C Load-Strain History Side (19) vs. Center (10) Transverse Plane.

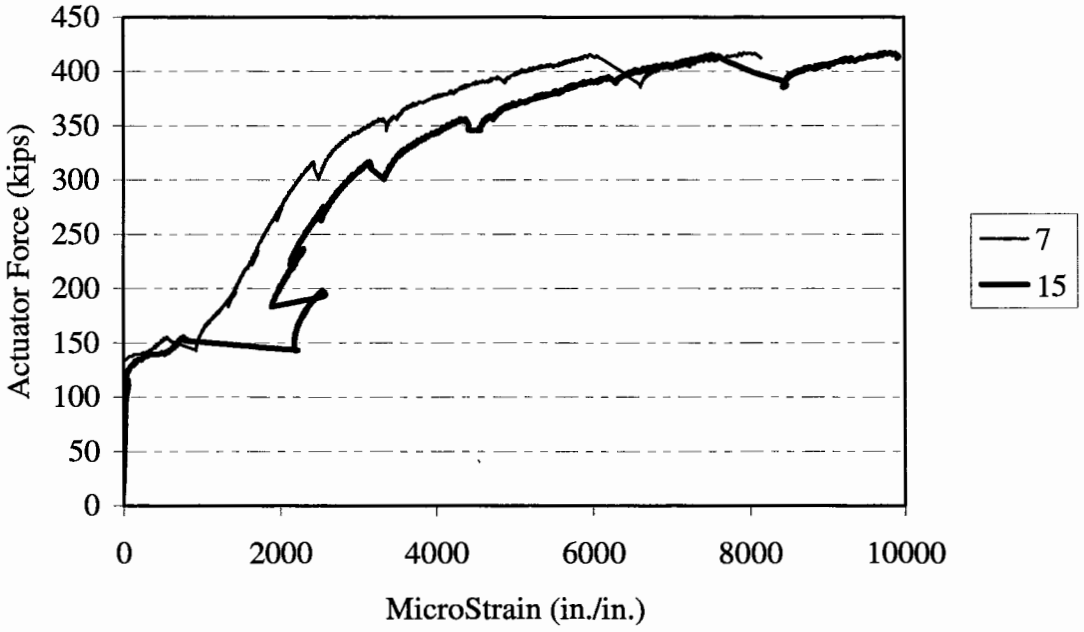

Figure B-3. Specimen 3C Load-Strain History Side (15) vs. Center (7) Transverse Plane.

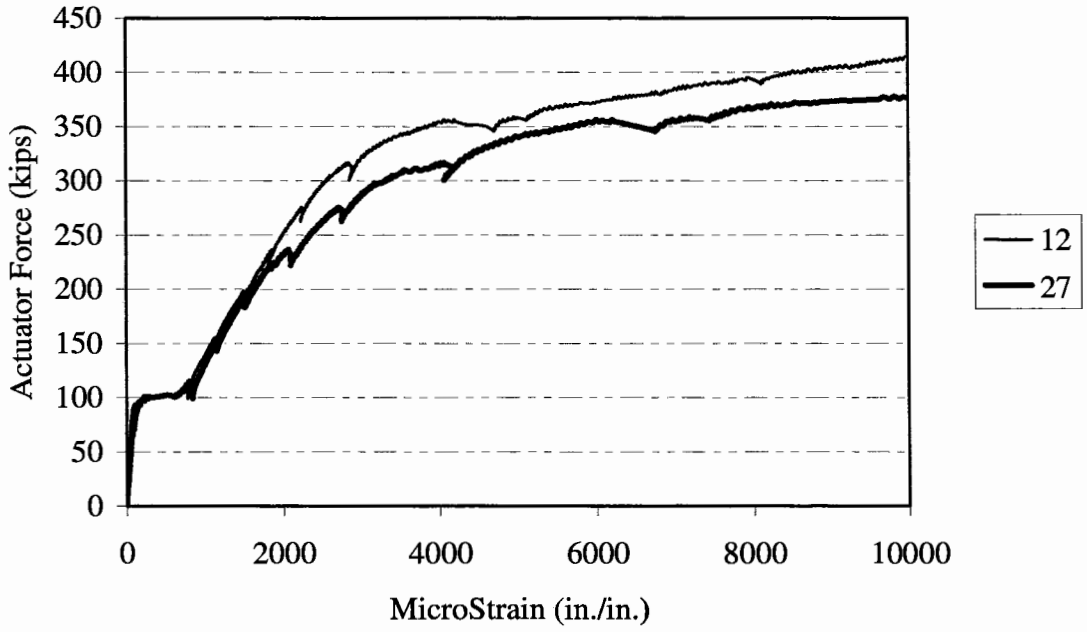

Figure B-4. Specimen 3C Load-Strain History Side (27) vs. Center (12) Transverse Plane.

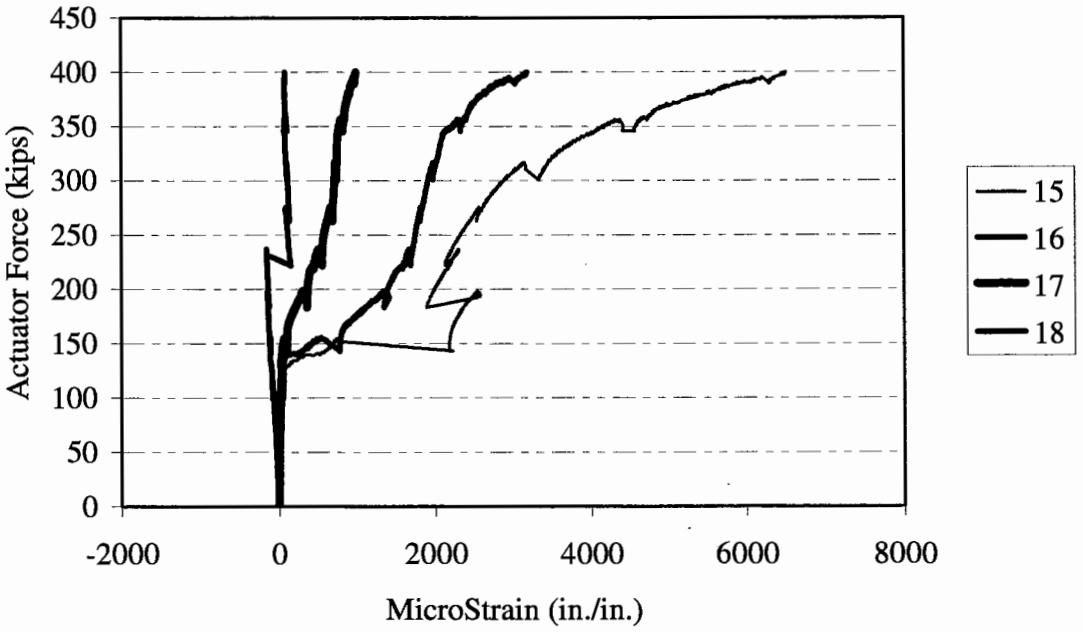

Figure B-5. Specimen 3C Strain Profile Through-Depth Side Face.

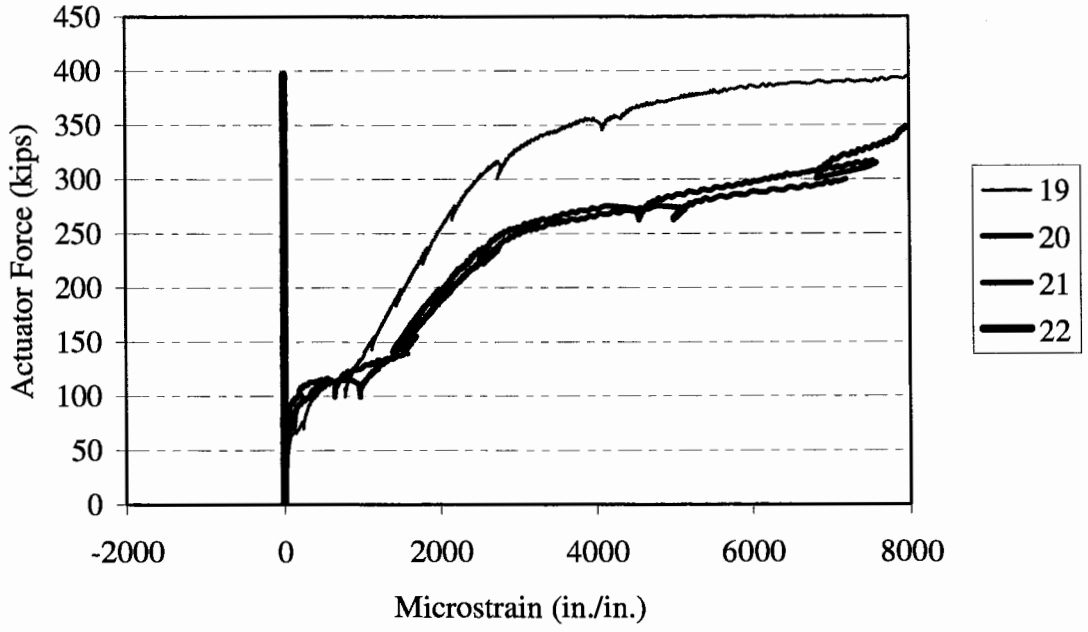

Figure B-6. Specimen 3C Strain Profile Through-Depth Side Face.

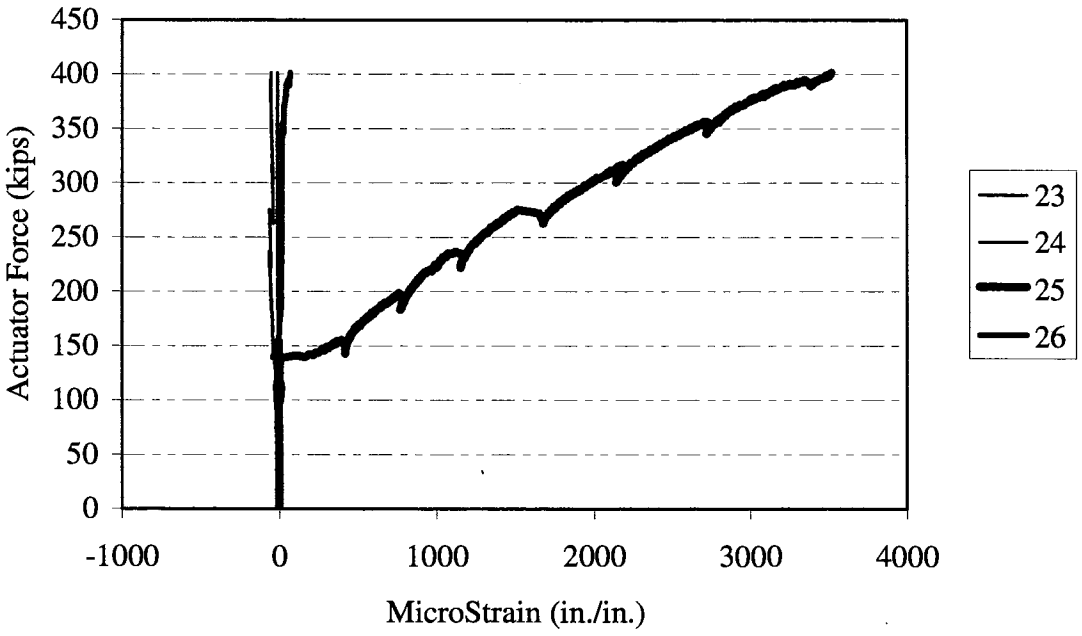

Figure B-7. Specimen 3C Strain Profile Transverse (Stirrup) Reinforcement.

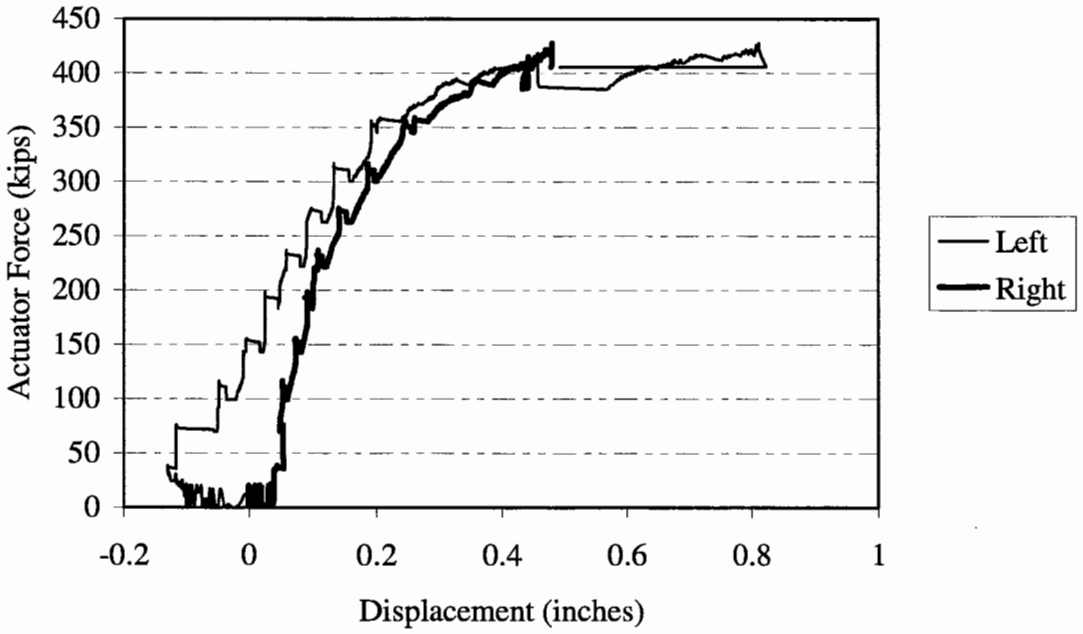

Figure B-8. Specimen 3C Load-Displacement History.

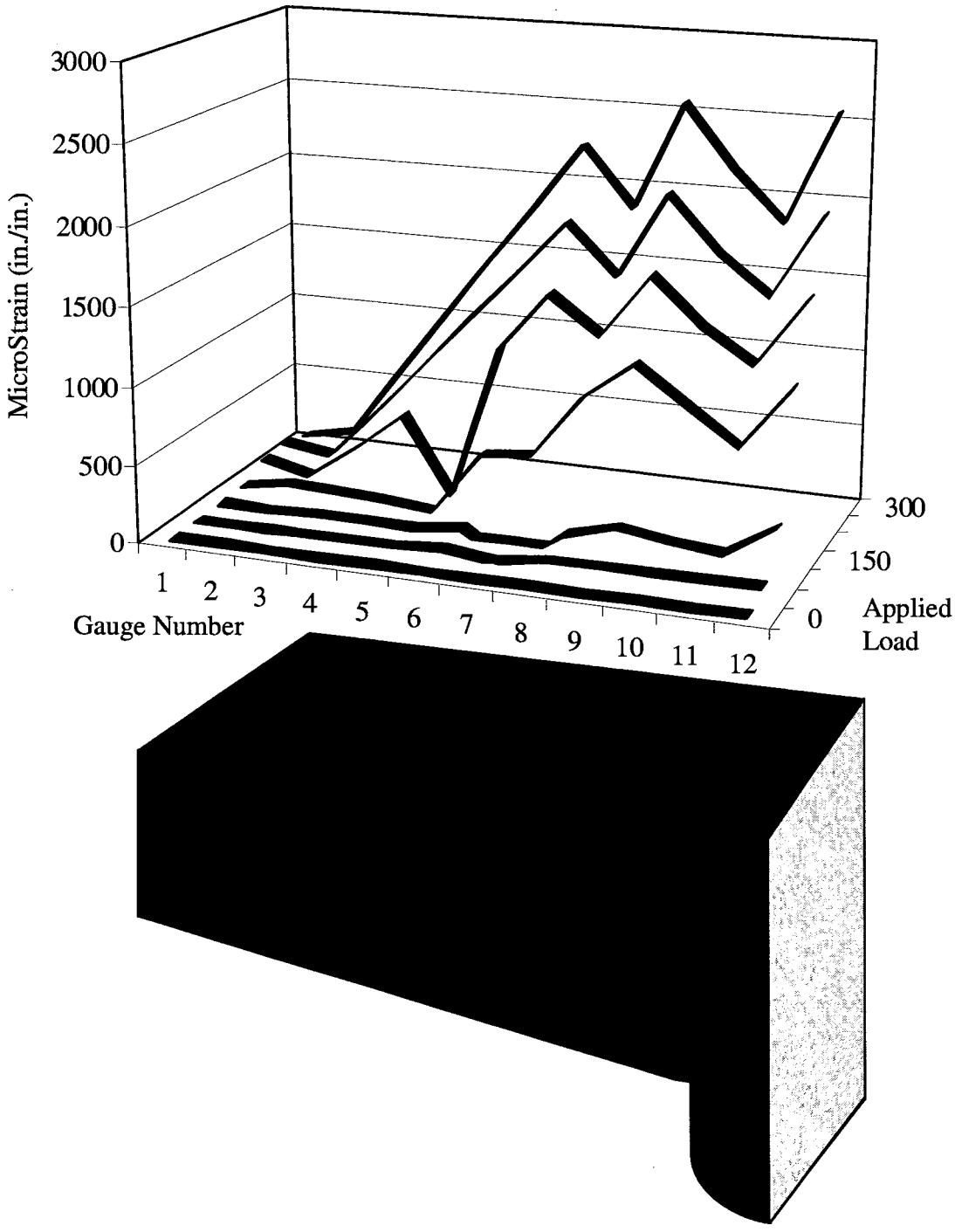

Figure B-9. Specimen 3C Longitudinal Reinforcement Strain Profile for Strain Gauges 1 Through 12.

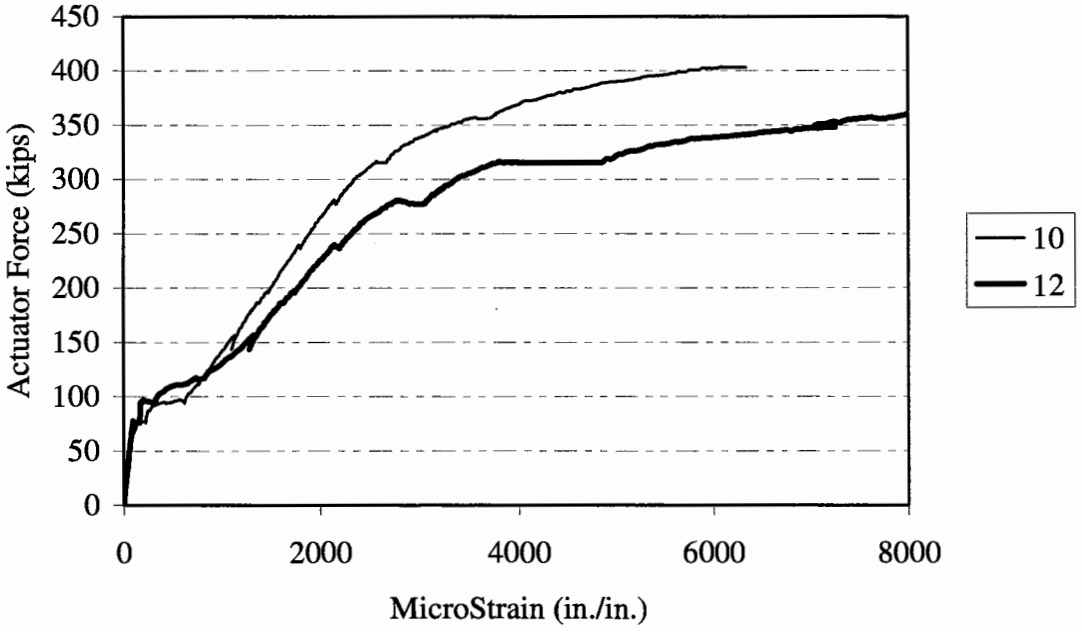

Figure B-10. Specimen 3D Load-Strain History Column Face (10) vs. Column Centerline (12).

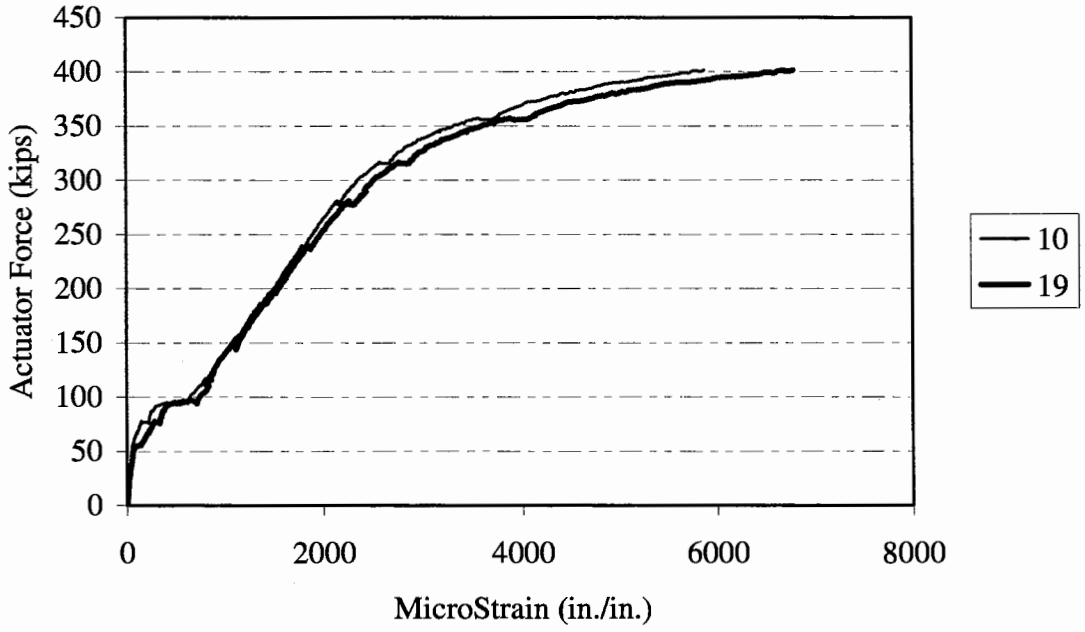

Figure B-11. Specimen 3D Load-Strain History Side (19) vs. Center (10) Transverse Plane.

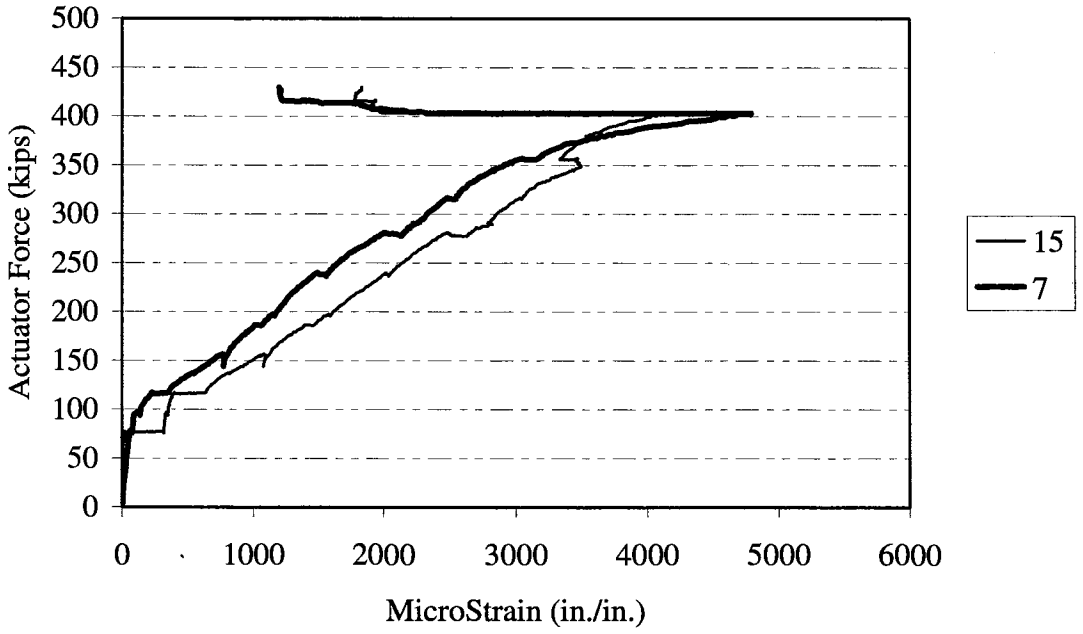

Figure B-12. Specimen 3D Load-Strain History Side (15) vs. Center (7) Transverse Plane.

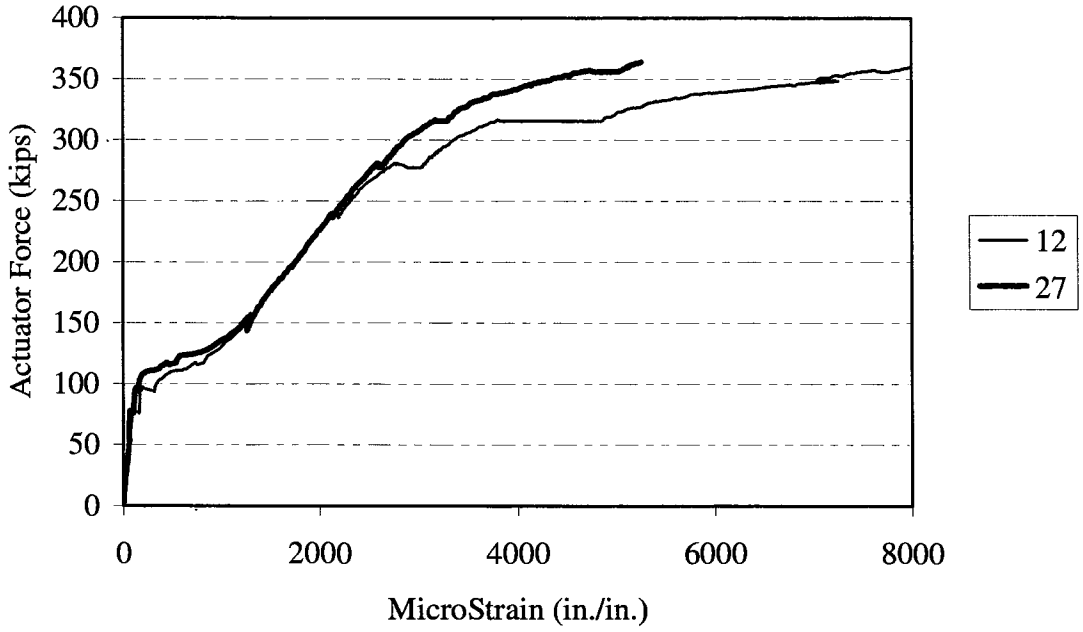

Figure B-13. Specimen 3D Load-Strain History Side (27) vs. Center (12) Transverse Plane.

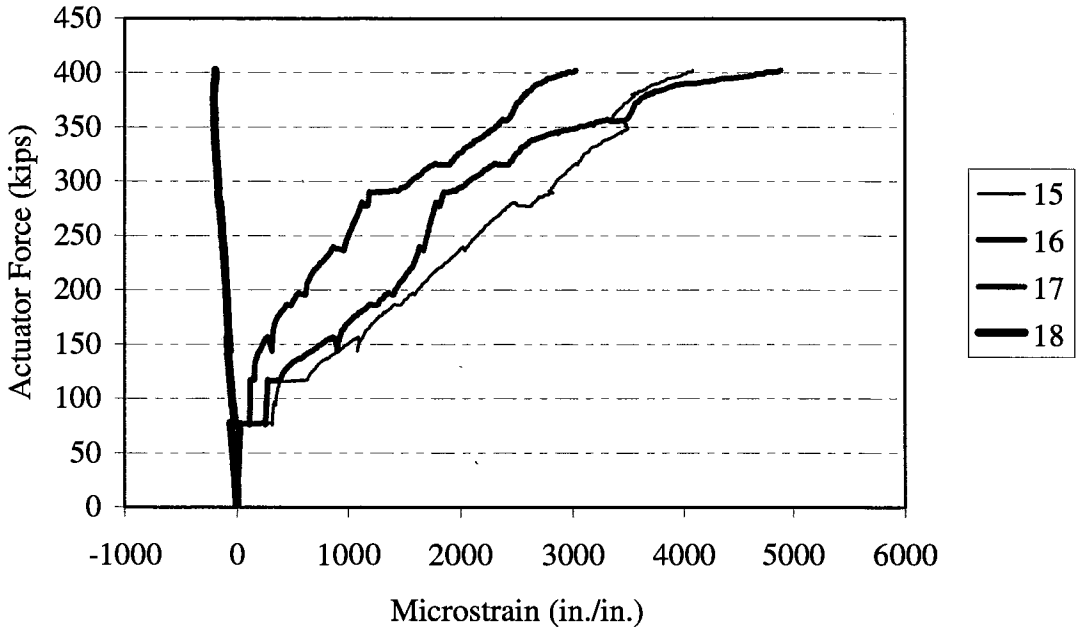

Figure B-14. Specimen 3D Strain Profile Through-Depth Side Face.

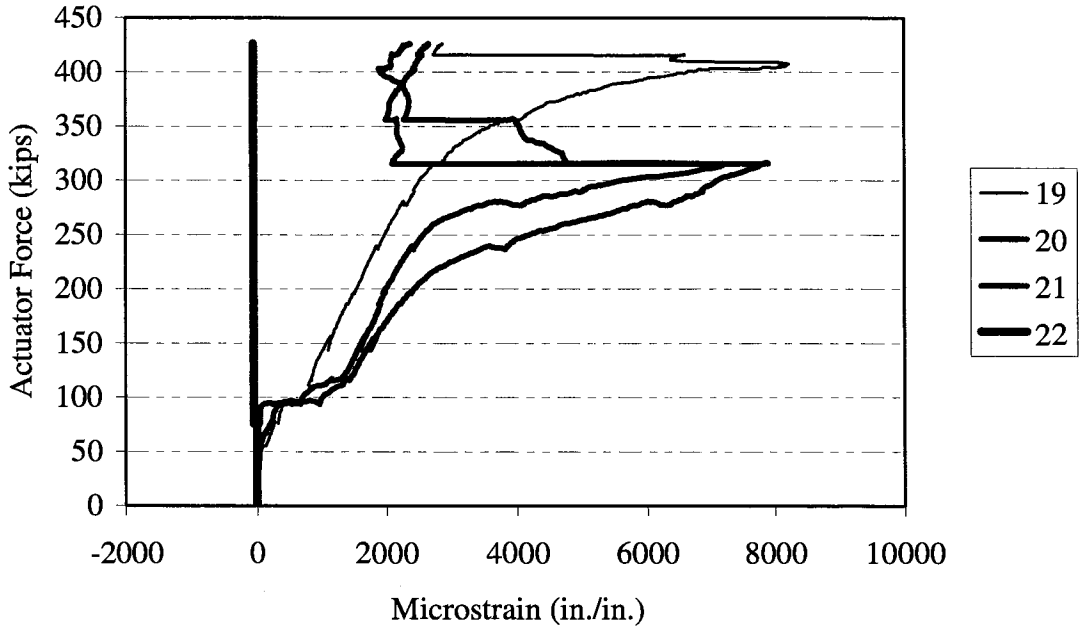

Figure B-15. Specimen 3D Strain Profile Through-Depth Side Face.

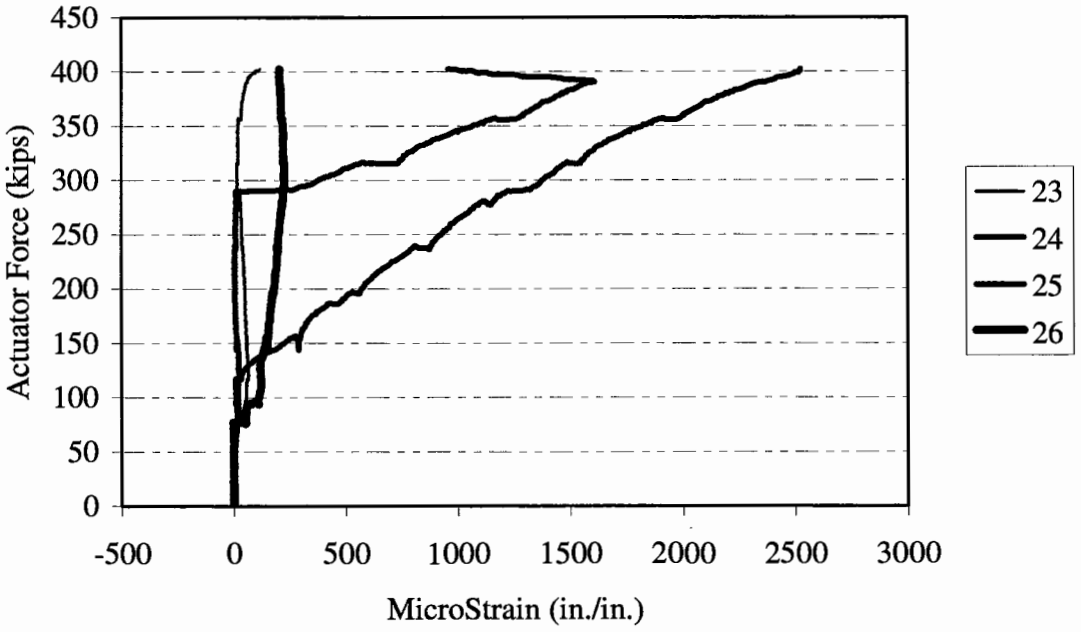

Figure B-16. Specimen 3D Strain Profile Transverse (Stirrup) Reinforcement.

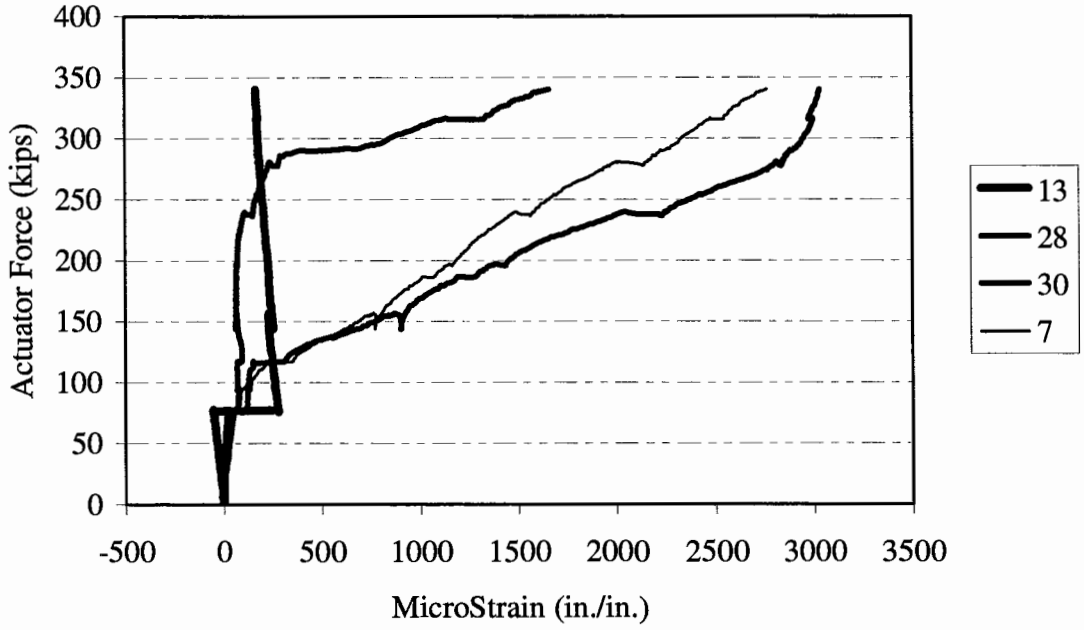

Figure B-17. Specimen 3D Strain Profile Through-Depth Centerline.

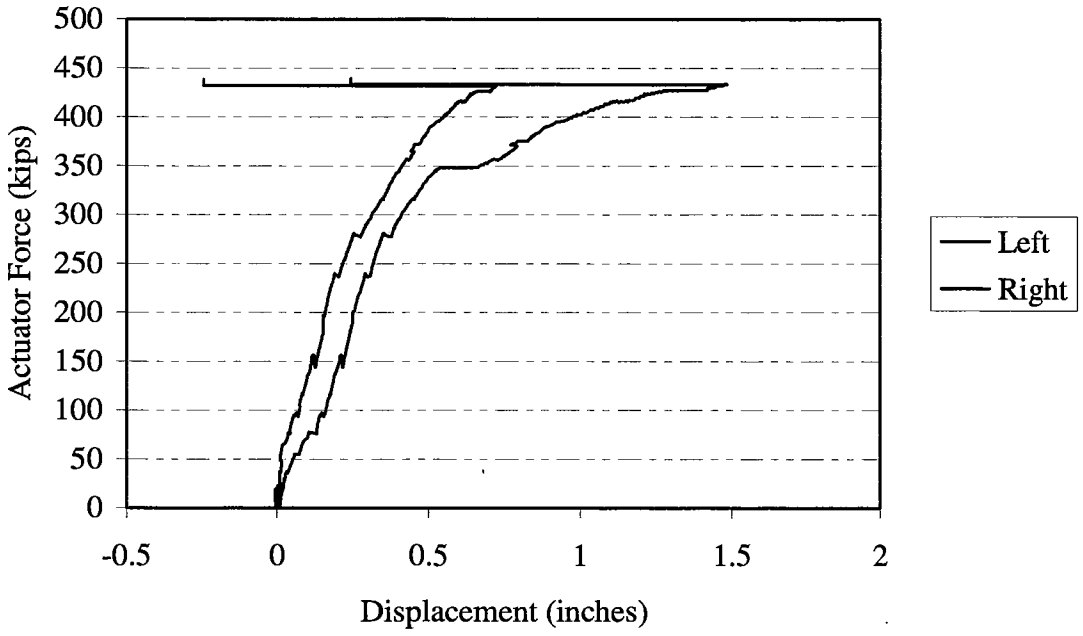

Figure B-18. Specimen 3D Load-Displacement History.

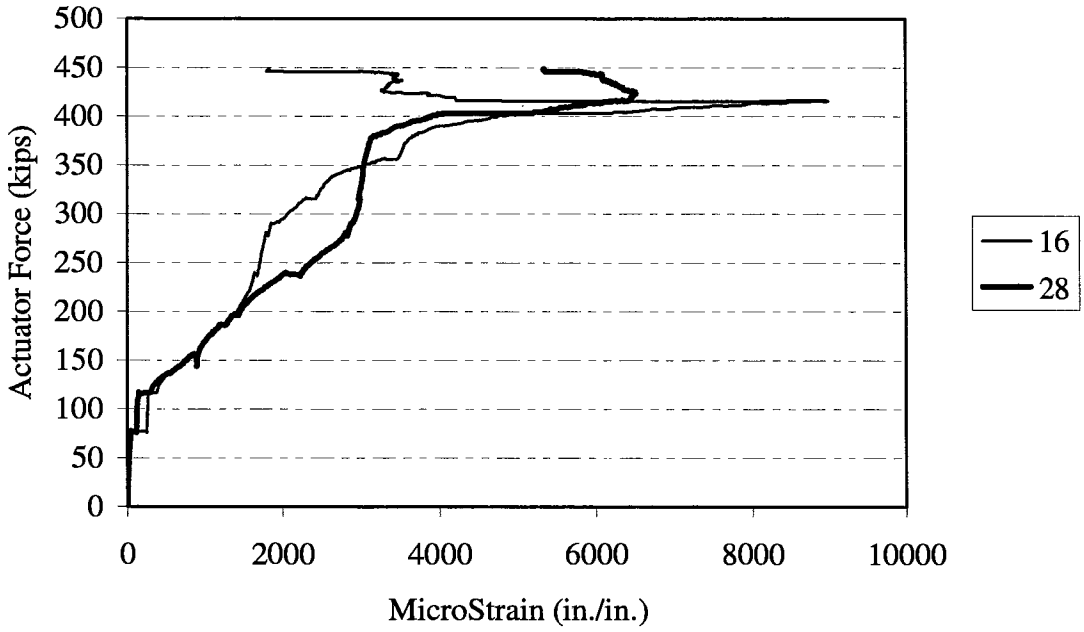

Figure B-19. Specimen 3D Load-Strain History Center (28) vs. Side (16) Transverse Plane.

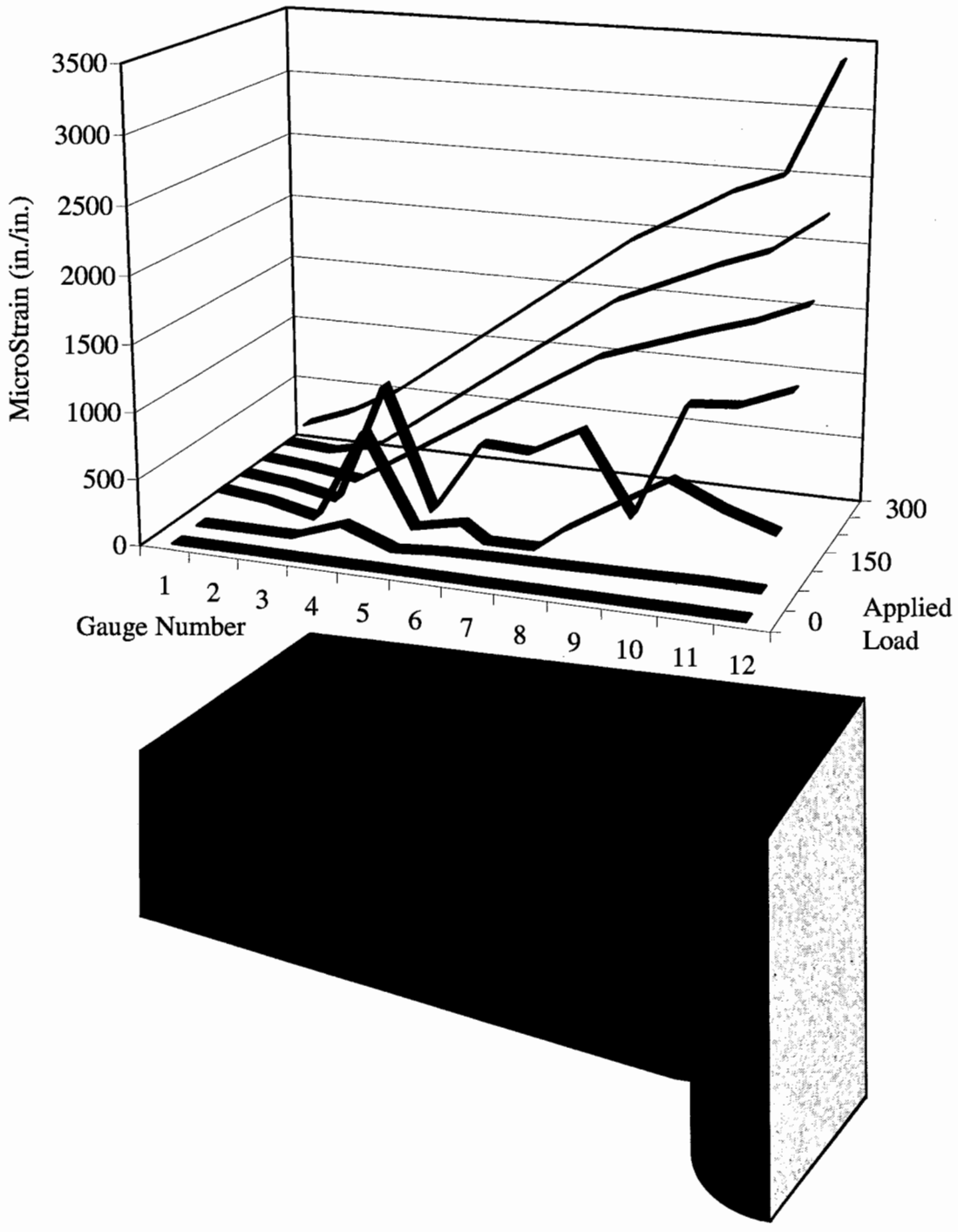

Figure B-20. Specimen 3D Longitudinal Reinforcement Strain Profile for Strain Gauges 1 Through 12.

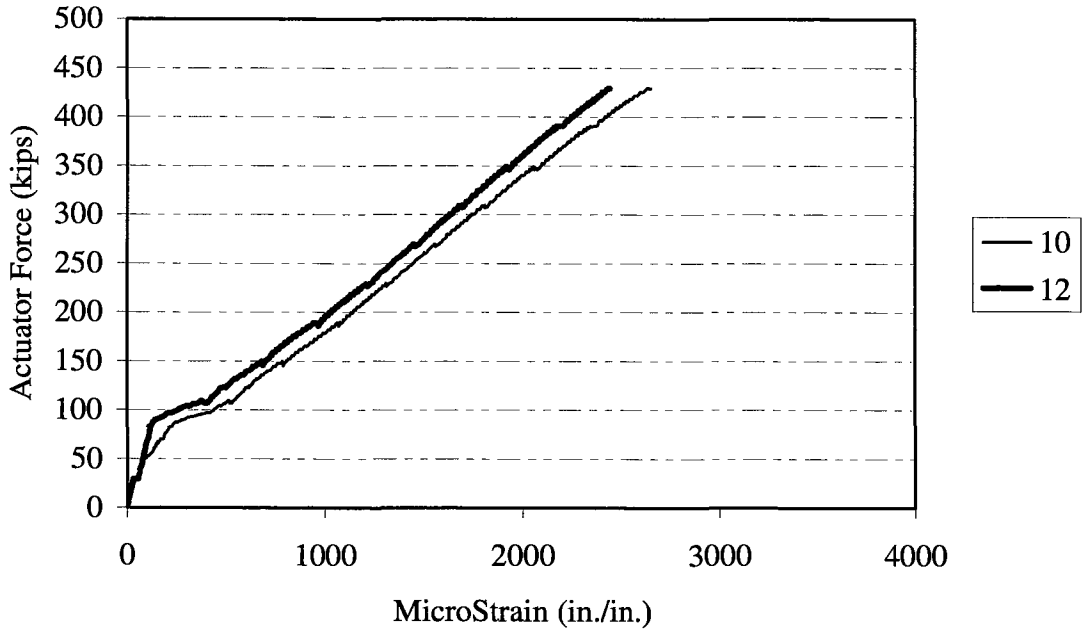

Figure B-21. Specimen 4C Load-Strain History Column face (10) vs. Column Centerline (12).

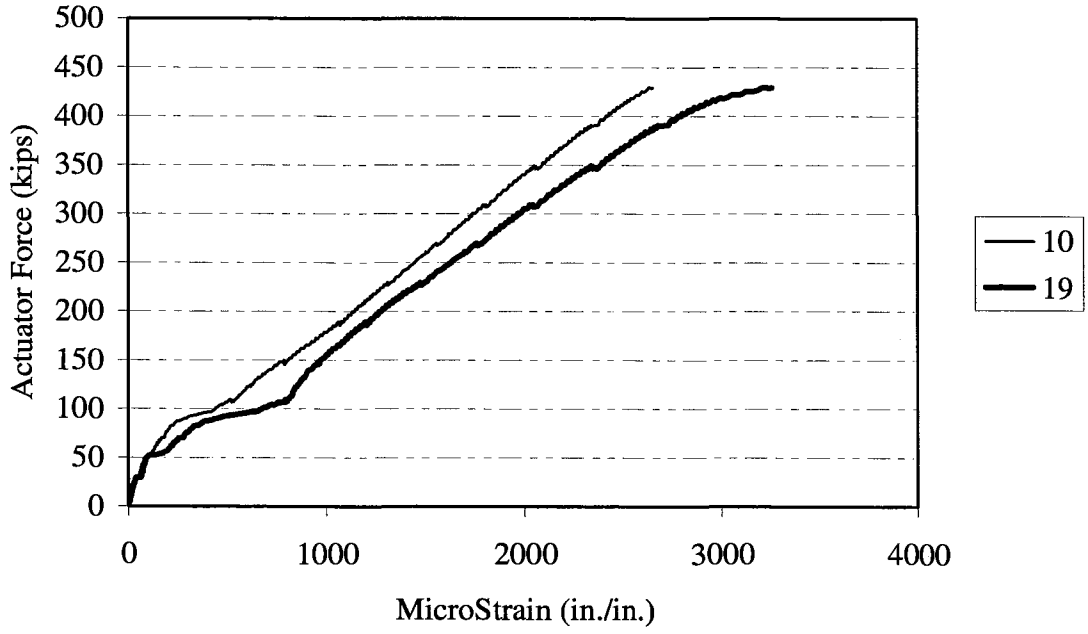

Figure B-22. Specimen 4C Load-Strain History Side (19) vs. Center (10) Transverse Plane.

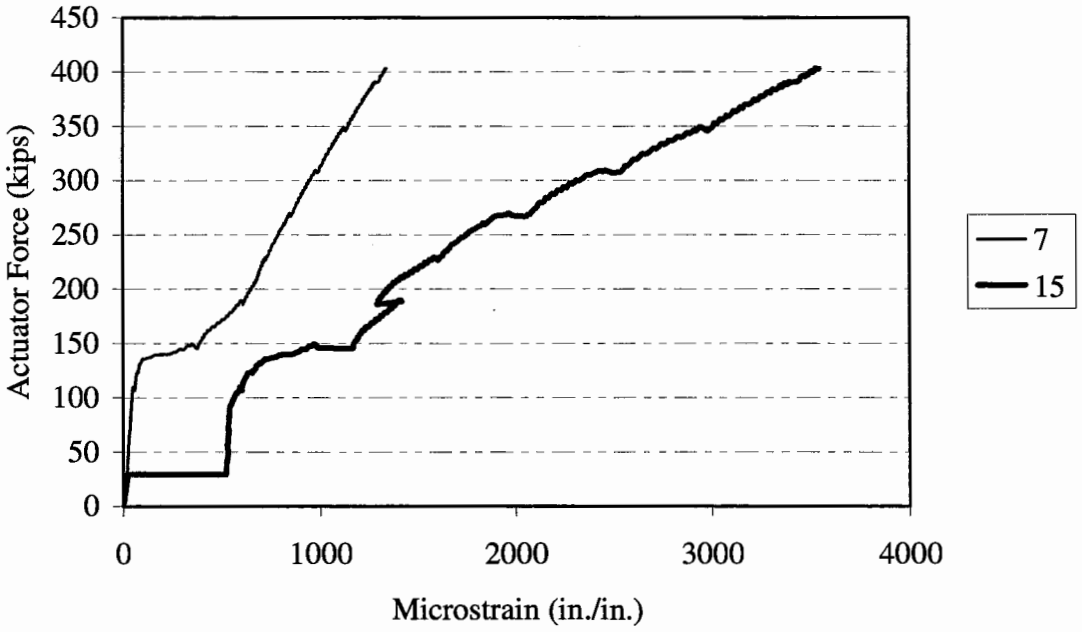

Figure B-23. Specimen 4C Load-Strain History Side (15) vs. Center (7) Transverse Plane.

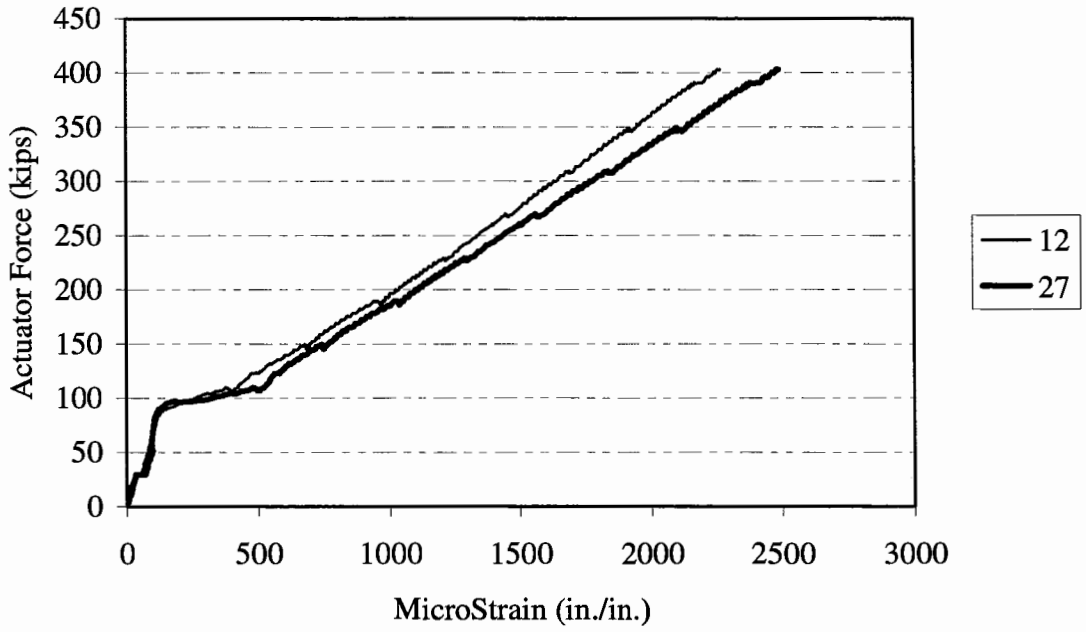

Figure B-24. Specimen 4C Load-Strain History Side (27) vs. Center (12) Transverse Plane.

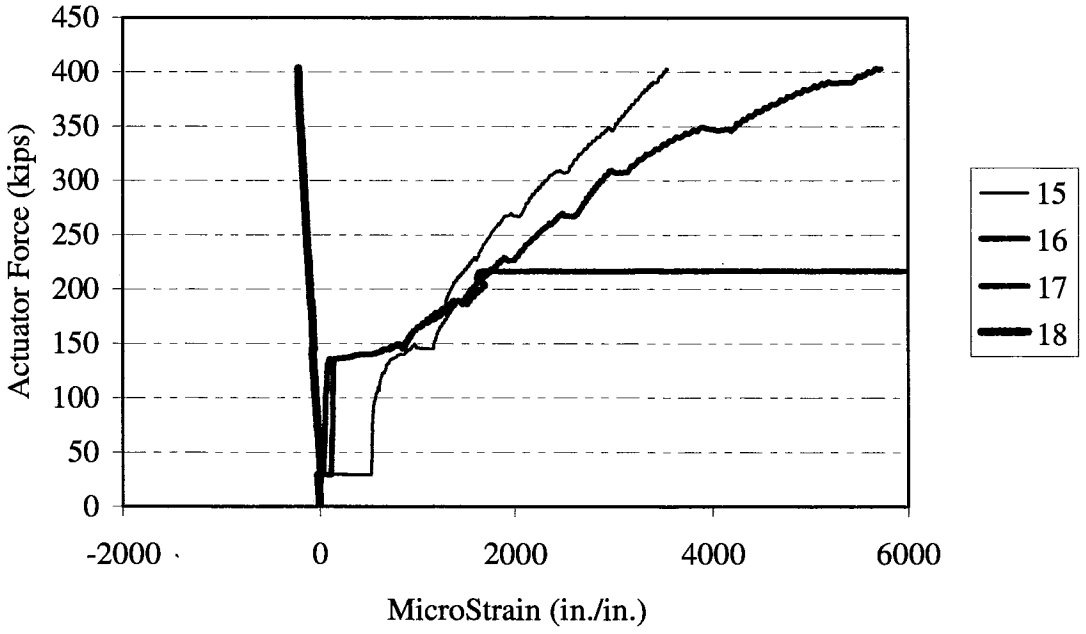

Figure B-25. Specimen 4C Strain Profile Through-Depth Side Face.

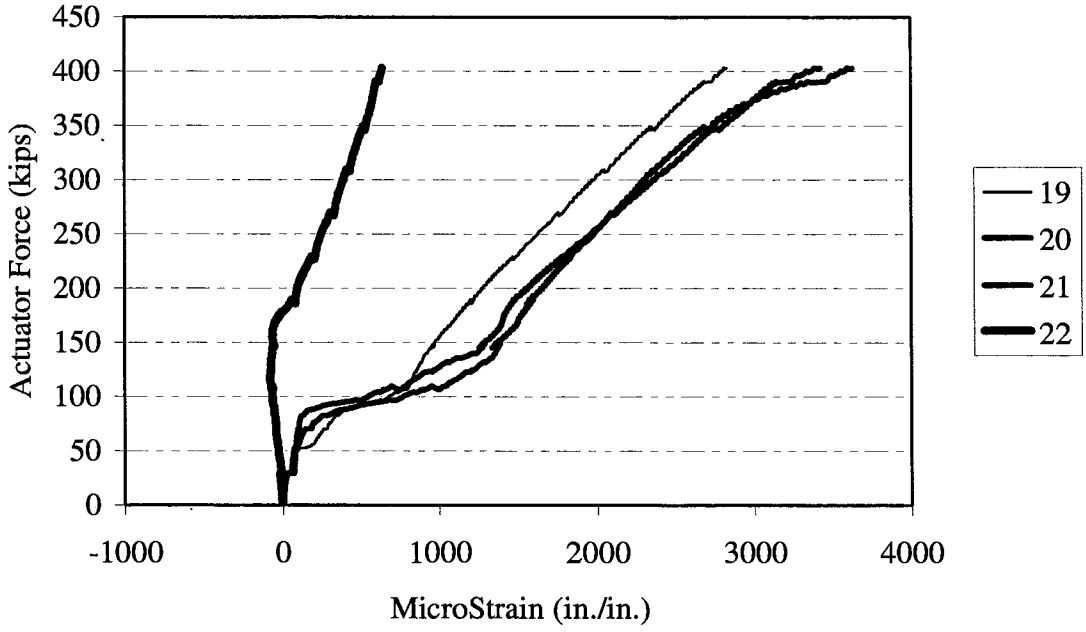

Figure B-26. Specimen 4C Strain Profile Through-Depth Side Face.

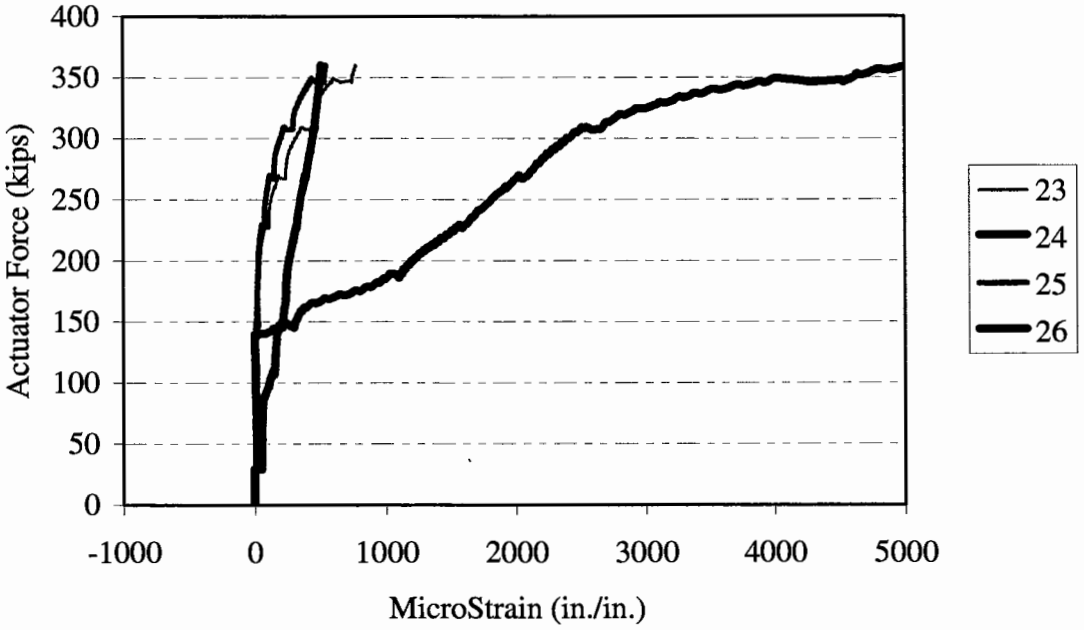

Figure B-27. Specimen 4C Strain Profile Transverse (Stirrup) Reinforcement.

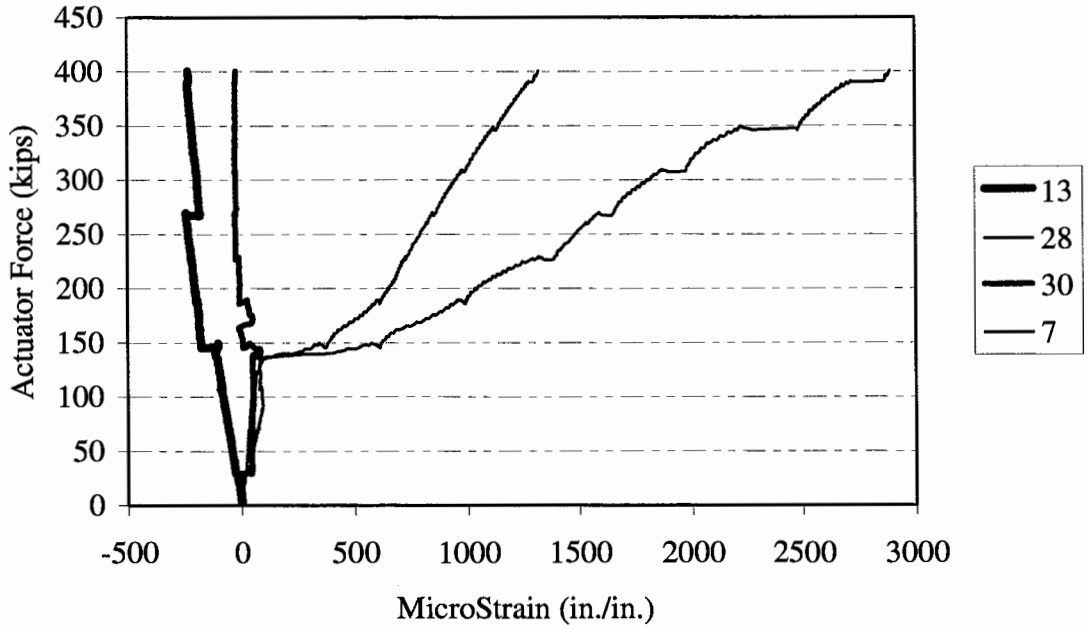

Figure B-28. Specimen 4C Strain Profile Through-Depth Centerline.

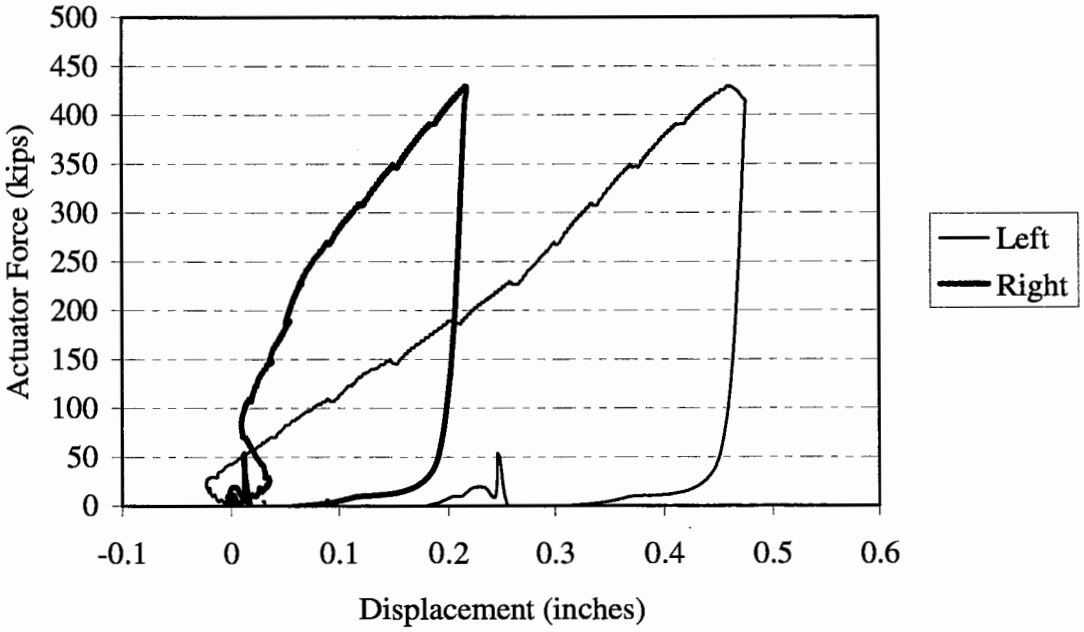

Figure B-29. Specimen 4C Load-Displacement History.

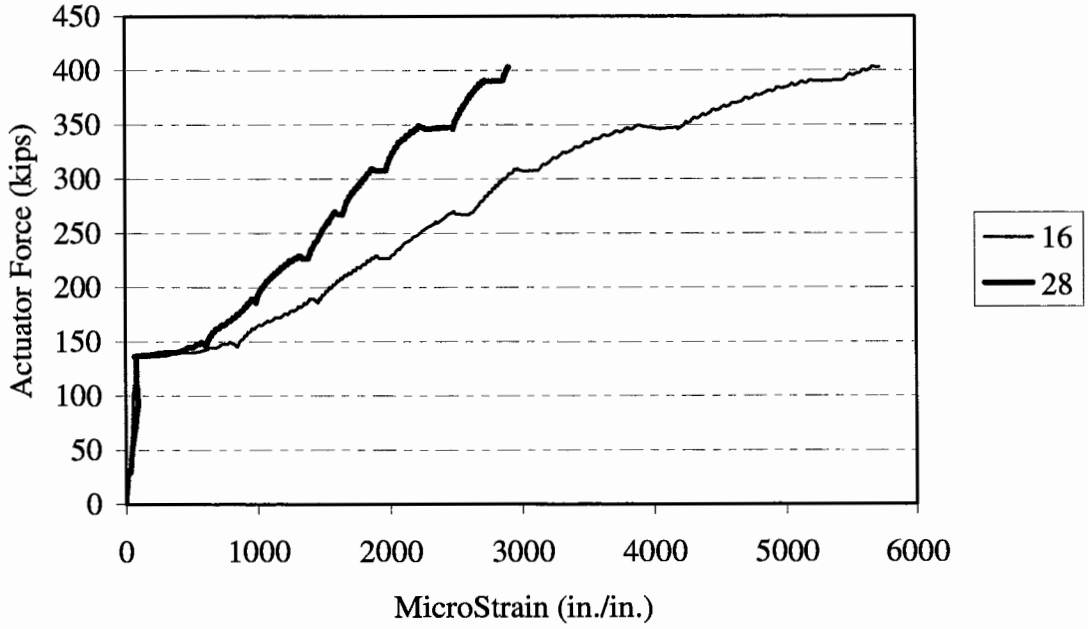

Figure B-30. Specimen 4C Load-Strain History Center (28) vs. Side (16) Transverse Plane.

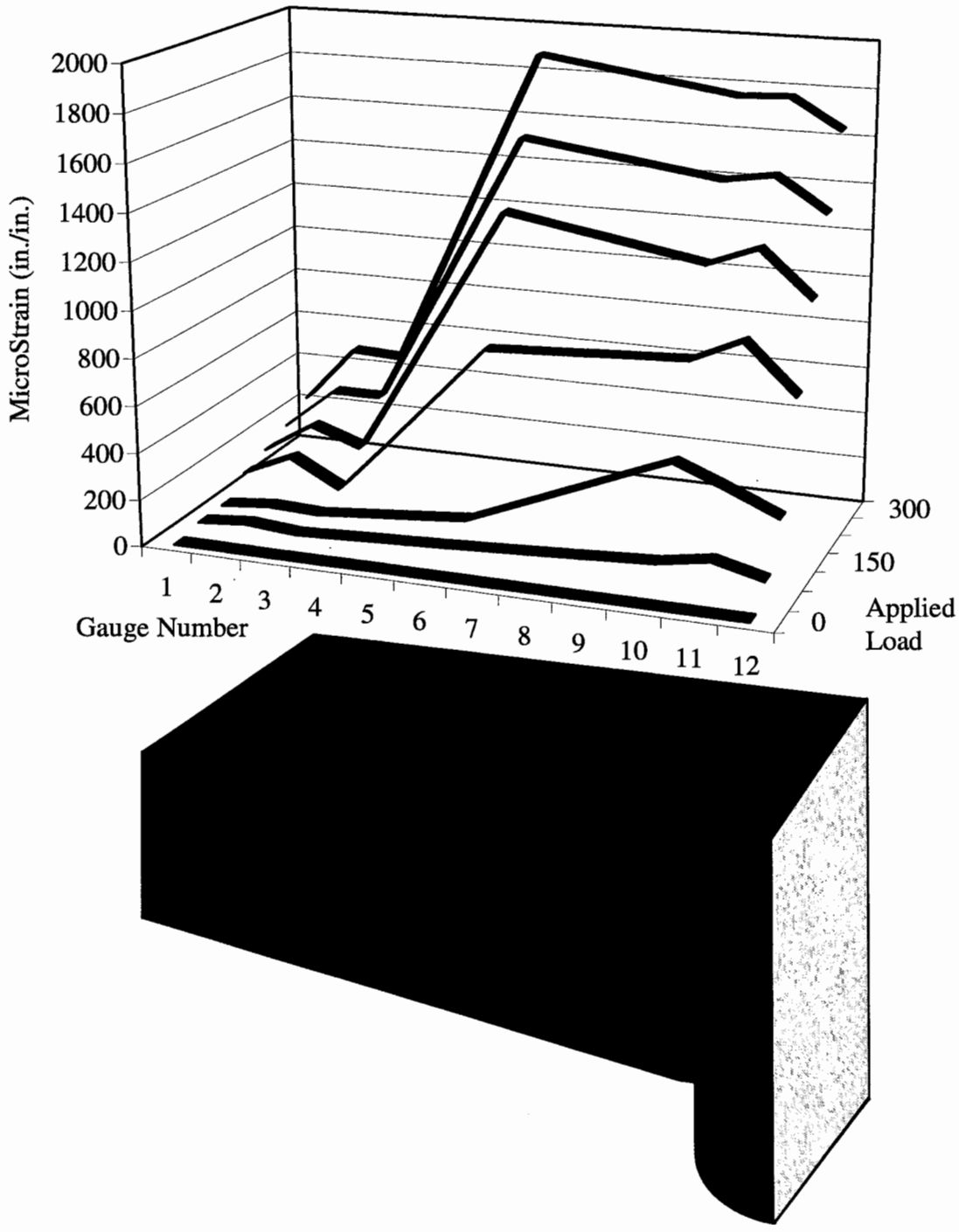

Figure B-31. Specimen 4C Longitudinal Reinforcement Strain Profile for Strain Gauges 1 Through 12.

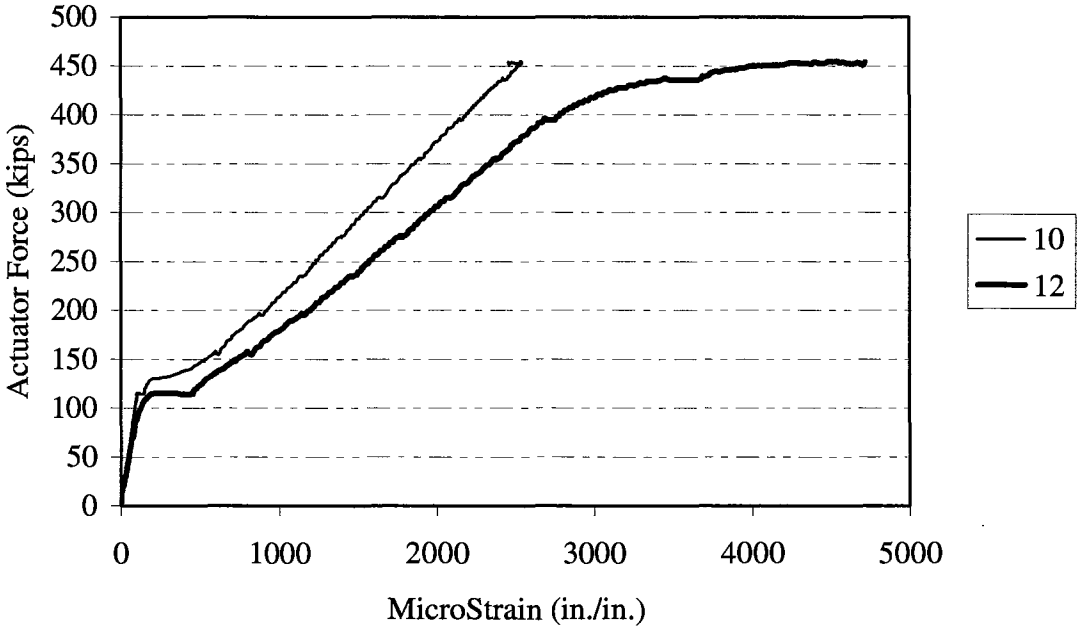

Figure B-32. Specimen 4E Load-Strain History Column Face (10) vs. Column Centerline (12).

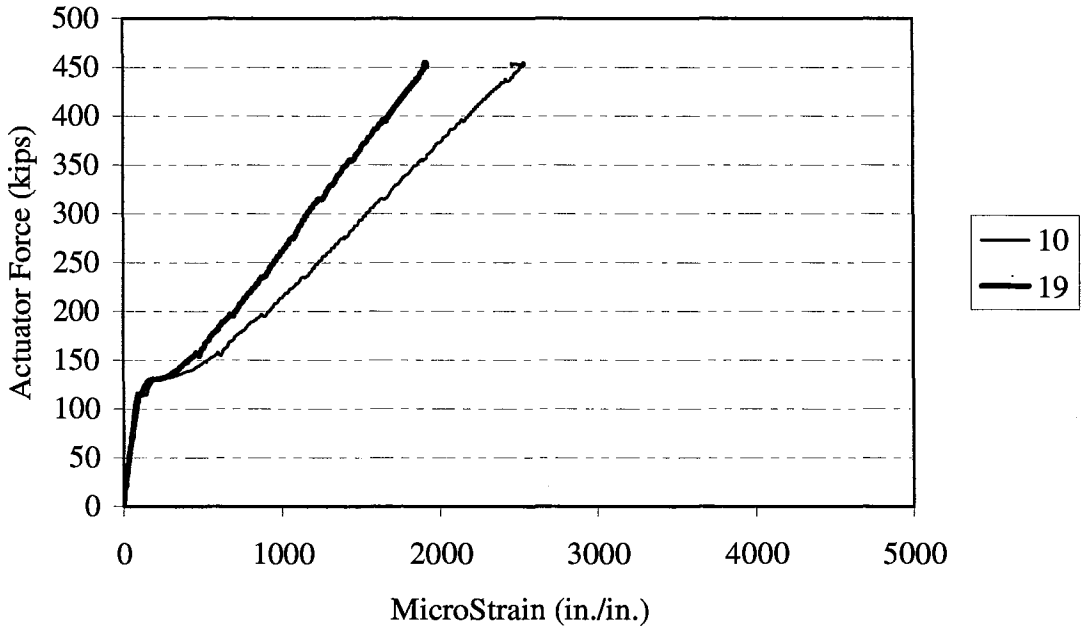

Figure B-33. Specimen 4E Load-Strain Profile Side (19) vs. Center (10) Transverse Plane.

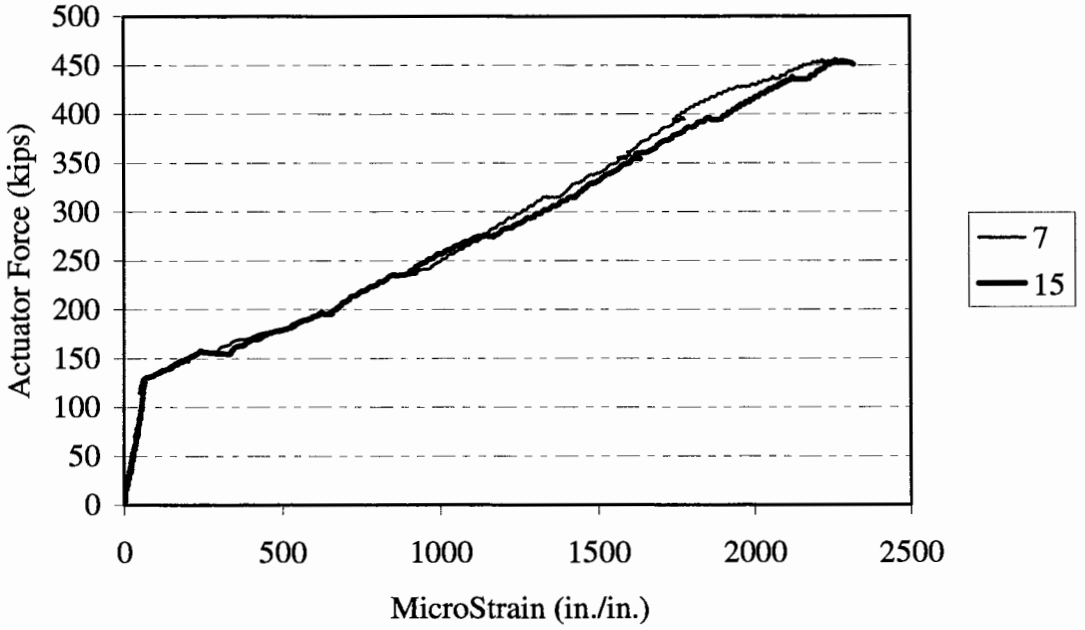

Figure B-34. Specimen 4E Load-Strain Profile Side (15) vs. Center (7) Transverse Plane.

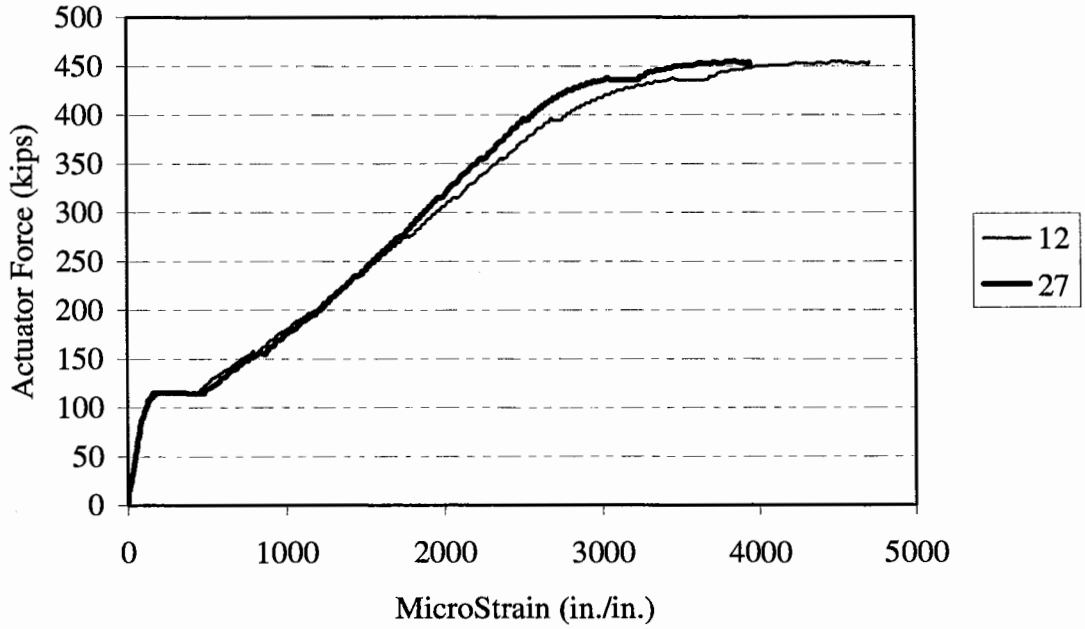

Figure B-35. Specimen 4E Load-Strain Profile Side (27) vs. Center (12) Transverse Plane.

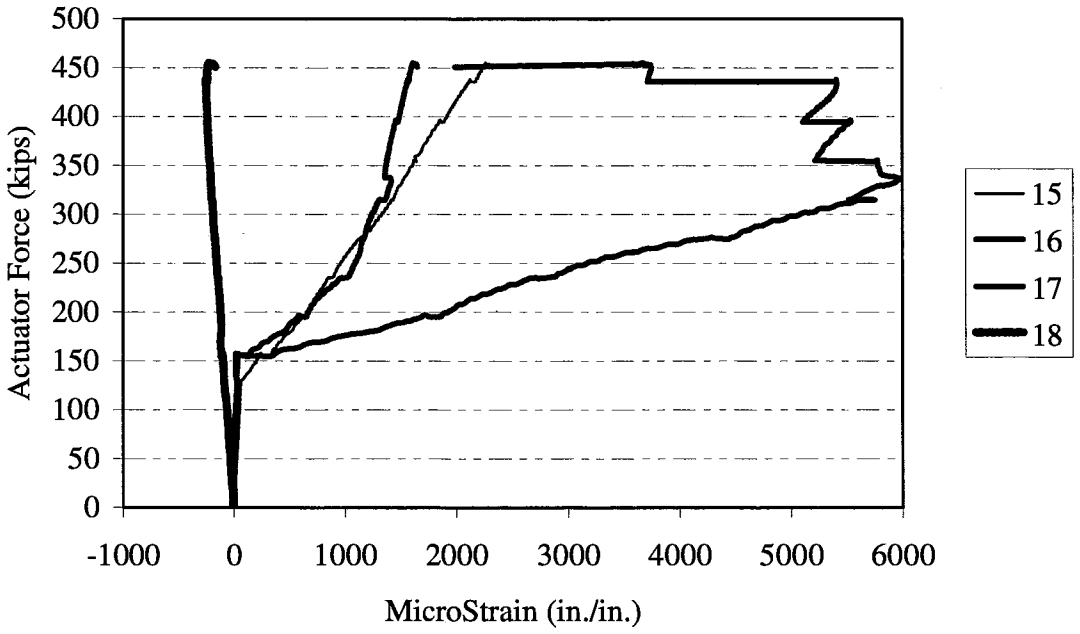

Figure B-36. Specimen 4E Strain Profile Through-Depth Side Face.

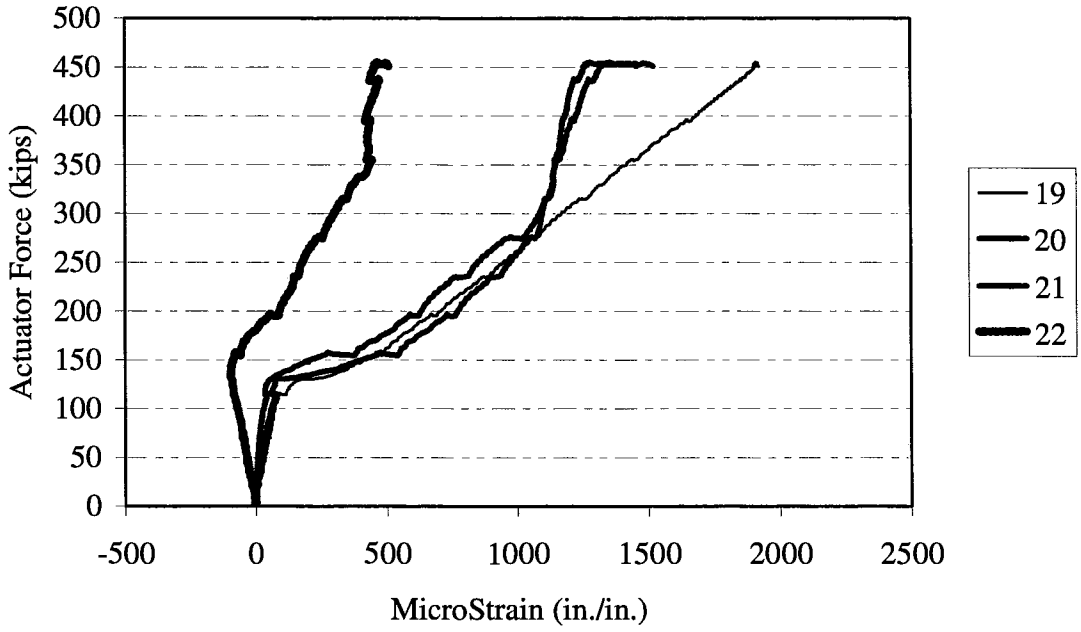

Figure B-37. Specimen 4E Strain Profile Through-Depth Side Face.

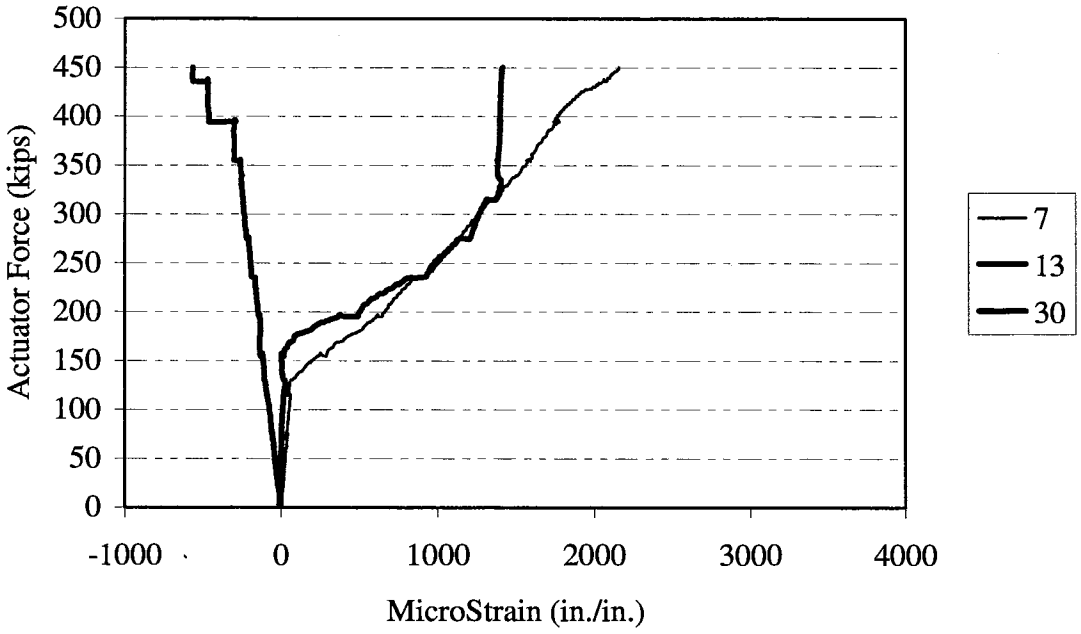

Figure B-38. Specimen 4E Strain Profile Through-Depth Centerline.

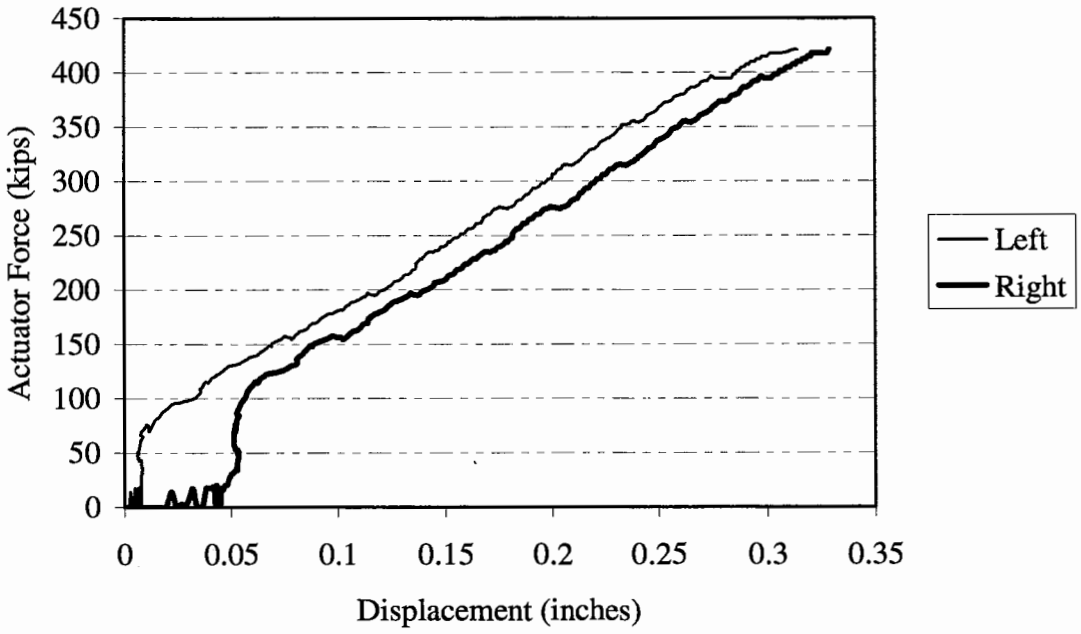

Figure B-39. Specimen 4E Load-Displacement History.

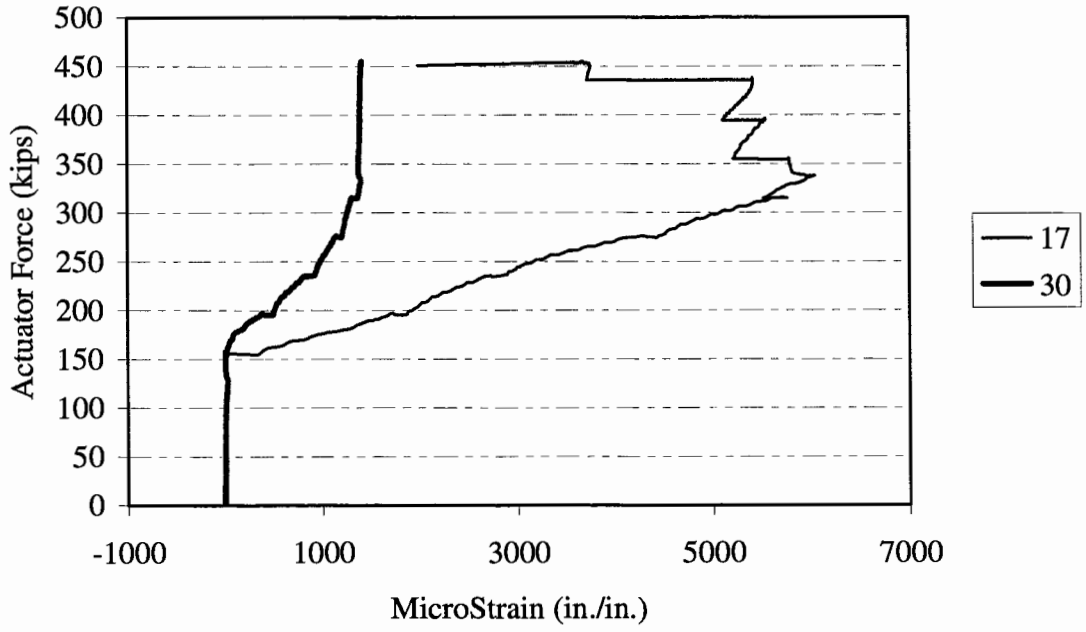

Figure B-40. Specimen 4E Strain Profile Center (30) vs. Side (17) Transverse Plane.

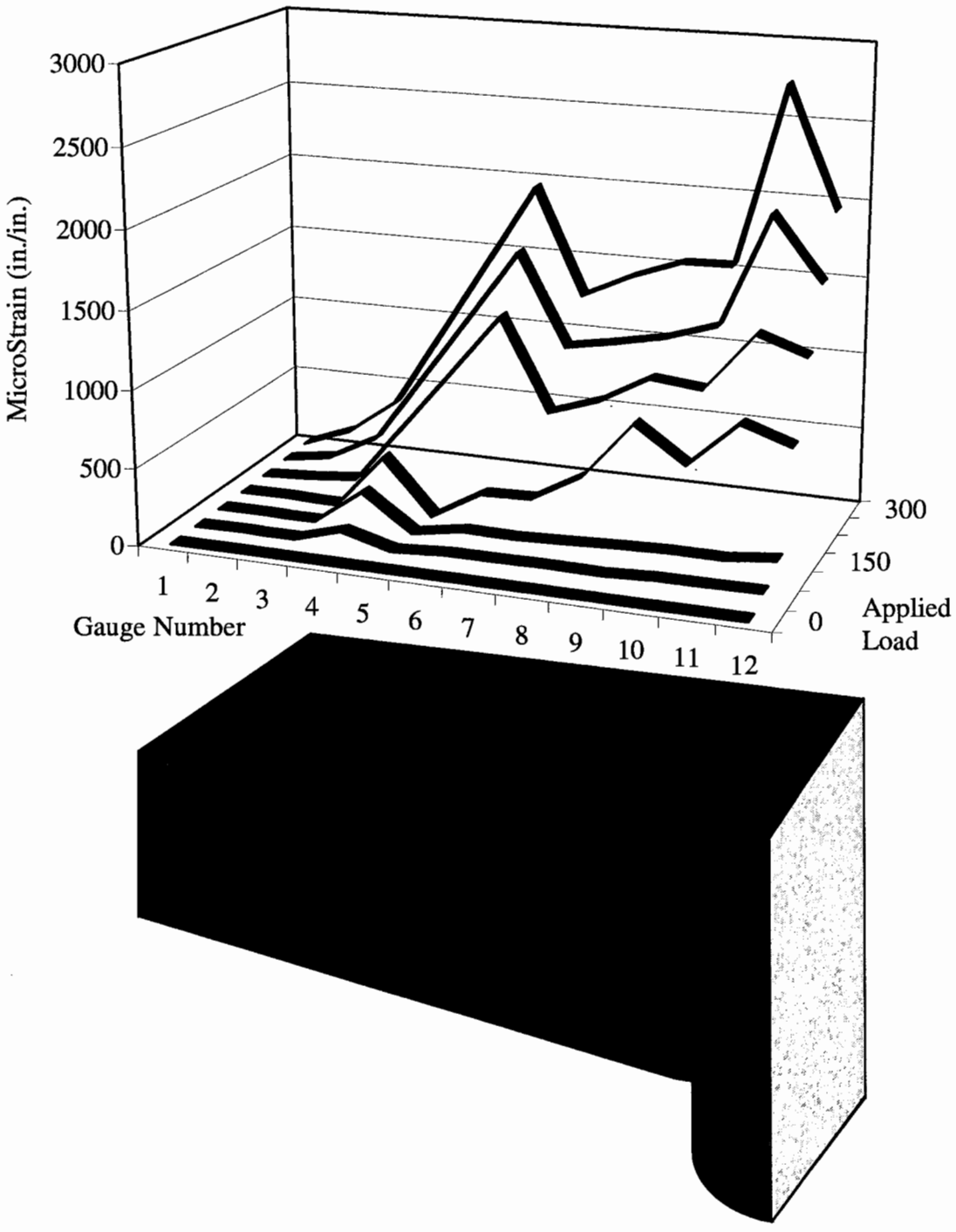

Figure B-41. Specimen 4E Longitudinal Reinforcement Strain Profile for Strain Gauges 1 Through 12.

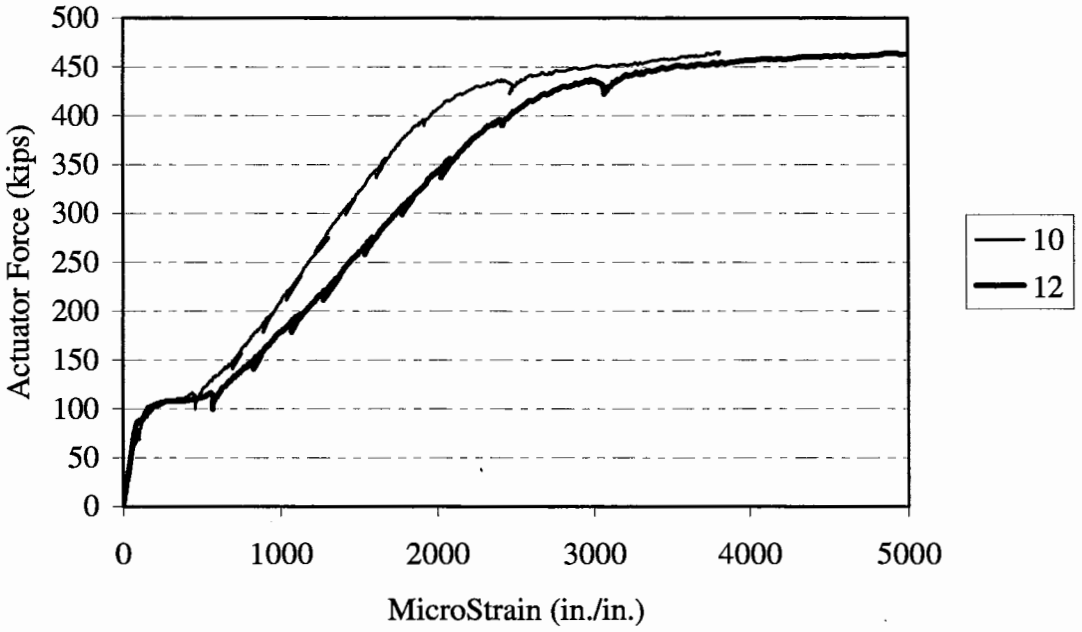

Figure B-42. Specimen 5D Load-Strain History Column Face (10) vs. Column Centerline (12).

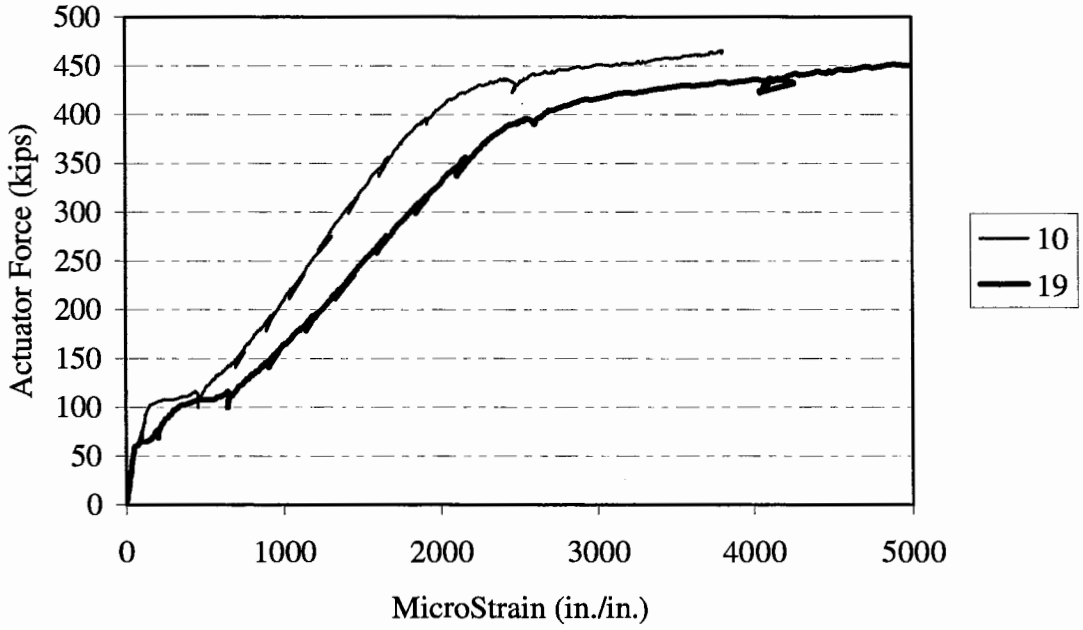

Figure B-43. Specimen 5D Load-Strain History Side (19) vs. Center (10) Transverse Plane.

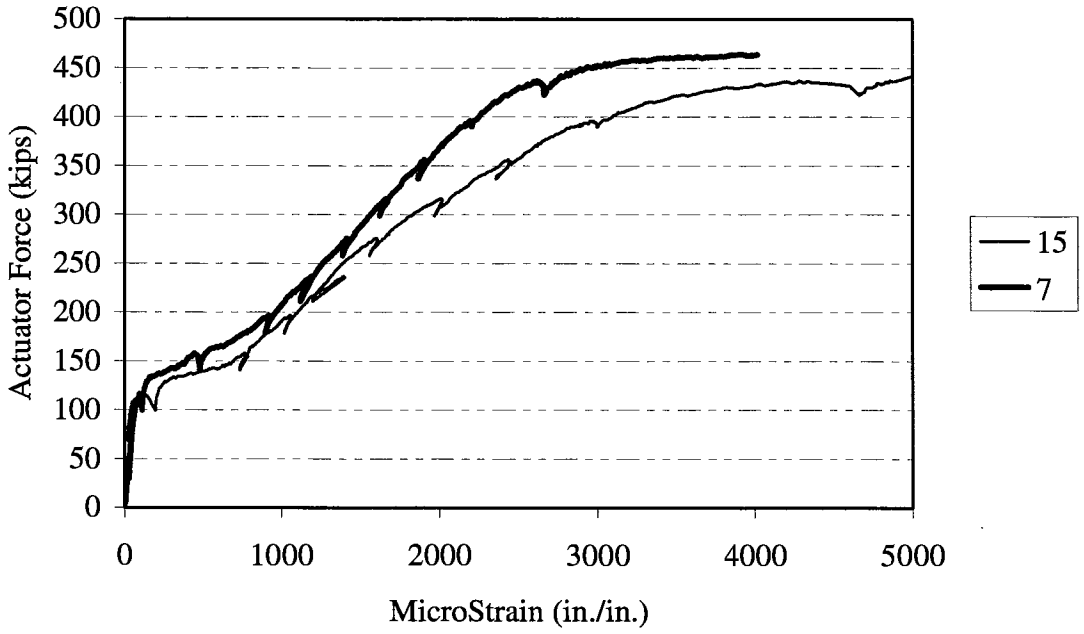

Figure B-44. Specimen 5D Load-Strain History Side (15) vs. Center (7) Transverse Plane.

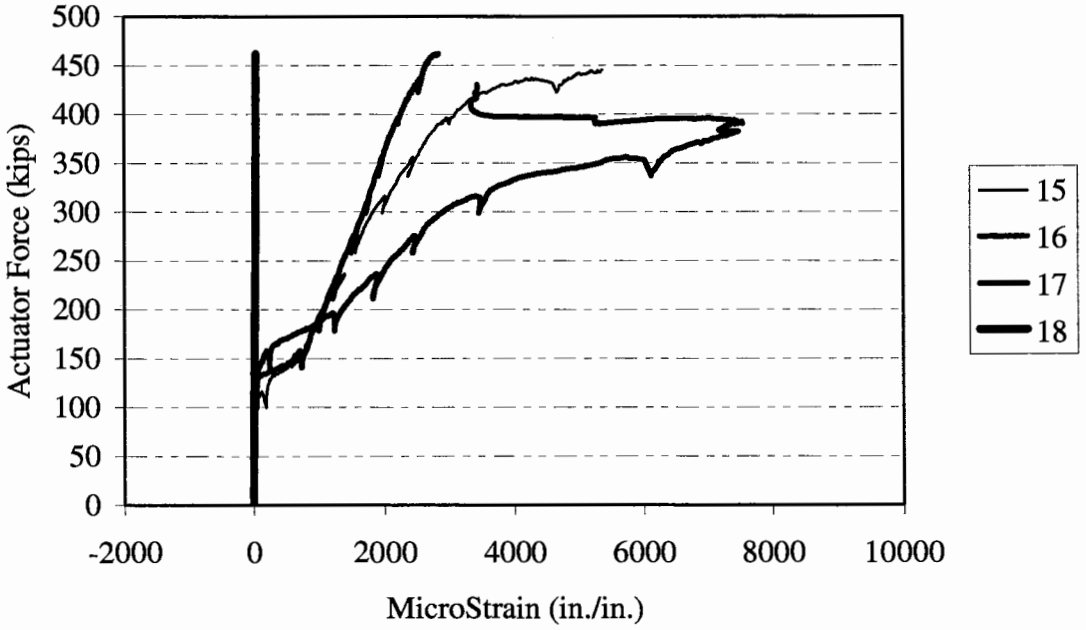

Figure B-45. Specimen 5D Strain Profile Through-Depth Side Face.

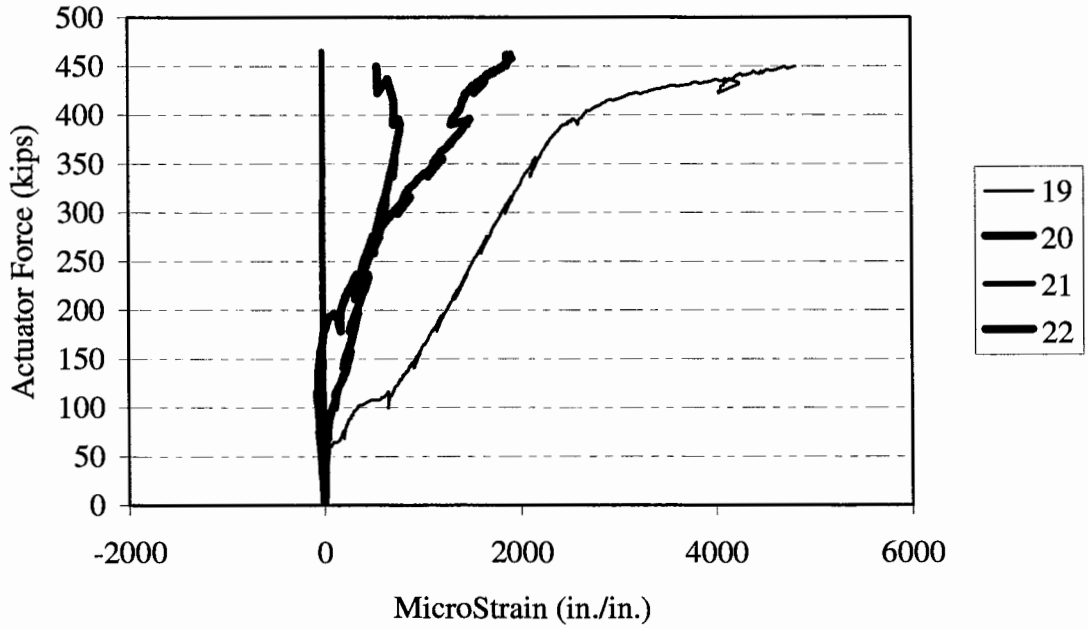

Figure B-46. Specimen 5D Strain Profile Through-Depth Side Face.

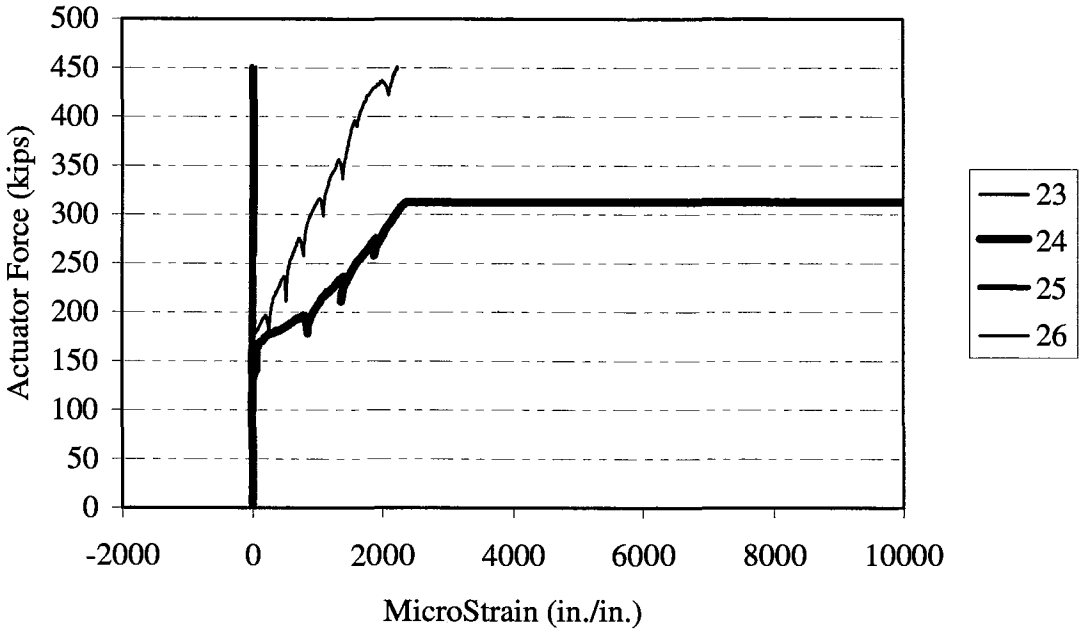

Figure B-47. Specimen 5D Strain Profile Transverse (Stirrup) Reinforcement.

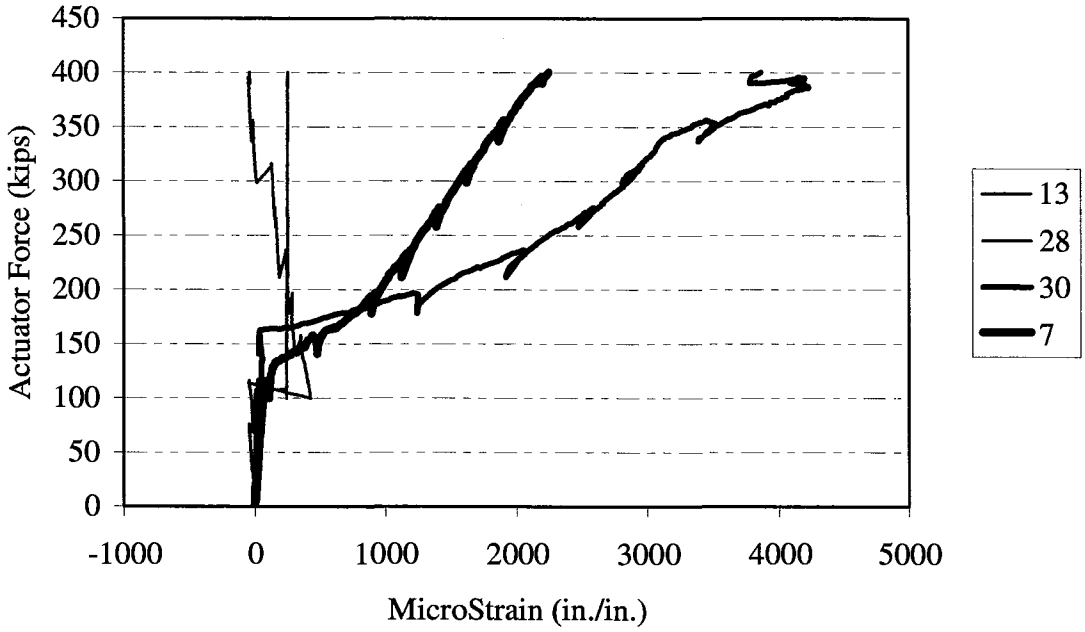

Figure B-48. Specimen 5D Strain Profile Through-Depth Centerline.

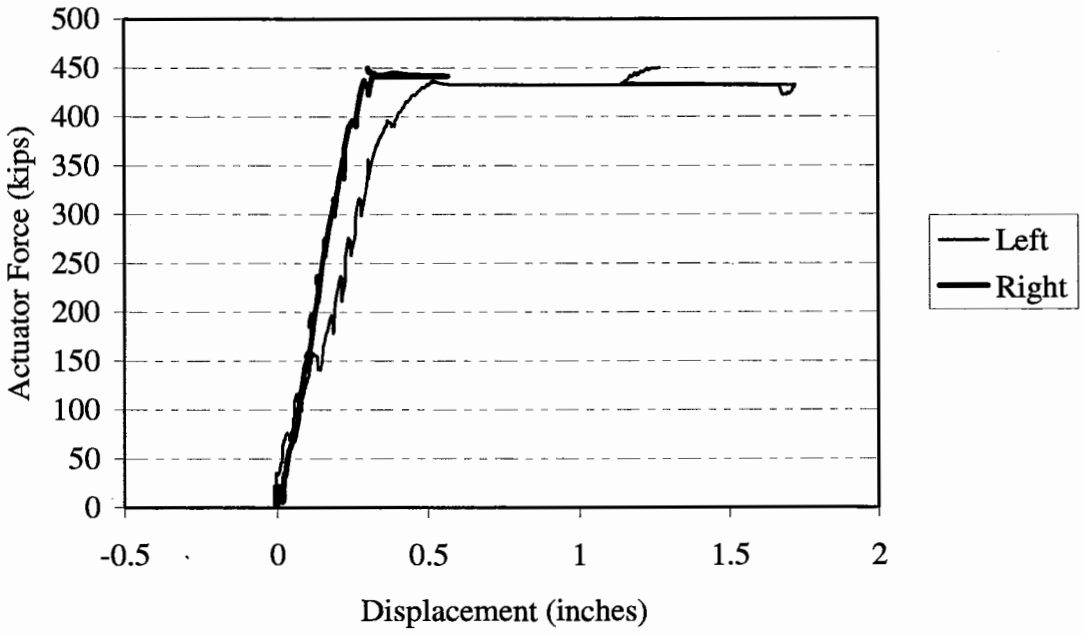

Figure B-49. Specimen 5D Load-Displacement History.

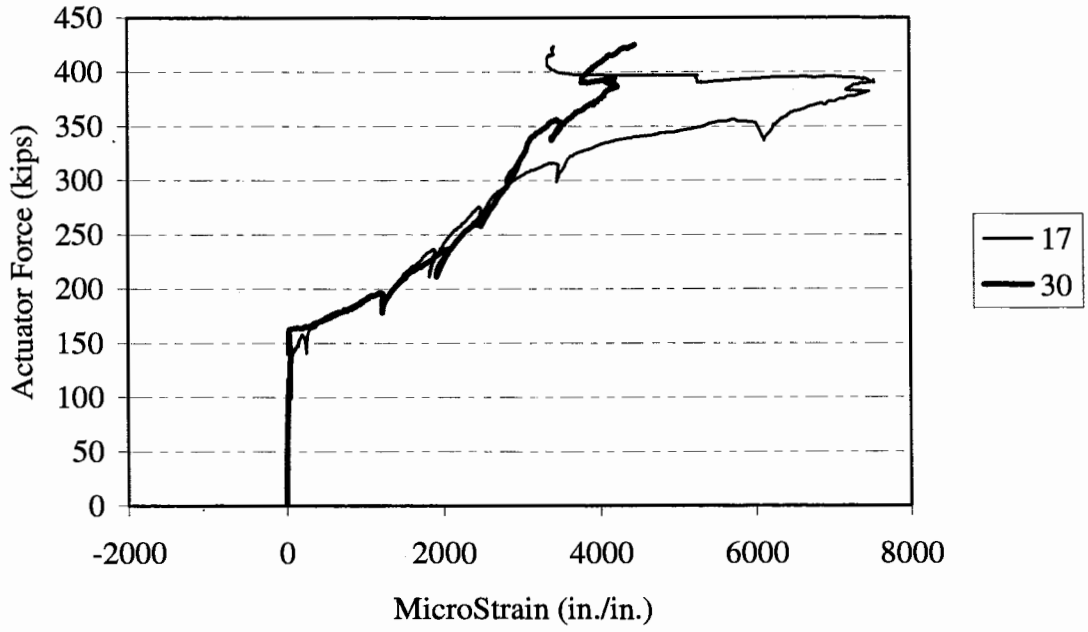

Figure B-50. Specimen 5D Strain Profile Center (30) vs. Side (17) Transverse Plane.

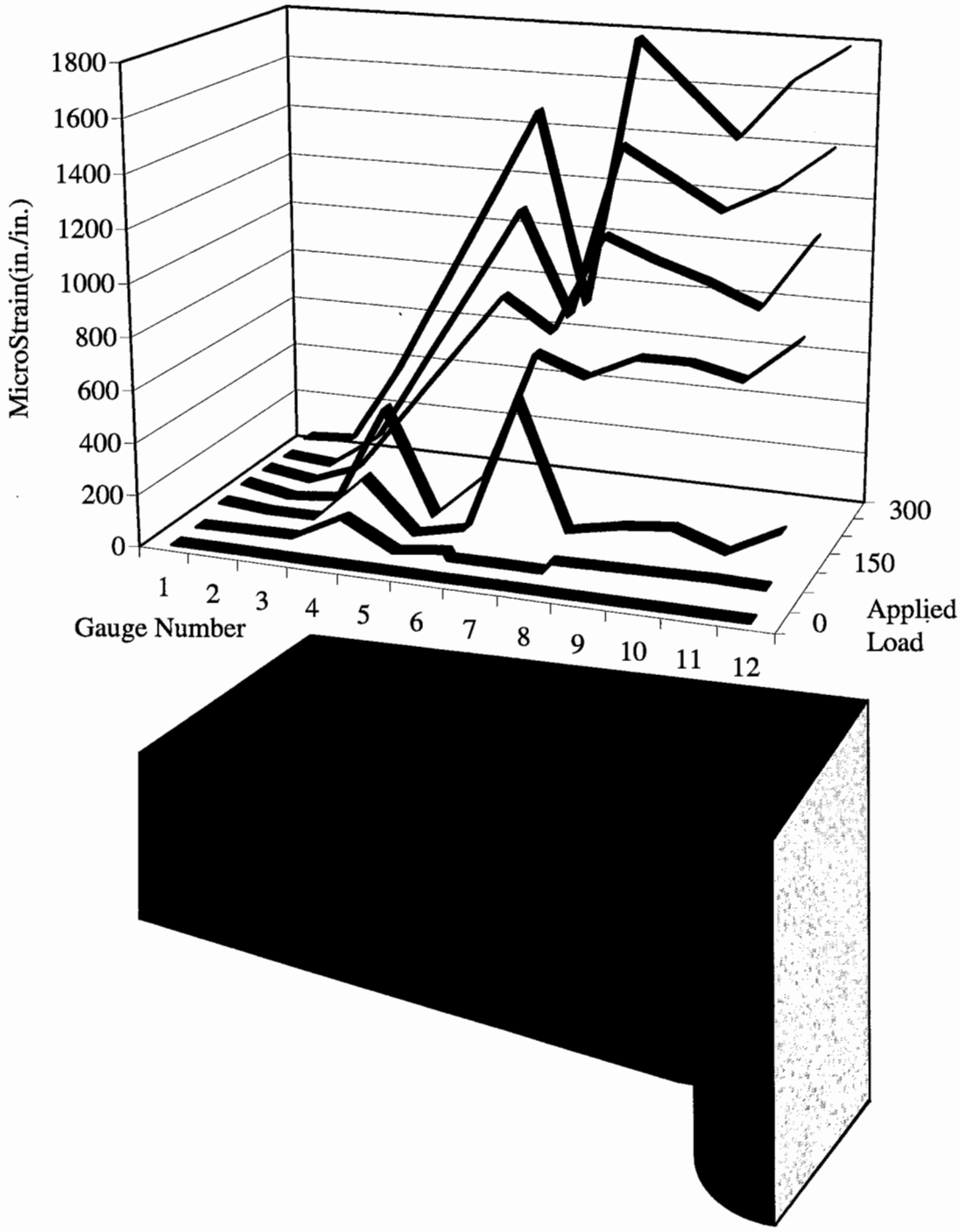

Figure B-51. Specimen 5D Longitudinal Reinforcement Strain Profile for Strain Gauges 1 Through 12.

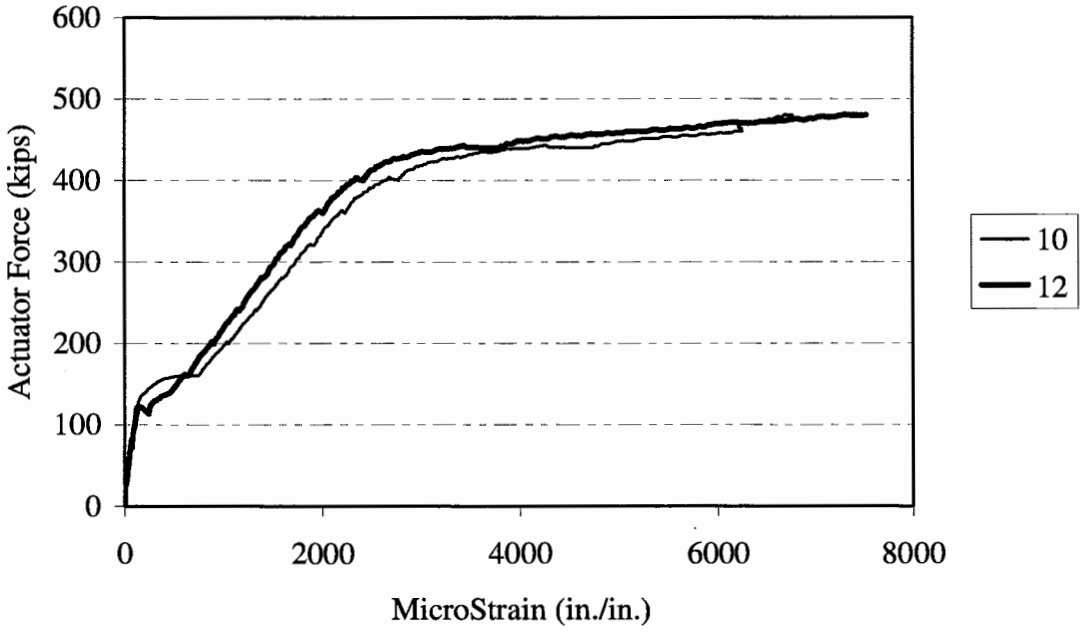

Figure B-52. Specimen 5E Load-Strain History Column Face (10) vs. Column Centerline (12).

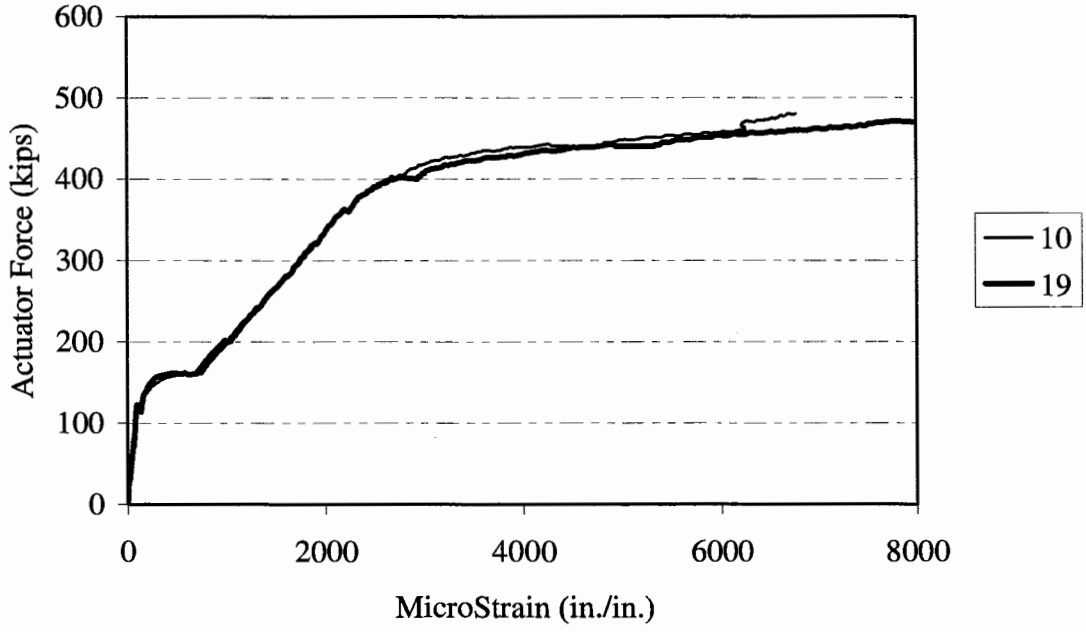

Figure B-53. Specimen 5E Load-Strain History Side (19) vs. Center (10) Transverse Plane.

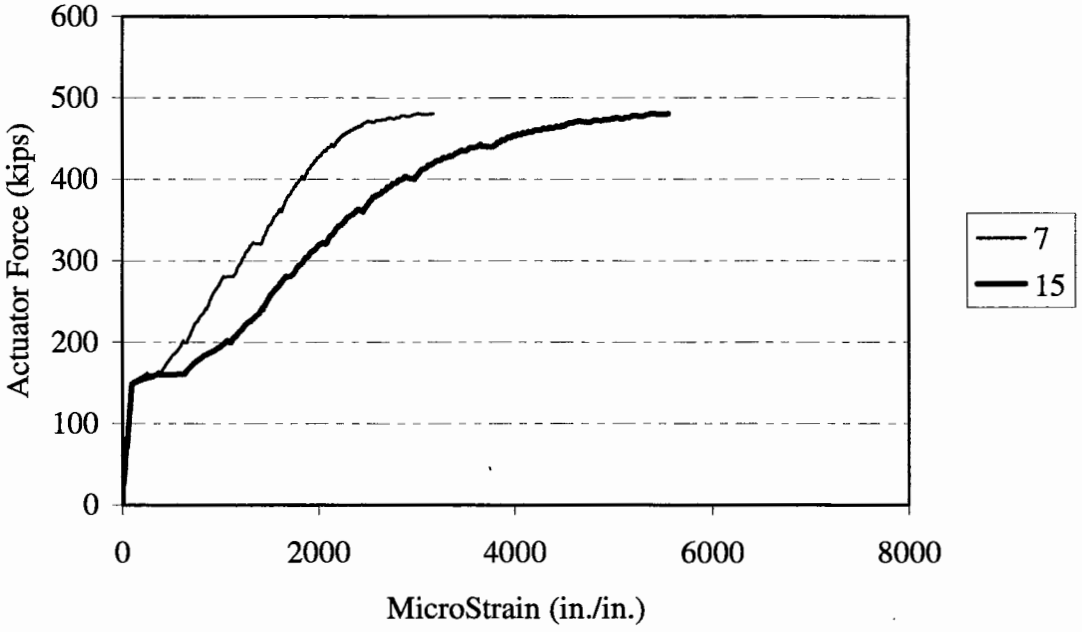

Figure B-54. Specimen 5E Load-Strain History Side (15) vs. Centerline (7) Transverse Plane.

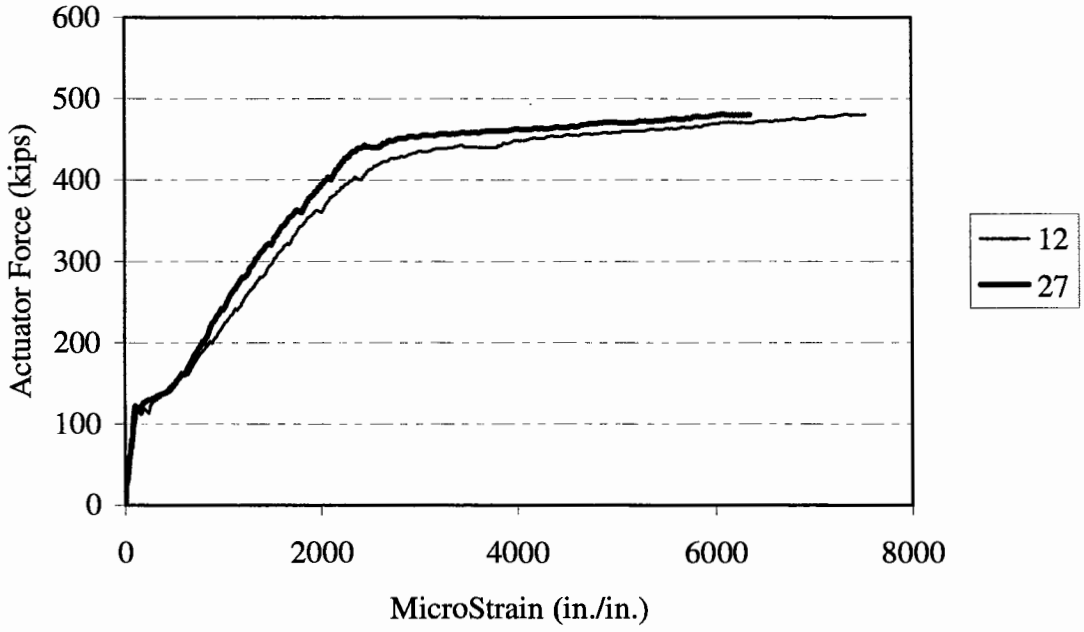

Figure B-55. Specimen 5E Load-Strain History Side (27) vs. Center (12) Transverse Plane.

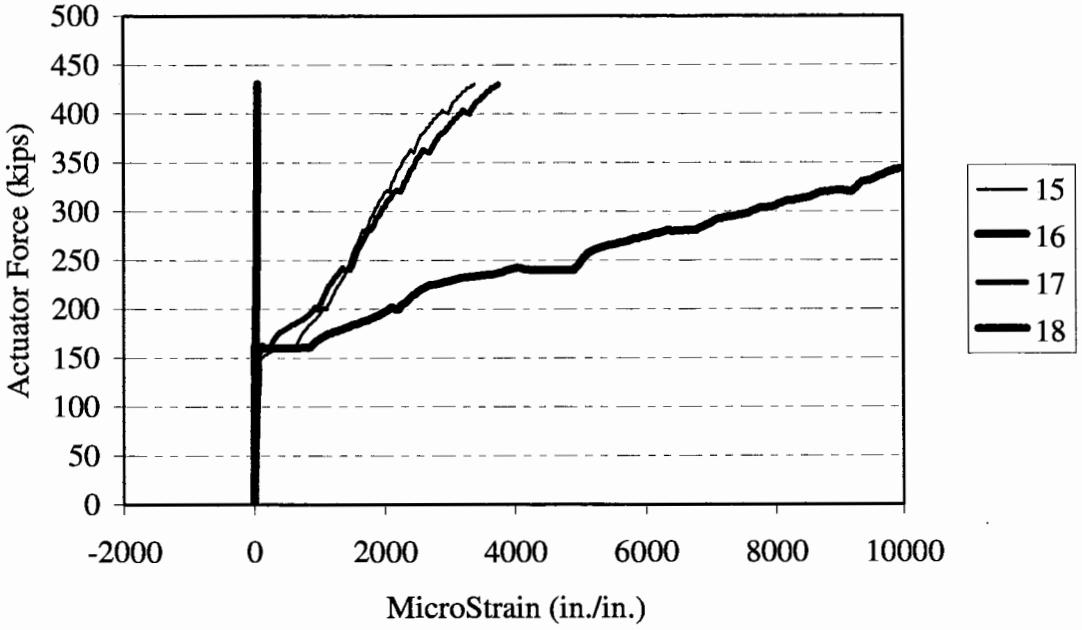

Figure B-56. Specimen 5E Strain Profile Through-Depth Side Face.

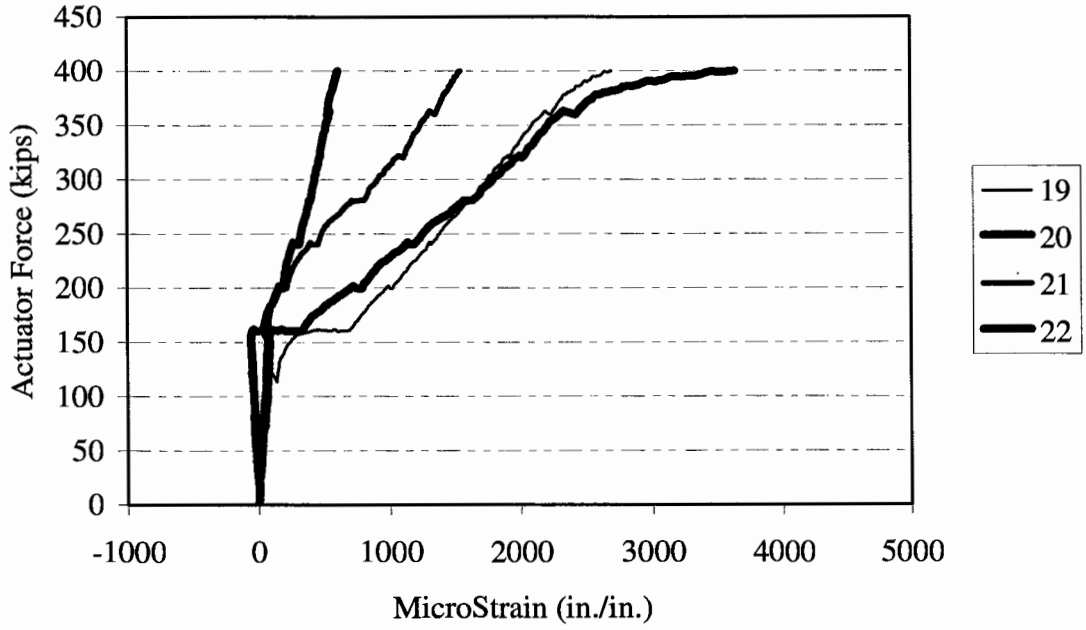

Figure B-57. Specimen 5E Strain Profile Through-Depth Side Face.

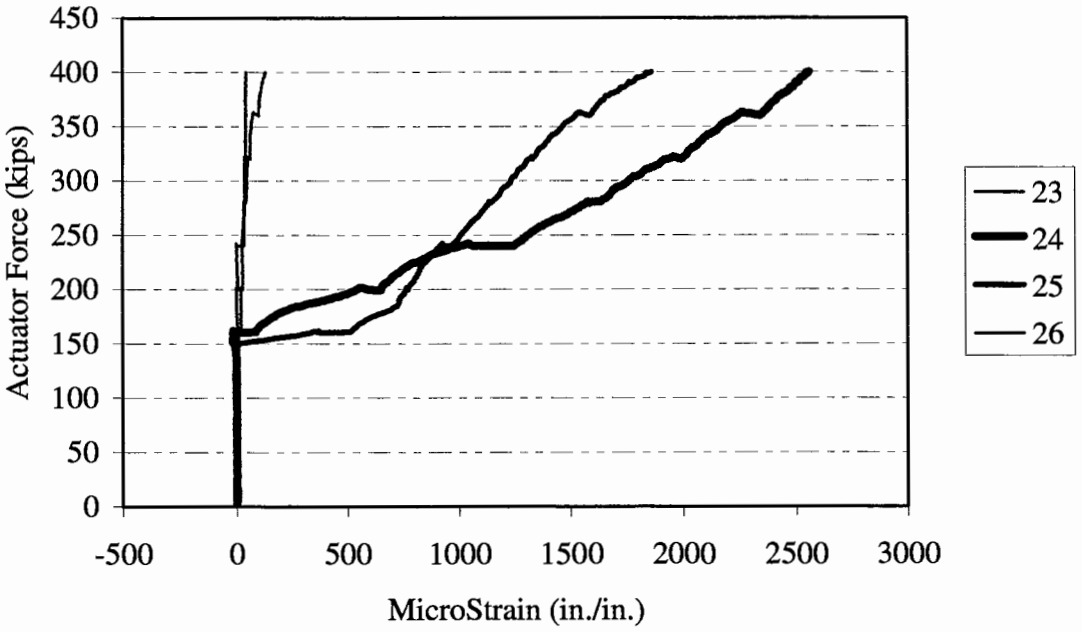

Figure B-58. Specimen 5E Strain Profile Through-Depth Side Face.

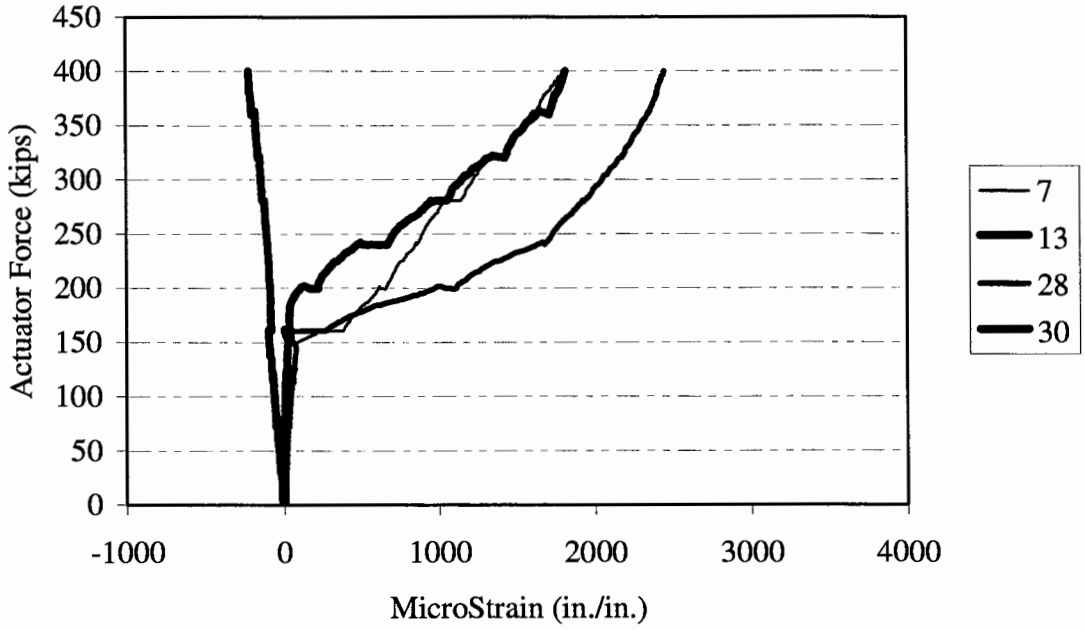

Figure B-59. Specimen 5E Strain Profile Through-Depth Centerline.

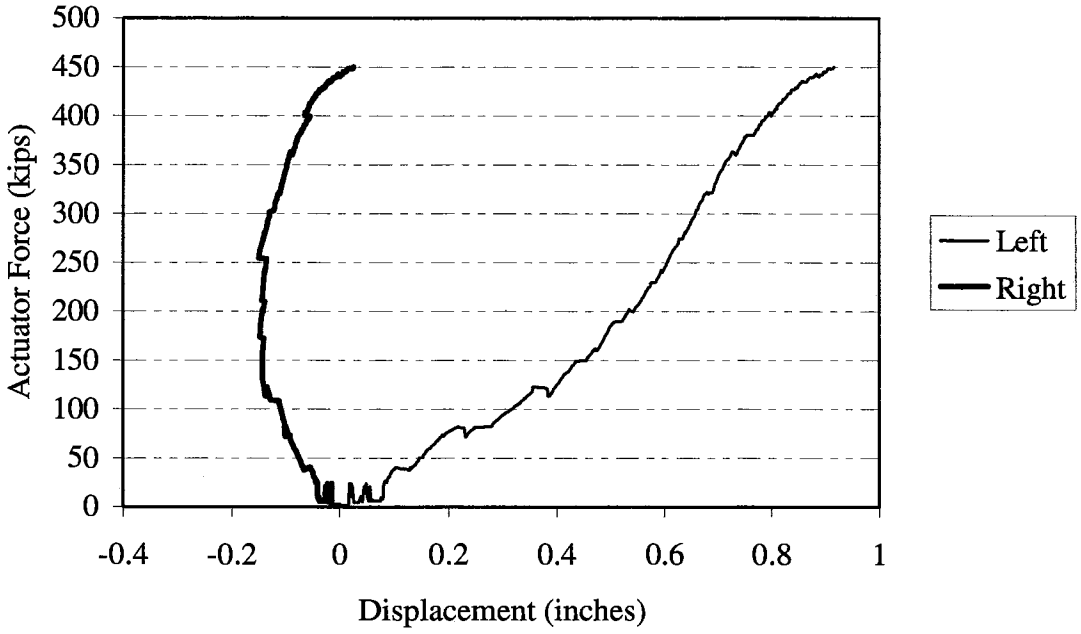

Figure B-60. Specimen 5E Load-Displacement History.

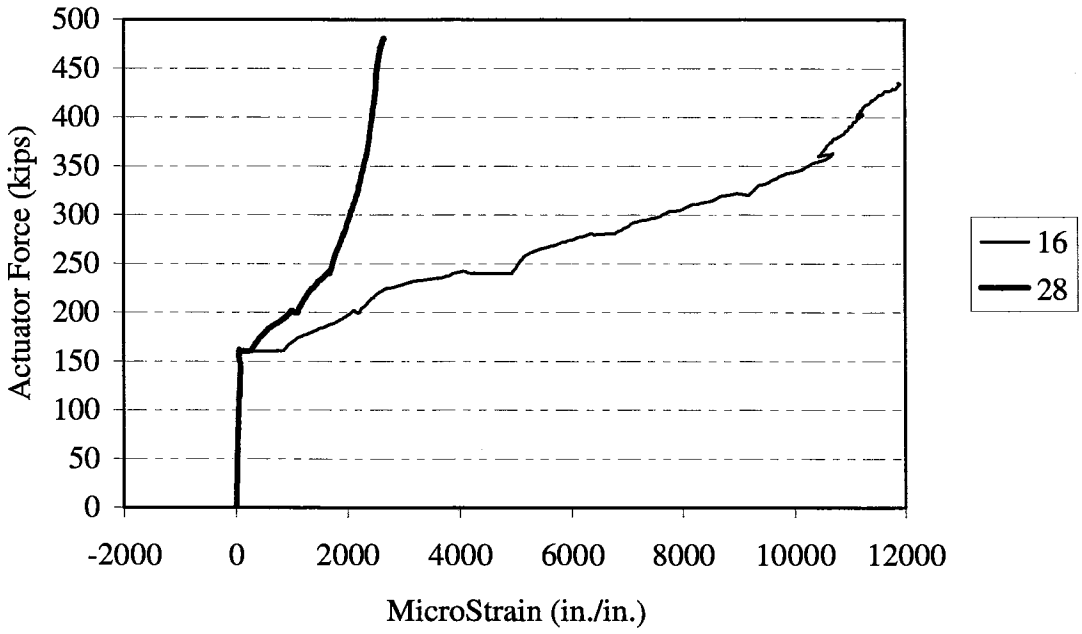

Figure B-61. Specimen 5E Load-Strain History Center (28) vs. Side (16) Transverse Plane.

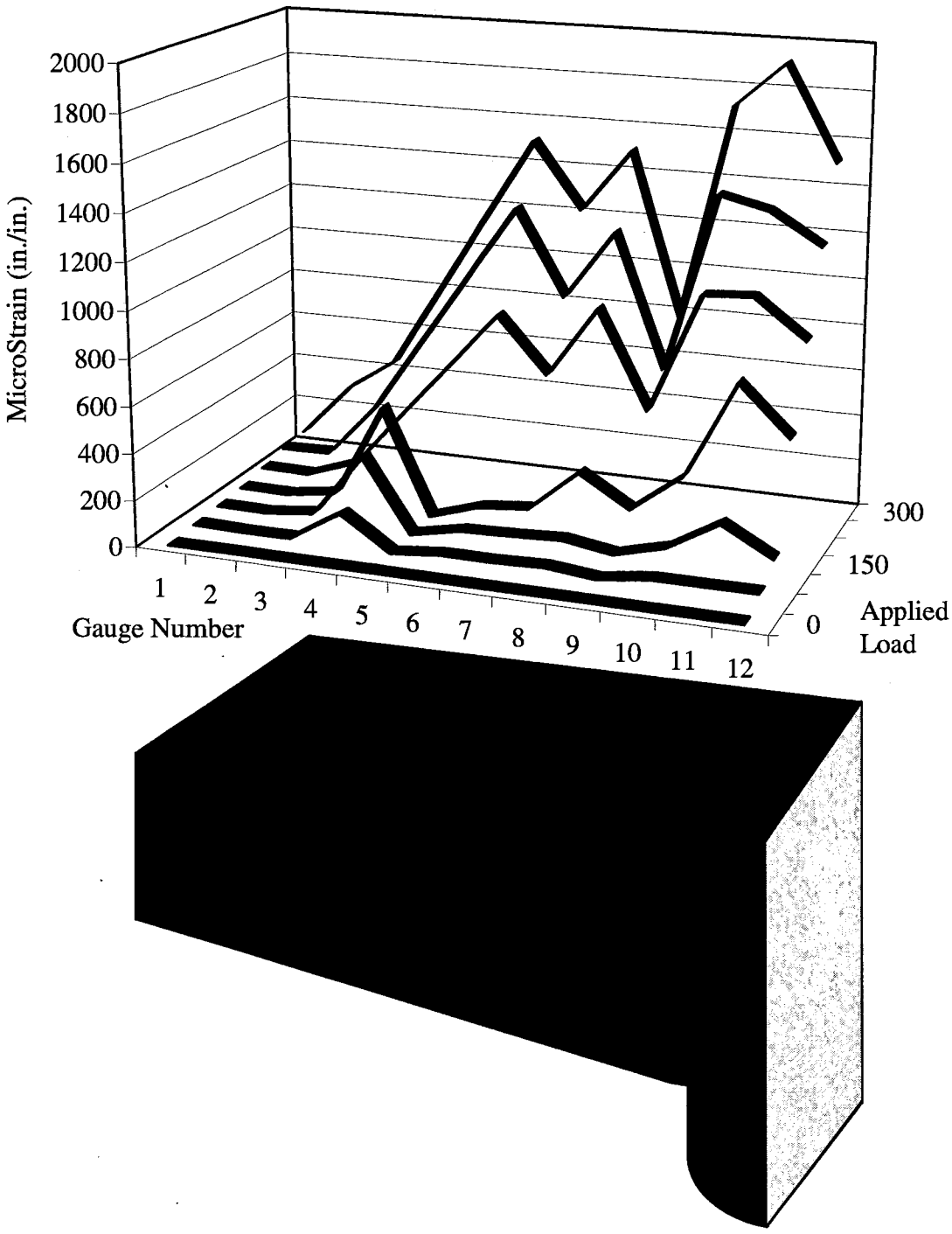

Figure B-62. Specimen 5E Longitudinal Reinforcement Strain Profile for Strain Gauges 1 Through 12.

APPENDIX C

GROUP #3 EXPERIMENTAL RESULTS

For this Appendix:

- The graphical data were intentionally terminated in order to reflect only that portion of testing necessary for illustrating a particular trend. Therefore, termination of the data series does not indicate failure of the specimen or completion of testing.

- Refer to Fig. 3.8 for illustration of strain gauge identification and locations.

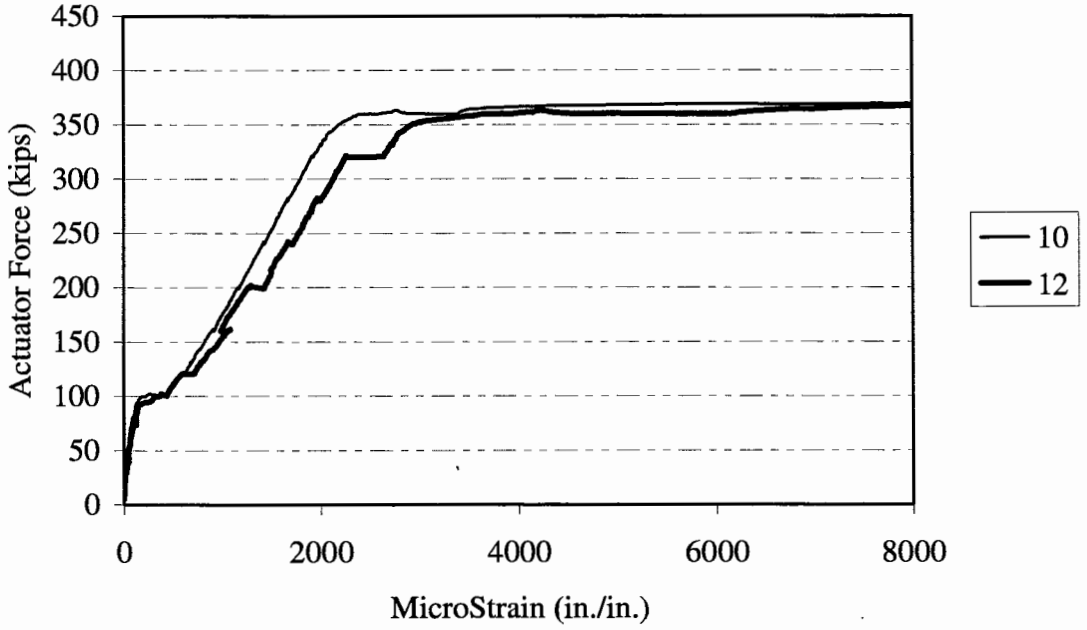

Figure C-1. Specimen 6F Load-Strain History
Column Face (10) vs. Column Centerline (12).

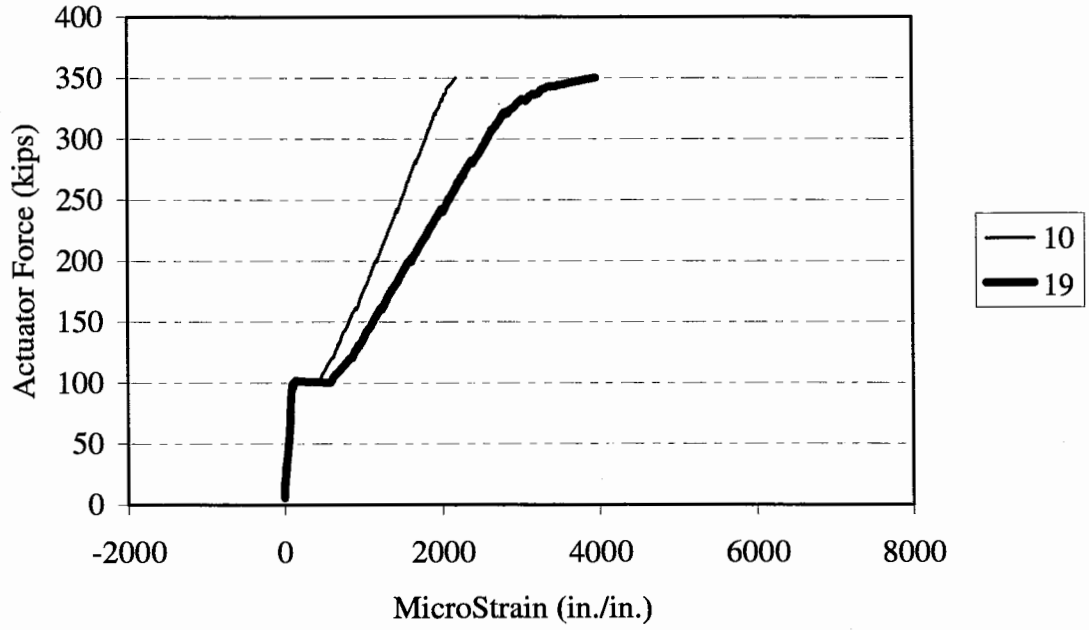

Figure C-2. Specimen 6F Load-Strain History
Side (19) vs. Center (10) Transverse Plane.

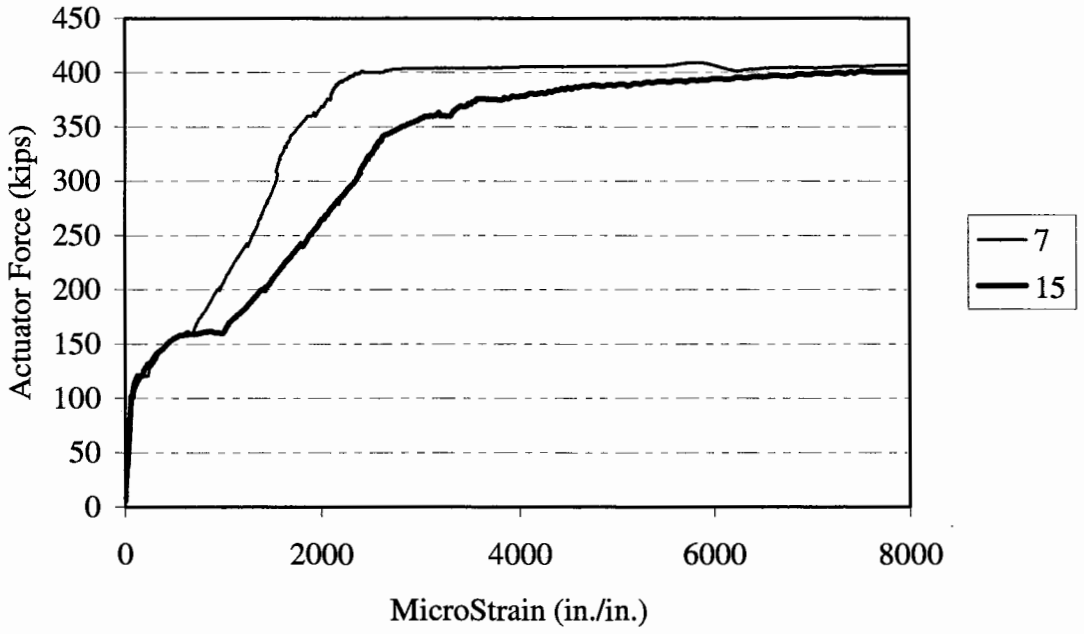

Figure C-3. Specimen 6F Load-Strain History Side (15) vs. Center (7) Transverse Plane.

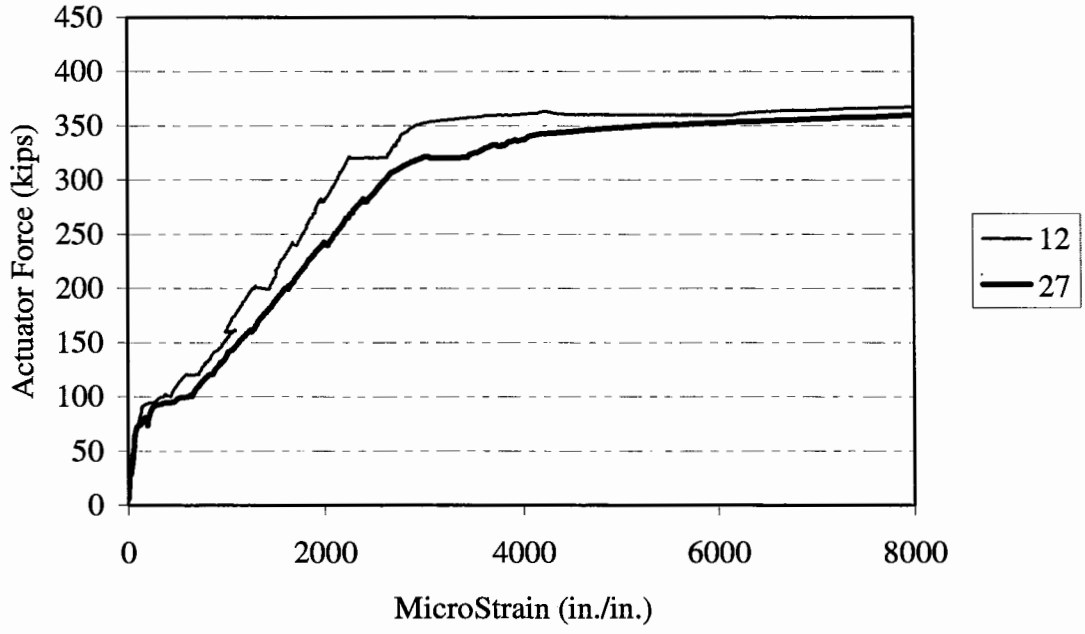

Figure C-4. Specimen 6F Load-Strain History Side (27) vs. Center (12) Transverse Plane.

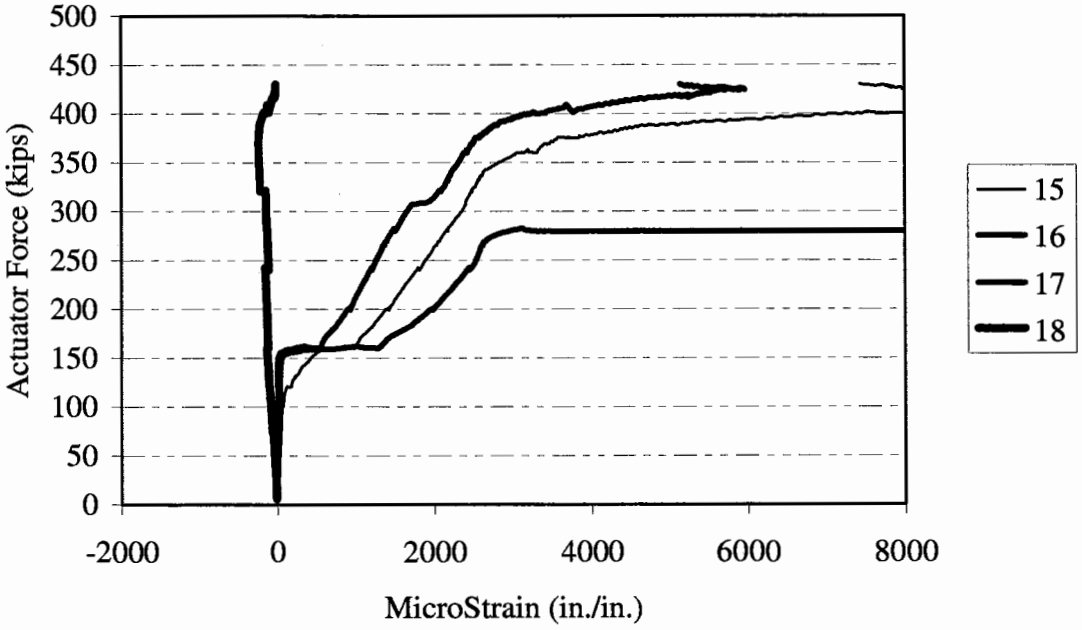

Figure C-5. Specimen 6F Strain Profile Through-Depth Side Face.

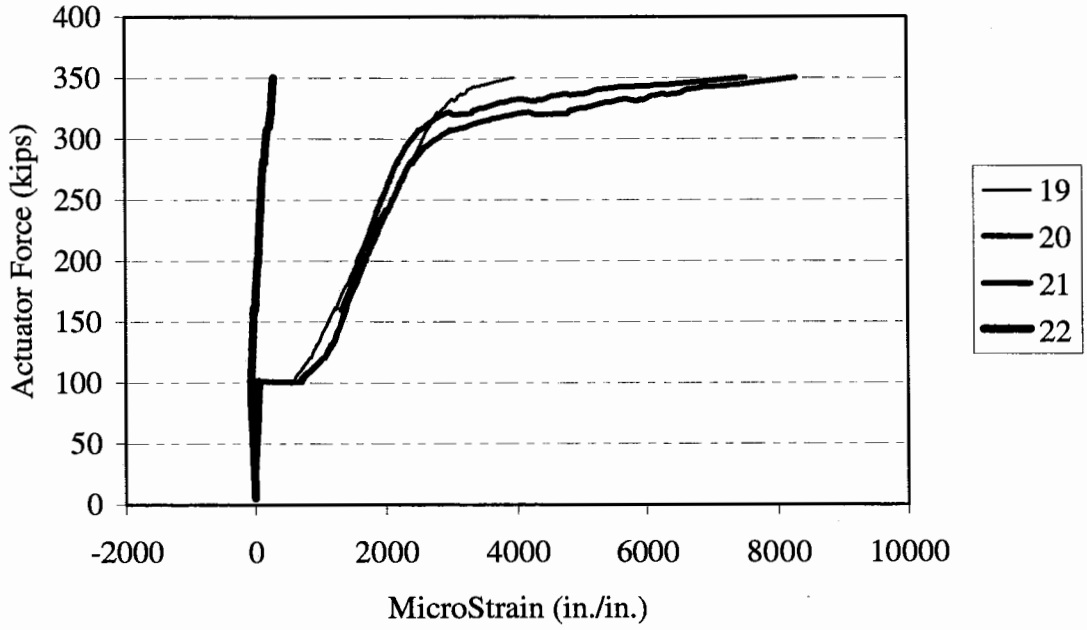

Figure C-6. Specimen 6F Strain Profile Through-Depth Side Face.

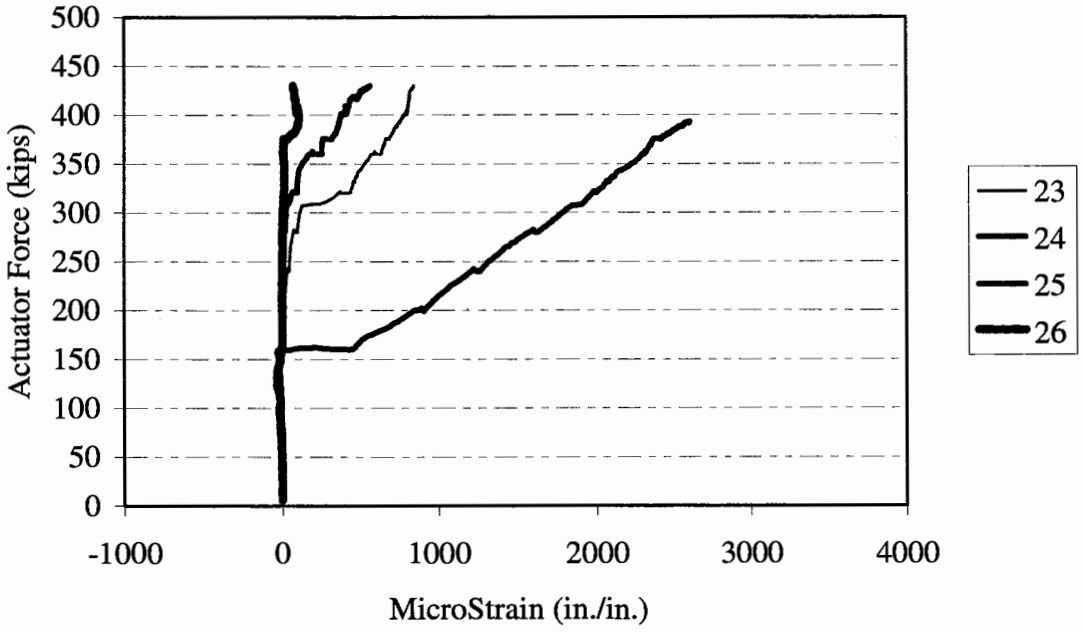

Figure C-7. Specimen 6F Strain Profile Transverse (Stirrup) Reinforcement.

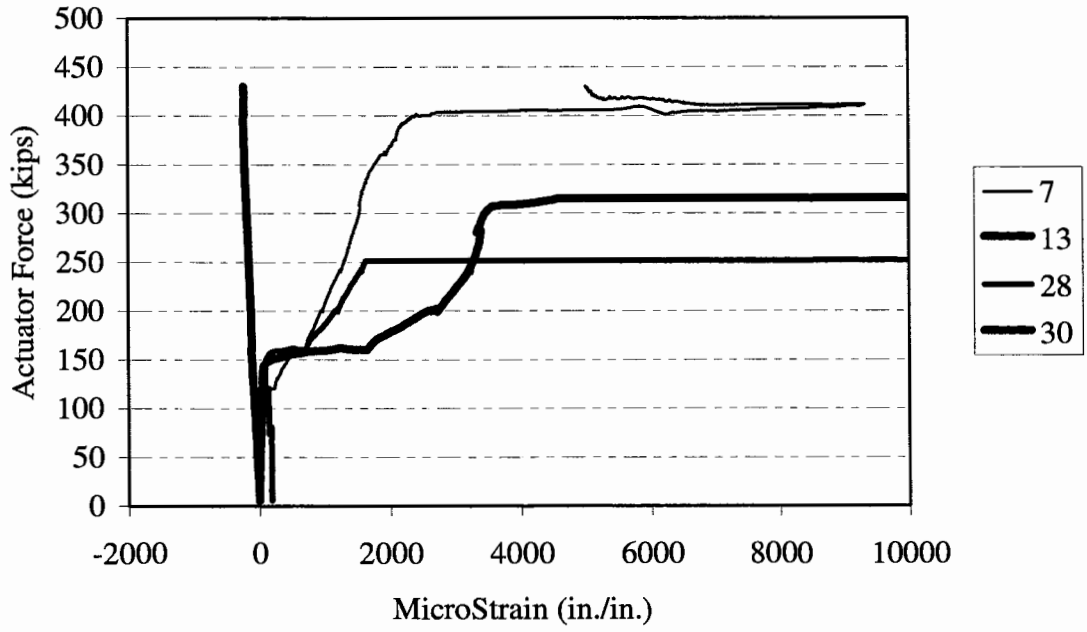

Figure C-8. Specimen 6F Strain Profile Through-Depth Centerline.

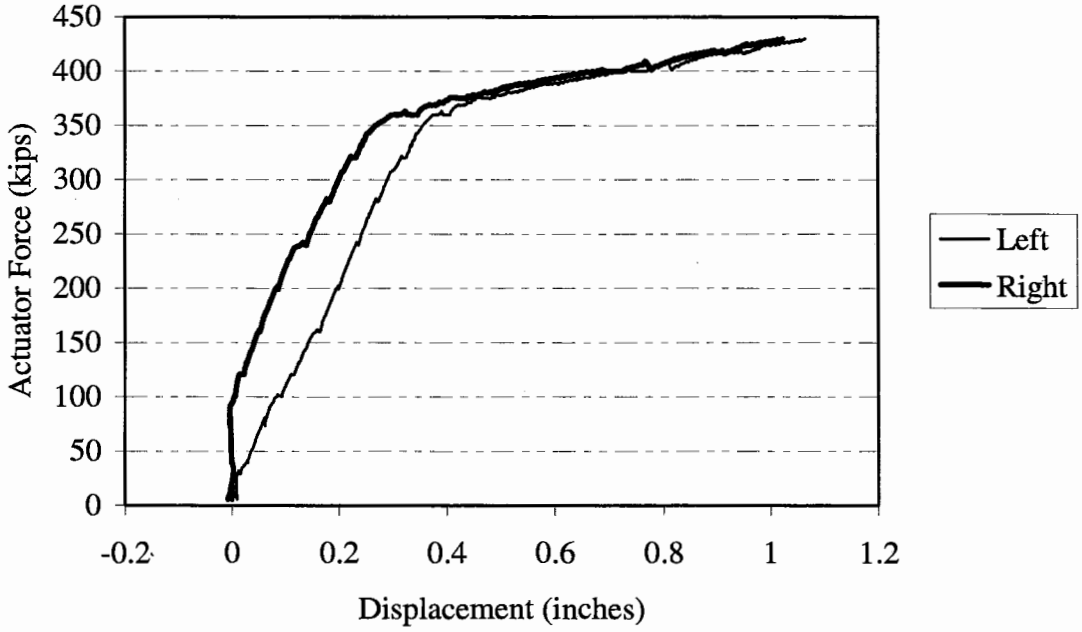

Figure C-9. Specimen 6F Load-Displacement History.

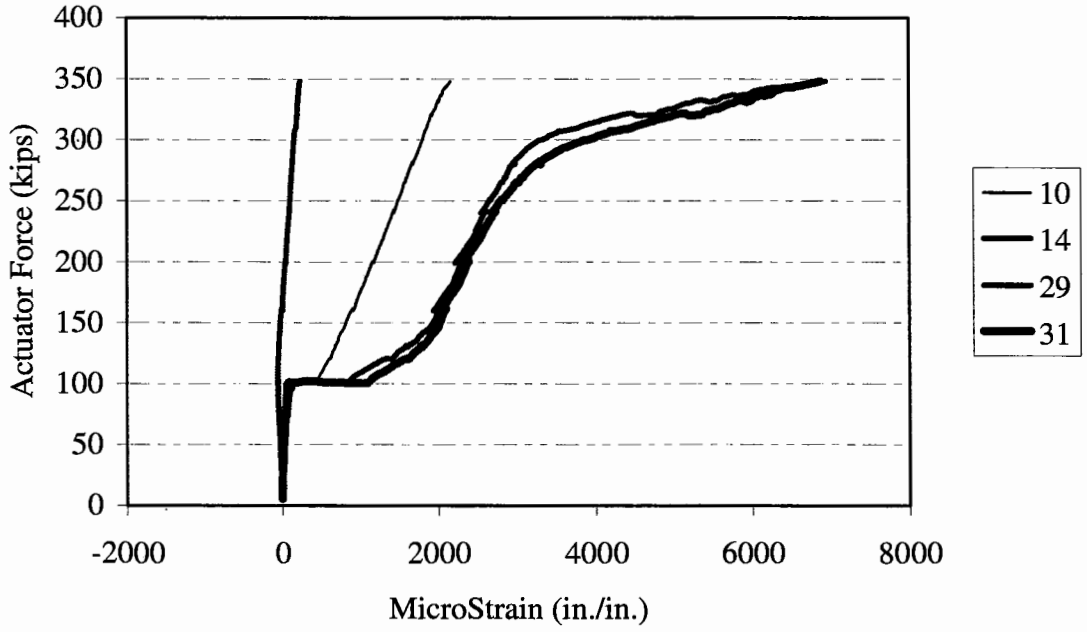

Figure C-10. Specimen 6F Strain Profile Through-Depth Centerline.

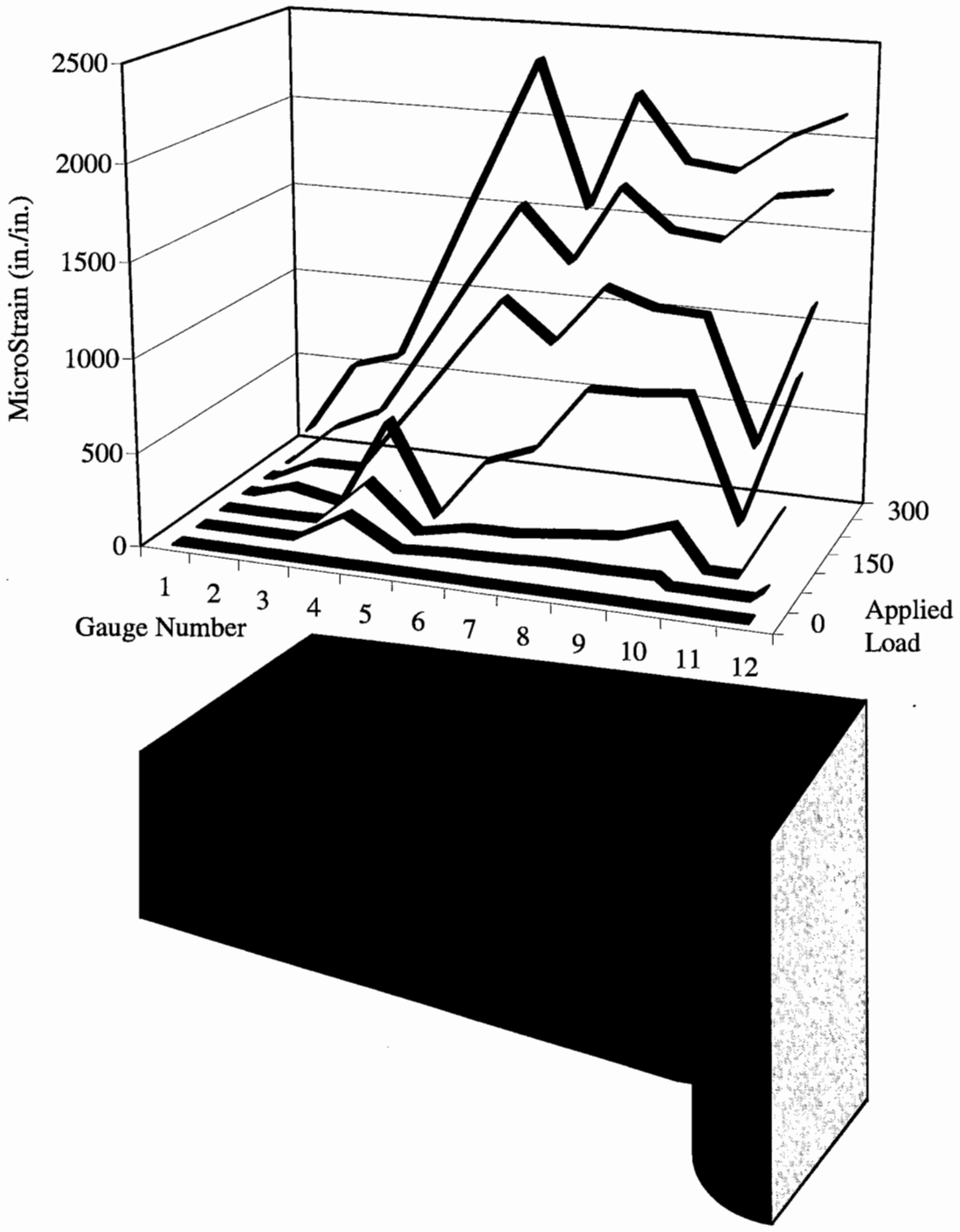

Figure C-11. Specimen 6F Longitudinal Reinforcement Strain Profile for Strain Gauges 1 Through 12.

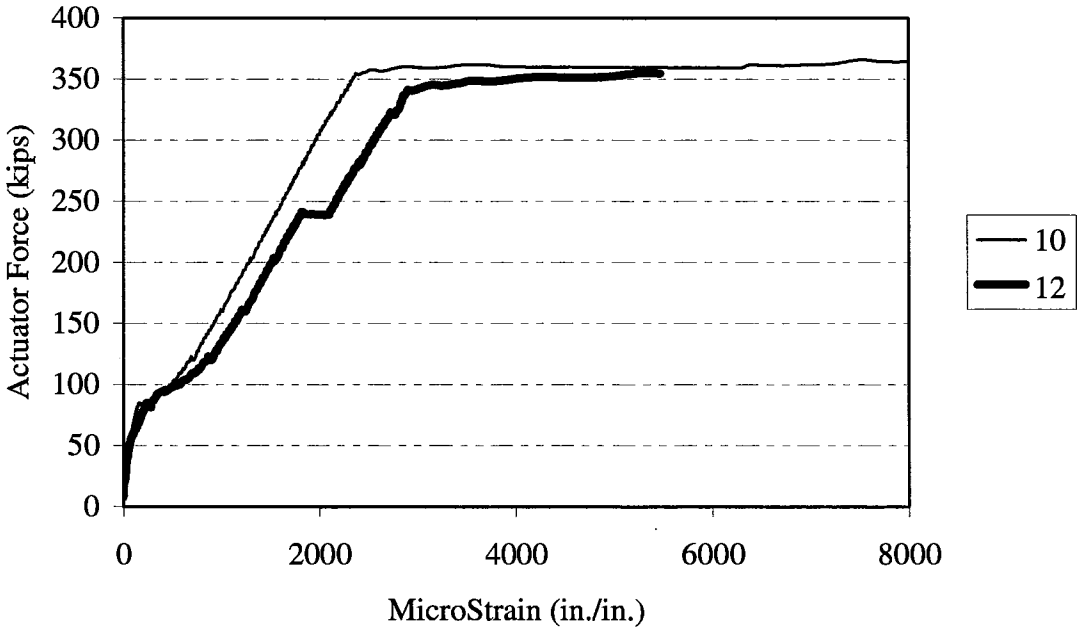

Figure C-12. Specimen 6G Load-Strain History Column Face (10) vs. Column Centerline (12).

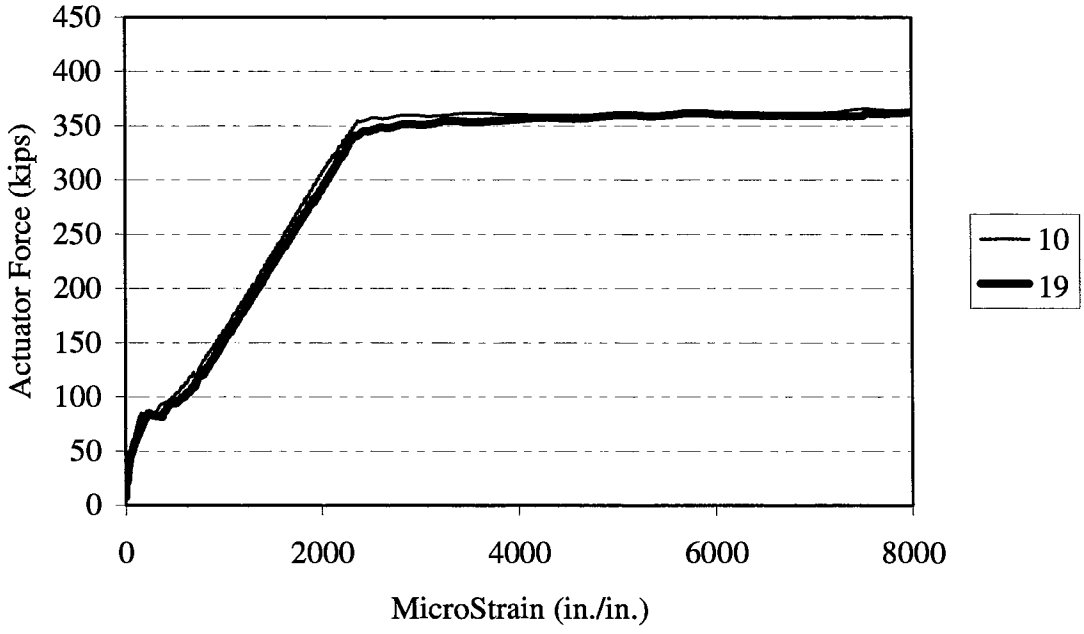

Figure C-13. Specimen 6G Load-Strain History Side (19) vs. Center (10) Transverse Plane.

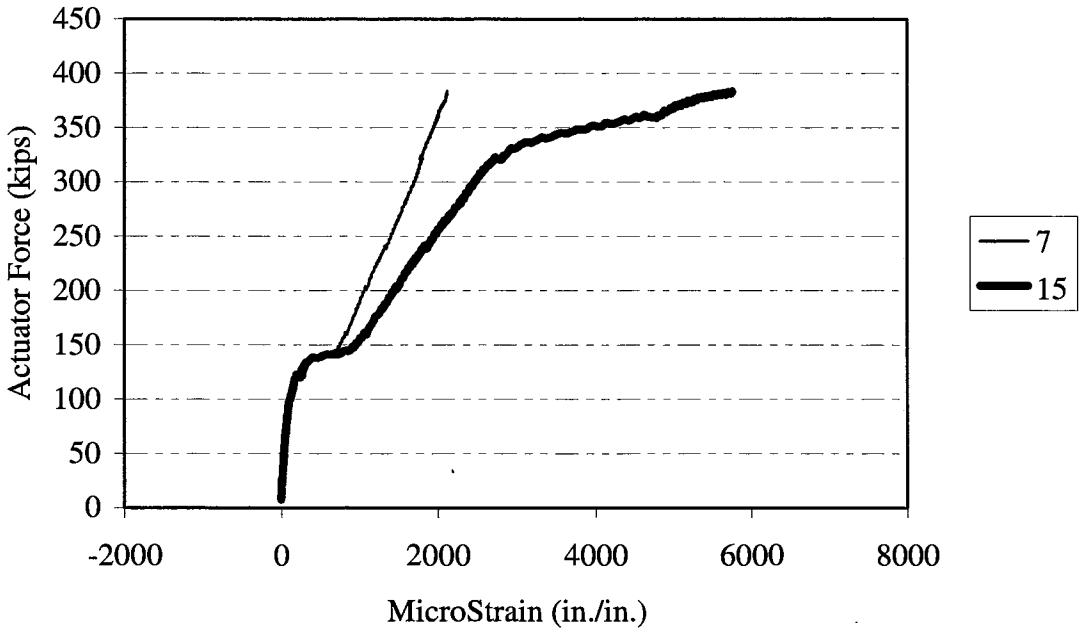

Figure C-14. Specimen 6G Load-Strain History Side (15) vs. Center (7) Transverse Plane.

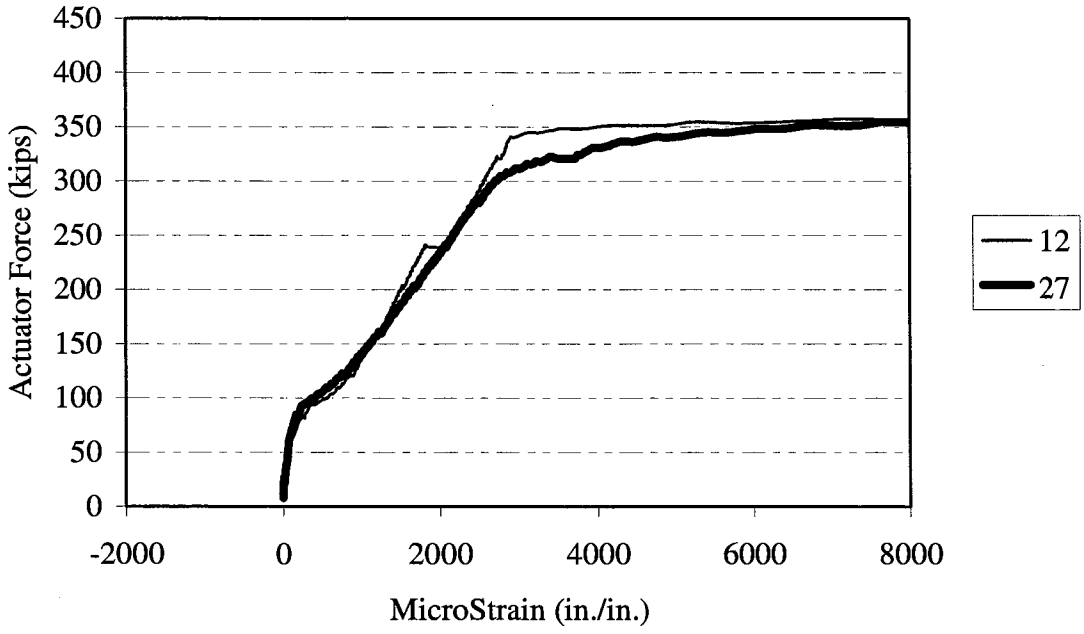

Figure C-15. Specimen 6G Load-Strain History Side (27) vs. Center (12) Transverse Plane.

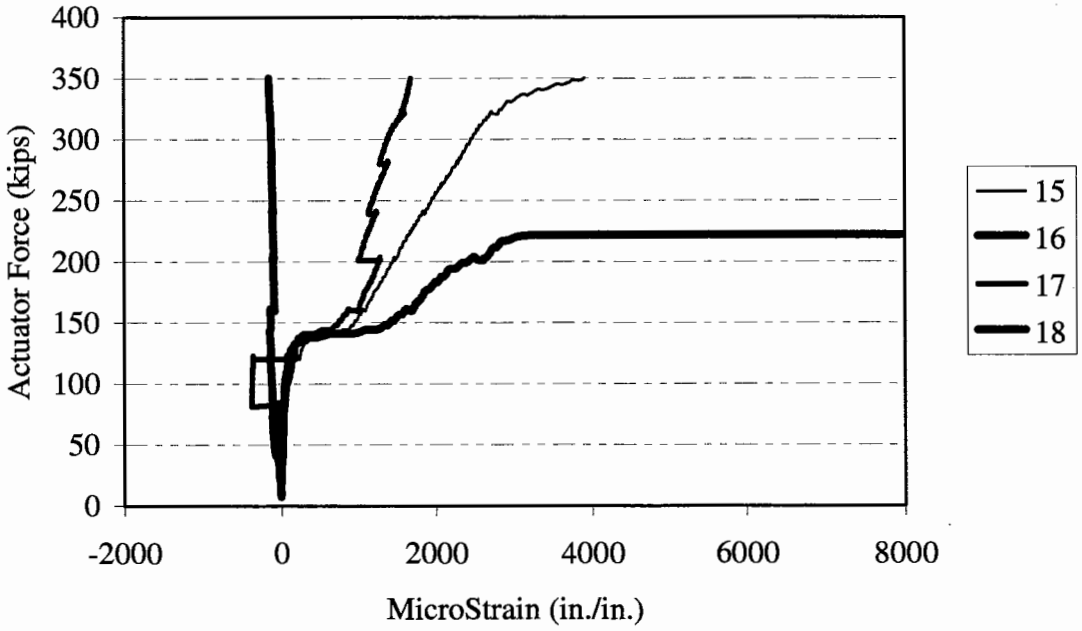

Figure C-16. Specimen 6G Strain Profile Through-Depth Side Face.

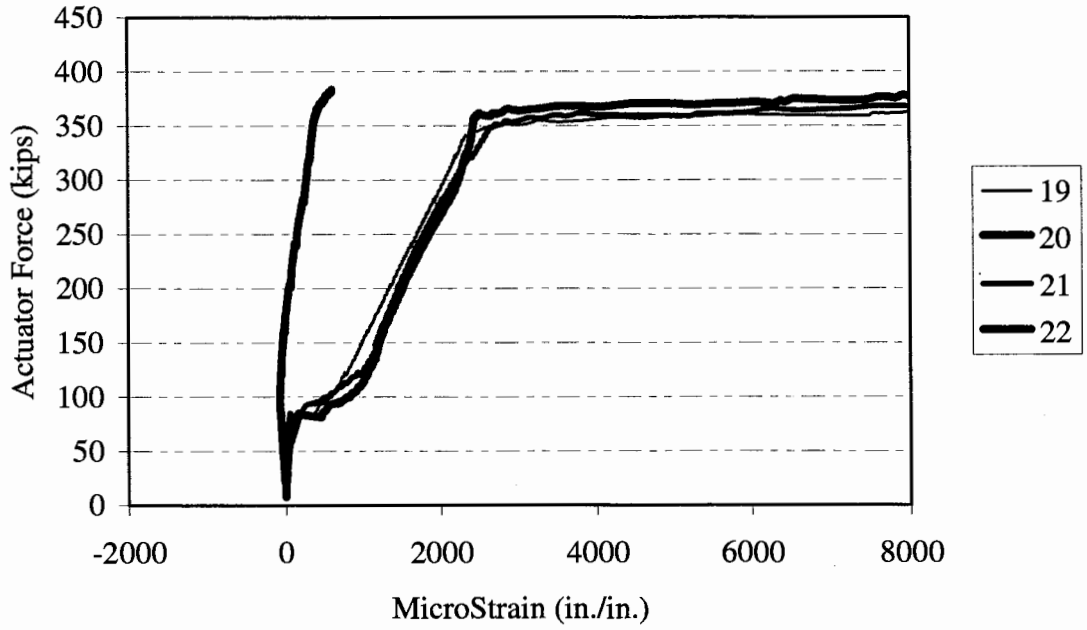

Figure C-17. Specimen 6G Strain Profile Through-Depth Side Face.

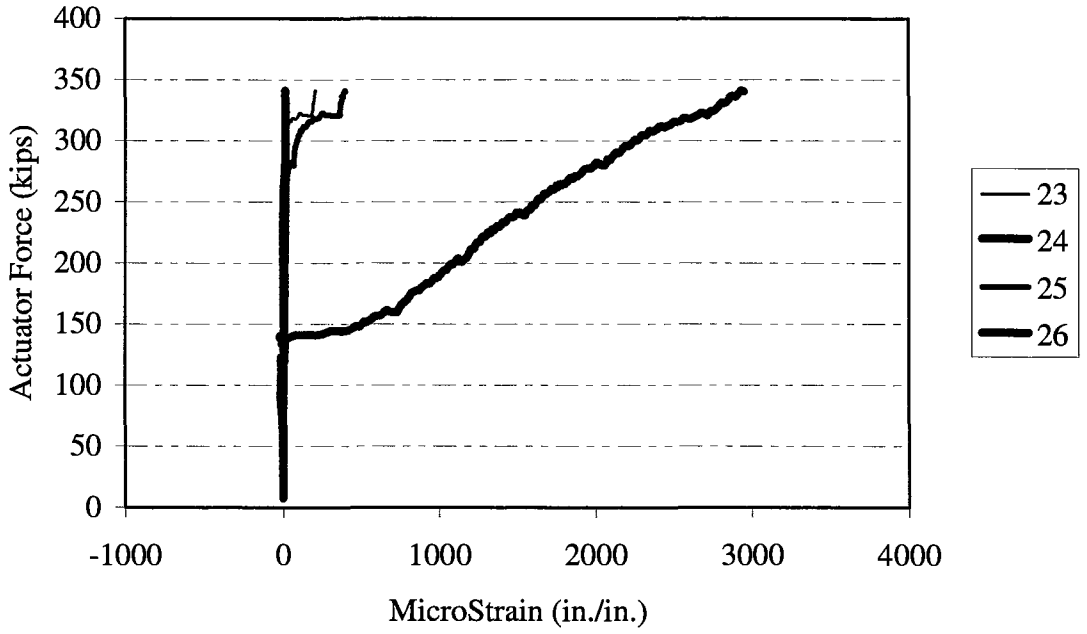

Figure C-18. Specimen 6G Strain Profile Transverse (Stirrup) Reinforcement.

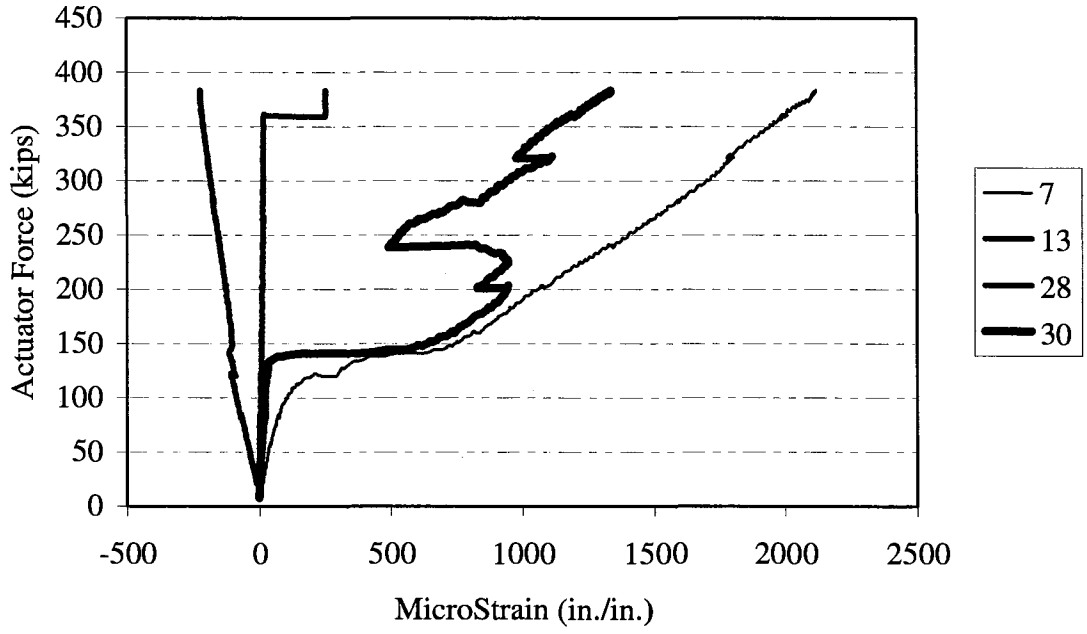

Figure C-19. Specimen 6G Strain Profile Through-Depth Centerline.

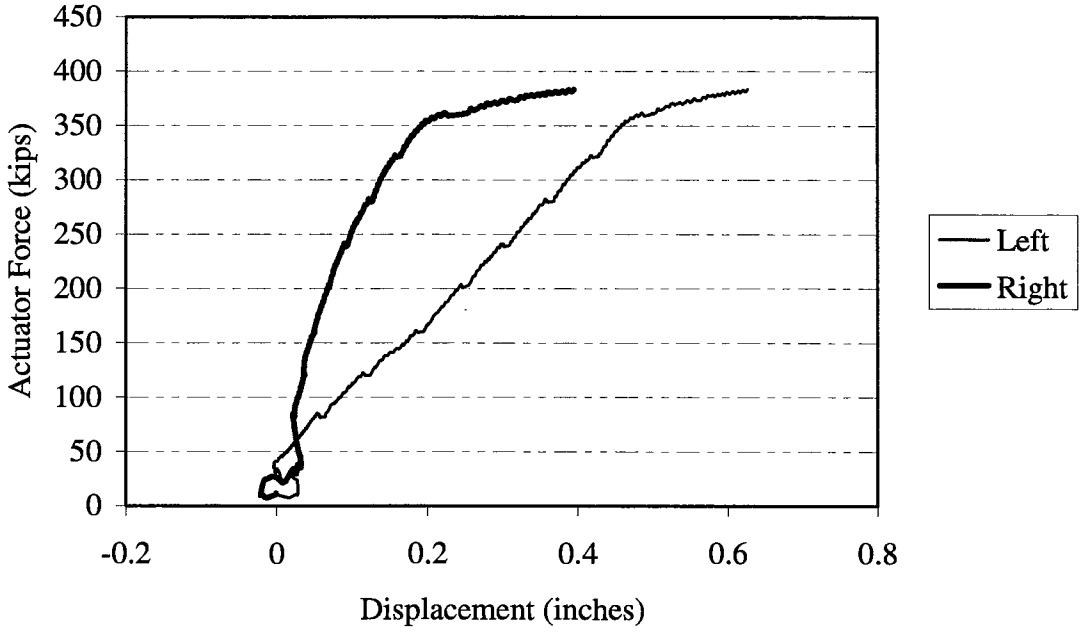

Figure C-20. Specimen 6G Load-Displacement History.

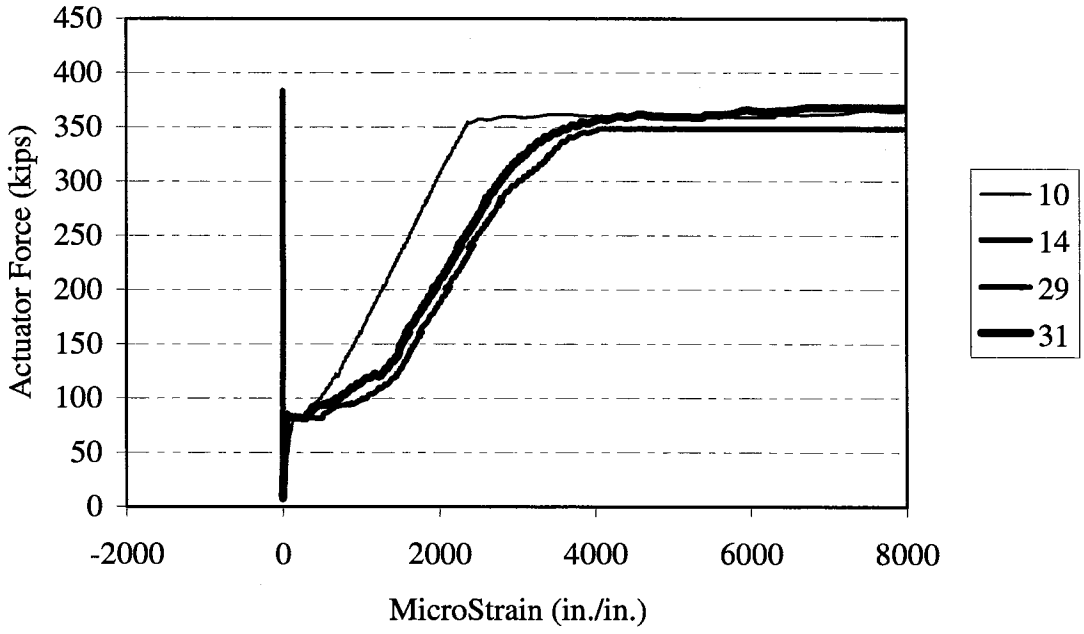

Figure C-21. Specimen 6G Strain Profile Through-Depth Centerline.

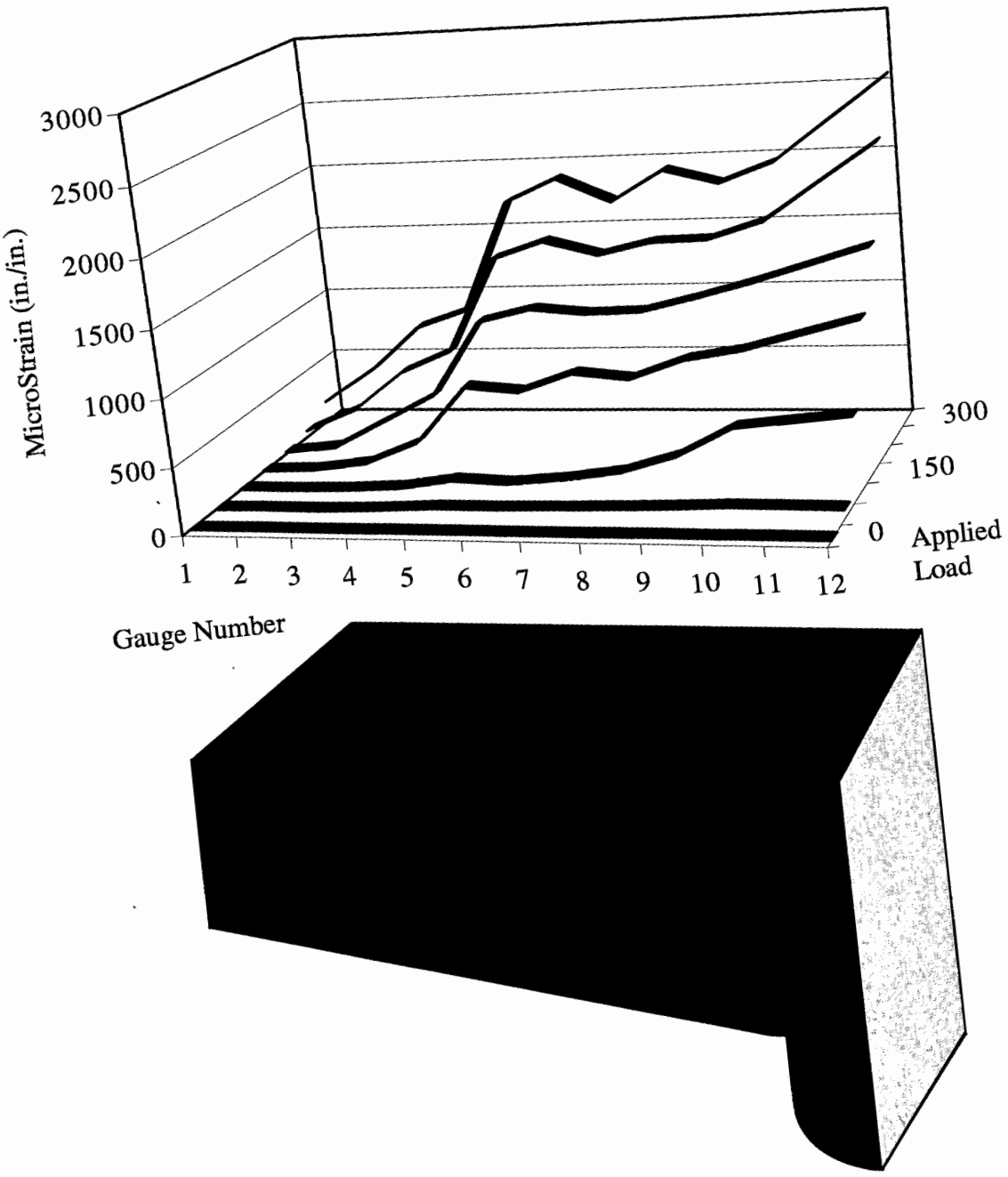

Figure C-22. Specimen 6G Longitudinal Reinforcement Strain Profile for Strain Gauges 1 Through 12.

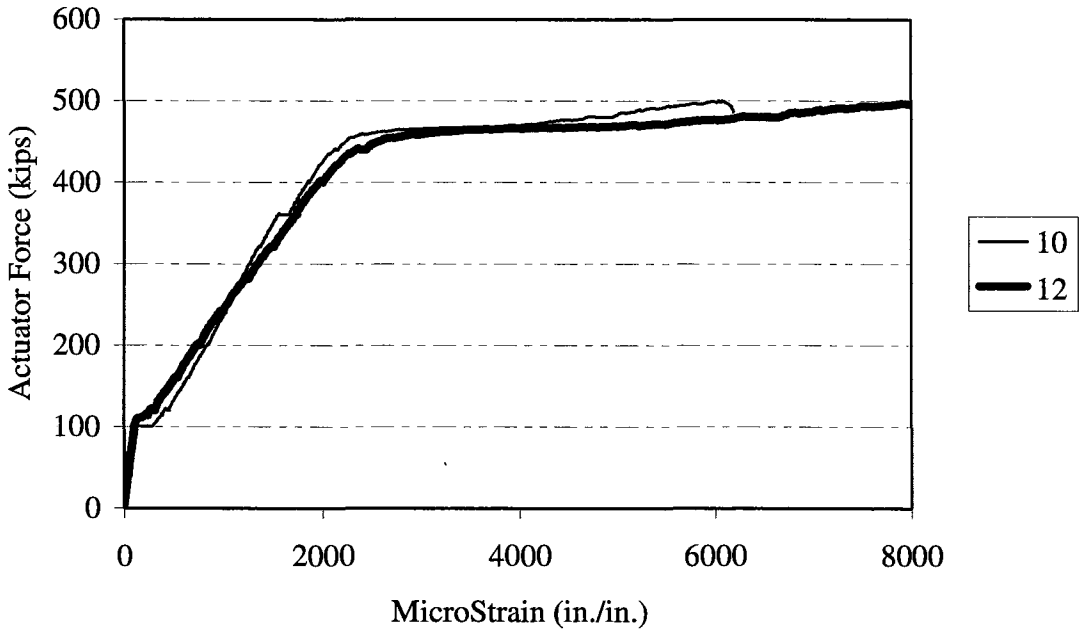

Figure C-23. Specimen 7F Load-Strain History Column Face (10) vs. Column Centerline (12).

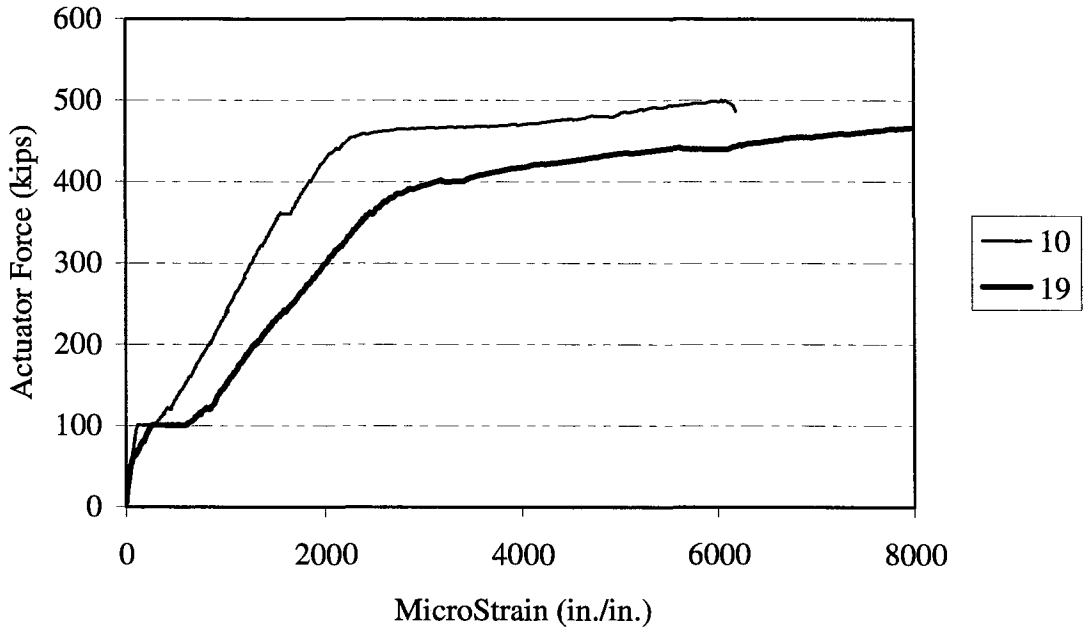

Figure C-24. Specimen 7F Load-Strain History Side (19) vs. Center (10) Transverse Plane.

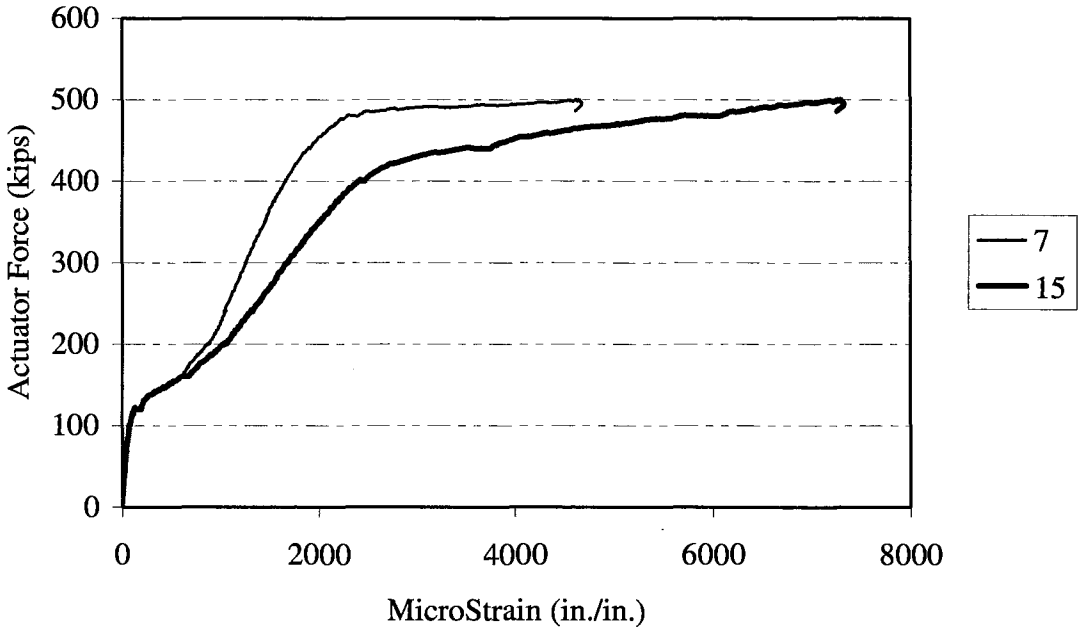

Figure C-25. Specimen 7F Load-Strain History Side (15) vs. Center (7) Transverse Plane.

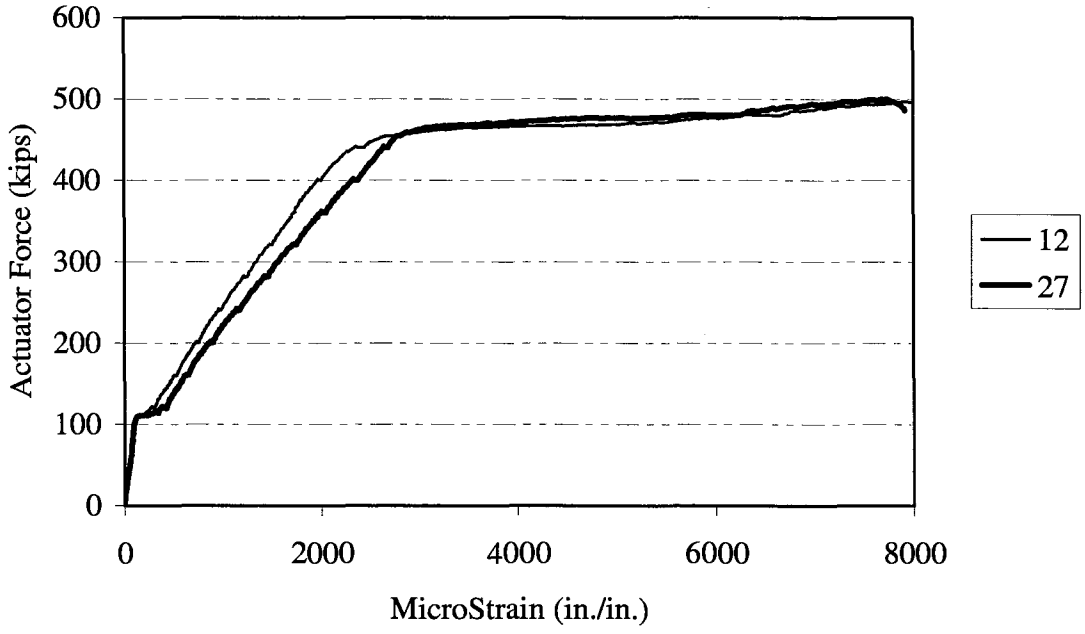

Figure C-26. Specimen 7F Load-Strain History Side (27) vs. Center (12) Transverse Plane.

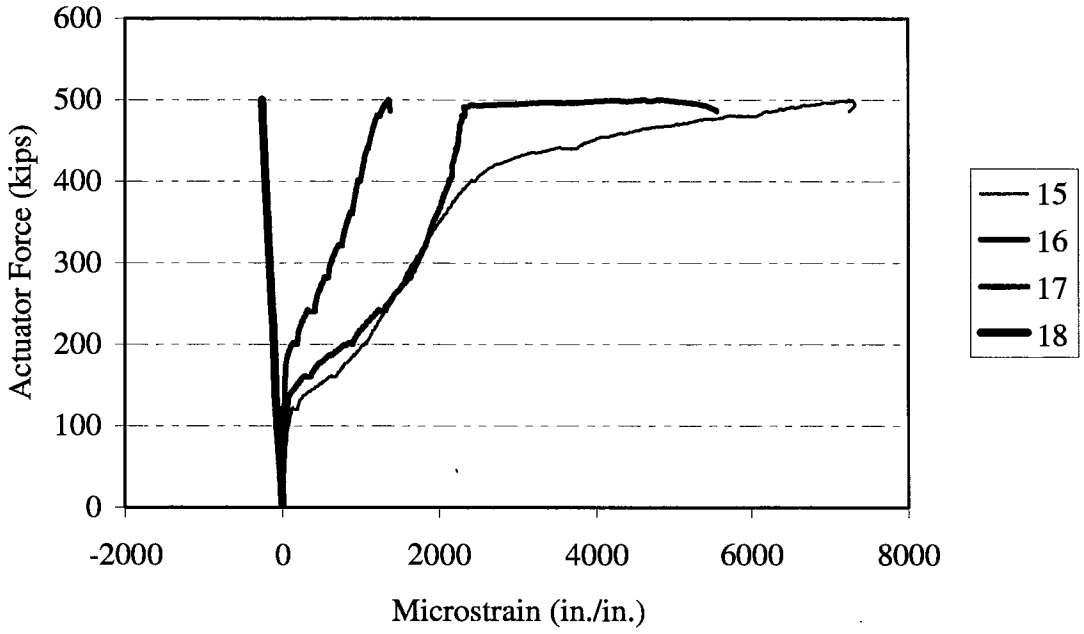

Figure C-27. Specimen 7F Strain Profile Through-Depth Side Face.

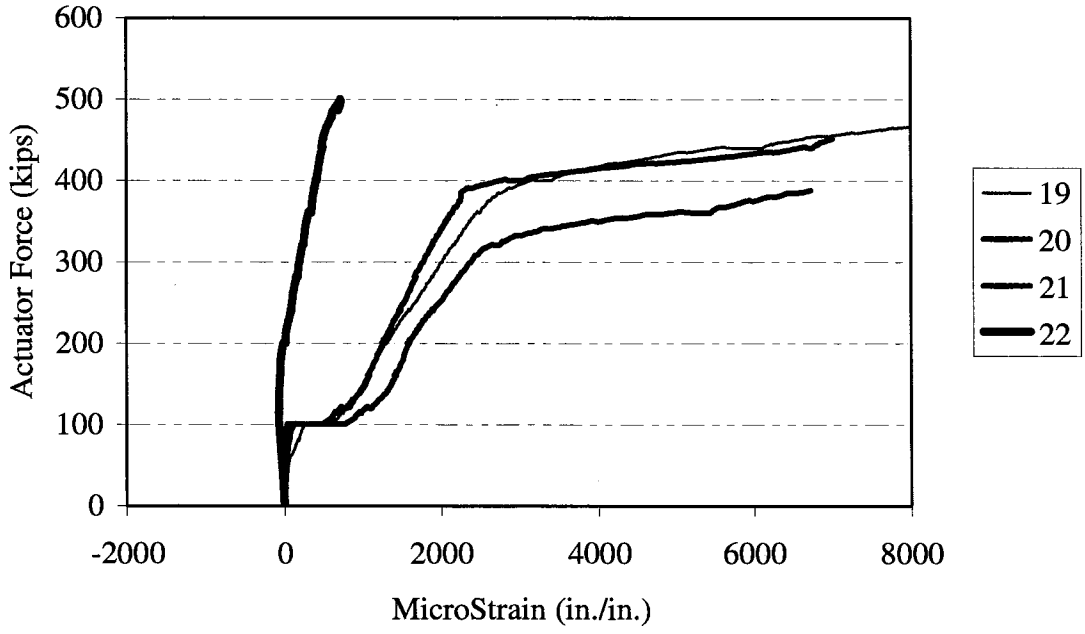

Figure C-28. Specimen 7F Strain Profile Through-Depth Side Face.

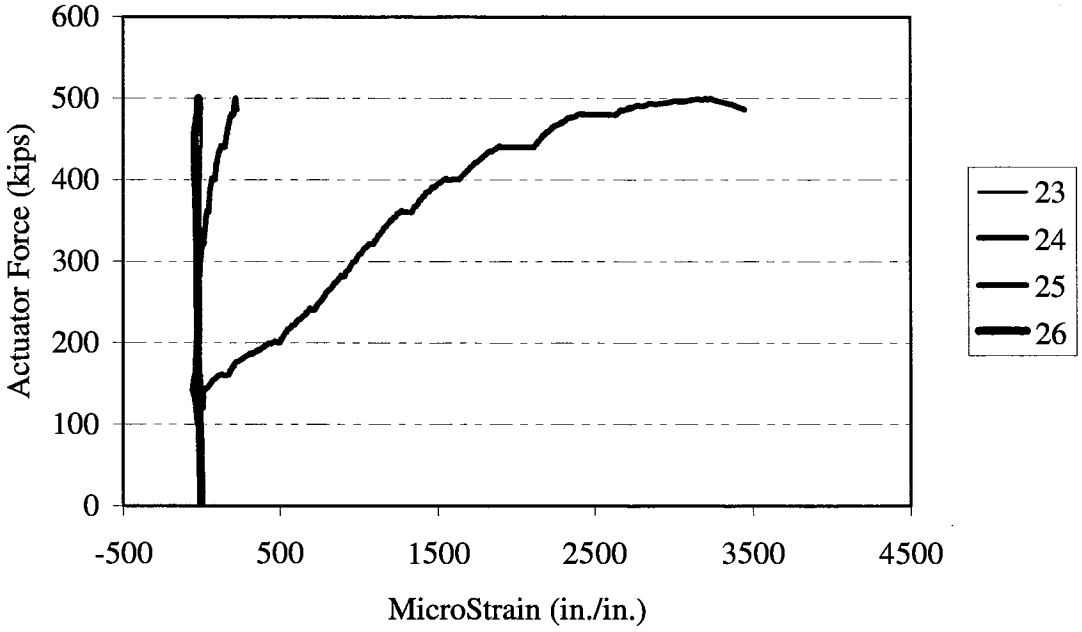

Figure C-29. Specimen 7F Strain Profile Transverse (Stirrup) Reinforcement.

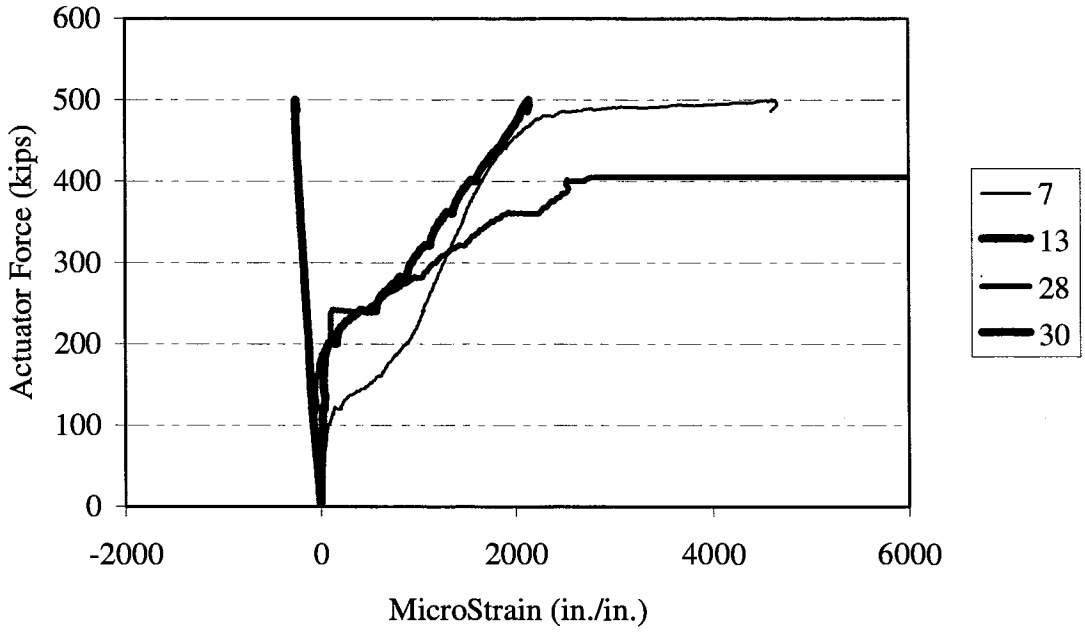

Figure C-30. Specimen 7F Strain Profile Through-Depth Centerline.

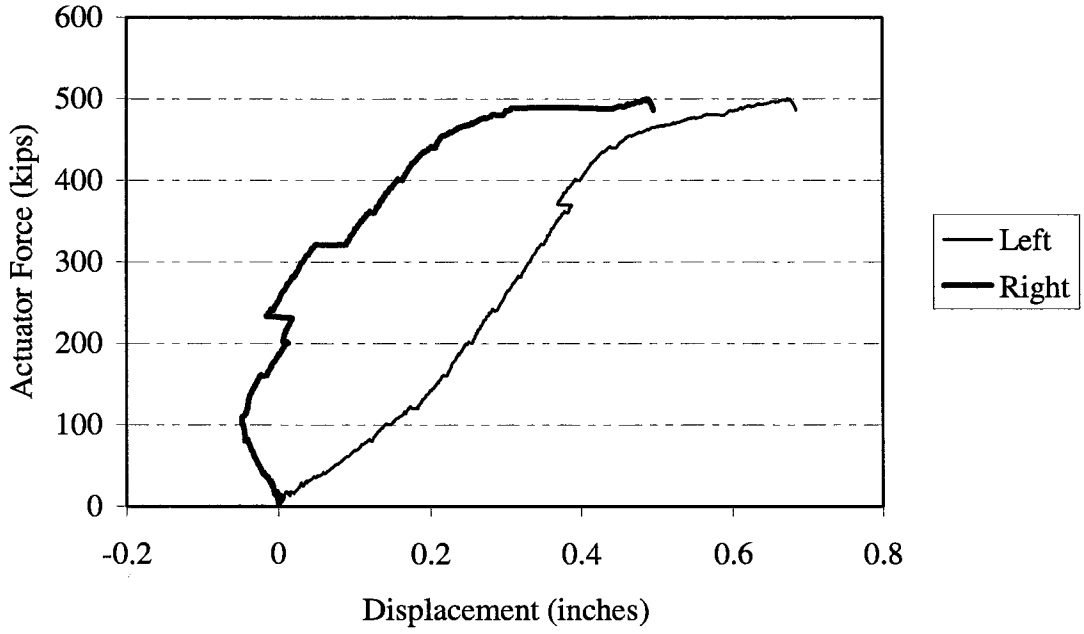

Figure C-31. Specimen 7F Load-Displacement History.

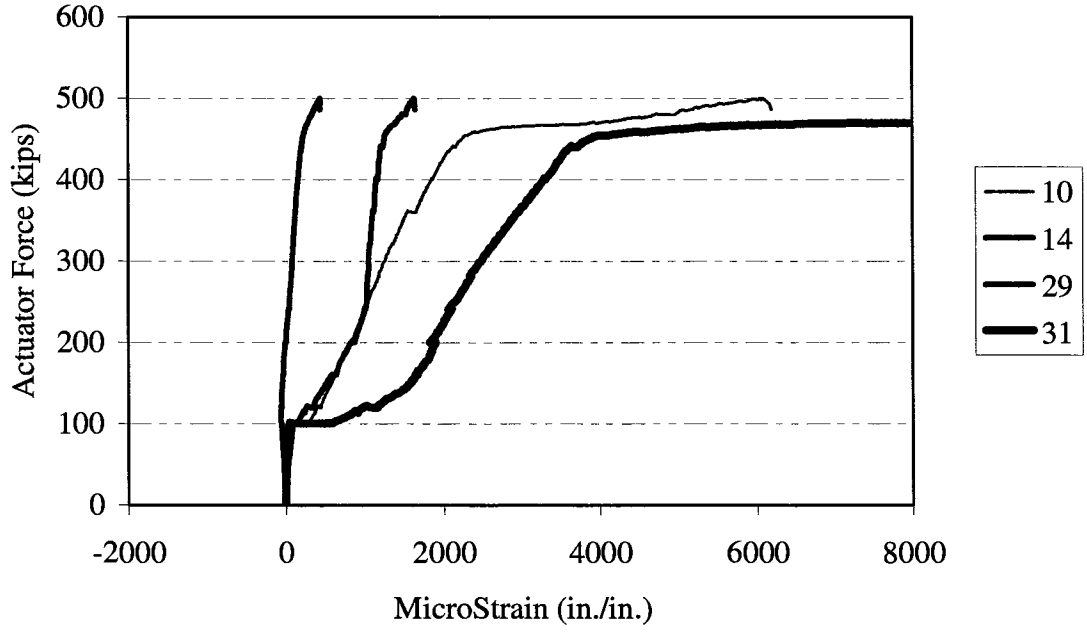

Figure C-32. Specimen 7F Strain Profile Through-Depth Centerline.

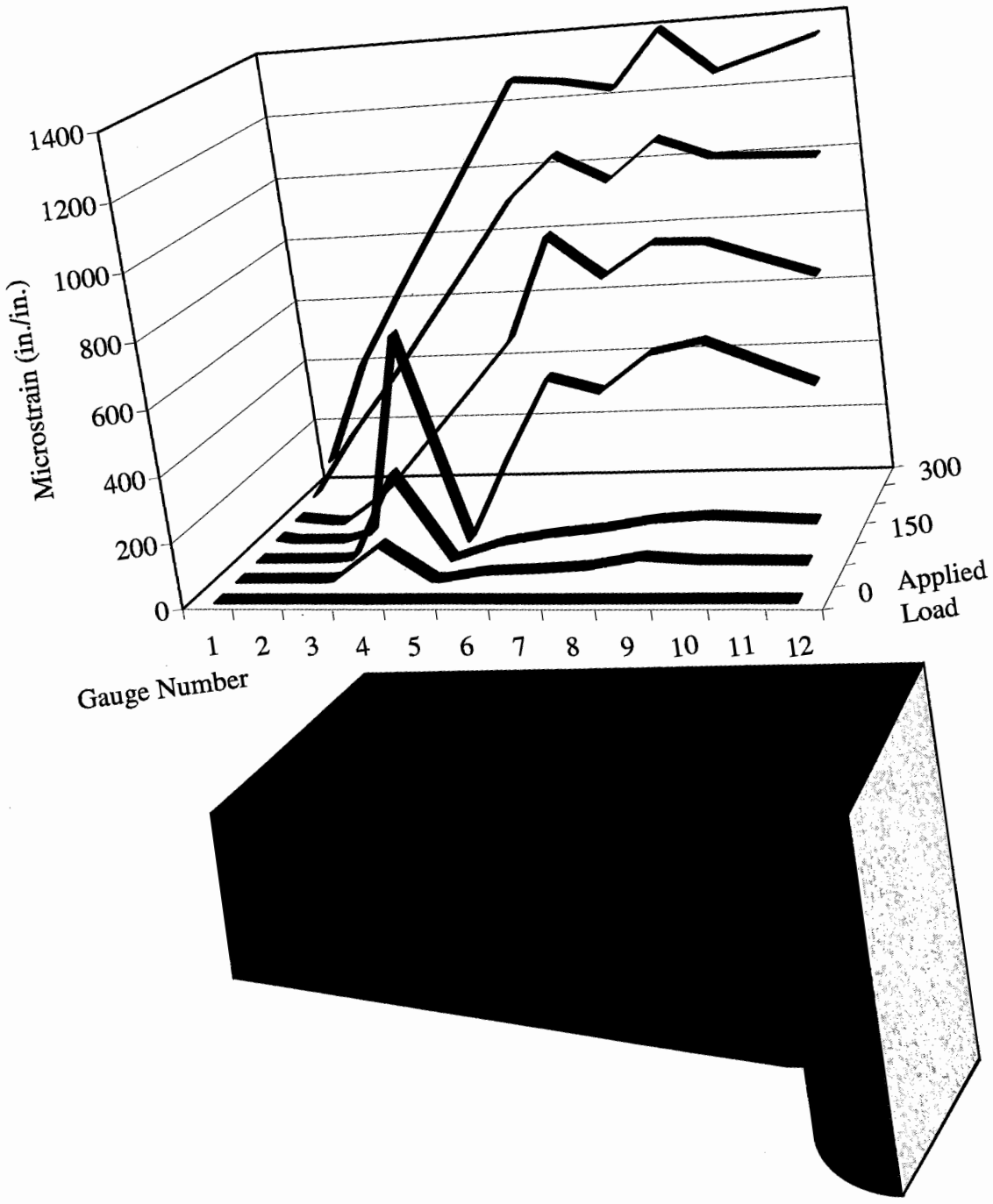

Figure C-33. Specimen 7F Longitudinal Reinforcement Strain Profile for Strain Gauges 1 Through 12.

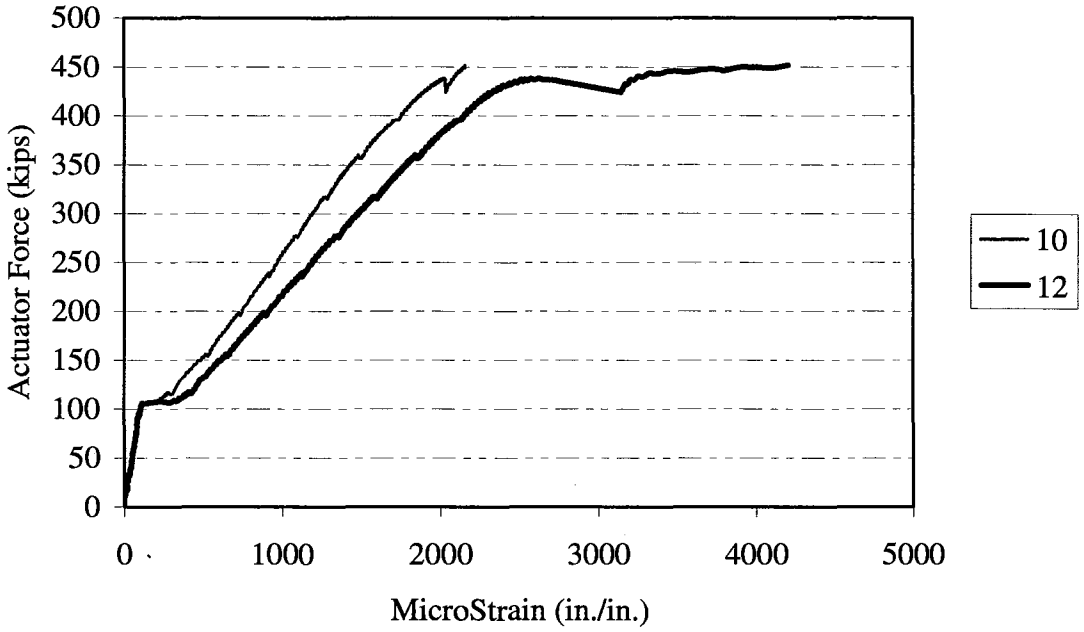

Figure C-34. Specimen 7H Load-Strain History Column face (10) vs. Column Centerline (12).

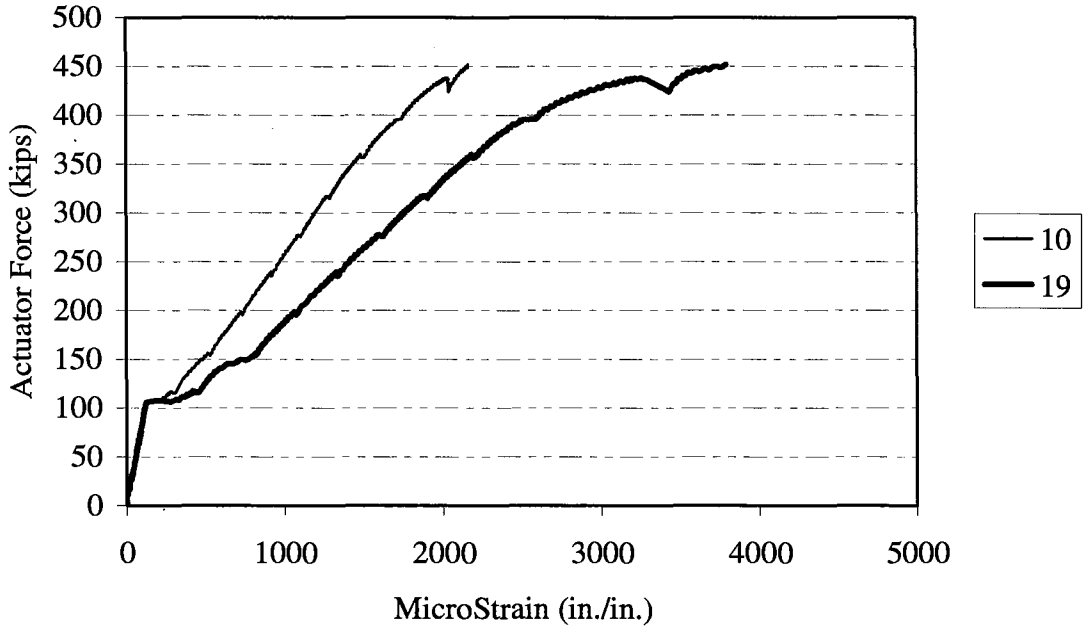

Figure C-35. Specimen 7H Load-Strain History Side (19) vs. Center (10) Transverse Plane.

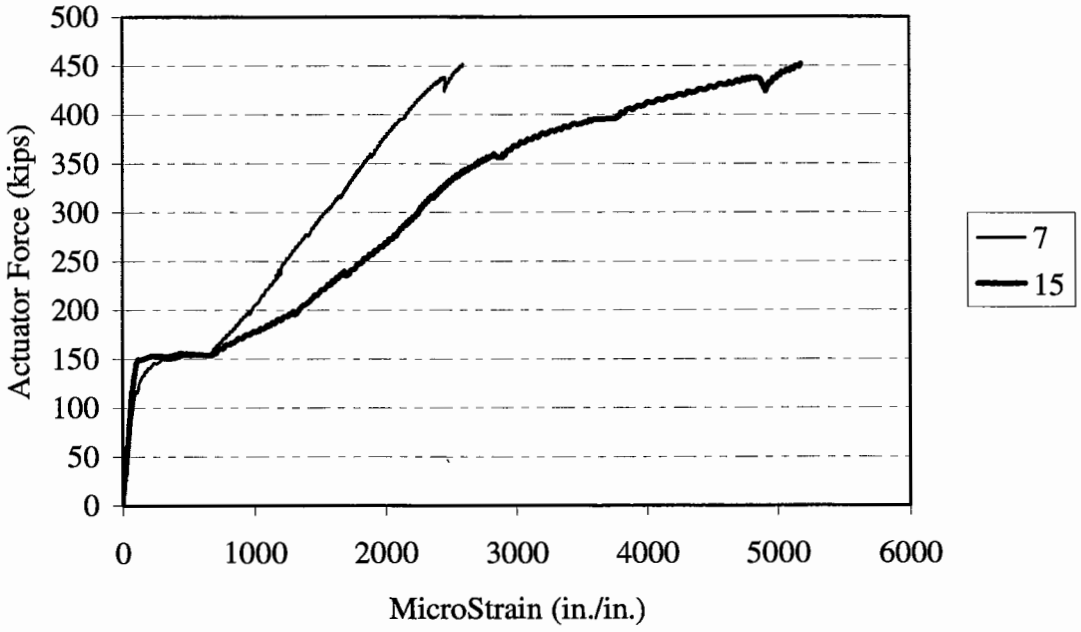

Figure C-36. Specimen 7H Load-Strain History Side (15) vs. Center (7) Transverse Plane.

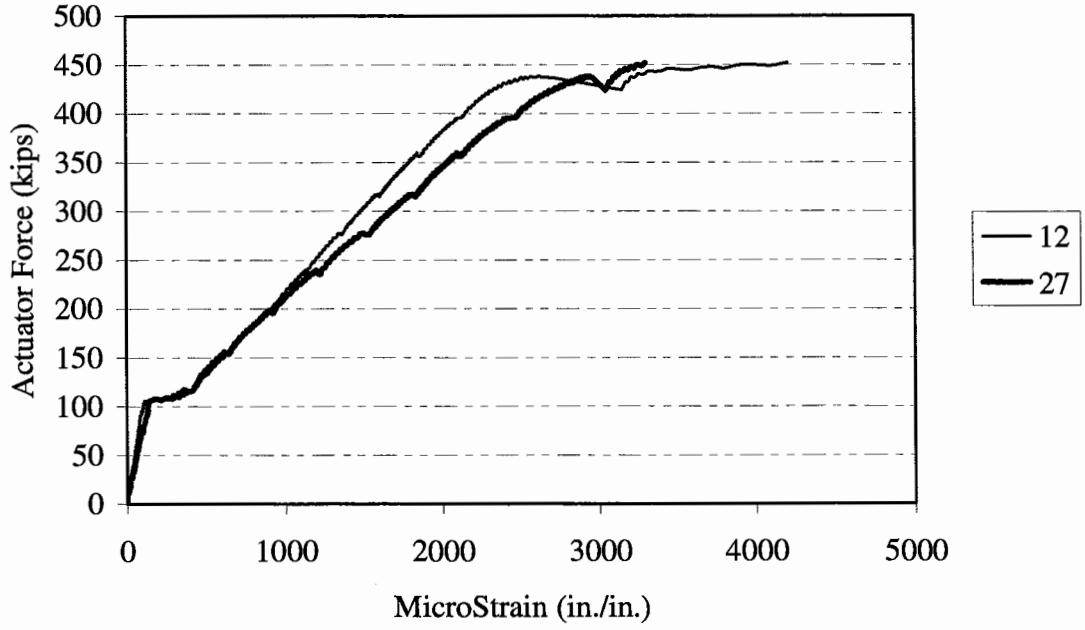

Figure C-37. Specimen 7H Load-Strain History Side (27) vs. Center (12) Transverse Plane.

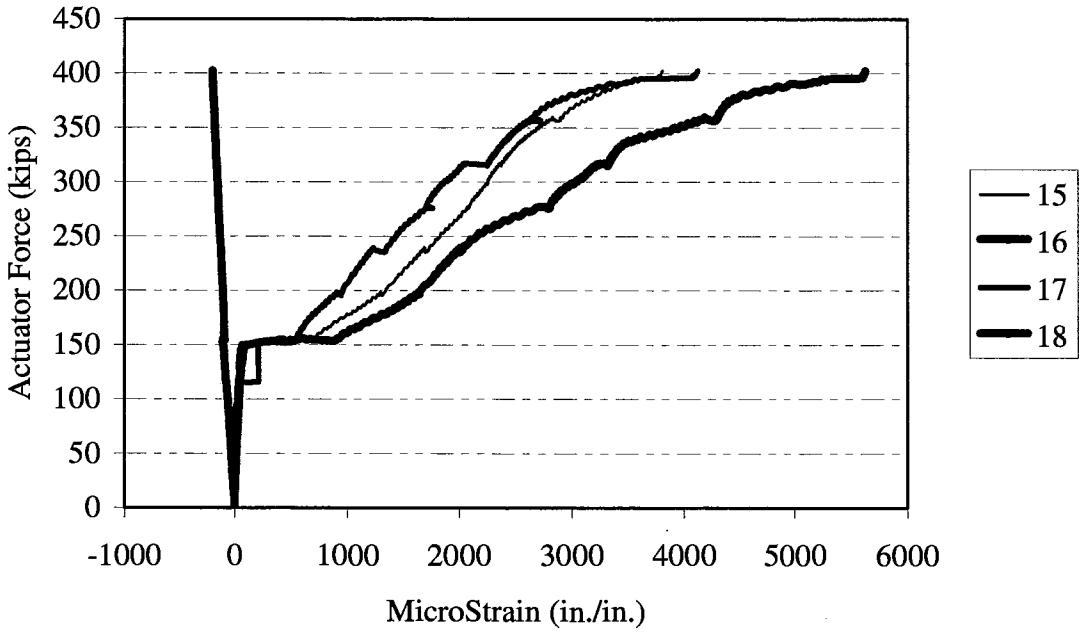

Figure C-38. Specimen 7H Strain Profile Through-Depth Side Face.

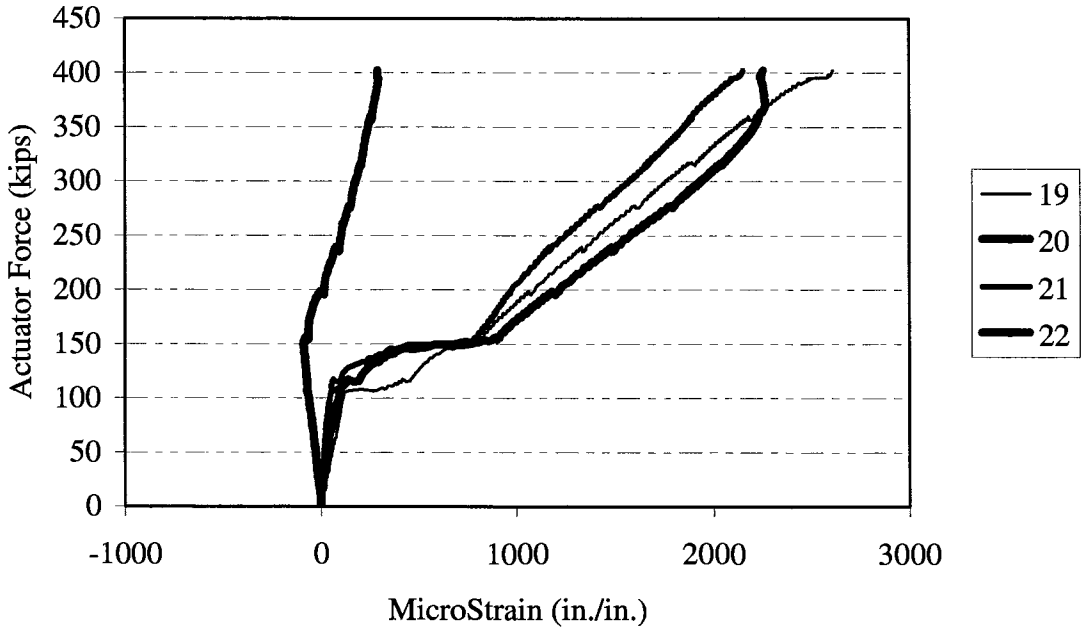

Figure C-39. Specimen 7H Strain Profile Through-Depth Side Face.

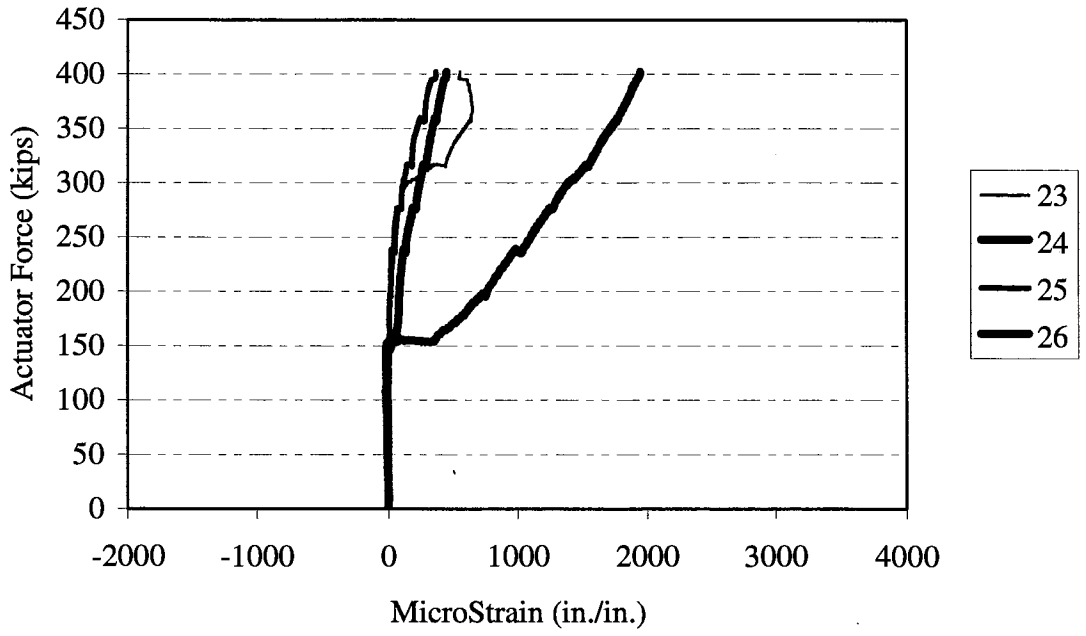

Figure C-40. Specimen 7H Strain Profile Transverse (Stirrup) Reinforcement.

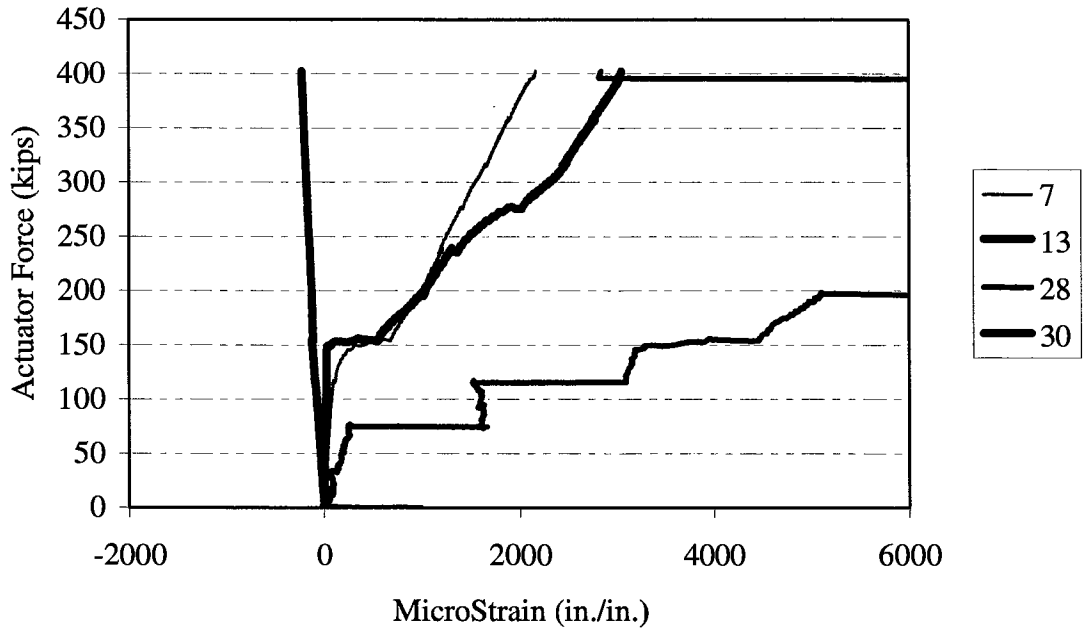

Figure C-41. Specimen 7H Strain Profile Through-Depth Centerline.

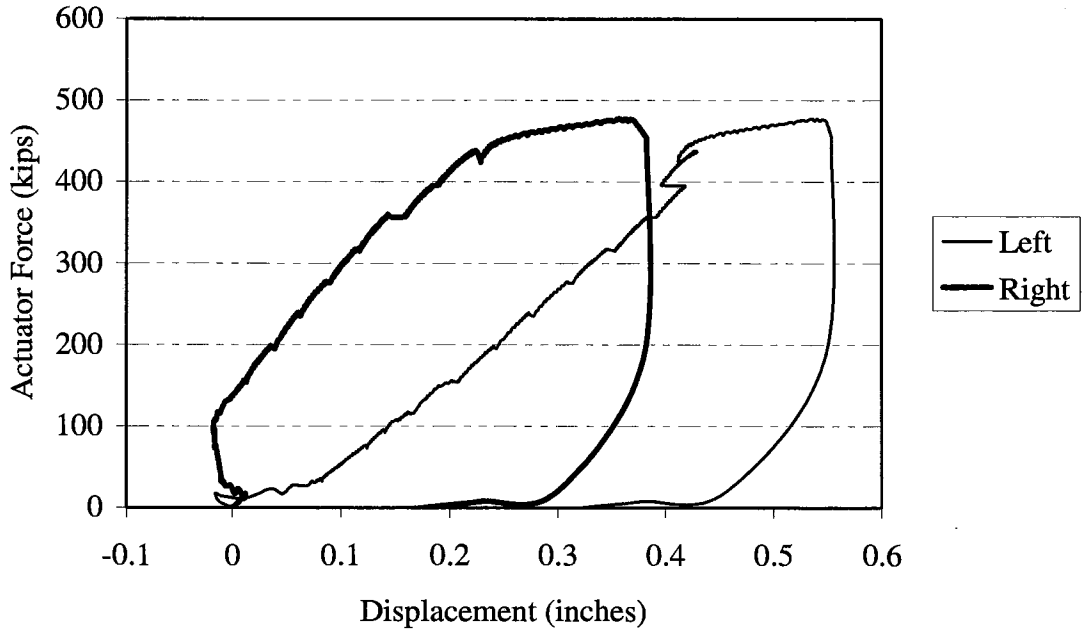

Figure C-42. Specimen 7H Load-Displacement History.

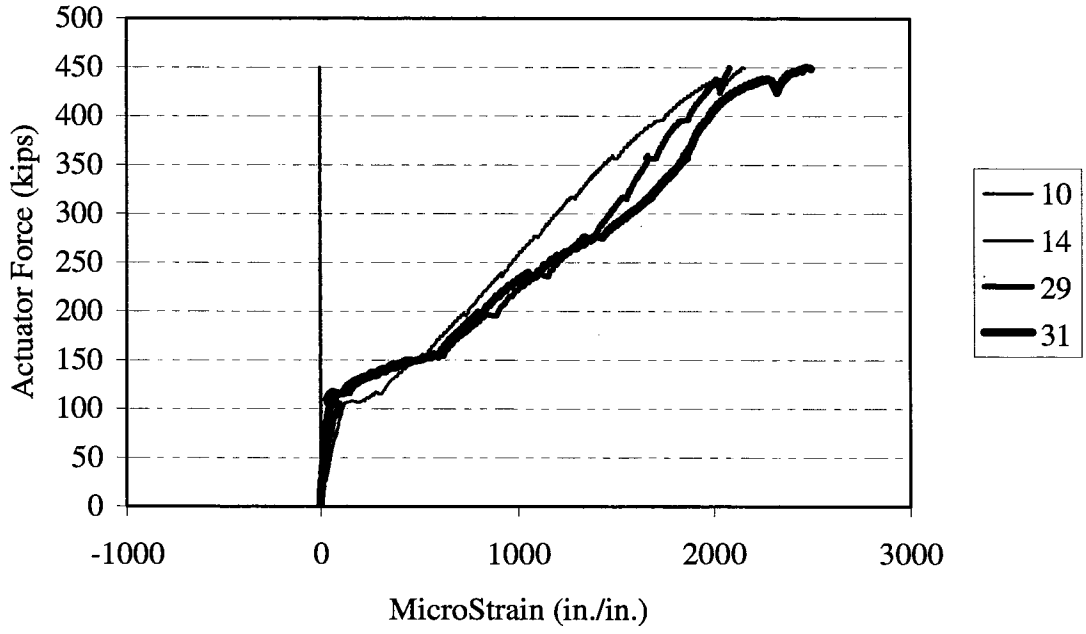

Figure C-43. Specimen 7H Strain Profile Through-Depth Centerline.

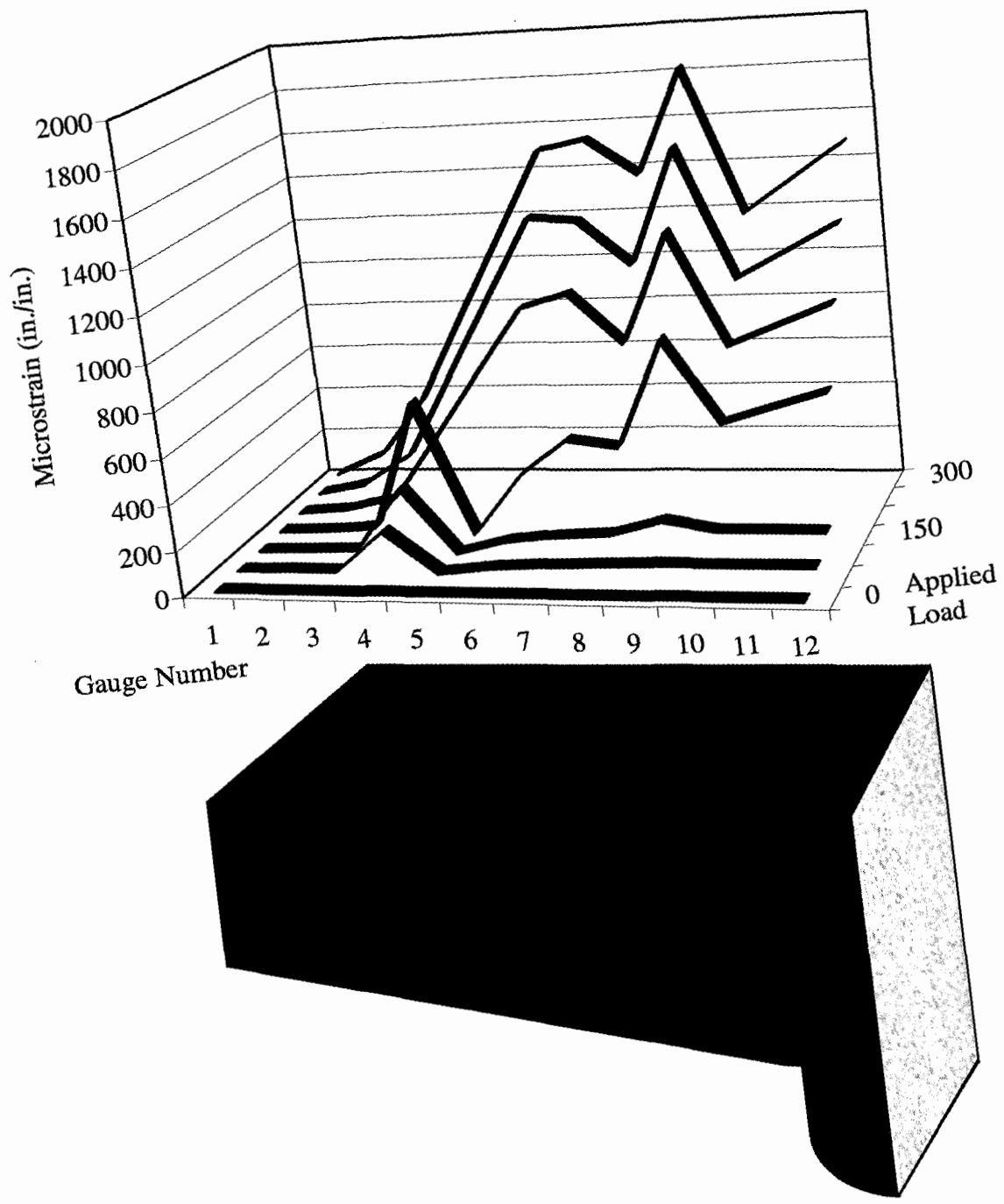

Figure C-44. Specimen 7H Longitudinal Reinforcement Strain Profile for Strain Gauges 1 Through 12.

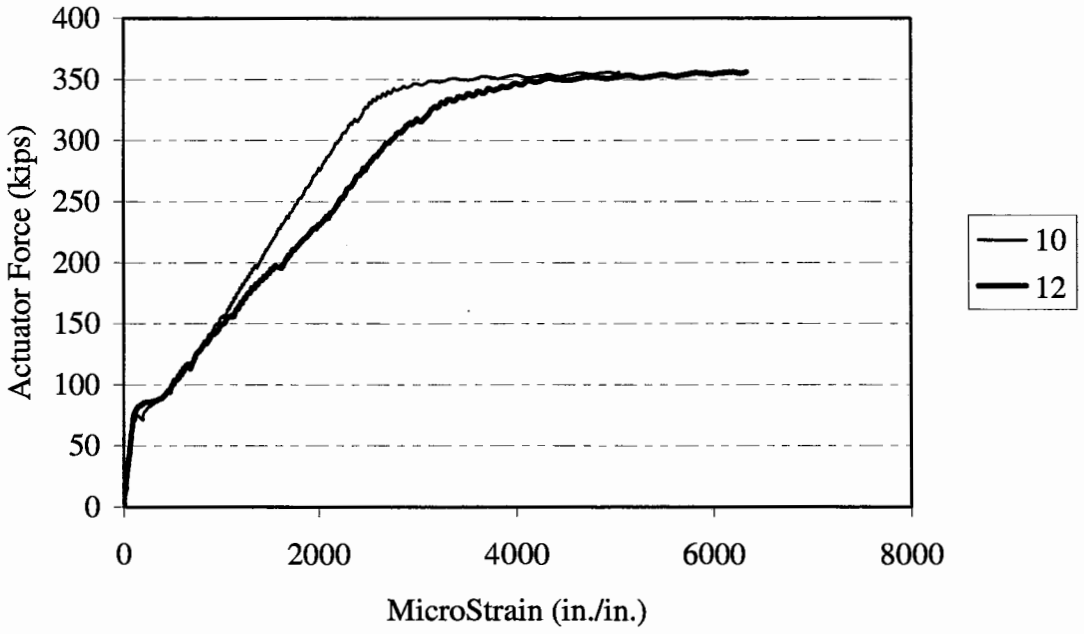

Figure C-45. Specimen 8G Load-Strain History Column Face (10) vs. Column Centerline (12).

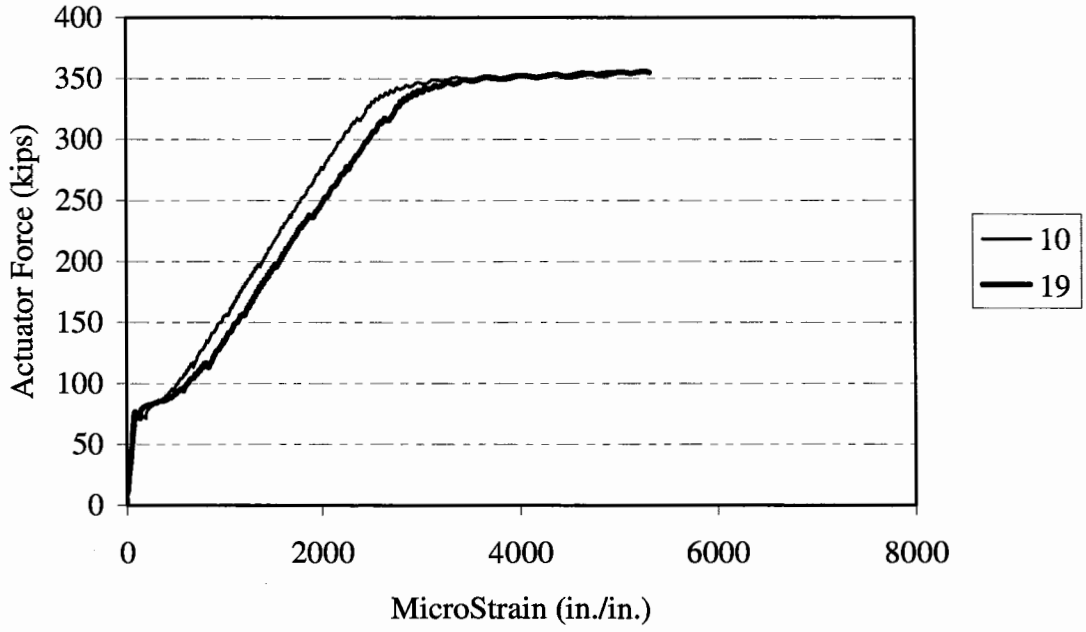

Figure C-46. Specimen 8G Load-Strain History Side (19) vs. Center (10) Transverse Plane.

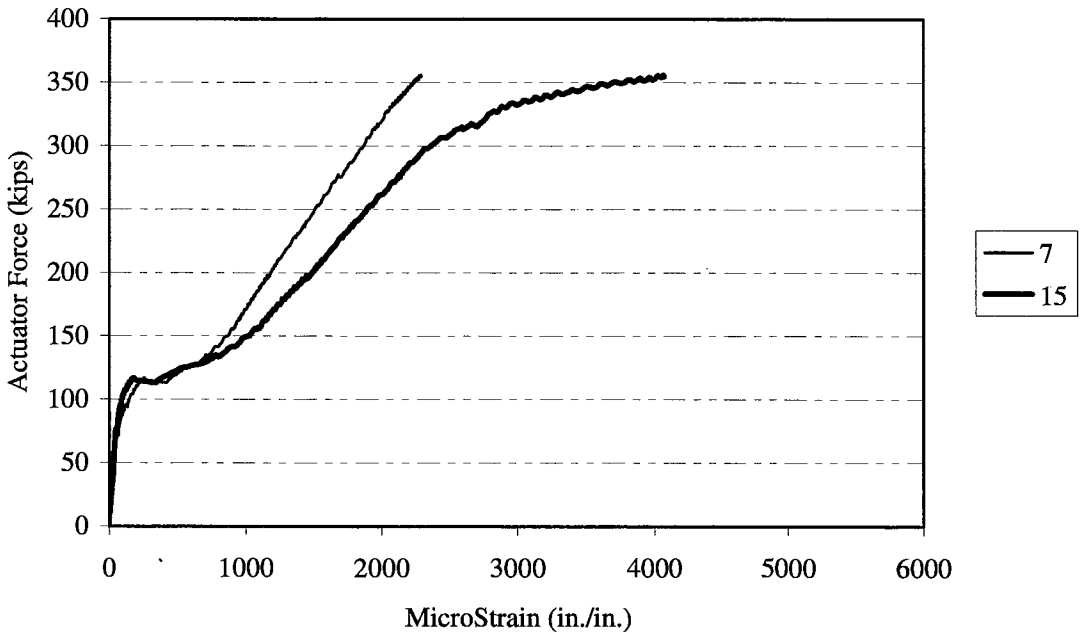

Figure C-47. Specimen 8G Load-Strain History Side (15) vs. Center (7) Transverse Plane.

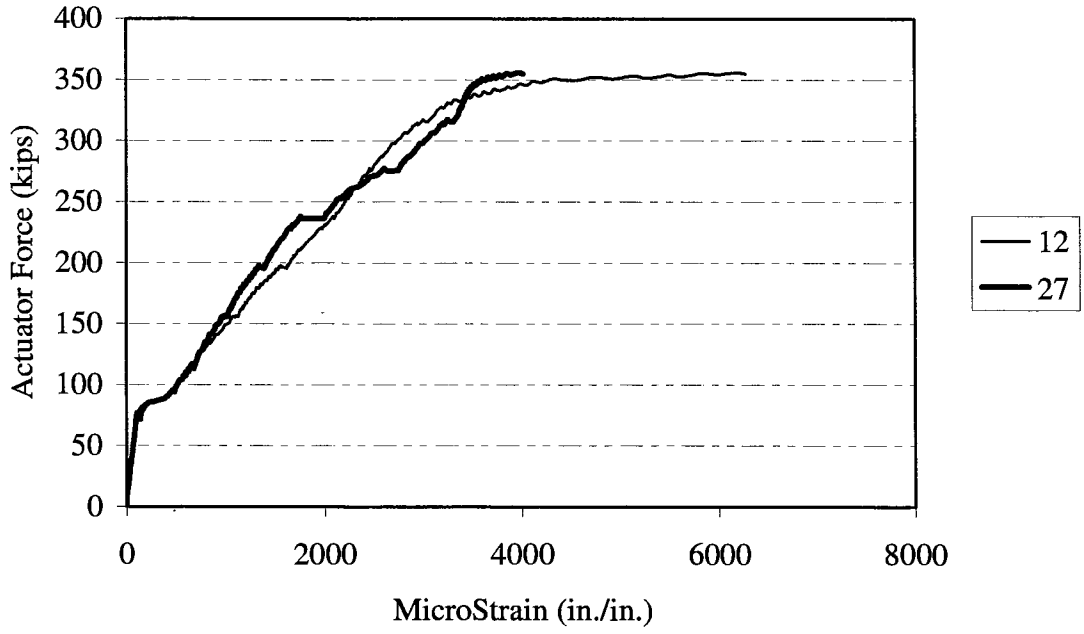

Figure C-48. Specimen 8G Load-Strain History Side (27) vs. Center (12) Transverse Plane.

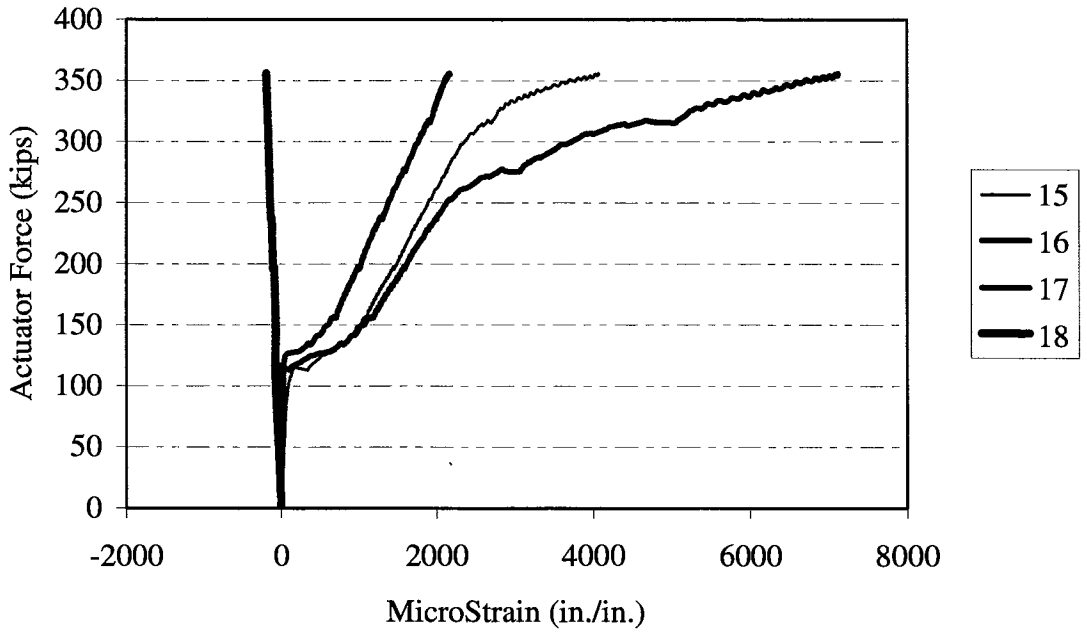

Figure C-49. Specimen 8G Strain Profile Through-Depth Side Face.

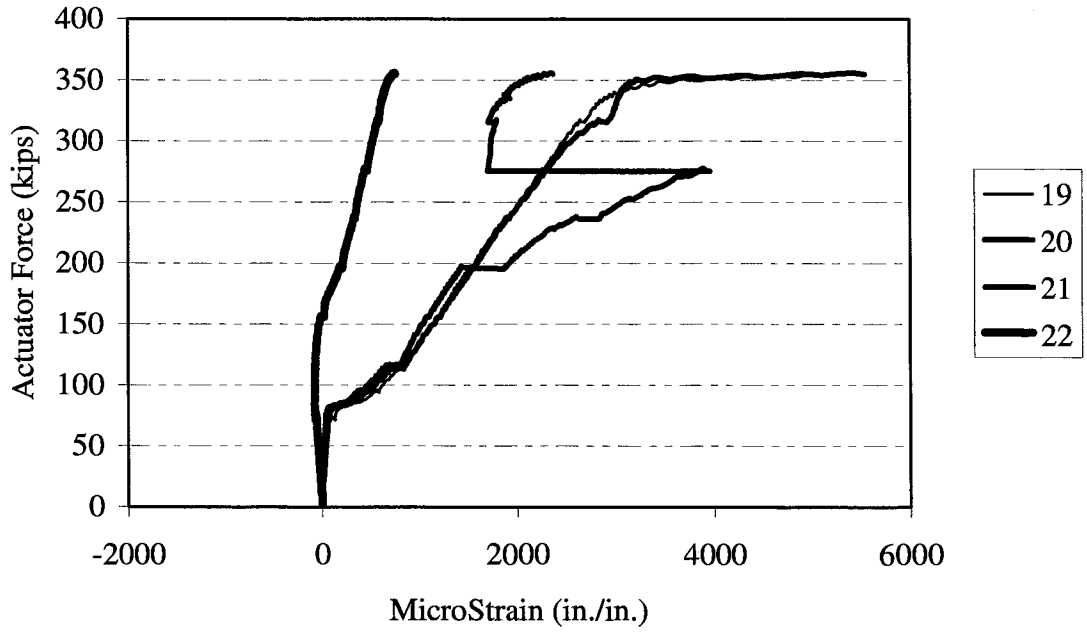

Figure C-50. Specimen 8G Strain Profile Through-Depth Side Face.

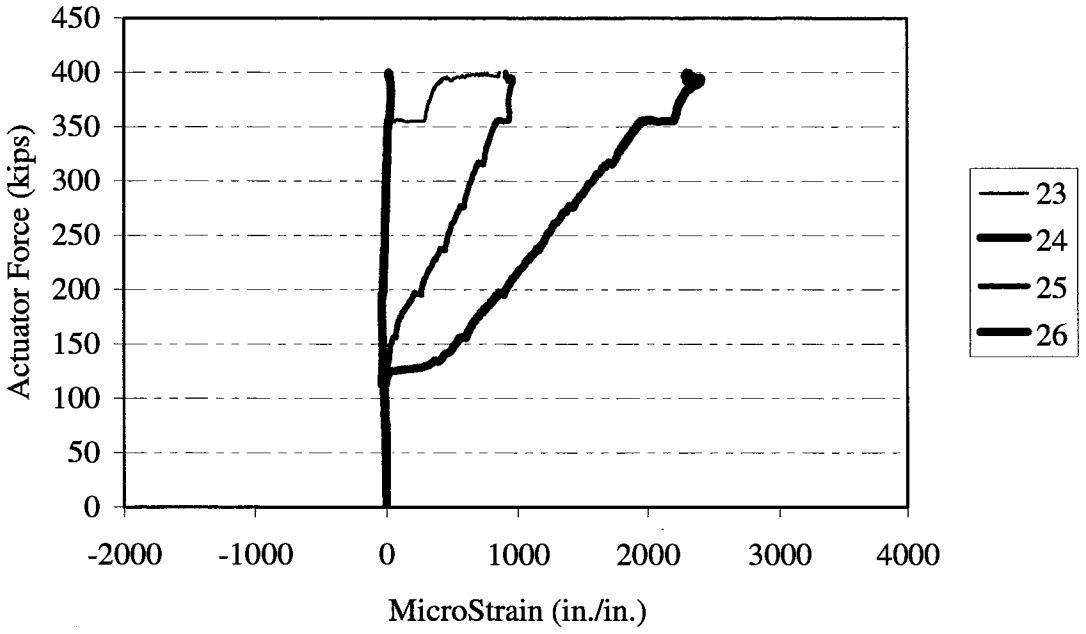

Figure C-51. Specimen 8G Strain Profile Transverse (Stirrup) Reinforcement.

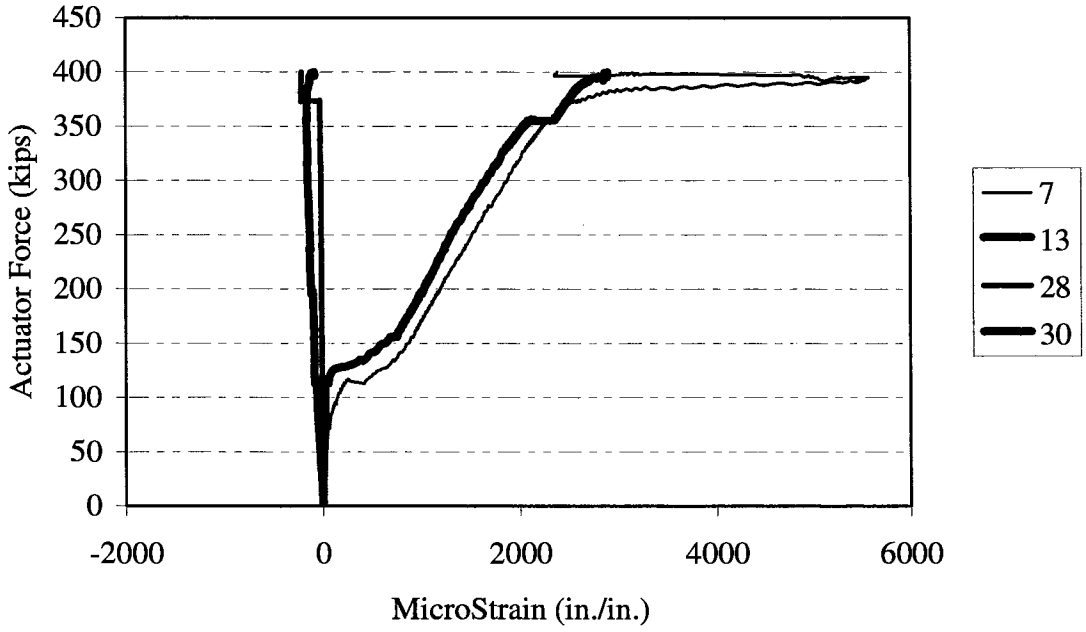

Figure C-52. Specimen 8G Strain Profile Through-Depth Centerline.

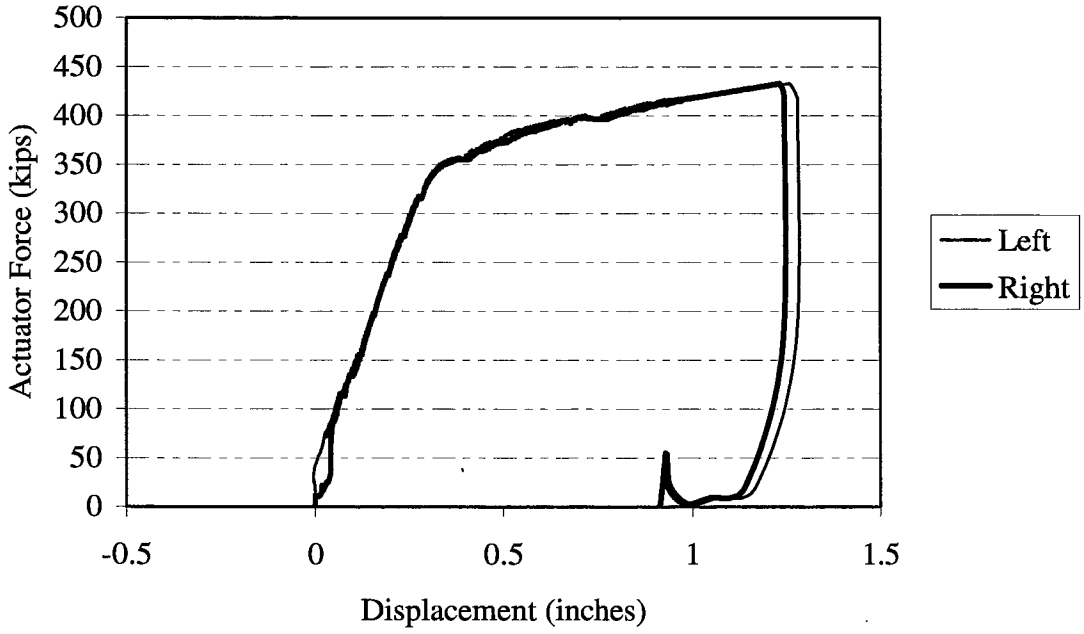

Figure C-53. Specimen 8G Load-Displacement History.

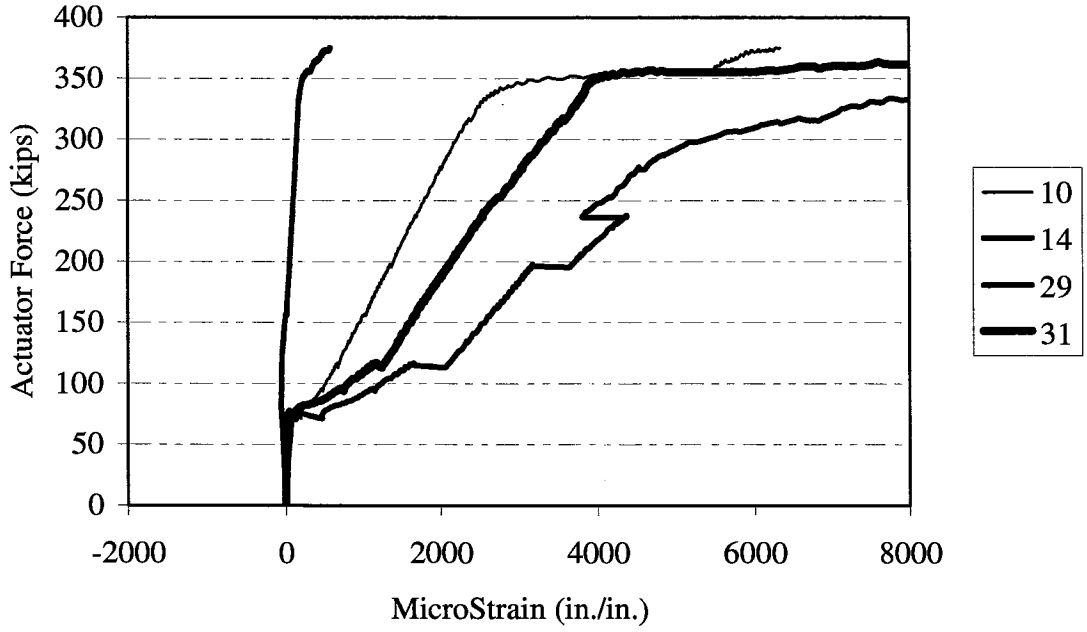

Figure C-54. Specimen 8G Strain Profile Through-Depth Centerline.

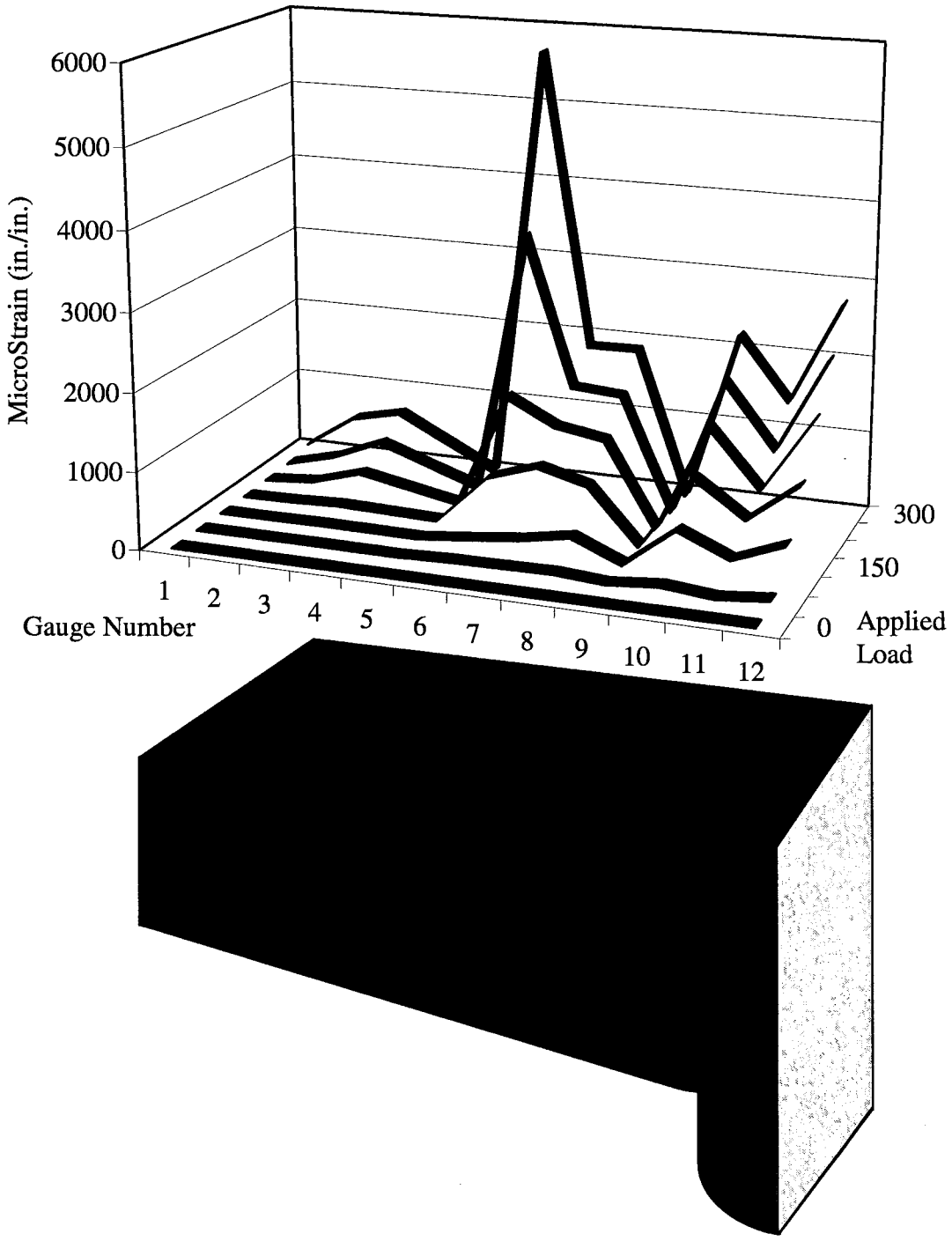

Figure C-55. Specimen 8G Longitudinal Reinforcement Strain Profile for Strain Gauges 1 Through 12.

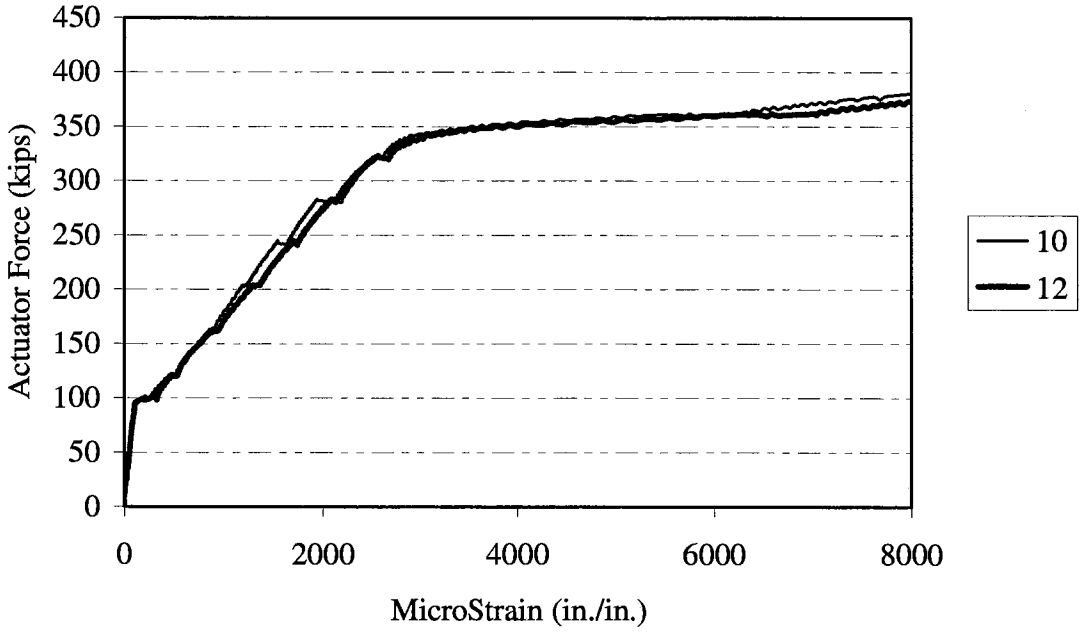

Figure C-56. Specimen 8H Load-Strain History Column Face (10) vs. Column Centerline (12).

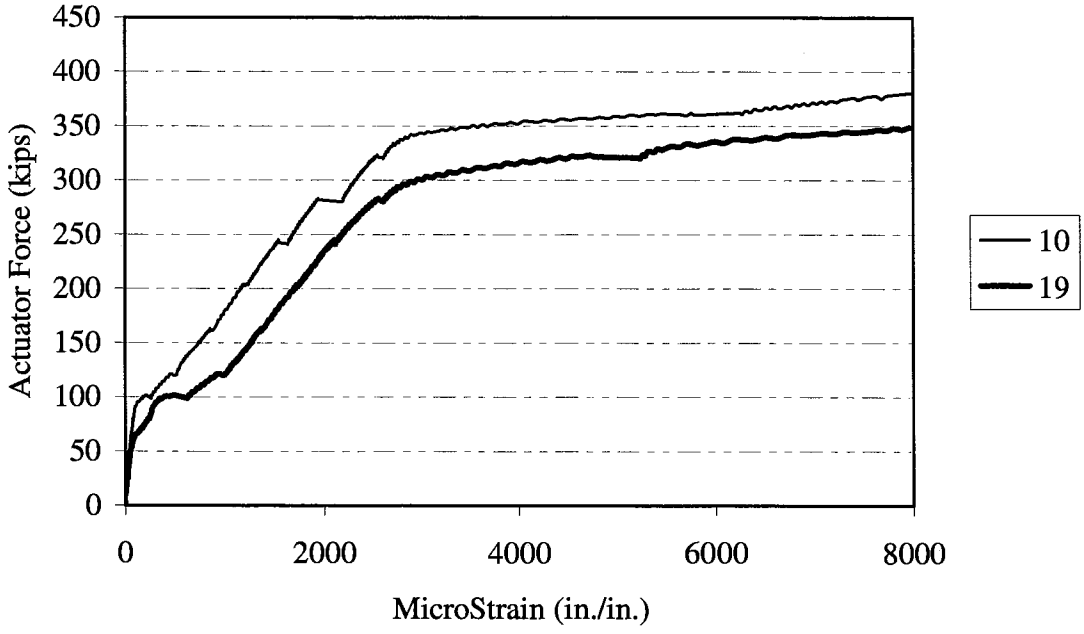

Figure C-57. Specimen 8H Load-Strain History Side (19) vs. Center (10) Transverse Plane.

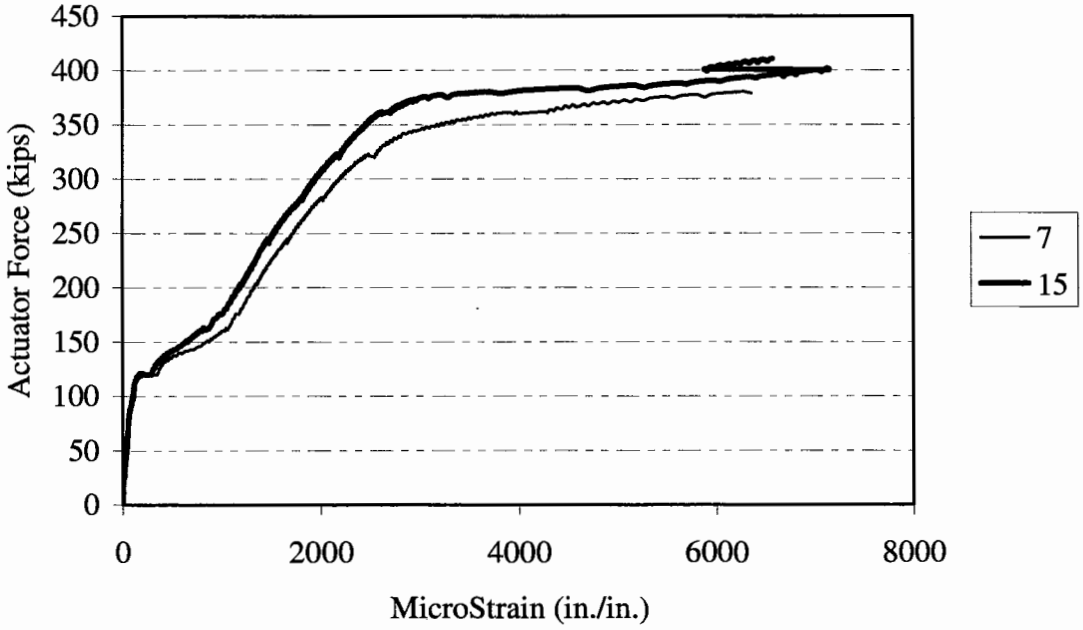

Figure C-58. Specimen 8H Load-Strain History Side (15) vs. Center (7) Transverse Plane.

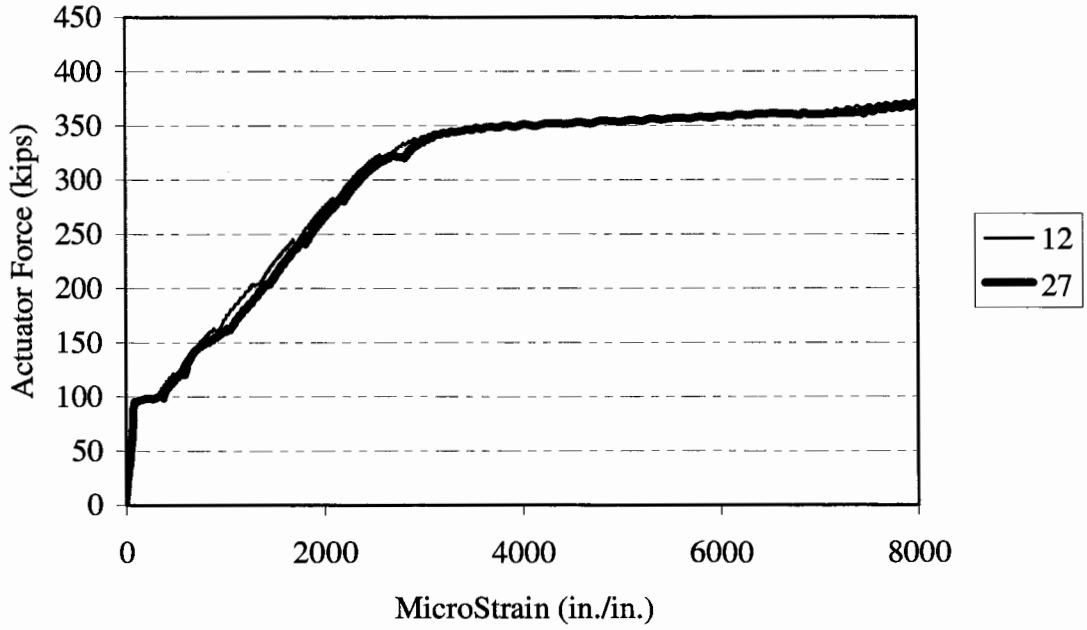

Figure C-59. Specimen 8H Load-Strain History Side (27) vs. center (12) Transverse Plane.

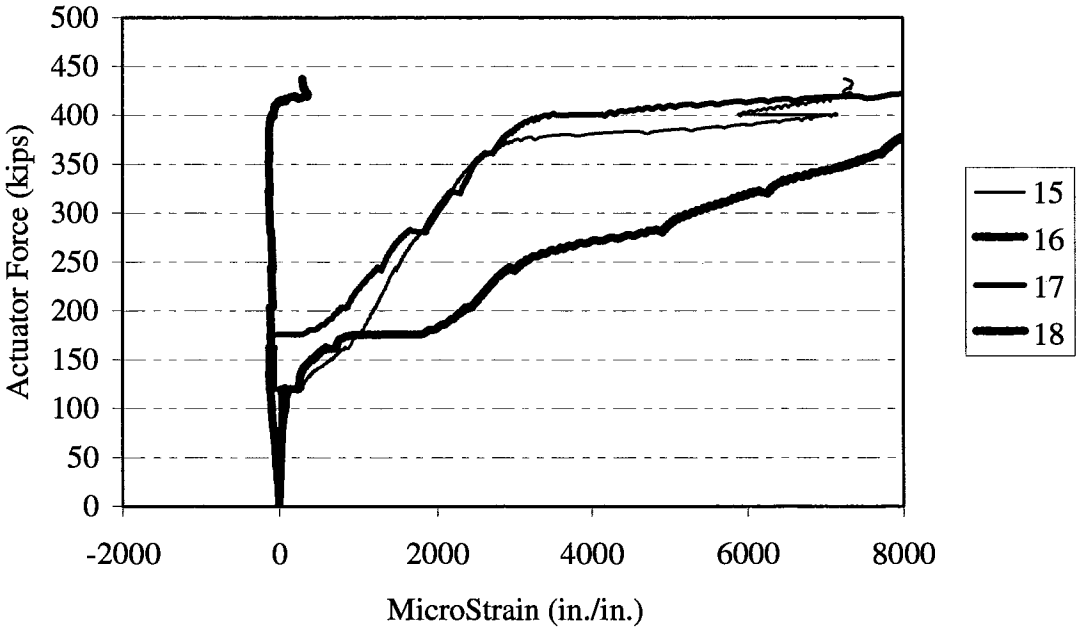

Figure C-60. Specimen 8H Strain Profile Through-Depth Side Face.

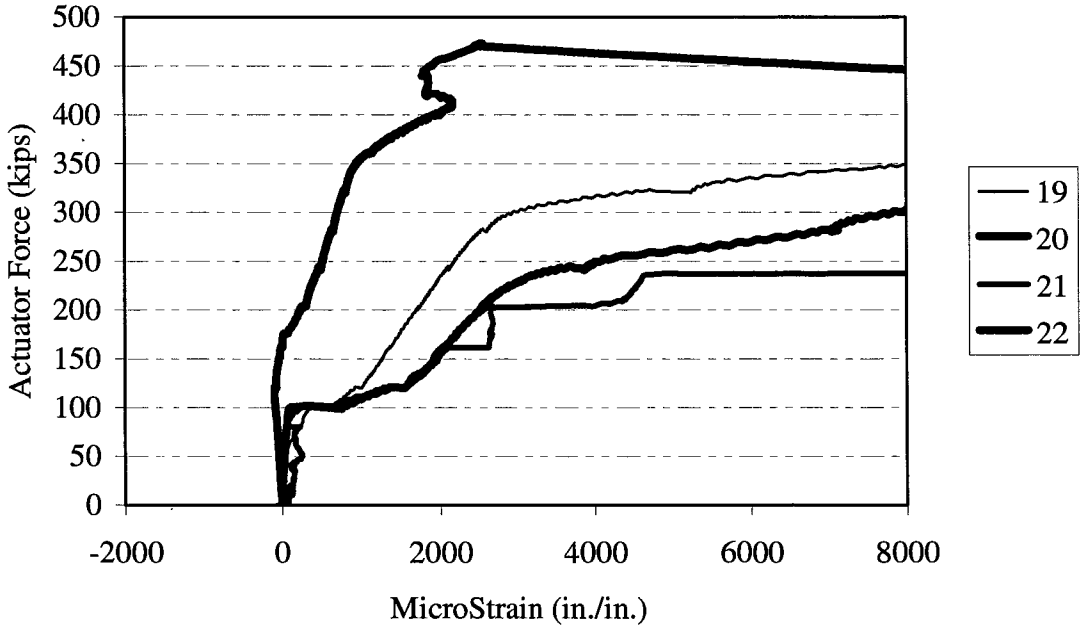

Figure C-61. Specimen 8H Strain Profile Through-Depth Side Face.

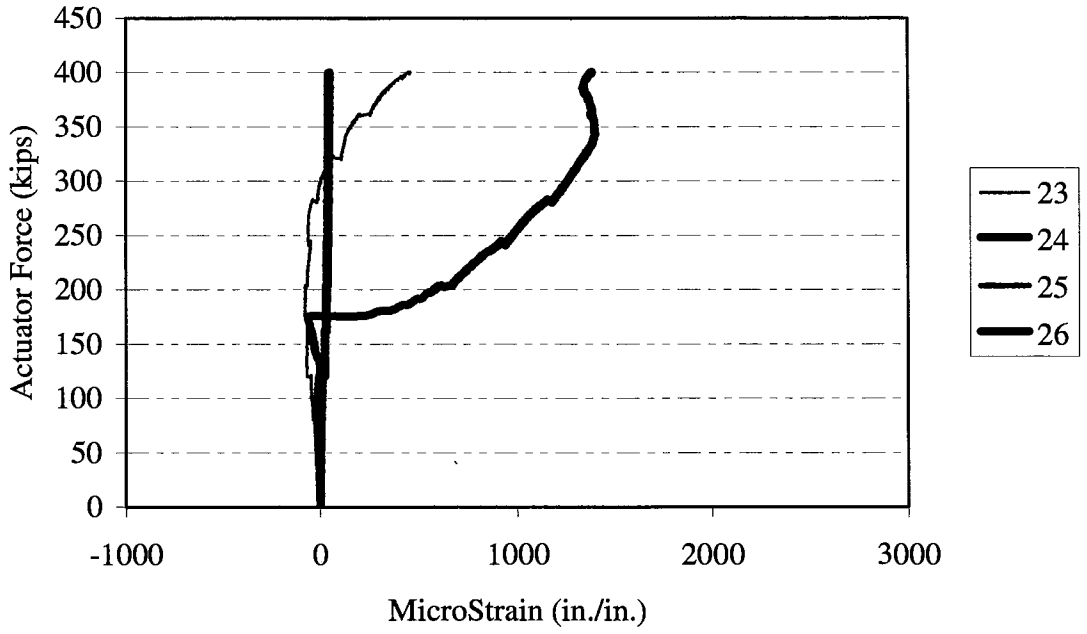

Figure C-62. Specimen 8H Strain Profile Transverse (Stirrup) Reinforcement.

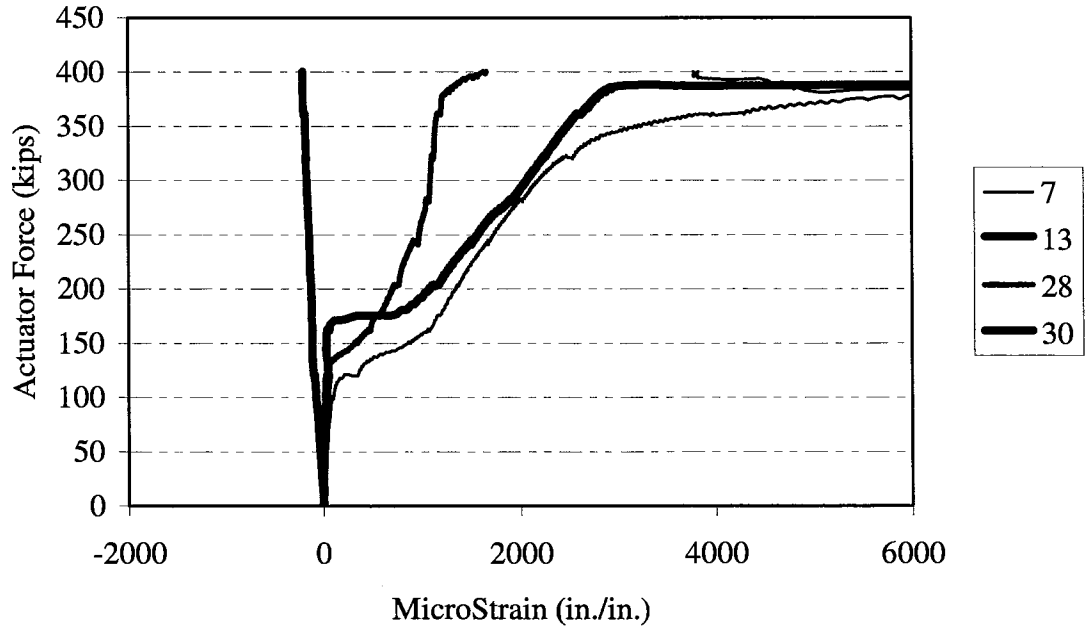

Figure C-63. Specimen 8H Strain Profile Through-Depth Centerline.

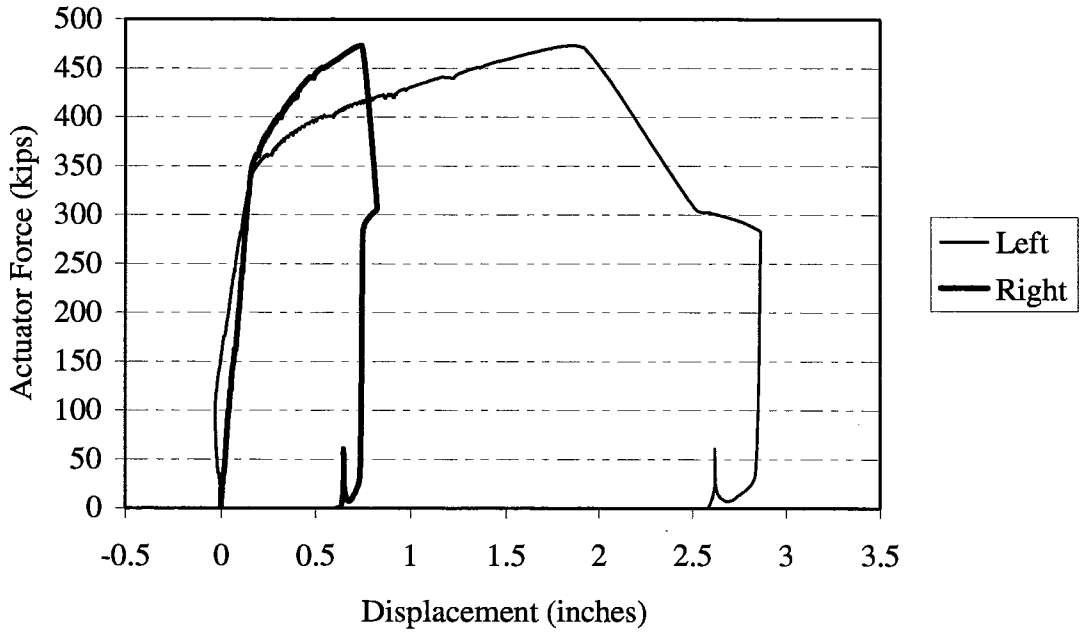

Figure C-64. Specimen 8H Load-Displacement History.

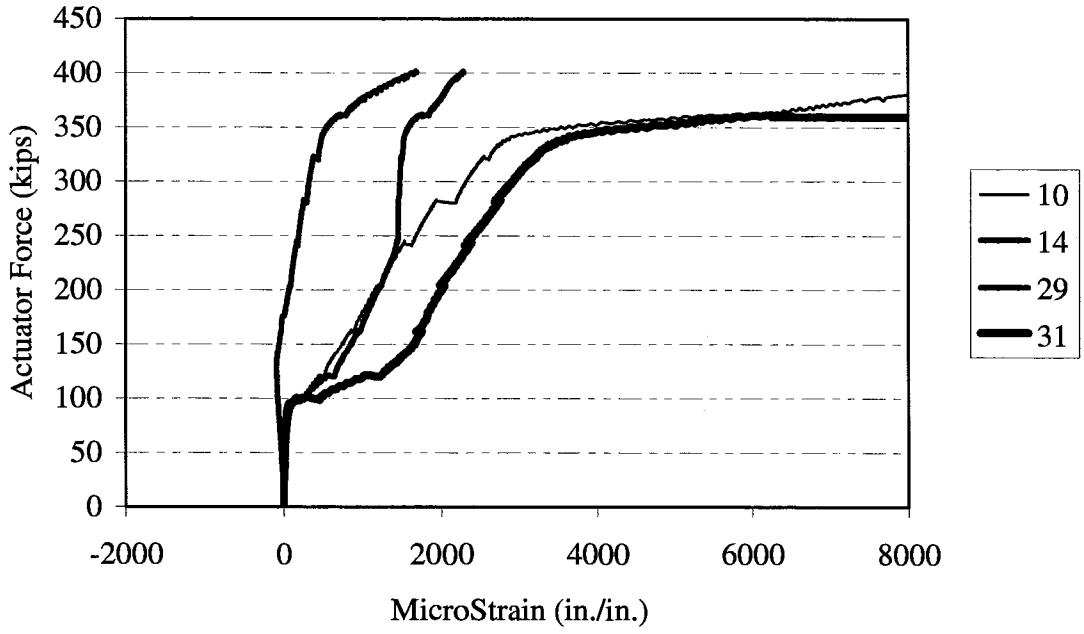

Figure C-65. Specimen 8H Strain Profile Through-Depth Centerline.

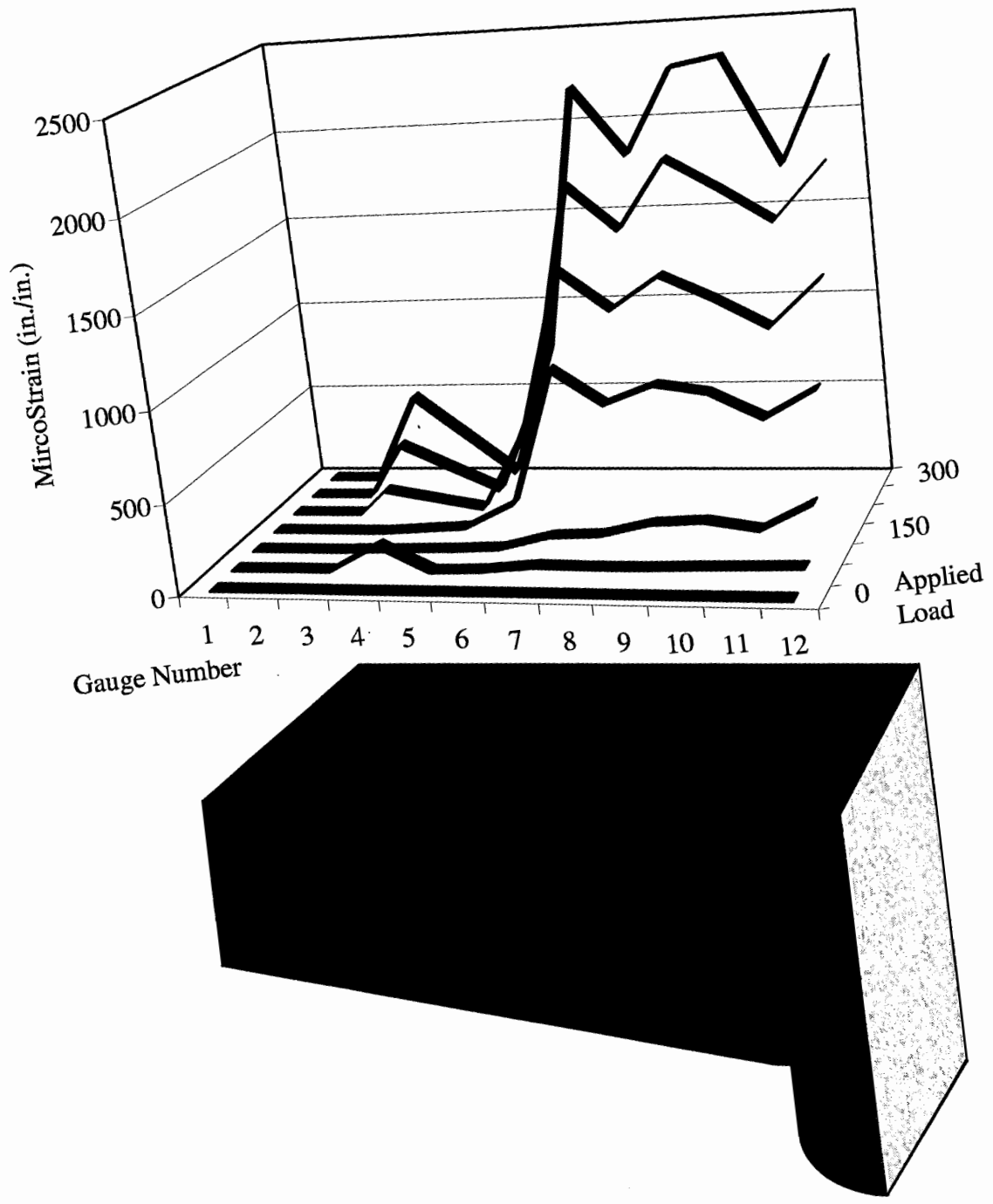

Figure C-66. Specimen 8H Longitudinal Reinforcement Strain Profile for Strain Gauges 1 Through 12.

APPENDIX D

APPLIED LOAD VERSUS EXPERIMENTAL AND ANALYTICAL STRAIN AT THE COLUMN FACE (GAUGE #10) FOR EACH SPECIMEN

For this Appendix;:

- P = applied load, and ε_{10} = strain reading at gauge #10.
- The yield strain (ε_y) indicated in the graphs is taken to be 60 ksi.
- The nominal flexural strength (M_n) indicated in the graphs was calculated from general beam flexure theory with $f'_c = 5500$ psi and $f_y = 60$ ksi.
- The graphical data have been intentionally terminated in order to reflect only that portion of testing that was necessary for illustrating a particular trend. Therefore, termination of the data series does not indicate failure of the specimen or completion of testing.

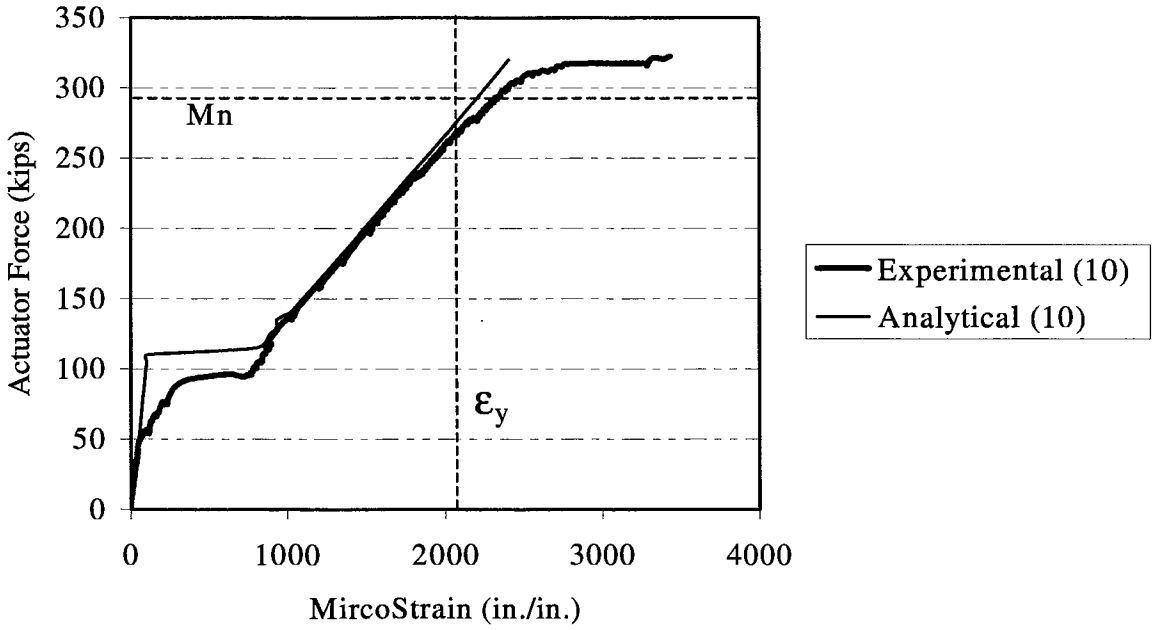

Figure D-1. Specimen 1A Experimental and Analytical P vs. ε_{10}.

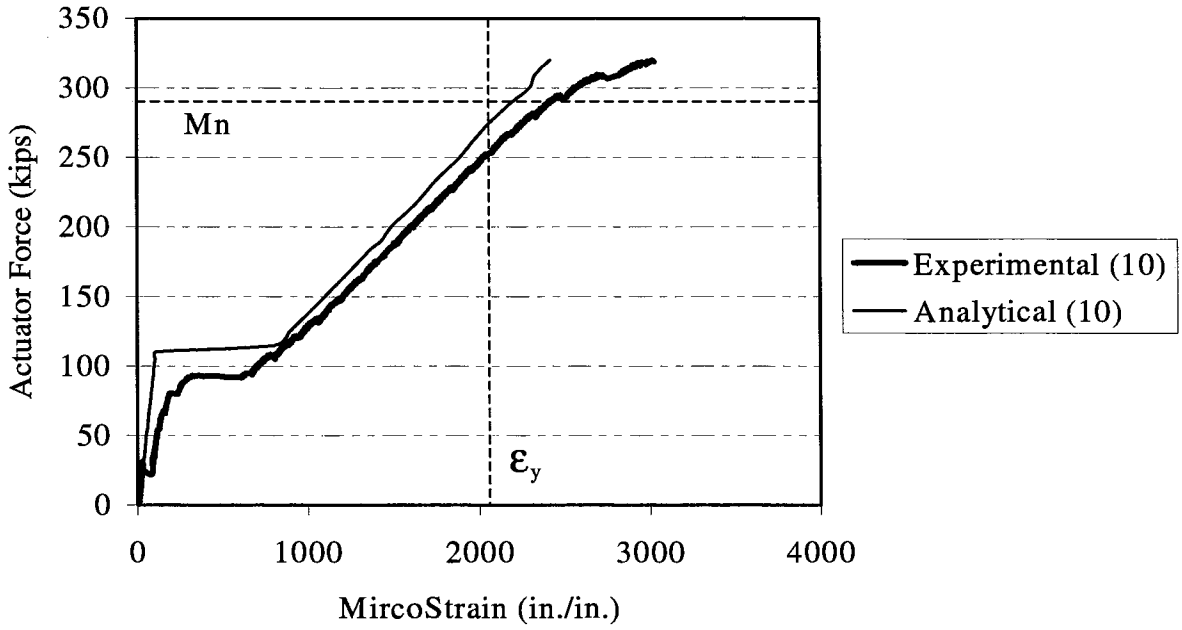

Figure D-2. Specimen 1B Experimental and Analytical P vs. ε_{10}.

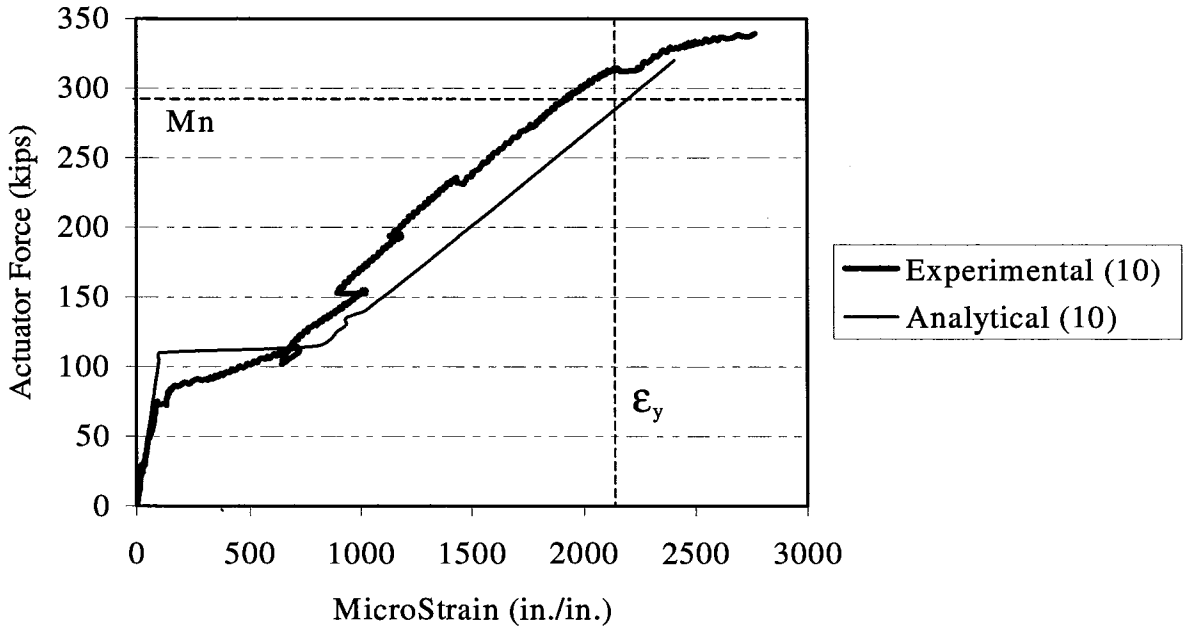

Figure D-3. Specimen 2A Experimental and Analytical P vs. ε_{10}.

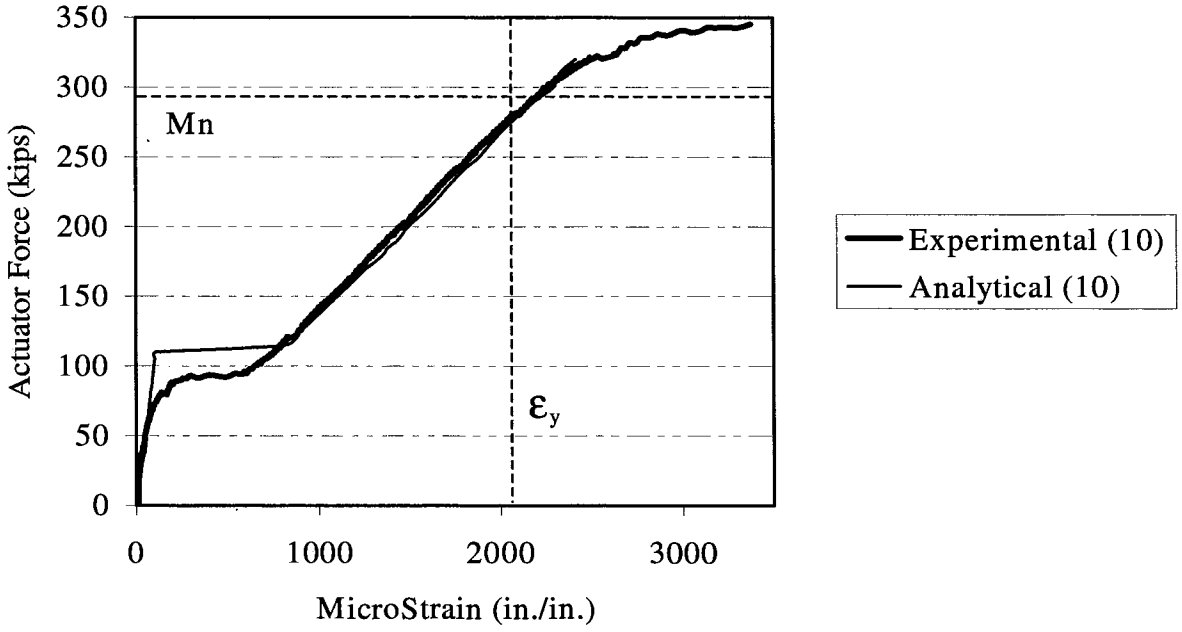

Figure D-4. Specimen 2B Experimental and Analytical P vs. ε_{10}.

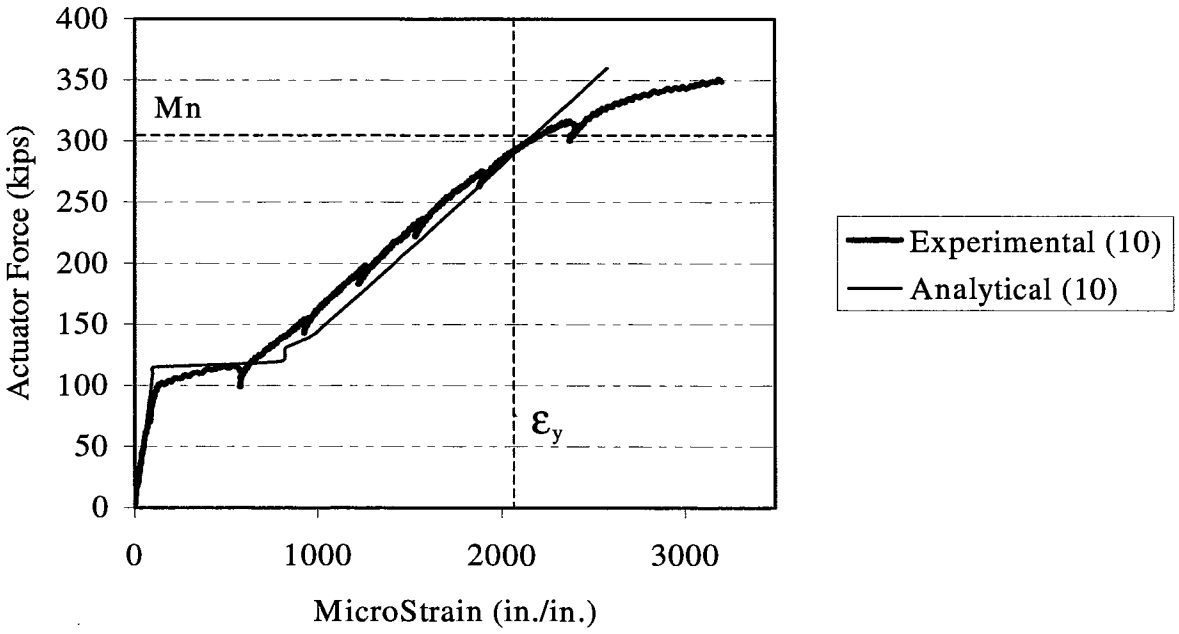

Figure D-5. Specimen 3C Experimental and Analytical P vs. ε_{10}.

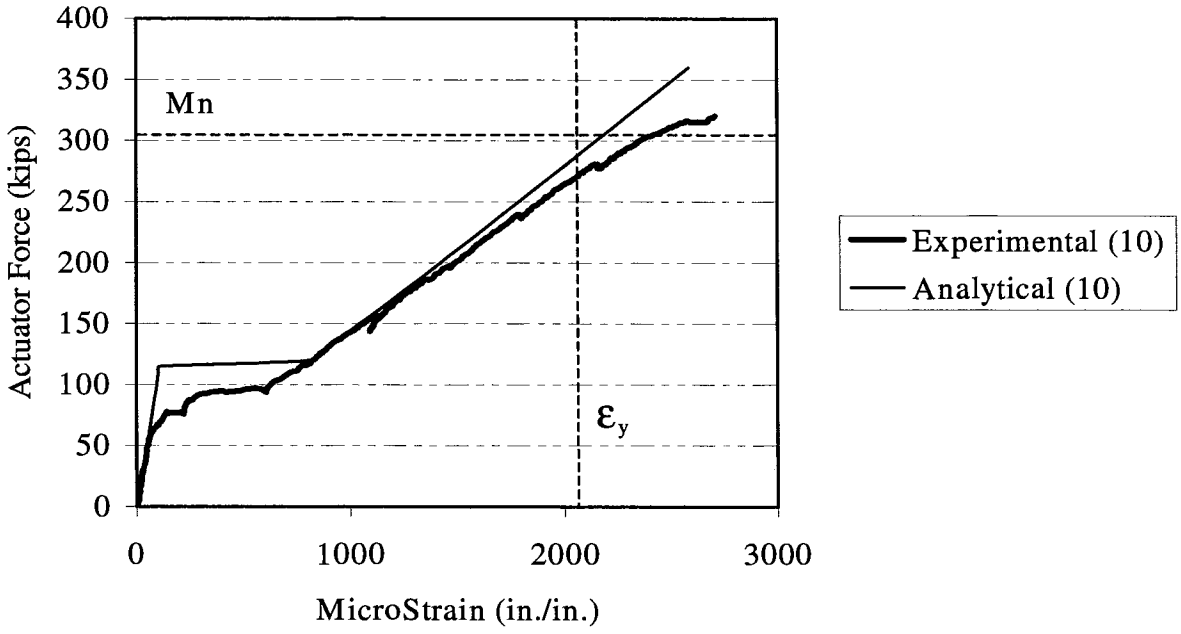

Figure D-6. Specimen 3D Experimental and Analytical P vs. ε_{10}.

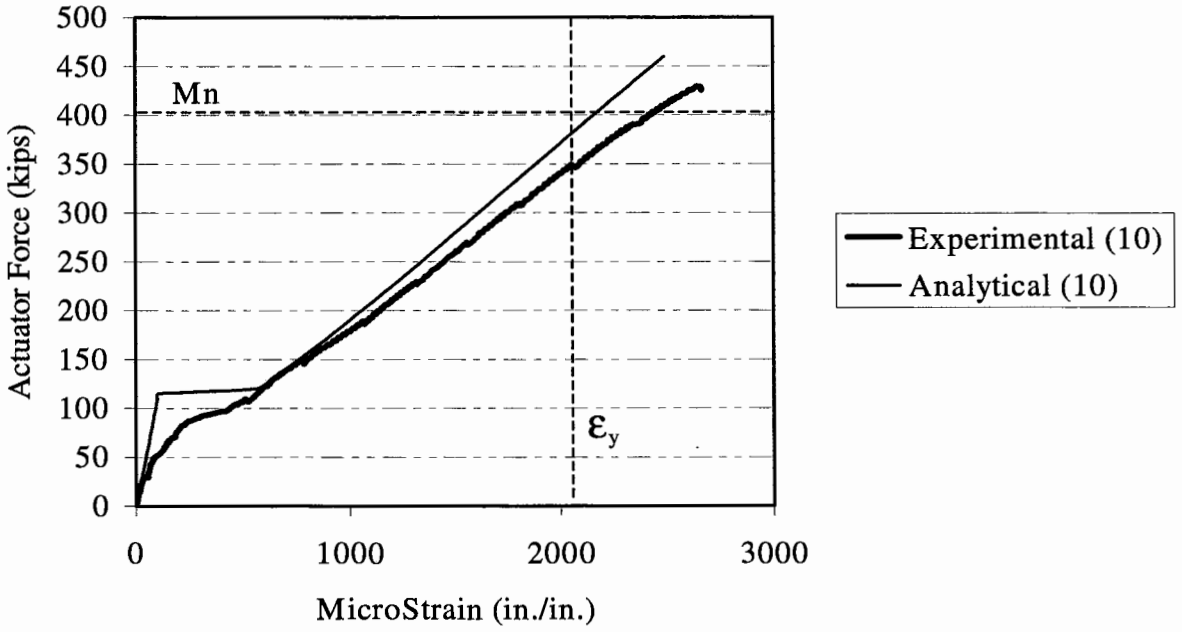

Figure D-7. Specimen 4C Experimental and Analytical P vs. ε_{10}.

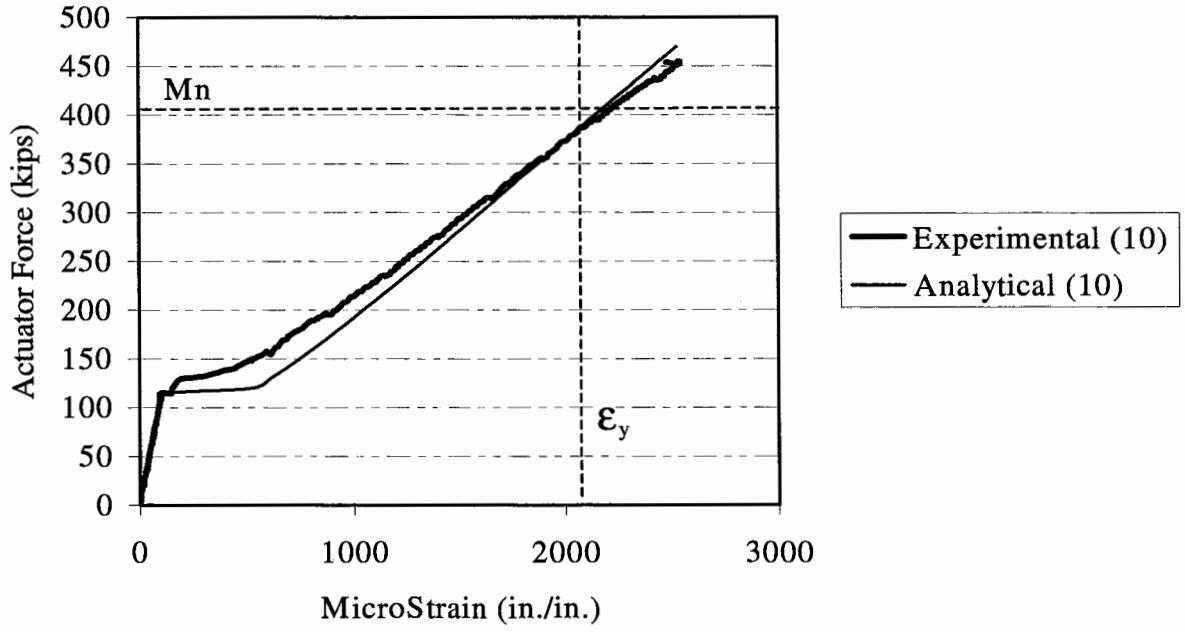

Figure D-8. Specimen 4E Experimental and Analytical P vs. ε_{10}.

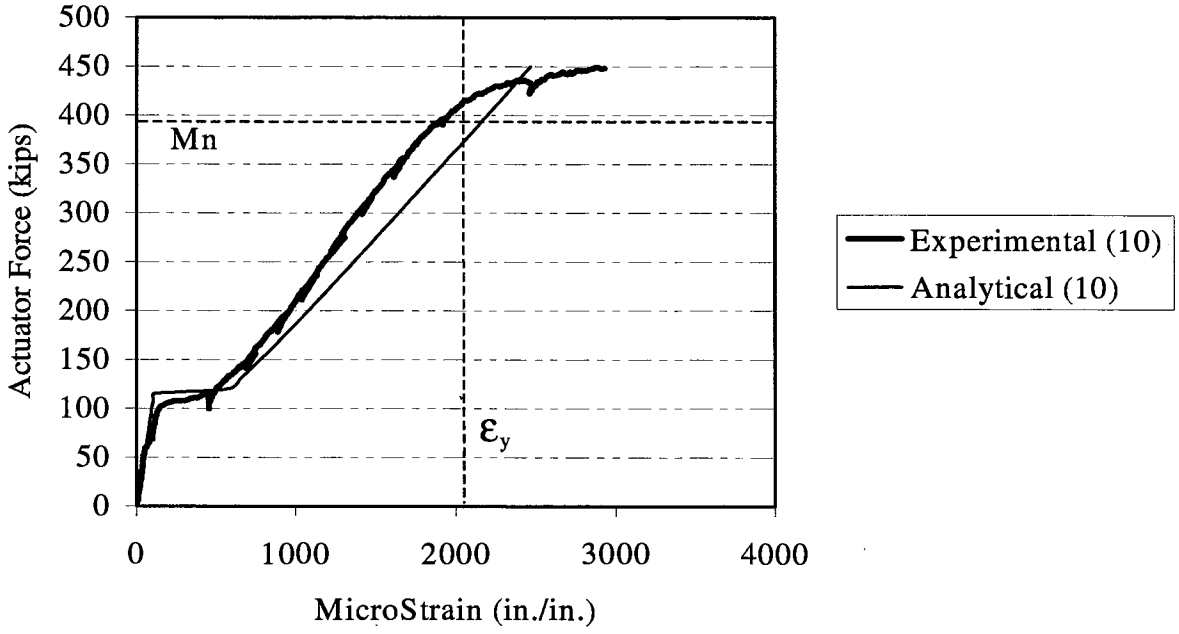

Figure D-9. Specimen 5D Experimental and Analytical P vs. ε_{10}.

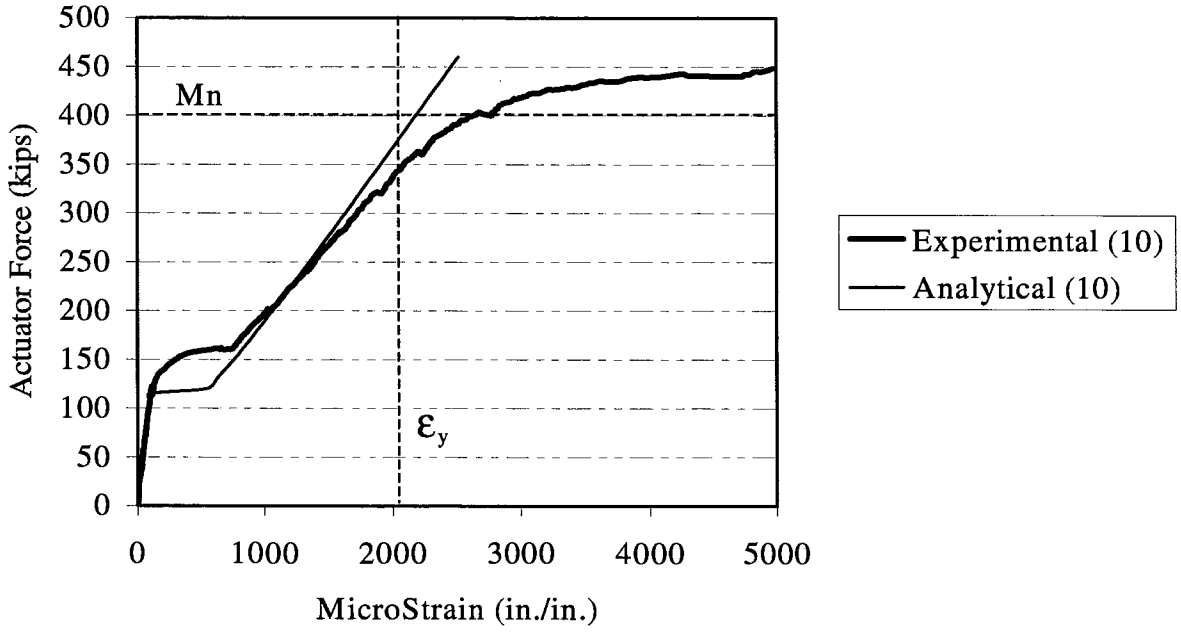

Figure D-10. Specimen 5E Experimental and Analytical P vs. ε_{10}.

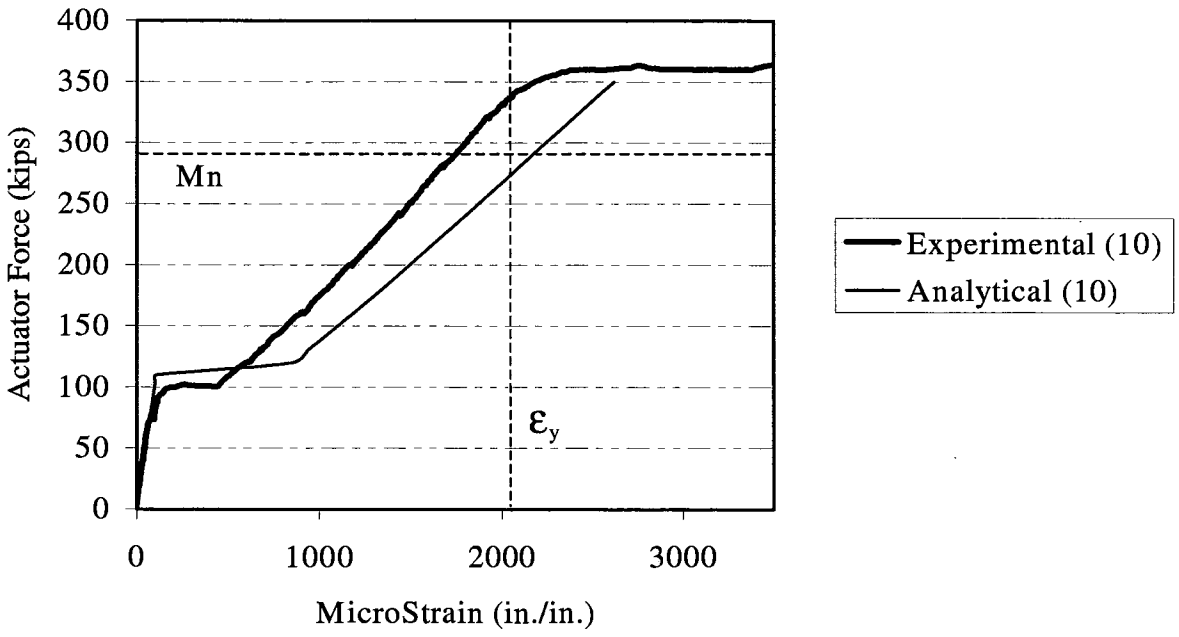

Figure D-11. Specimen 6F Experimental and Analytical P vs. ε_{10}.

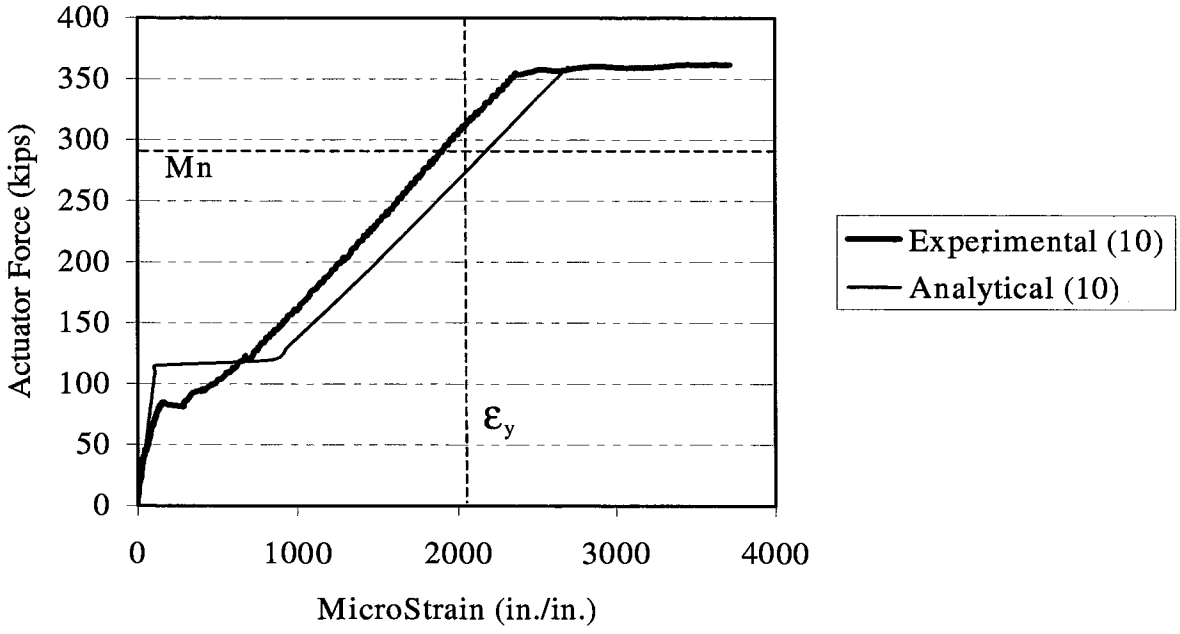

Figure D-12. Specimen 6G Experimental and Analytical P vs. ε_{10}.

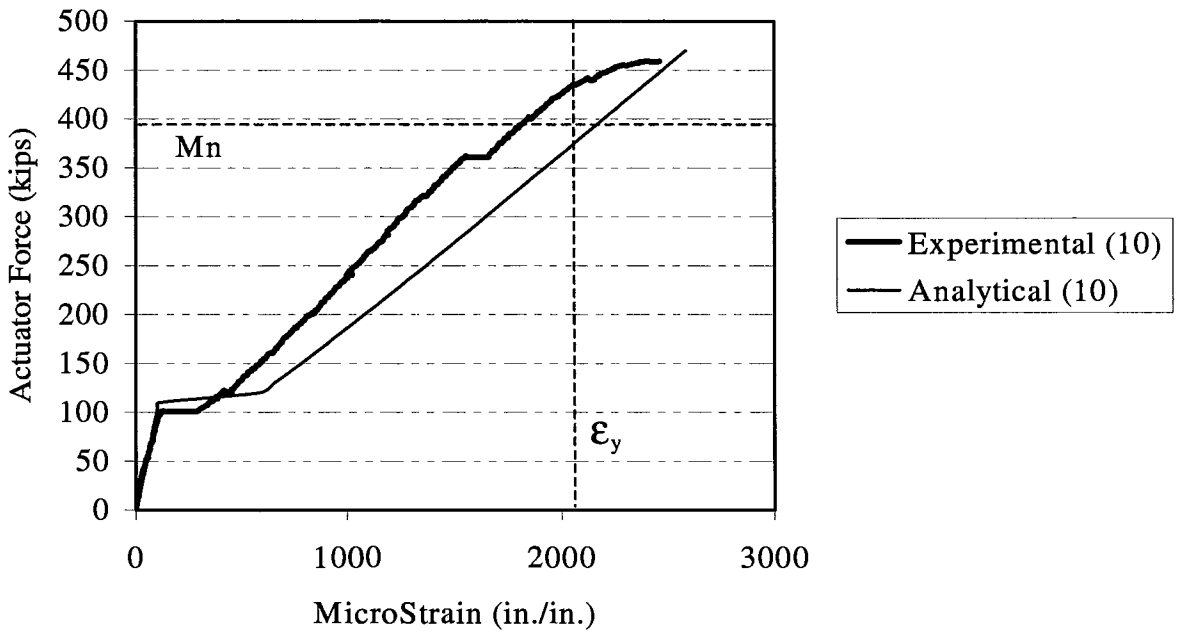

Figure D-13. Specimen 7F Experimental and Analytical P vs. ε_{10}.

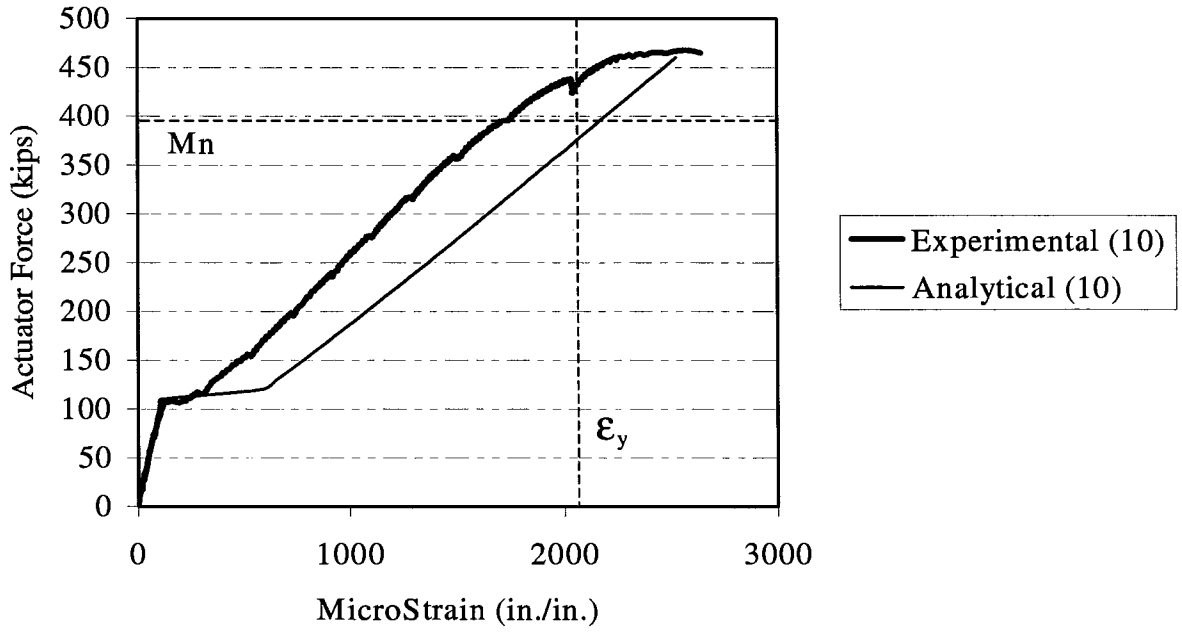

Figure D-14. Specimen 7H Experimental and Analytical P vs. ε_{10}.

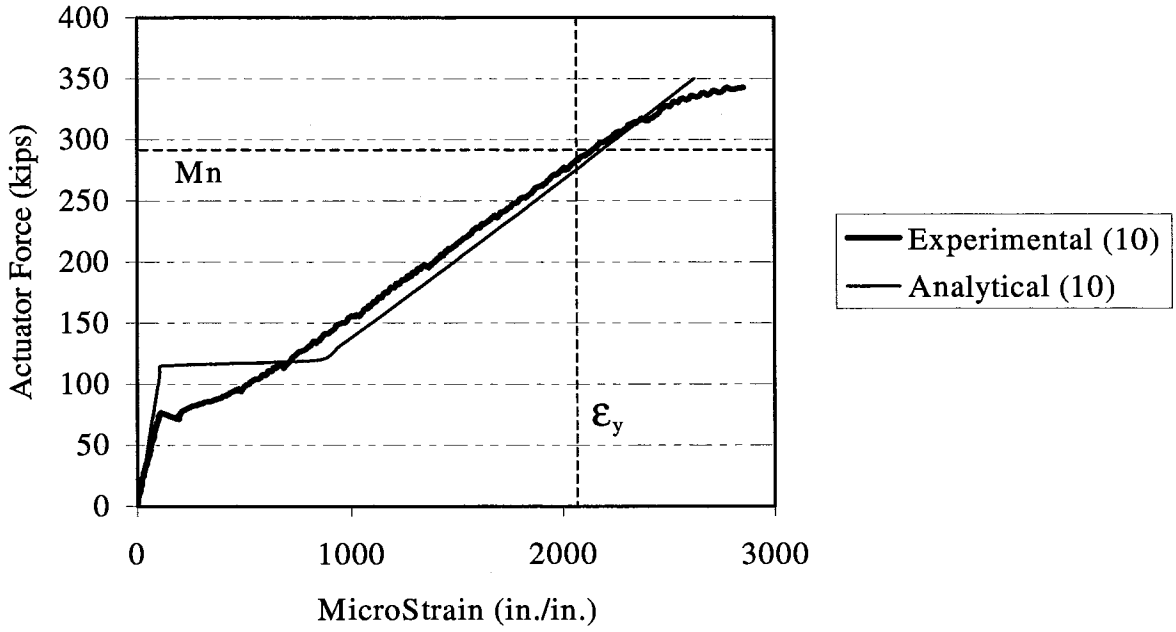

Figure D-15. Specimen 8G Experimental and Analytical P vs. ε_{10}.

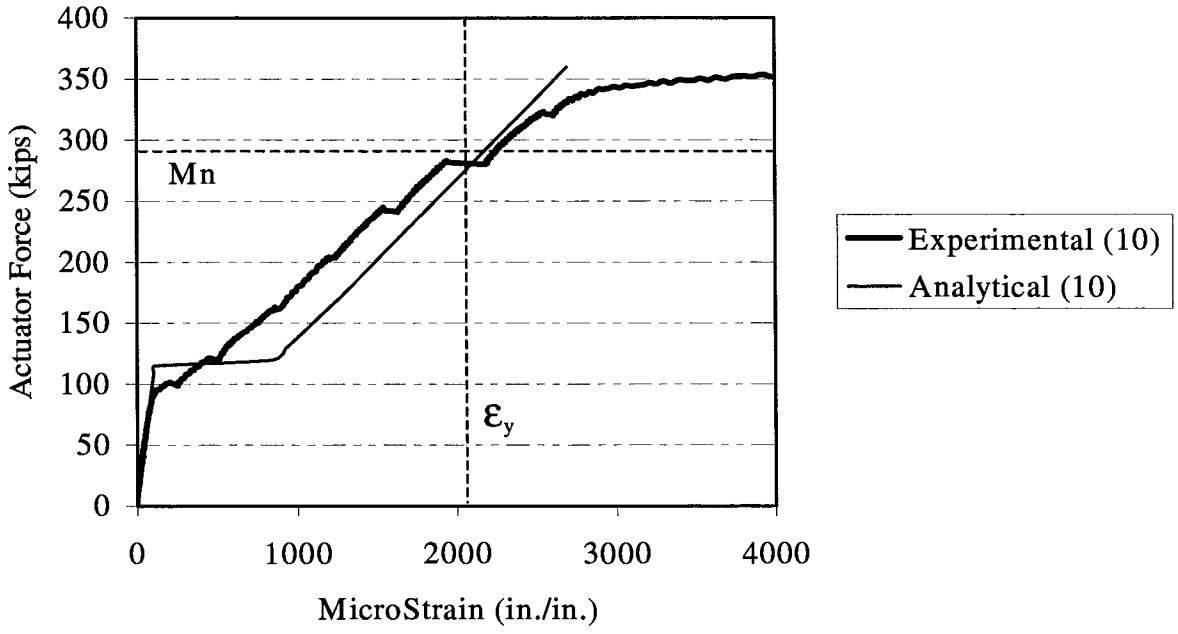

Figure D-16. Specimen 8H Experimental and Analytical P vs. ε_{10}.

APPENDIX E

BENT CAP SPECIMEN PHOTOGRAPHS

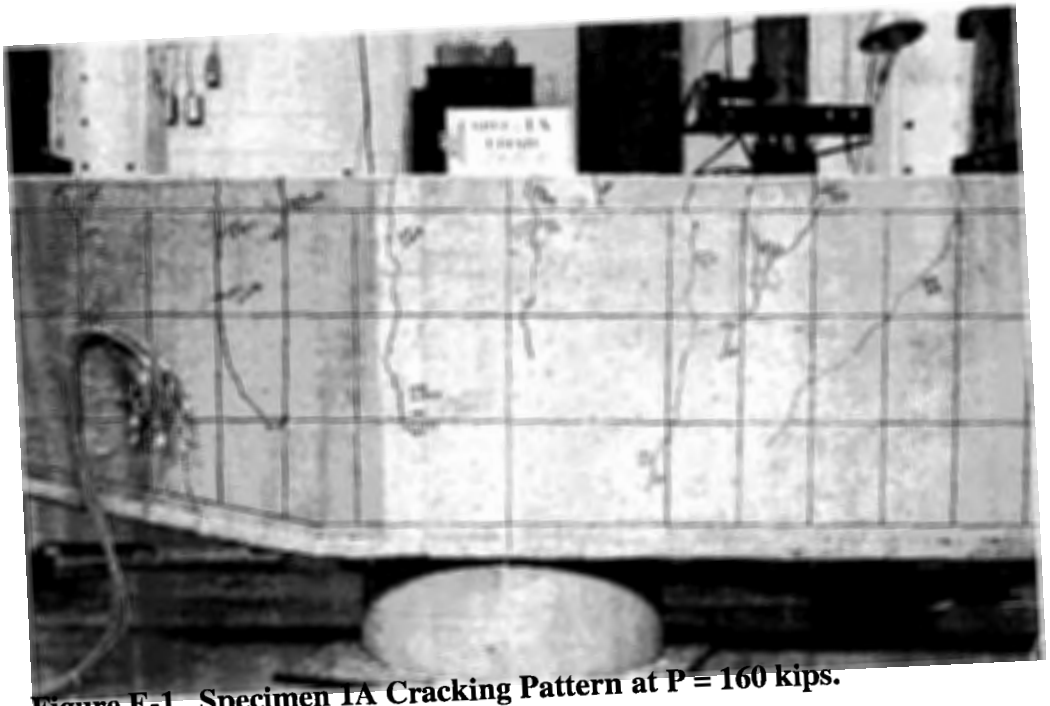

Figure E-1. Specimen 1A Cracking Pattern at P = 160 kips.

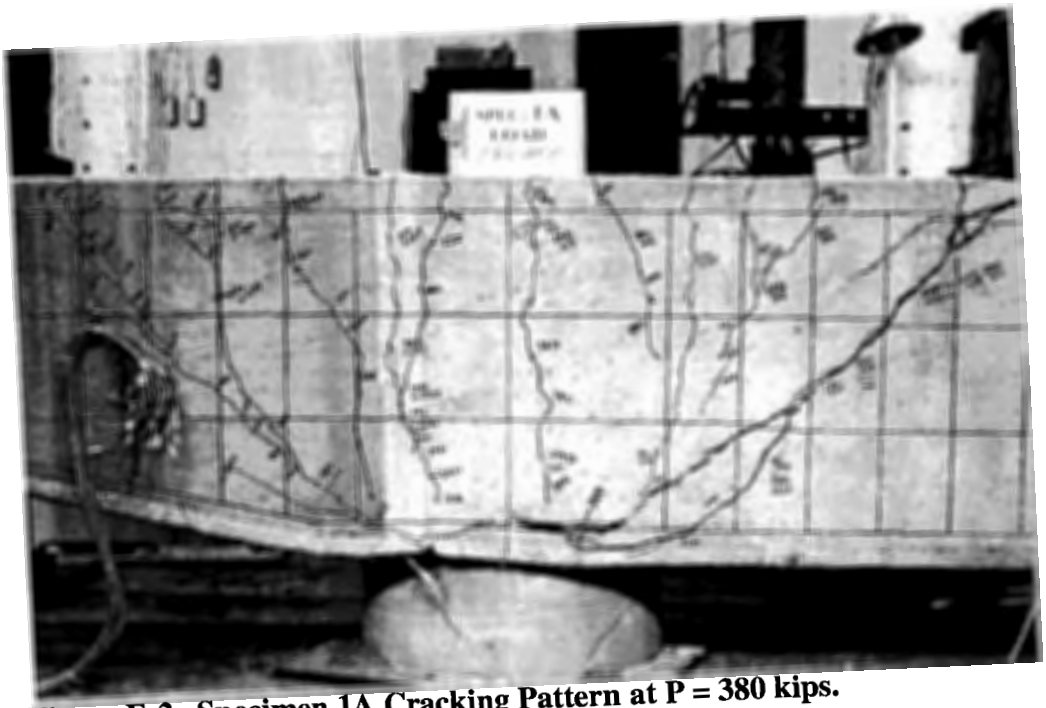

Figure E-2. Specimen 1A Cracking Pattern at P = 380 kips.

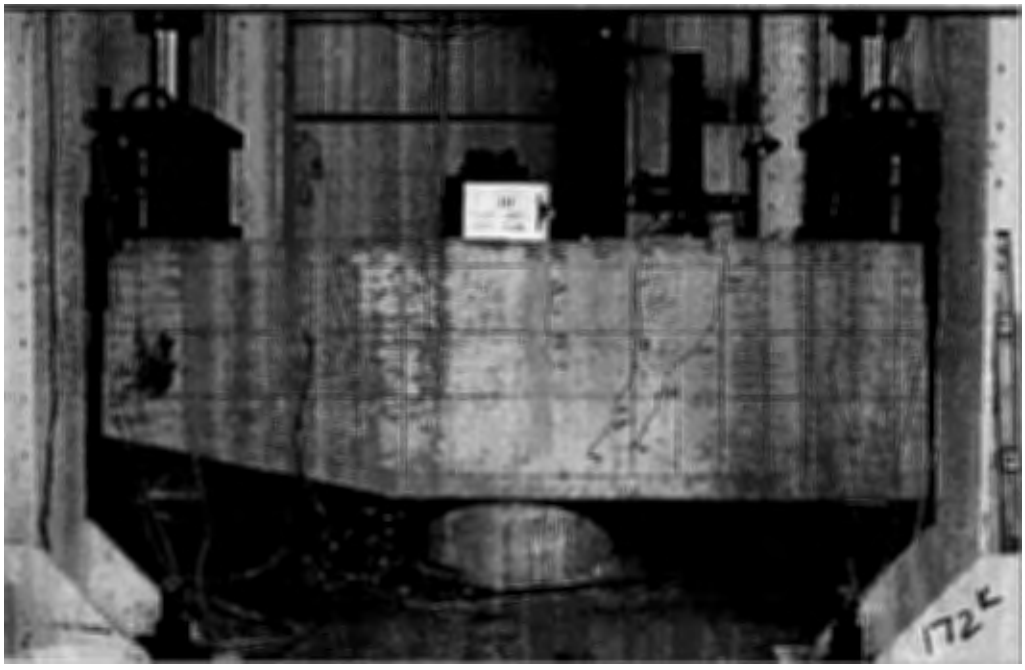

Figure E-3. Specimen 1B Cracking Pattern at P = 172 kips.

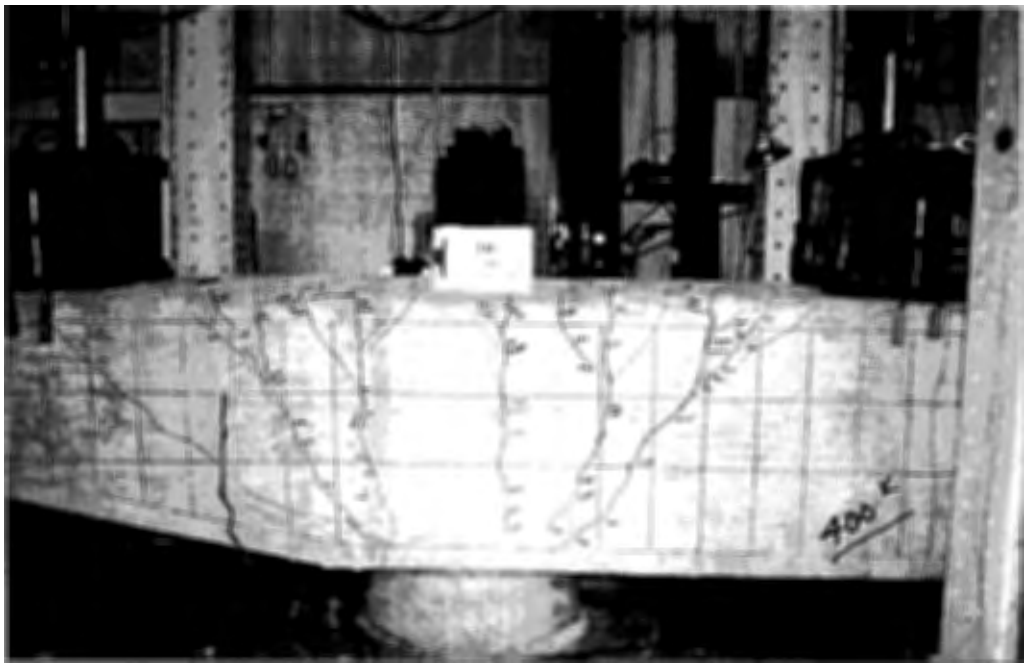

Figure E-4. Specimen 1B Cracking Pattern at P = 400 kips.

Figure E-5. Specimen 2A Cracking Pattern at P = 160 kips.

Figure E-6. Specimen 2A Cracking Pattern at P = 400 kips.

Figure E-7. Specimen 2B Cracking Pattern at P = 160 kips.

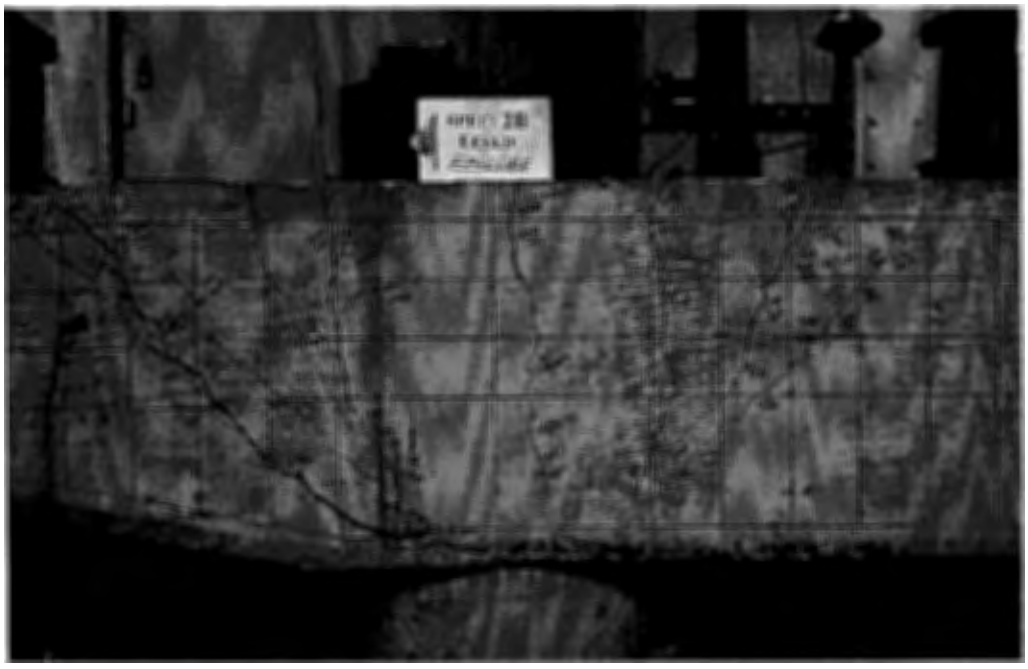

Figure E-8. Specimen 2B Cracking Pattern at P = 390 kips.

Figure E-9. Specimen 3C Cracking Pattern at P = 160 kips.

Figure E-10. Specimen 3C Cracking Pattern at P = 420 kips.

Figure E-11. Specimen 3D Cracking Pattern at P = 280 kips.

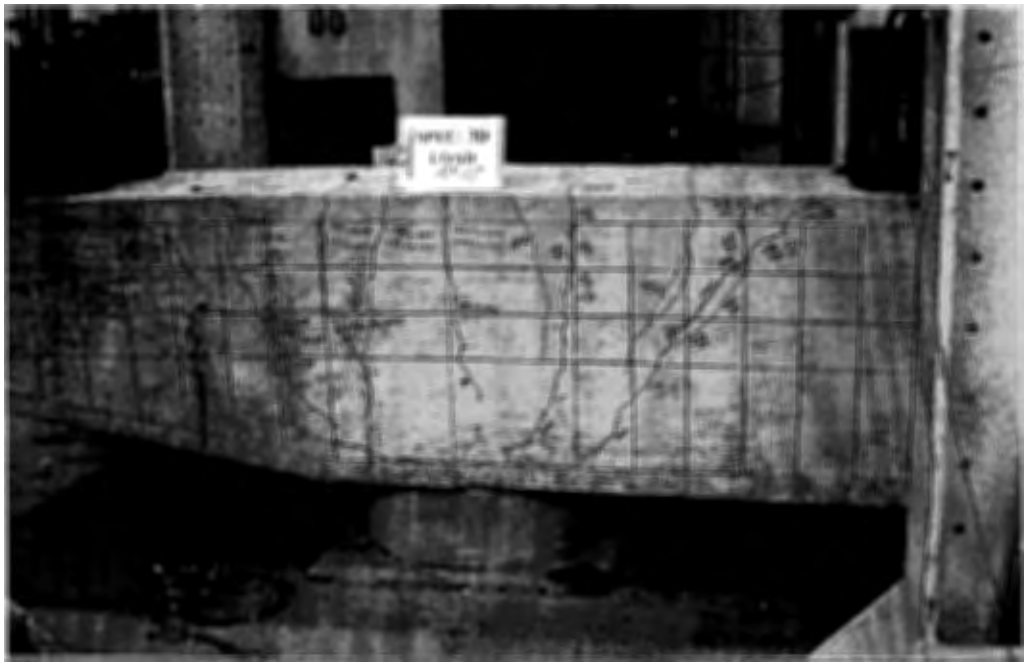

Figure E-12. Specimen 3D Cracking Pattern at P = 450 kips.

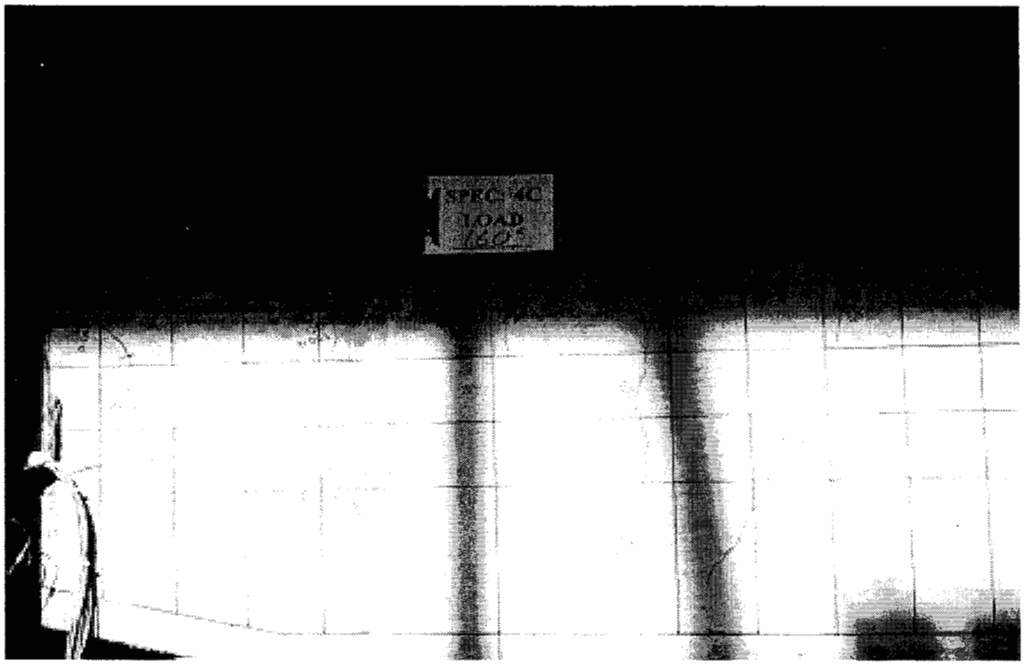

Figure E-13. Specimen 4C Cracking Pattern at P = 160 kips.

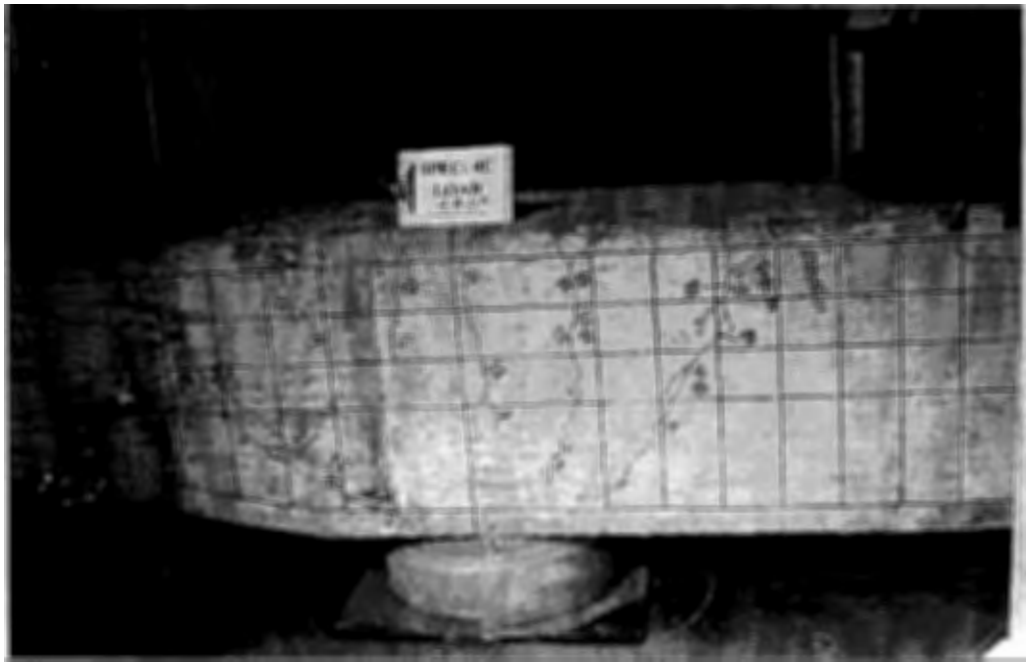

Figure E-14. Specimen 4C Cracking Pattern at P = 440 kips.

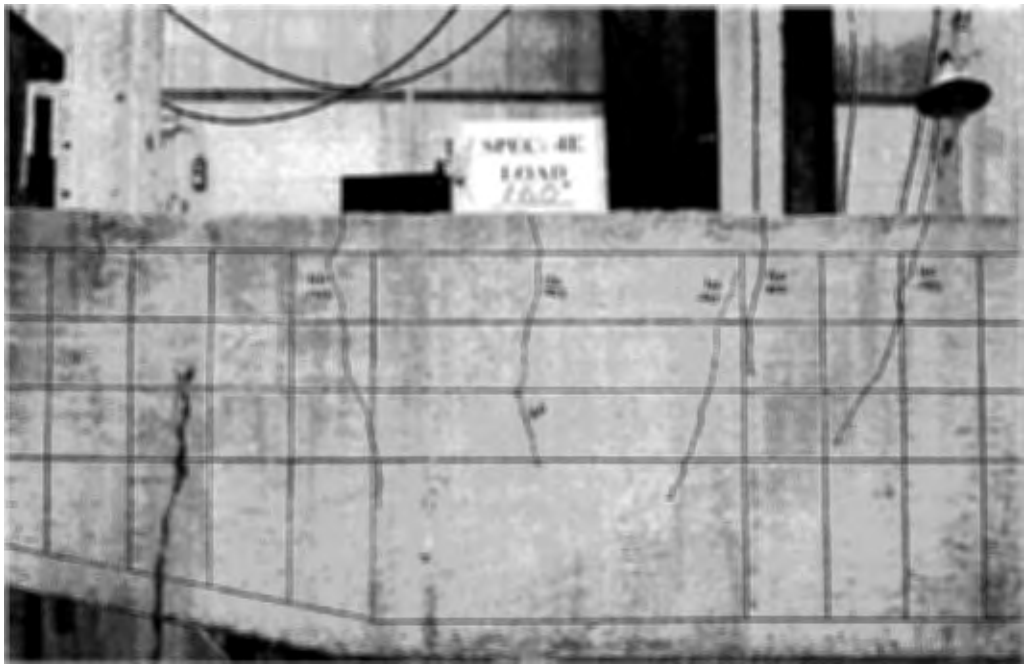

Figure E-15. Specimen 4E Cracking Pattern at P = 160 kips.

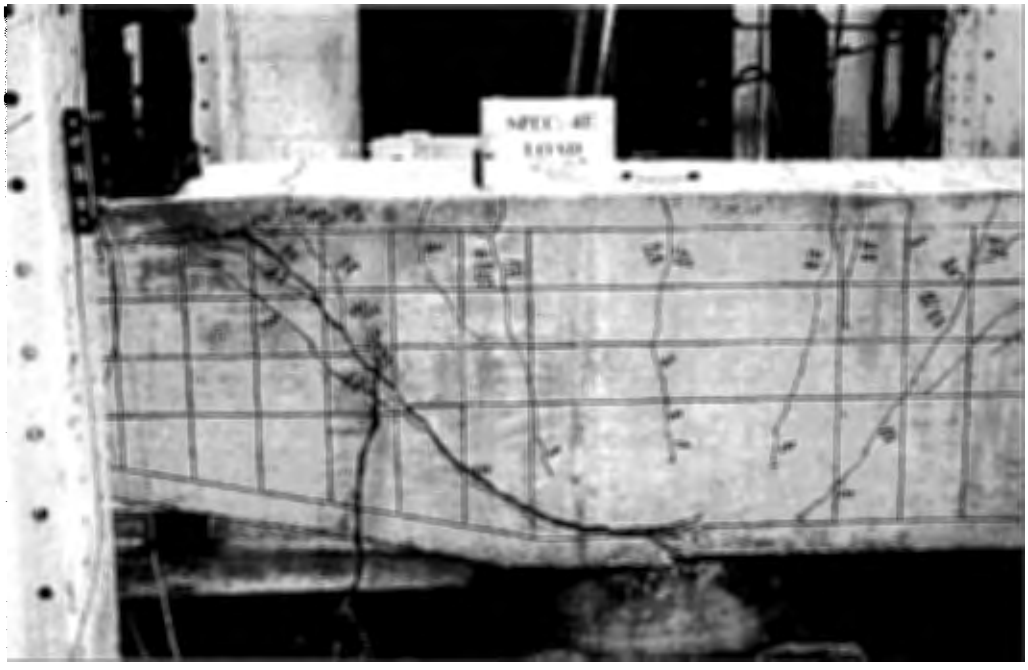

Figure E-16. Specimen 4E Cracking Pattern at P = 460 kips.

Figure E-17. Specimen 5D Cracking Pattern at P = 160 kips.

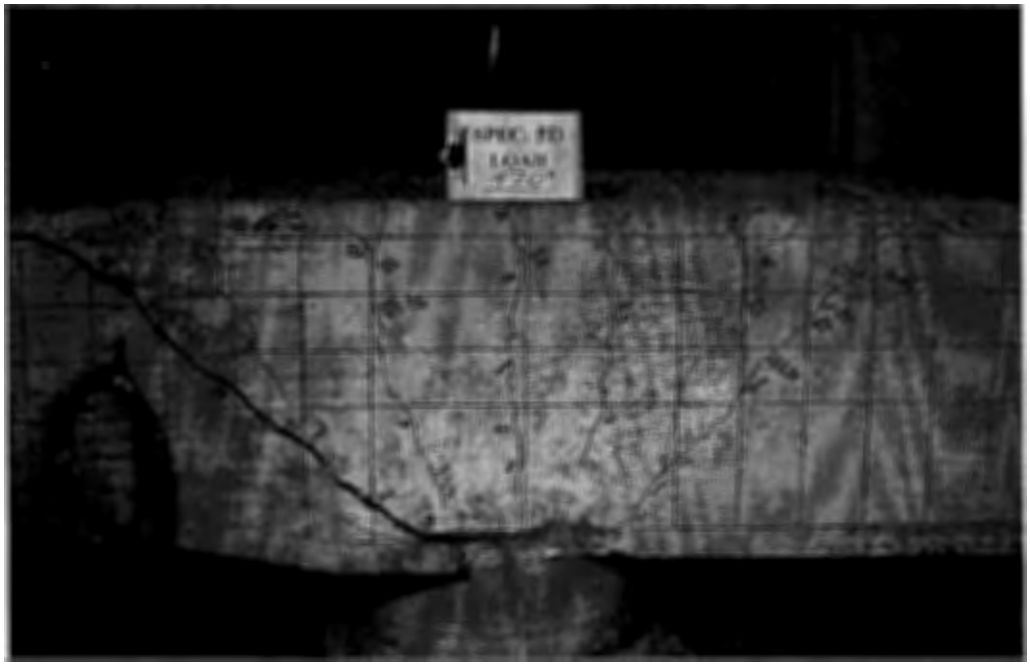

Figure E-18. Specimen 5D Cracking Pattern at P = 470 kips.

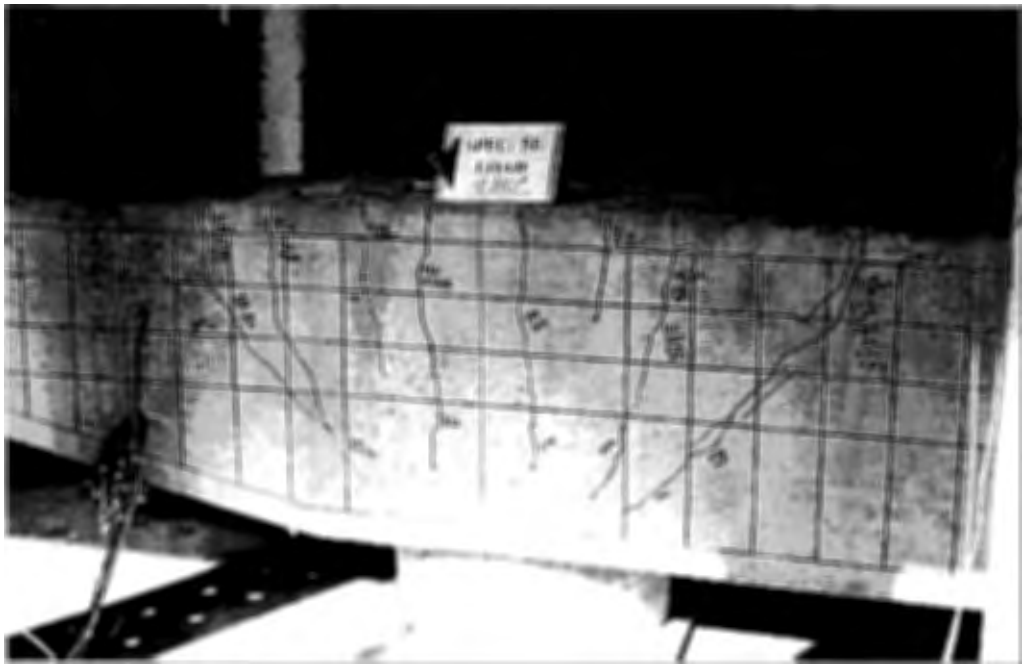

Figure E-19. Specimen 5E Cracking Pattern at P = 480 kips.

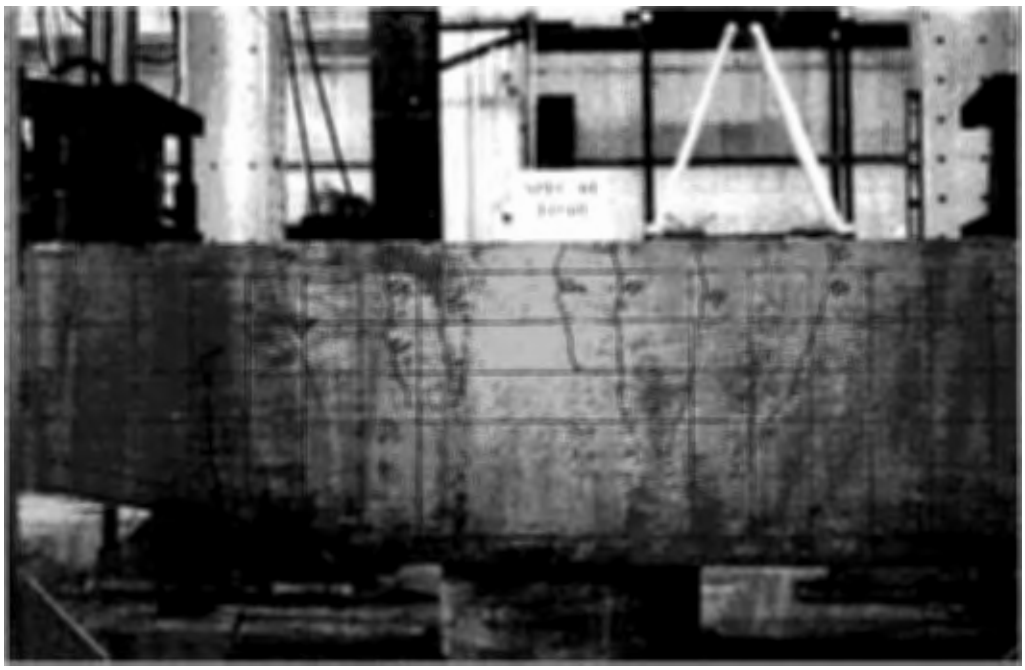

Figure E-20. Specimen 6F Cracking Pattern at P = 160 kips.

Figure E-21. Specimen 6F Cracking Pattern at P = 420 kips.

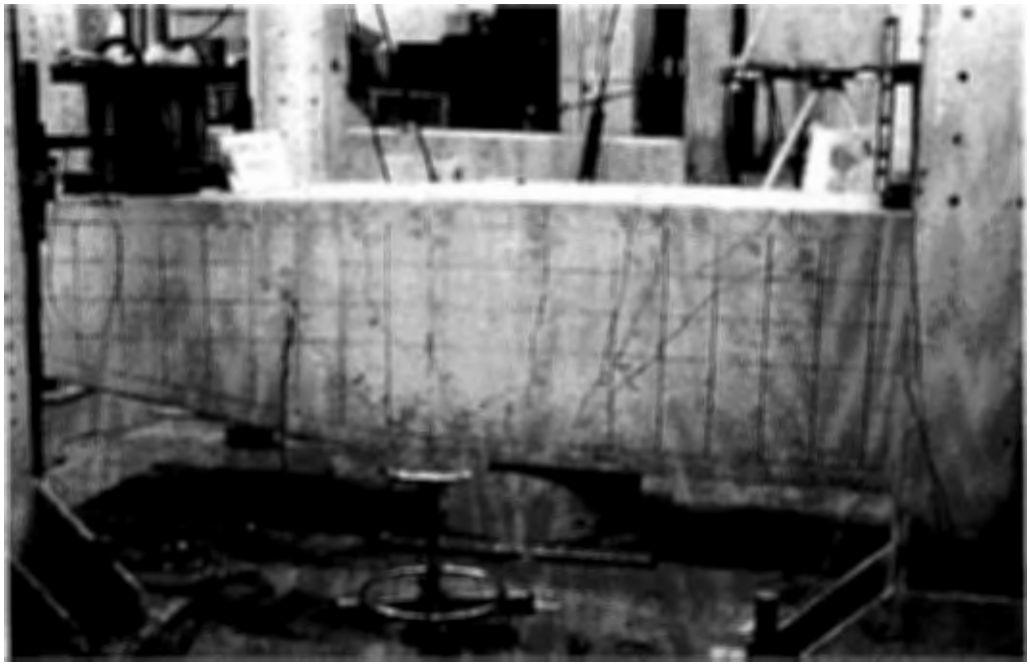

Figure E-22. Specimen 6G Cracking Pattern at P = 360 kips.

Figure E-23. Specimen 7F Cracking Pattern at P = 160 kips.

Figure E-24. Specimen 7F Cracking Pattern at P = 500 kips.

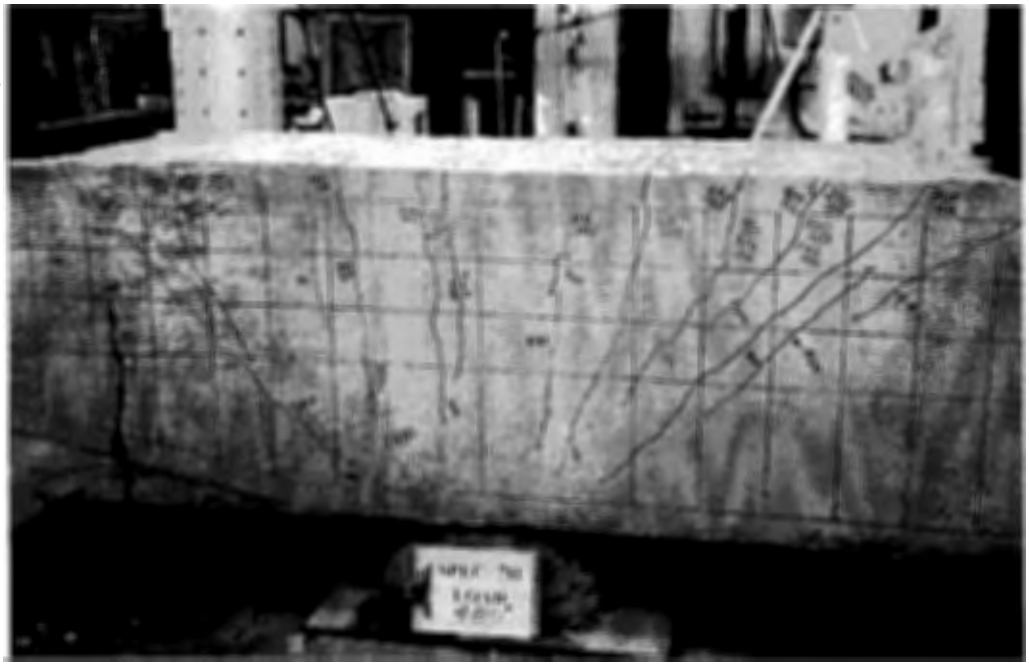

Figure E-25. Specimen 7H Cracking Pattern at P = 480 kips.

Figure E-26. Specimen 8G Cracking Pattern at P = 160 kips.

Figure E-27. Specimen 8G Cracking Pattern at P = 440 kips.

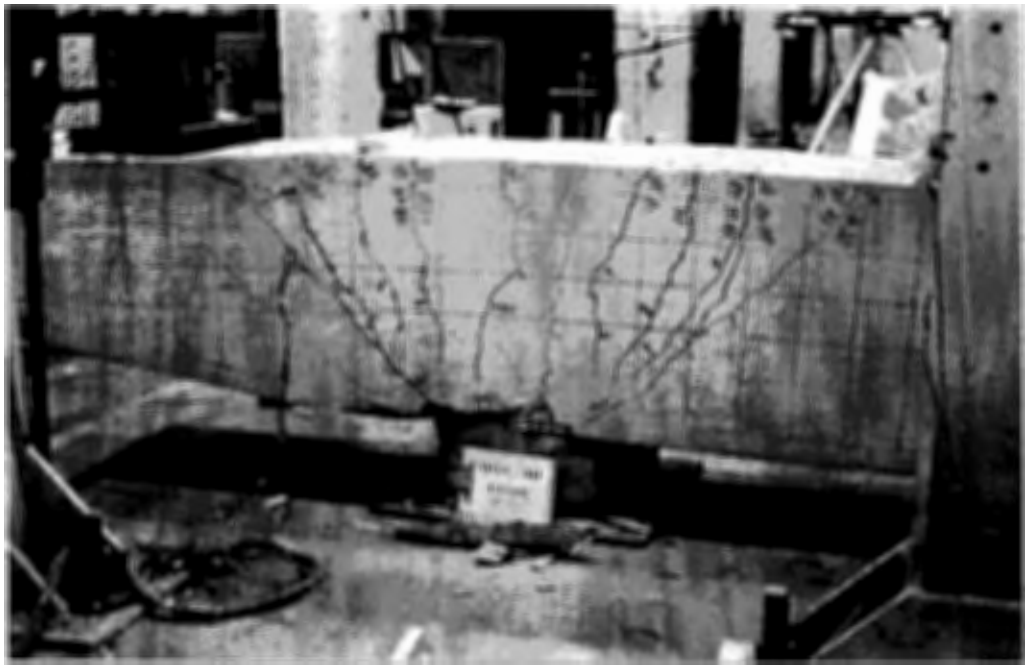

Figure E-28. Specimen 8H Cracking Pattern at P = 470 kips.

APPENDIX F

NOTATION AND TERMS

This report uses the following notation:

a : shear span measured from the support reaction to the centroid of the applied load

A : effective tension area of concrete having the same centroid as the flexural steel, per flexural reinforcement bar (in.^{2}/bar)

A_s : area of flexural tension reinforcement

A_{sc} : area of flexural compression reinforcement

A_{sp} : area of flexural tension reinforcement being provided

A_{sr} : area of flexural tension reinforcement required so that f_s = 36 ksi

A_v : area of transverse vertical shear reinforcement

A_{vh} : area of horizontal shear reinforcement

b : transverse width of flexural member

β : crack width gradient for projecting crack width at the level of the reinforcement to the crack width at the extreme concrete fiber

c : distance from the extreme concrete fiber in compression to the neutral axis

c_c : clear distance from the extreme concrete fiber in tension to the surface of the nearest tension reinforcement

d : effective depth of member, measured from the extreme concrete fiber in compression to the centroid of the flexural tension reinforcement

d' : distance from the extreme concrete fiber in compression to the centroid of the flexural compression reinforcement

d_c : distance from the extreme concrete fiber in compression to the centroid of the flexural tensile reinforcement

E_c : concrete modulus of elasticity

E_s : steel reinforcement modulus of elasticity

ε_{cc} : strain at the level of the steel compression reinforcement

ε_{ct} : strain at the level of the extreme concrete fiber in tension

ε_s : steel tensile strain

ε_{st} : steel tensile strain in flexural analytical model

f'_c : concrete 28 day compressive strength

f_{cc} : concrete stress at the level of the extreme concrete fiber in compression

f_{ce} : effective concrete strength for compression struts within strut-and-tie model

f_{ct} : concrete stress at the level of the extreme concrete fiber in tension

f_r : concrete modulus of rupture, taken to be equivalent to $7.5*(f'_c)^{1/2}$

f_{sa} : maximum allowable flexural service stress

f_{sc} : steel stress at the level of the steel compression reinforcement

f_{st} : steel stress at the level of the steel tension reinforcement

f_y : specified yield stress of steel reinforcement

F_{cc} : resultant transverse plane concrete compressive force

F_{ct} : resultant transverse plane concrete tensile force

F_{sc} : resultant transverse plane steel compressive force

h : height (depth) of flexural member

h_1 : $(1 - k) * d$, where k = distance from the neutral axis to the compression face divided by the effective depth, d

jd : length of the internal moment arm of a flexural member, measured from the resultant of the internal tensile force to the resultant of the internal compressive force

l_n : clear span distance between the faces of two adjacent supports

M_n : nominal moment capacity of flexural section, where f_y = 60 ksi

M_{pr} : probable moment capacity causing formation of plastic hinge, with f_y = 75 ksi

P : magnitude of applied load

R : $(h - k d) / h_1$

s : maximum spacing of flexural tension reinforcement bars or transverse shear reinforcement

s_c : longitudinal crack spacing along concrete tension surface

t_s : side cover measured from the centroid of the nearest reinforcement bar

v_1 : effective concrete compressive strength reduction factor

v_2 : effective concrete compressive strength reduction factor

V_c : nominal shear strength provided by the concrete

ϕV_n : reduced member nominal shear strength by superposition of concrete and steel shear strengths ($\phi = 0.85$)

V_s : nominal shear strength provided by the steel reinforcement

V_u : ultimate applied shear force

w_c : general crack width measurement

w_{max} : maximum observed crack width

w_s : maximum side face crack width

x : distance from the neutral axis to the uncracked concrete tension fiber

This report uses the following terms:

AASHTO	:	American Association of State Highway and Transportation Officials
ACI 318	:	American Concrete Institute, Committee 318
ASCE	:	American Society of Civil Engineers
ASD	:	Allowable Stress Design
CEB	:	Comitě Euro-International du Běton
CSA	:	Canadian Standards Association
CHBDC	:	Canadian Highway Bridge Design Code
LFD	:	Load Factor Design
LRFD	:	Load and Resistance Factor Design
RC	:	Reinforced Concrete
TxDOT	:	Texas Department of Transportation